MAPPING PSYCHOPATHOLOGY WITH fMRI AND EFFECTIVE CONNECTIVITY ANALYSIS

EDITED BY: Baojuan Li, Adeel Razi and Karl J. Friston
PUBLISHED IN: Frontiers in Human Neuroscience

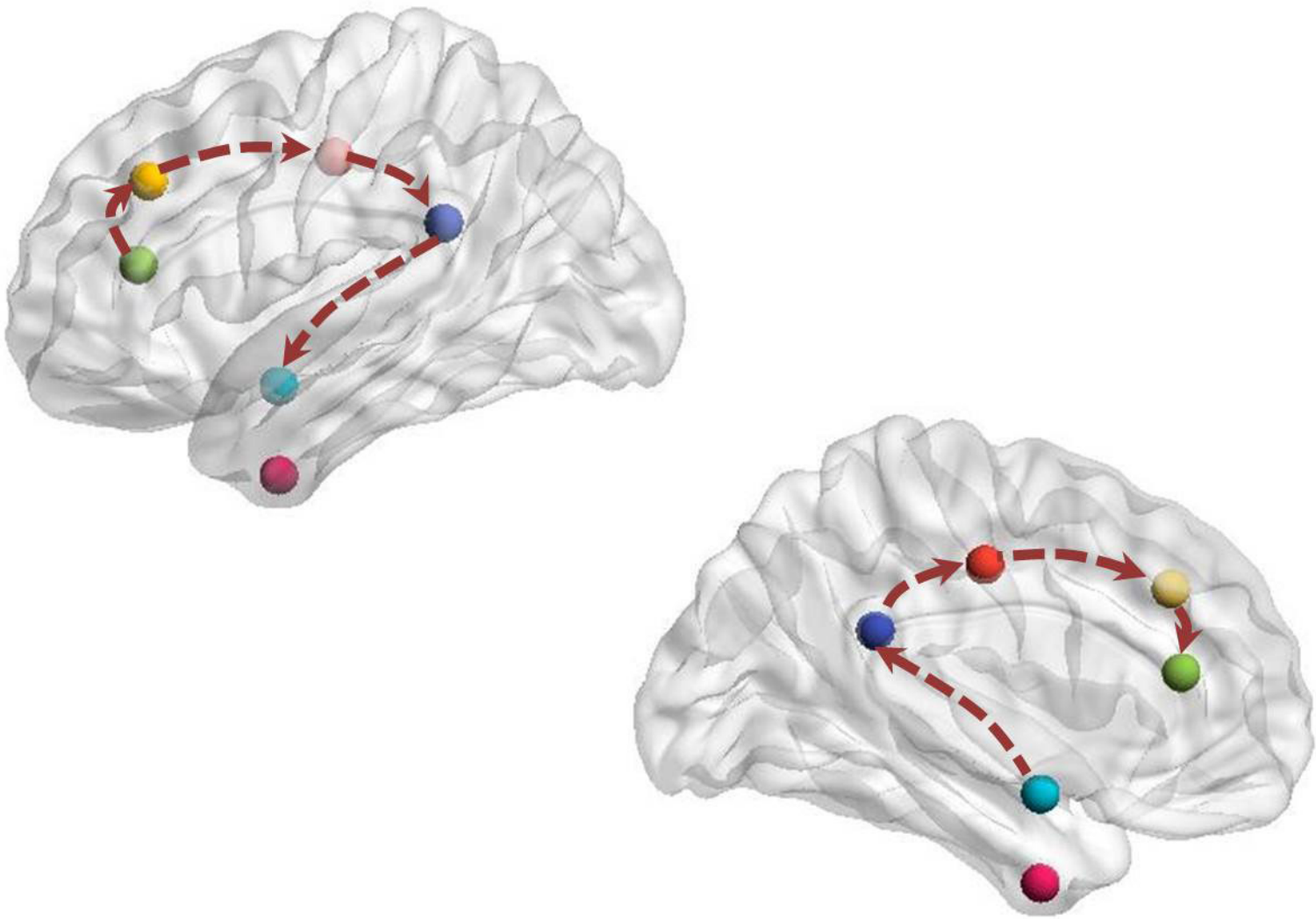

frontiers Research Topics

frontiers

ISSN 1664-8714
ISBN 978-2-88945-207-1
DOI 10.3389/978-2-88945-207-1

About Frontiers

Frontiers is more than just an open-access publisher of scholarly articles: it is a pioneering approach to the world of academia, radically improving the way scholarly research is managed. The grand vision of Frontiers is a world where all people have an equal opportunity to seek, share and generate knowledge. Frontiers provides immediate and permanent online open access to all its publications, but this alone is not enough to realize our grand goals.

Frontiers Journal Series

The Frontiers Journal Series is a multi-tier and interdisciplinary set of open-access, online journals, promising a paradigm shift from the current review, selection and dissemination processes in academic publishing. All Frontiers journals are driven by researchers for researchers; therefore, they constitute a service to the scholarly community. At the same time, the Frontiers Journal Series operates on a revolutionary invention, the tiered publishing system, initially addressing specific communities of scholars, and gradually climbing up to broader public understanding, thus serving the interests of the lay society, too.

Dedication to Quality

Each Frontiers article is a landmark of the highest quality, thanks to genuinely collaborative interactions between authors and review editors, who include some of the world's best academicians. Research must be certified by peers before entering a stream of knowledge that may eventually reach the public - and shape society; therefore, Frontiers only applies the most rigorous and unbiased reviews.

Frontiers revolutionizes research publishing by freely delivering the most outstanding research, evaluated with no bias from both the academic and social point of view.

By applying the most advanced information technologies, Frontiers is catapulting scholarly publishing into a new generation.

What are Frontiers Research Topics?

Frontiers Research Topics are very popular trademarks of the Frontiers Journals Series: they are collections of at least ten articles, all centered on a particular subject. With their unique mix of varied contributions from Original Research to Review Articles, Frontiers Research Topics unify the most influential researchers, the latest key findings and historical advances in a hot research area! Find out more on how to host your own Frontiers Research Topic or contribute to one as an author by contacting the Frontiers Editorial Office: **researchtopics@frontiersin.org**

MAPPING PSYCHOPATHOLOGY WITH fMRI AND EFFECTIVE CONNECTIVITY ANALYSIS

Topic Editors:
Baojuan Li, Fourth Military Medical University, China
Adeel Razi, University College London, UK
Karl J. Friston, University College London, UK

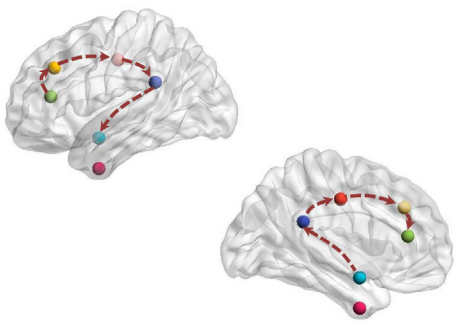

Effective connectivity analysis models causal interactions among brain regions
Image by Baojuan Li

There is a growing appreciation that many psychiatric (and neurological) conditions can be understood as functional disconnection syndromes – as reflected in aberrant functional integration and synaptic connectivity. This Research Topic considers recent advances in understanding psychopathology in terms of aberrant effective connectivity – as measured noninvasively using functional magnetic resonance imaging (fMRI).

Recently, there has been increasing interest in inferring directed connectivity (effective connectivity) from fMRI data. Effective connectivity refers to the influence that one neural system exerts over another and quantifies the directed coupling among brain regions – and how they change with pathophysiology. Compared to functional connectivity, effective connectivity allows one to understand how brain regions interact with each other in terms of context sensitive changes and directed coupling – and therefore may provide mechanistic insights into the neural basis of psychopathology.

Established models of effective connectivity include psychophysiological interaction (PPI), structural equation modeling (SEM) and dynamic causal modelling (DCM). DCM is unique because it explicitly models the interaction among brain regions in terms of latent neuronal activity. Moreover, recent advances in DCM such as stochastic and spectral DCM, make it possible to characterize the interaction between different brain regions both at rest and during a cognitive task.

Citation: Li, B., Razi, A., Friston, K. J., eds. (2017). Mapping Psychopathology with fMRI and Effective Connectivity Analysis. Lausanne: Frontiers Media. doi: 10.3389/978-2-88945-207-1

Table of Contents

frontiers in Human Neuroscience

EDITORIAL
published: 31 March 2017
doi: 10.3389/fnhum.2017.00151

Editorial: Mapping Psychopathology with fMRI and Effective Connectivity Analysis

Baojuan Li[1,2]*, *Adeel Razi*[3,4] *and Karl J. Friston*[3]

[1] School of Biomedical Engineering, Fourth Military Medical University, Xi'an, China, [2] Athinoula A. Martinos Center for Biomedical Imaging, Department of Radiology, Massachusetts General Hospital and Harvard Medical School, Boston, MA, USA, [3] The Wellcome Trust Centre for Neuroimaging, University College London, London, UK, [4] Department of Electronic Engineering, NED University of Engineering and Technology, Karachi, Pakistan

Keywords: effective connectivity, fMRI, neuropsychiatric disorders, psychophysiological interactions, dynamic causal modeling, Granger causality

Editorial on the Research Topic

Mapping Psychopathology with fMRI and Effective Connectivity Analysis

Distributed networks of interacting brain systems—rather than a single area—are usually involved in the execution of a specific cognitive task. Recent advances in neuroimaging techniques now allow us to see how these interacting brain regions are integrated and cooperate with each other to prosecute cognitive operations (Razi and Friston, 2016). Brain connectivity analyses based on electroencephalography (EEG), magnetoencephalography (MEG), and functional magnetic resonance imaging (fMRI) signals characterize neuronal responses in terms of how brain activity is induced by external stimuli and propagates among distributed brain regions, and thus may help answer key questions about functional brain architectures. The insights that brain connectivity analyses offer is also crucial for us to elucidate the neurobiological correlates underlying many neuropsychiatric disorders.

Functional connectivity and effective connectivity are generally used to measure functional integration in neuroimaging. The former examines (undirected) statistical dependencies (e.g., temporal correlations) between brain regions and has been extensively studied to characterize brain networks at rest. However, understanding the precise mechanisms mediating cognitive processes depend on directed information flow within brain networks. Thus, the current research topic focuses on mapping psychopathology with (directed) effective connectivity analysis, which models causal interactions among brain regions. We attempt to further improve current understanding of the neural mechanisms of major neuropsychiatric disorders by exploring how signals are transmitted differently from one region to another in healthy controls and patients. This comparison may help explain the pathophysiology and psychopathology seen in these disorders—at a network and possibly synaptic level.

In this research topic, we invited world-renowned experts to present their recent work that have utilized various models of directed connectivity; including psychophysiological interactions (PPI), Granger causality (GC), and dynamic causal modeling (DCM) to investigate directed connectivity in healthy subjects and patients with neuropsychiatric disorders. The papers in this research topic further our knowledge of the neurobiological mechanisms underlying neurological and psychiatric disorders. We will see that young people with OCD exhibit increased dorsal anterior cingulate cortex (dACC) modulatory effects during the performance of working memory tasks (Diwadkar et al.). There is also new evidence suggesting that neurodegenerative disorders like Parkinson's disease (Yan et al.) and Huntington's disease (Minkova et al.) are characterized by impaired causal

OPEN ACCESS

Edited and reviewed by:
Srikantan S. Nagarajan, University of California, San Francisco, USA

***Correspondence:**
Baojuan Li
libjuan@163.com

Received: *16 December 2016*
Accepted: *14 March 2017*
Published: *31 March 2017*

Citation:
Li B, Razi A and Friston KJ (2017) Editorial: Mapping Psychopathology with fMRI and Effective Connectivity Analysis. Front. Hum. Neurosci. 11:151. doi: 10.3389/fnhum.2017.00151

interactions of the motor control system (Dowlati et al.) speaking to the interesting notion that age-dependent neural mechanisms may be important for understanding aberrant belief states associated with psychopathology. Interestingly, abnormalities in brain effective connectivity are also seen clearly in resting state in subjects with schizophrenia (Cui et al.), smoking addiction (Tang et al.), idiopathic generalized epilepsy (Wei et al.) and cocaine users (Ray et al.). In addition, it is exciting to see that effective connectivity analysis may furnish a new framework to understand fatigue and depression (Stephan et al.). We believe these findings have the potential to invigorate and advance our understanding of the neurobiological mechanisms of major neuropsychiatric disorders, thus improving the prevention, diagnosis and treatment of these disorders.

Looking into the future, we anticipate a shift toward new methods that can measure effective connectivity among specific cell types (e.g., lamina-specific connectivity). For example, methods that use detailed biophysical modeling based on canonical microcircuits and neural mass models for functional MRI data (Friston et al., in press) or that combine other modalities—like optogenetics—with fMRI (Bernal-Casas et al., 2017). These new methods will be very useful within the context of detecting early and selective abnormalities in specific cell types in various forms of dementia. For example, frontotemporal lobar degeneration (FTLD) has been previously shown to selectively target Von Economo neurons in fronto-insular regions (Seeley et al., 2006) and that pathogenic *huntingtin* protein selectively targets striatal spiny projection neurons (Ehrlich, 2012). More detailed and informed models of effective connectivity may also be very useful for furthering recent (and exciting) developments in understanding compensatory mechanisms in presymptomatic neurodegeneration that could potentially translate to the discovery of reliable neuronal biomarkers of disease progression (Klöppel et al., 2015). We envisage that computational modeling of dementia will usher a new era of functional integration research, by increasing our understanding of mechanisms by which molecular lesions engender specific meso and macro scale neural network damage that maps onto specific phenotypes (Gilson et al., 2016).

A complete understanding of complex (many-to-many) protein-network-phenotype mappings will be crucial for the early diagnosis and development of interventional therapies for slowing and preventing dementia. In psychiatry, computational modeling has already given a birth to the new field of computational psychiatry that constitutes a new paradigm for translational research and clinical decision making (Montague et al., 2012; Friston et al., 2014). The potential for developing new treatments for psychiatric illnesses that go beyond addressing symptoms is promising and any computational modeling that can precisely characterize aberrant connectivity may play a central role in predicting an individual's clinical trajectory (Stephan and Mathys, 2014; Friston, 2016).

AUTHOR CONTRIBUTIONS

All authors listed, have made substantial, direct and intellectual contribution to the work, and approved it for publication.

ACKNOWLEDGMENTS

This work was funded by the National Natural Science Foundation of China (81301199) and the Wellcome Trust Principal Research Fellowship (Ref: 088130/Z/09/Z).

REFERENCES

Bernal-Casas, D., Lee, H. J., Weitz, A. J., and Lee, J. H. (2017). Studying brain circuit function with dynamic causal modeling for optogenetic fMRI. *Neuron* 93, 522–532.e5. doi: 10.1016/j.neuron.2016.12.035

Ehrlich, M. E. (2012). Huntington's disease and the striatal medium spiny neuron: cell-autonomous and non-cell-autonomous mechanisms of disease. *Neurotherapeutics* 9, 270–284. doi: 10.1007/s13311-012-0112-2

Friston, K. (2016). "Computational nosology and precision psychiatry: a proof of concept," in *Computational Psychiatry: New Perspectives on Mental Illness*, *Strüngmann Forum Reports.* eds A. Redish, and J. Gordon (Cambridge, MA: MIT Press), 20.

Friston, K. J., Preller, K. H., Mathys, C. Cagnan, H., Heinzle, J., Razi, A., et al. (in press). Dynamic causal modelling revisited. *NeuroImage*. doi: 10.1016/j.neuroimage.2017.02.045

Friston, K. J., Stephan, K. E., Montague, R., and Dolan, R. J. (2014). Computational psychiatry: the brain as a phantastic organ. *Lancet Psychiatry* 1, 148–158. doi: 10.1016/S2215-0366(14)70275-5

Gilson, M., Moreno-Bote, R., Ponce-Alvarez, A., Ritter, P., and Deco, G. (2016). Estimation of directed effective connectivity from fMRI functional connectivity hints at asymmetries of cortical connectome. *PLoS Comput. Biol.* 12:e1004762. doi: 10.1371/journal.pcbi.1004762

Klöppel, S., Gregory, S., Scheller, E., Minkova, L., Razi, A., Durr, A., et al. (2015). Compensation in preclinical Huntington's disease: evidence from the track-on HD study. *EBio Med.* 2, 1420–1429. doi: 10.1016/j.ebiom.2015.08.002

Montague, P. R., Dolan, R. J., Friston, K. J., and Dayan, P. (2012). Computational psychiatry. *Trends Cogn. Sci.* 16, 72–80. doi: 10.1016/j.tics.2011.11.018

Razi, A., and Friston, K. J. (2016). The Connected Brain Causality, models, and intrinsic dynamics. *IEEE Signal Process. Mag.* 33, 14–35. doi: 10.1109/MSP.2015.2482121

Seeley, W. W., Carlin, D. A., Allman, J. M., Macedo, M. N., Bush, C., Miller, B. L., et al. (2006). Early frontotemporal dementia targets neurons unique to apes and humans. *Ann. Neurol.* 60, 660–667. doi: 10.1002/ana.21055

Stephan, K. E., and Mathys, C. (2014). Computational approaches to psychiatry. *Curr. Opin. Neurobiol.* 25, 85–92. doi: 10.1016/j.conb.2013.12.007

Conflict of Interest Statement: The authors declare that the research was conducted in the absence of any commercial or financial relationships that could be construed as a potential conflict of interest.

frontiers in Human Neuroscience

ORIGINAL RESEARCH
published: 09 November 2016
doi: 10.3389/fnhum.2016.00563

Effective Connectivity within the Mesocorticolimbic System during Resting-State in Cocaine Users

Suchismita Ray[1], Xin Di[2] and Bharat B. Biswal[2]*

[1] Center of Alcohol Studies, Rutgers, The State University of New Jersey, Piscataway, NJ, USA, [2] New Jersey Institute of Technology, Newark, NJ, USA

Objective: Although effective connectivity between brain regions has been examined in cocaine users during tasks, no effective connectivity study has been conducted on cocaine users during resting-state. In the present functional magnetic resonance imaging study, we examined effective connectivity in resting-brain, between the brain regions within the mesocorticolimbic dopamine system, implicated in reward and motivated behavior, while the chronic cocaine users and controls took part in a resting-state scan by using a spectral Dynamic causal modeling (spDCM) approach.

Method: As part of a study testing cocaine cue reactivity in cocaine users (Ray et al., 2015b), 20 non-treatment seeking cocaine-smoking (abstinent for at least 3 days) and 17 control participants completed a resting state scan and an anatomical scan. A mean voxel-based time series data extracted from four key brain areas (ventral tegmental area, VTA; nucleus accumbens, NAc; hippocampus, medial frontal cortex) within the mesocorticolimbic dopamine system during resting-state from the cocaine and control participants were used as input to the spDCM program to generate spDCM analysis outputs.

Results: Compared to the control group, the cocaine group had higher effective connectivity from the VTA to NAc, hippocampus and medial frontal cortex. In contrast, the control group showed a higher effective connectivity from the medial frontal cortex to VTA, from the NAc to medial frontal cortex, and on the hippocampus self-loop.

Conclusions: The present study is the first to show that during resting-state in abstaining cocaine users compared to controls, the VTA initiates an enhanced effective connectivity to NAc, hippocampus and medial frontal cortex areas within the mesocorticolimbic dopamine system, the brain's reward system. Future studies of effective connectivity analysis during resting-state may eventually be used to monitor treatment outcome.

Keywords: connectivity, cocaine, fMRI, mesocorticolimbic system, resting state connectivity

OPEN ACCESS

Edited by:
Baojuan Li,
Massachusetts General Hospital, USA

Reviewed by:
Bonnie J. Nagel,
Oregon Health & Science University, USA
Xia Liang,
National Institute on Drug Abuse, USA

****Correspondence:***
Suchismita Ray
shmita@rci.rutgers.edu

Received: *27 June 2016*
Accepted: *25 October 2016*
Published: *09 November 2016*

Citation:
Ray S, Di X and Biswal BB (2016) Effective Connectivity within the Mesocorticolimbic System during Resting-State in Cocaine Users. Front. Hum. Neurosci. 10:563. doi: 10.3389/fnhum.2016.00563

INTRODUCTION

The mesocorticolimbic system has been associated with reward, motivation, and goal-directed behavior. Drugs of abuse enhance extracellular dopamine concentration in components of the mesocorticolimbic system, including the ventral striatum (nucleus accumbens, NAc), extended amygdala, hippocampus, anterior cingulate, prefrontal cortex, and insula, which are triggered by

dopaminergic projections essentially from the ventral tegmental area (VTA; Jasinska et al., 2014). Based on earlier studies (Jay, 2003; Kelley, 2004; Nestler, 2005), although the mesocorticolimbic system responds to natural rewards such as food, water, and sex, drugs of abuse induce a larger response in this system than physiological stimuli. Past research suggests that the drugs of abuse "hijack" the neurobiological mechanisms by which the brain reacts to reward, creates reward-related memories, and summarizes action repertoires leading to the reward (Everitt and Robbins, 2005; Kalivas and O'Brien, 2008). According to Volkow et al. (2006, 2008), through repeated drug use, drug related cues become conditioned stimuli and evoke dopamine release and craving; and over time, the incentive salience of these cues is heightened (Robinson and Berridge, 1993). This phenomenon of heightened salience of the drug cues has been demonstrated in human neuroimaging studies by increased blood oxygenation level dependent (BOLD) activation in areas including the prefrontal cortex [medial prefrontal cortex (mPFC), orbital frontal cortex, dorsolateral prefrontal cortex], VTA, anterior cingulate cortex, insula, NAc, amygdala, and hippocampus in response to drug cues relative to neutral cues in chronic drug users (see Jasinska et al., 2014 for review).

A major focus of the recent neuroimaging studies has been to understand not just which individual brain locations are activated by drug cues, but how individual brain regions are integrated, i.e., functional connectivity. Functional connectivity has been examined in cocaine users in resting-state (Gu et al., 2010; Wilcox et al., 2011; Cisler et al., 2013; Ray et al., 2015a) and also when they performed tasks (a finger-tapping and an attention task; Tomasi et al., 2010; Hanlon et al., 2011). According to Fox and Raichle (2007), resting state functional connectivity, typically assessed by the correlation of spontaneous fluctuations of BOLD signals in different regions of the 'resting' brain, is believed to provide a measure of the brain's functional organization. Resting state functional connectivity between the regions within the mesocorticolimbic system in cocaine users has been examined by Gu et al. (2010). Results showed that cocaine users compared to controls had a reduced functional connectivity within this system. However, functional connectivity studies are limited in that although they provide information about the interaction of brain regions of interest (ROIs), these studies do not assess how one region influences another.

Effective connectivity on the other hand refers to the causal influence that one brain region employs over another, and thus add an important information on the consequences of chronic drug use on the mesocorticolimbic system. To the best of our knowledge, only three functional magnetic resonance imaging (fMRI) effective connectivity studies have been done with cocaine users. As part of the study described here, we have reported effective connectivity among brain regions within the drug cue processing network using IMaGES (Ramsey et al., 2010), a Bayesian search algorithm, while chronic cocaine users viewed cocaine-related picture cues (Ray et al., 2015b). During cocaine cue exposure, cocaine users demonstrated a unique feed-forward effective connectivity pattern between the ROIs of the drug-cue processing network (amygdala→hippocampus→dorsal striatum→insula→medial frontal cortex, dorsolateral prefrontal cortex, anterior cingulate cortex) that was absent when the controls viewed the cocaine cues. Using a stochastic dynamic causal modeling (DCM) approach, Ma et al. (2014) showed that cocaine subjects differed from controls in that effective connectivity from inferior frontal cortex to striatum was less affected by an immediate working memory task in the cocaine compared to the control group, and the effective connectivity from middle frontal gyrus to the striatum was less affected by the delayed working memory task in the cocaine compared to the control group. And Ma et al. (2015) utilized an fMRI-based stochastic DCM to study the effective neuronal connectivity associated with response inhibition in cocaine dependent subjects, elicited under performance of a Go/NoGo task with two levels of NoGo difficulty (Easy and Hard). The DCM analysis revealed that prefrontal-striatal connectivity was influenced during the NoGo conditions for both groups. In cocaine dependent subjects, the effective connectivity from left anterior cingulate cortex to left caudate was more negative during the Hard NoGo conditions.

The goal of this study was to expand Gu et al.'s (2010) study by examining effective connectivity among regions within the mesocorticolimbic dopamine system (**Figure 1**) in cocaine users during resting-state, when there are no demands being placed, such as cognitive tasks or viewing drug cues. This provided a measure of baseline effective connectivity, utilizing baseline BOLD signal, within the mesocorticolimbic system in cocaine users (Liu et al., 2011). Since there is no demand on task, resting-state data unburden subject compliance, and training demands, and thus makes it interesting for studies of development and clinical populations. An analysis of baseline connectivity might shed light on the interpretation of prior research that has found an increased connectivity in cocaine users (vs. controls) in response to, for example, a cognitive task. Conceivably, such a finding might be due to a characteristically higher resting state level of connectivity for cocaine users; if true, then a conclusion that higher connectivity is due to a cognitive task would be called into question. In the present fMRI study, we examined effective connectivity in resting-brain, more specifically, between the brain regions within the mesocorticolimbic dopamine system while the chronic cocaine users took part in a resting-state scan. We collected resting-state fMRI data from cocaine smokers who were non-treatment seekers and were abstinent from cocaine use for 72 h and age-matched healthy controls with no experience with cocaine.

Although originally developed for task based fMRI (Friston et al., 2003), several methodological developments have made it possible to use DCM to model effective connectivity during resting-state (Daunizeau et al., 2012; Di and Biswal, 2014; Friston et al., 2014). One of the recent developments is to inverse DCM models at the frequency spectrum domain (Friston et al., 2014). In the current study, we applied this spectral DCM (spDCM) approach on resting-state fMRI data collected from chronic cocaine users and controls to examine effective connectivity among four key regions within the mesocorticolimbic dopamine system: VTA, NAc, hippocampus, and medial frontal cortex. We first set fully connected models for the two groups. We then adopted a Bayesian model reduction approach to identify optimal

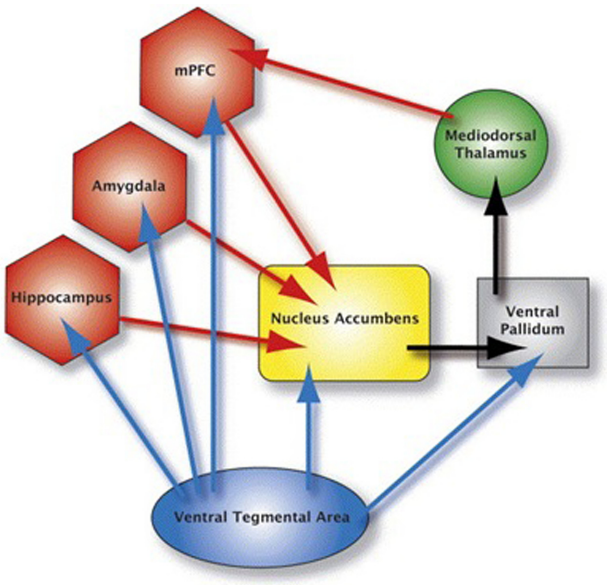

FIGURE 1 | This figure depicts the mesocorticolimbic system. The blue arrows represent dopaminergic pathways: the red arrows represent glutamatergic pathways; black arrows represent GABAergic pathways. Brain areas anterior cingulate, insula, orbital frontal cortex and dorsolateral prefrontal cortex are not shown in the figure.

models for the two groups (Friston and Penny, 2011). More specifically, based on research conducted by Gu et al. (2010), we hypothesized that the cocaine group compared to the control group would show a decreased effective connectivity pattern between the four regions within the mesocorticolimbic dopamine system as a result of chronic cocaine use during resting-state.

MATERIALS AND METHODS

Participants

Twenty (15M; 5F) non-treatment seeking chronic cocaine smokers abstaining from cocaine use for 72 h, and 17 (13M; 4F) age-, education-, and ethnic-background matched healthy control participants took part in the study (**Table 1**). The two groups did not significantly differ with regard to their age, education, alcohol use quantity, nicotine use frequency and quantity, and caffeine use frequency and quantity.

The main inclusion criteria for the study participants included English as their first language, no report of childhood learning disability or special education, right handedness, and near 20/20 vision (or corrected). The main exclusion criteria for the study participants included serious medical conditions, a history of psychiatric or neurological disorder or treatment, lifetime diagnosis of any substance use disorder of the prospective participant's biological mother (to rule out prenatal exposure effects), MRI contraindications, alcohol abuse and dependence including past dependence on alcohol, and for women, pregnancy. Participants were excluded if they reported any history of anxiety or depression in their recent past.

TABLE 1 | Demographic and substance use information for cocaine users and controls.

	Cocaine (*n*=20)	Control (*n*=17)		
	Mean, Range (*SD*)	**Mean, Range (*SD*)**	***t*-stats**	***p***
Age (years)	46 (6.4)	46 (7)	0.10	0.92
Education (years)	13.4 (2.4)	13.5 (2.1)	−0.17	0.86
Race/Ethnicity				
Caucasian	7	5		
African American	11	11		
Hispanic	2	1		
Female (*n*)	5	4		
Cocaine Use by All Users				
Frequency (days/week)	3, 2–6 (1.2)	NA		
Duration of use (years)	16, 3–34 (8)	NA		
Money spent ($/week)	$220, $70–550 (131)	NA		
Cocaine Use by Non-cocaine dependent/abusers				
Frequency (days/week)	3, 2–6 (1.5)			
Duration of use (years)	9, 3–19 (6)			
Money spent ($/week)	$172, $80–350 (93)			
Alcohol Use				
Frequency (days/month)	1.9, 1–2.5 (0.55)	4.0, 2.5–6.5 (1.4)	−4.89	0.00*
Quantity (drinks/occasion)	2.1, 1–3.5 (0.92)	1.7, 1–2 (0.42)	0.92	0.37
Drinkers (#)	13	6		
Nicotine Use				
Frequency (days/week)	5.1, 1–7 (2.3)	5.7, 3–7 (2.3)	−0.40	0.70
Quantity (cigarettes/day)	6.3, 1.5–13 (3.0)	2.8, 2.5–3 (0.29)	2.00	0.07
Smokers (#)	13	6		
Caffeine Use				
Frequency (days/week)	4.4, 1–7 (2.5)	3.6, 1–7 (2.4)	0.78	0.44
Quantity (cups/day)	1.3, 1–2 (0.43)	1.3, 1–4 (0.90)	0.26	0.80
Caffeine users (#)	13	11		
Clinical Characteristics				
DSM-IV-R cocaine dependence	10	NA		
DSM-IV-R cocaine abuse	3	NA		
Cocaine non-dependent/abusers	7			

**Denotes significant group difference.*

Participants were included in the cocaine group if they currently spent a minimum of $70 per week on cocaine and had a history of smoking cocaine for at least two times per week for the past 6 months (assessed by self-report). Participants in the cocaine group were instructed to abstain from cocaine for at least 72 h before their study appointment. The primary current drug of choice for the cocaine group was cocaine and they did not meet a DSM-IV-TR diagnosis of abuse or dependence for any other drugs, as confirmed by SCID (First et al., 1997). Half of the cocaine users did not meet DSM-IV-TR criteria for cocaine dependence, and seven did meet criteria for abuse or dependence.

Ten out of 20 cocaine users never tried any other drugs in their lifetime and nine others experimented with marijuana once or two times in their lifetime ranging from 15 to 30 years back. Only one used marijuana one time in his/her lifetime 3 weeks before the study. Participants were included in the control group if they did not have any current or past drug use history and had no alcohol abuse history in their first degree family members. Ten out of 17 controls never tried any drugs in their lifetime and seven others experimented with marijuana once or two times in their lifetime ranging from 30 to 43 years back. Family history of alcohol abuse was assessed by using a semi-structured diagnostic instrument called Family History Assessment Module (Cloninger and Reich, 1991). None of the participants in the cocaine or in the control group reported any history of anxiety or depression during the past 2 weeks on the day of the telephone screening interview which took place within 7 days of the study.

On the day of the study, all participants gave written informed consent and took a urine screen to rule out pregnancy in women, and to ensure negative urine toxicology for cocaine, methamphetamine, THC, opiate and benzodiazepines (One Step Multi-Drug Screen Test Panel). Abstinence from alcohol was confirmed with a breathalyzer. At the end of the study, participants were compensated with a gift certificate worth $100 for their participation and were paid for their transportation expenses (Ray et al., 2015b). This research was approved by the Rutgers University Institutional Review Board.

Procedure

Each participant completed a resting-state scan and a high resolution anatomical MPRAGE (magnetization-prepared rapid acquisition with gradient echo) scan. During resting-state scan, participants were instructed to lie quietly without any movements while they visually fixated on a cross for 6 min. All participants completed resting-state scan first and then took part in the cue exposure task. All participants were administered a cocaine-craving questionnaire (CCQ-Brief; Sussner et al., 2006) before the resting-state scan started. They had to rate their craving for cocaine on a seven-point scale (1 = Strongly Disagree, 7 = Strongly Agree).

Image Acquisition

Imaging data were collected using a 3T Siemens Trio head-only fMRI scanner equipped with a standard Siemens head coil. While participants visually fixated on the cross, T2*-weighted echo planar images were acquired (35 axial slices, voxel size 3 mm × 3 mm × 3 mm, interslice gap 1 mm, matrix size 64 mm × 64 mm, FOV = 192 mm, TR = 2000 ms, TE = 25 ms, flip angle = 90°) covering the entire brain. A sagittal T1-weighed structural scan (TR = 1900 ms, TE = 2.52 ms, matrix = 256 × 256, FOV = 256 mm, voxel size 1 mm × 1 mm × 1 mm, 176 1-mm slices with 0.5 mm gap) was acquired in order to co-register it with the fMRI data (Ray et al., 2015b).

ROIs Selection

Based on prior publications in the field of addiction (see section 3.3.1. of Jasinska et al., 2014) we selected four ROIs within the mesocorticolimbic dopamine system as key nodes for effective connectivity analysis during resting-state. These four ROIs included VTA, NAc, hippocampus and medial frontal cortex. We selected these four regions: (1) VTA because regions within the mesocorticolimbic system are innervated by dopaminergic projections predominantly from the VTA, (2) VTA directly sends its projection to NAc (ventral striatum) implicated in reward and motivation, (3) hippocampus is responsible for memory related to past drug use, and (4) medial frontal cortex is implicated in continuation of drug seeking behavior (Jasinska et al., 2014). These four regions well represent mesocorticolimbic system (**Figure 2**).

Data Preprocessing

For each participant, in the first step, first five time-points were removed from that participant's BOLD fMRI data to account for T1-relaxation effects. In the next step, the participant's BOLD fMRI data were motion corrected with respect to the mean image of that participant. Following motion correction, each participant's BOLD fMRI data were co-registered to the anatomical images for that participant. Following co-registration, each participant's anatomical images were segmented into gray matter, white matter, cerebrospinal fluid (CSF) images and the deformation fields were derived to transform each participant's BOLD fMRI data into the MNI standard space. Lastly, 24 head motion parameters (Friston et al., 1996), the first five principle components of signals from white matter, and first five principle components of signals from CSF were regressed out for every voxel using linear regression.

In order to study effective connectivity patterns of the mesocorticolimbic dopamine system, we defined a total of four brain regions based on Jasinska et al. (2014). For each cocaine participant, a mean voxel based time series was extracted from each of these four ROIs (bilateral) using the AFNI program '3dmaskave', and used as input to the spDCM analysis in modeling the causal interactions between the ROIs during resting-state. For these four ROIs, the mean voxel based time series for the right brain area (i.e., right hippocampus) and the left brain area (i.e., left hippocampus) were averaged to create the

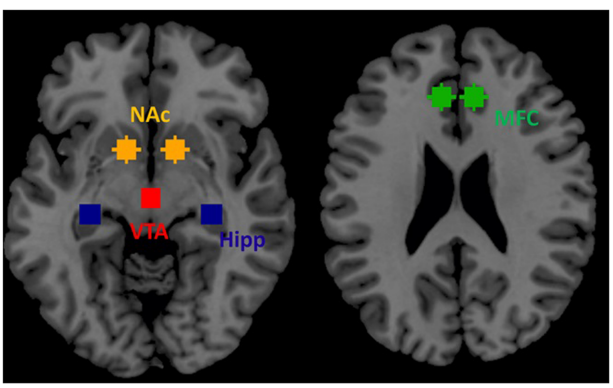

FIGURE 2 | Four regions of interest (ROIs) within the mesocorticolimbic system that were used for spDCM analysis.

mean voxel based time series for that brain area (hippocampus). A mean voxel-based time series data extracted from the same ROIs during resting-state from the control participants were used as input to the spDCM program to generate an additional spDCM analysis output.

Dynamic Causal Modeling

SPM 12 (with updates 6685) was used to perform spDCM analysis. For each subject, we first built a DCM with all endogenous connectivity specified (full model). All other types of connectivity, i.e., B, C, and D parameters, were set as zero. We used spectrum DCM framework to inverse the model for each subject (Friston et al., 2014). We next employed a network discovery procedure to optimize the DCMs for each group, separately (Friston and Penny, 2011). This procedure tests all the models nested in the full model, and chose the model with highest posterior probability. We then adopted Bayesian parameter averaging (BPA) approach to obtain model parameters for each group, separately (Razi et al., 2015). To compare connectivity parameters between the two groups, we compared model parameters from the full models between the two groups by using the BPA approach. Group differences in connectivity were identified using false discovery rate (FDR) at $p < 0.05$ correcting for the total 16 (4×4) connectivity parameters.

RESULTS

Motion Comparison

All participants met the motion threshold (0.5 mm) as set for the study. That is, for all participants, the mean frame-wise displacement was less than 5 mm. A group level unpaired *t*-test revealed that groups did not differ in mean frame-wise displacement ($p = 0.8120$). The average mean frame-wise displacement was 0.177 mm in the cocaine group and 0.185 mm in the control group.

Craving Results

For each participant, craving scores were obtained (Sussner et al., 2006) before the resting state scan. Results showed that cocaine users did not show significantly higher craving rating compared to controls [$t(35) = 1.02$, $p = 0.31$; 1.23 ($SD = 1.03$) vs. 1 ($SD = 0$)].

Dynamic Causal Modeling

Model optimization procedure gave slightly different model structures for the two groups. For the cocaine group, the effective connectivity from the VTA to medial frontal cortex and effective connectivity from the medial frontal cortex to hippocampus were removed. While for the control group, the effective connectivity from the NAc to medial frontal cortex and effective connectivity from medial frontal cortex to VTA were removed. The effective connectivity structures along with averaged connectivity parameters for the two groups are shown in **Figure 3**.

Group differences in effective connectivity parameters of the full model between the two groups are shown in **Figure 4**.

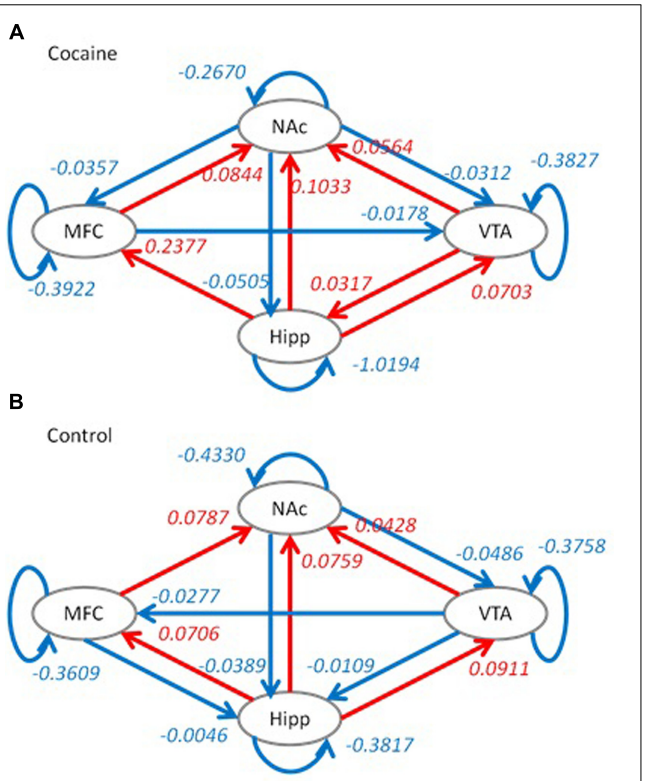

FIGURE 3 | Optimized dynamic causal models (DCMs) for the cocaine group (A) and the control group **(B)**. Red color indicates positive effective connectivity, while blue color indicates negative effective connectivity. Numbers represent averaged effective connectivity strengths using Bayesian parameter averaging. Hipp, hippocampus; MFC, medial frontal cortex; VTA, ventral tegmental area; NAc, nucleus accumbens.

Compared to the control group, the cocaine group had higher effective connectivity for seven connections (red arrows), and reduced effective connectivity for three connections (blue arrows). The cocaine group showed higher effective connectivity from the VTA to NAc, hippocampus and medial frontal cortex. In addition, the effective connectivity from the hippocampus to NAc, the reciprocal effective connectivity between the hippocampus and medial frontal cortex, and the self-effective connectivity of the NAc also showed a greater effective connectivity in the cocaine group compared to the control group. In contrast, the control group showed a higher effective connectivity from the medial frontal cortex to VTA, from the NAc to medial frontal cortex, and on the hippocampus self-loop.

DISCUSSION

The objective of this fMRI study was to compare effective connectivity among four key brain regions within the mesocorticolimbic dopamine system in chronic cocaine users to healthy controls during resting-state, when there are no demands being placed, such as cognitive tasks or viewing drug cues. This provided us a measure of baseline effective

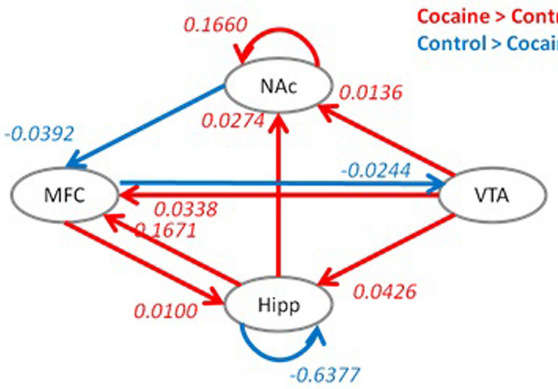

FIGURE 4 | Group differences in effective connectivity parameters between the cocaine and control groups. Red indicates a greater effective connectivity in the cocaine group compared to the control group, and blue indicates a reduced effective connectivity in the cocaine group compared to the control group. Significant group differences were identified after false discovery rate (FDR) correction at $p < 0.05$. Hipp, hippocampus; MFC, medial frontal cortex; VTA, ventral tegmental area; NAc, nucleus accumbens.

connectivity within the mesocorticolimbic dopamine system in chronic users of cocaine which is not available by measuring effective connectivity while the cocaine users perform a task. To examine effective connectivity, we employed one of the recently developed DCM models which utilizes the frequency spectrum domain (spDCM; Friston et al., 2014).

According to Jasinska et al. (2014), drugs of abuse enhance extracellular dopamine concentration in components of the mesocorticolimbic system, including the NAc, extended amygdala, hippocampus, anterior cingulate, prefrontal cortex, and insula, which are triggered by dopaminergic projections essentially from the VTA (Jasinska et al., 2014). Since VTA sends projections to multiple areas within the mesocorticolimbic system, we decided that these connections would provide a good way to compare cocaine users with controls during resting-state. Our results provided a mixed support of our hypothesis. More specifically, group differences in effective connectivity pattern revealed that the control group compared to the cocaine group showed a higher effective connectivity from the medial frontal cortex to VTA, from the NAc to medial frontal cortex, and on the hippocampus self-loop, consistent with our hypothesis. However, contrary to our hypothesis, the cocaine group compared to the control group showed a greater effective connectivity from the VTA to all three other areas within the mesocorticolimbic dopamine system, that is, NAc, hippocampus and medial frontal cortex (**Figure 4**). Perhaps neuroplasticity within the mesocorticolimbic dopamine reward system as a result of chronic cocaine use may account for these differences in effective connectivity patterns between cocaine users and controls. We speculate that the higher effective connectivity from the medial frontal cortex to VTA and from the NAc to medial frontal cortex represent better cortical and subcortical communications in controls compared to cocaine users. More specifically, higher effective connectivity from the medial frontal cortex to VTA demonstrates control participants' higher cortical cognitive control on subcortical region (VTA; Ridderinkhof et al., 2004) that may have implications for reducing drug seeking behavior.

We further speculate that may be the effective connectivity alterations throughout the mesocorticolimbic reward system revealed during resting-state in chronic users of cocaine play a role in maintaining problematic drug use. An enhanced causal influence of VTA on NAc, hippocampus and medial frontal cortex in cocaine users compared to control is consistent with Jasinska et al. (2014), who suggested that drugs of abuse increase dopaminergic projections predominantly from the VTA to other areas within the mesocorticolimbic system.

The present study extends upon the previous research including research by Gu et al. (2010) by establishing for the first time that during resting-state in abstaining cocaine users, the VTA created an enhanced effective connectivity to NAc, hippocampus and medial frontal cortex in cocaine users compared to controls within the brain's reward system. The present findings are, however, contrary to Gu et al. (2010) who showed a reduced functional connectivity between regions within the mesocorticolimbic system, including between VTA and ventral striatum, between amygdala and mPFC, and between hippocampus and dorsal mPFC during resting-state in cocaine users compared to controls. Yet the majority of participants in Gu et al.'s (2010) study did not abstain from cocaine during the resting-state scan, so their findings may reflect, in part, the acute effects of cocaine, which change resting-state functional connectivity.

Resting-state functional connectivity has been linked to self-monitoring and introspective processes (Eryilmaz et al., 2011). We speculate that, during the resting-state scan, a greater effective connectivity from the VTA to hippocampus within the mesocorticolimbic dopamine system in cocaine users compared to controls may reflect persistent thoughts of the cocaine users' long-term memory of drug use (Tiffany, 1990; Spaniol et al., 2009; Jasinska et al., 2014), consistent with the activation of hippocampus by VTA. We also speculate that an enhanced effective connectivity from the VTA to medial frontal cortex in cocaine users compared to controls may reflect activation of decision making and motivated behavior related to continued drug use (Balleine et al., 2007; Jasinska et al., 2014). In future studies, participants might be interviewed post-scan to understand the content of their thoughts while they were inside the scanner. As potential system-level biomarkers of chronic cocaine use, the alterations within the mesocorticolimbic dopamine system may be usefully applied in treatment development and monitoring treatment outcome. It would be particularly useful to examine whether therapeutic interventions change the enhanced effective connectivities that were found in cocaine users within this system which may imply a positive treatment outcome.

Next, we would like to mention a couple of limitations of this study. First, although we matched the cocaine smoking and control groups based on their age, educational and ethnic/racial background, controls drank significantly more alcohol than the cocaine-using group (**Table 1**). However, importantly, alcohol

use was still very low for both groups (<1 drink/day), therefore, was unlikely to affect our findings. This does, however, restrict our conclusions to a 'pure' cocaine-using group and may not be generalizable to cocaine users who abuse alcohol as well. Second, we acknowledge that we had a small sample size. There were only five female cocaine smokers in our study, thus, we could not investigate any potential sex differences in our resting-state study outcome. Third, due to limitation of the BPA approach that does not allow us to put alcohol and nicotine usage as covariates in group level analysis, we could not use alcohol use frequency and nicotine use quantity as covariates. However, alcohol usage frequency was actually significantly lower in the cocaine group than the control group, and conversely nicotine use quantity was higher in the cocaine group than the control group (non-significant). Despite these limitations, the results of the present study provide a model of effective connectivity among four regions within the mesocorticolimbic dopamine system during resting-state in individuals who are chronic users of cocaine. An important issue in interpreting results of a cross-sectional study, such as ours, is whether differences between groups are a consequence of chronic drug use or alternatively, reflect pre-existing differences that predispose some individuals to addiction. This can be investigated in future studies that will utilize a longitudinal design.

To conclude, the present study is the first to show that during resting-state in abstaining cocaine users compared to controls, the VTA initiates an enhanced effective connectivity to NAc, hippocampus and medial frontal cortex areas within the mesocorticolimbic dopamine system, the brain's reward system. Future studies of effective connectivity analysis during resting-state may eventually be used to monitor treatment outcome.

AUTHOR CONTRIBUTIONS

SR, designed and ran the study, and wrote the manuscript. XD, conducted the analysis, and wrote part of the results section. BB helped with the design, addressed reviewers' concerns, and edited the manuscript.

FUNDING

This research was supported by National Institute on Drug Abuse grants K01DA029047 and R01DA038895.

ACKNOWLEDGMENTS

We are grateful to Ashley Aya, Alexis Budhi, JesseGabriel Tecson, and Brian Foster for assistance with subject recruitment, data collection, and data coding.

REFERENCES

Balleine, B. W., Delgado, M. R., and Hikosaka, O. (2007). The role of the dorsal striatum in reward and decision-making. *J. Neurosci.* 27, 8161–8165. doi: 10.1523/JNEUROSCI.1554-07.2007

Cisler, J. M., Elton, A., Kennedy, A. P., Young, J., Smitherman, S., Andrew James, G., et al. (2013). Altered functional connectivity of the insular cortex across prefrontal networks in cocaine addiction. *Psychiatry Res.* 213, 39–45. doi: 10.1016/j.pscychresns.2013.02.007

Cloninger, R., and Reich, T. (1991). *Family History Assessment Module. Based on HELPER Family Data Interview*. St. Louis, MO: Washington University School of Medicine.

Daunizeau, J., Stephan, K. E., and Friston, K. J. (2012). Stochastic dynamic causal modelling of fMRI data: should we care about neural noise? *Neuroimage* 62:464481. doi: 10.1016/j.neuroimage.2012.04.061

Di, X., and Biswal, B. B. (2014). Identifying the default mode network structure using dynamic causal modeling on resting-state functional magnetic resonance imaging. *Neuroimage* 86, 53–59. doi: 10.1016/j.neuroimage.2013.07.071

Eryilmaz, H., Van De Ville, D., Schwartz, S., and Vuilleumier, P. (2011). Impact of transient emotions on functional connectivity during subsequent resting state: A wavelet correlation approach. *Neuroimage* 54, 2481–2491. doi: 10.1016/j.neuroimage.2010.10.021

Everitt, B. J., and Robbins, T. W. (2005). Neural systems of reinforcement for drug addiction: from actions to habits to compulsion. *Nat. Neurosci.* 8, 1481–1489. doi: 10.1038/nn1579

First, M. B., Spitzer, R. L., Gibbon, M., and Williams, J. B. W. (1997). *Structured Clinical Interview for DSM-IV Axis I Disorders-Patient Edition (SCID-I/P, Version 2.0,* 4/97 revision). New York, NY: New York State Psychiatric Institute.

Fox, M. D., and Raichle, M. E. (2007). Spontaneous fluctuations in brain activity observed with functional magnetic resonance imaging. *Nat. Rev. Neurosci.* 8, 700–711. doi: 10.1038/nrn2201

Friston, K., and Penny, W. (2011). Post hoc Bayesian model selection. *Neuroimage* 56, 2089–2099. doi: 10.1016/j.neuroimage.2011.03.062

Friston, K. J., Harrison, L., and Penny, W. (2003). Dynamic causal modelling. *Neuroimage* 19, 1273–1302. doi: 10.1016/S1053-8119(03)00202-7

Friston, K. J., Kahan, J., Biswal, B., and Razi, A. (2014). A DCM for resting state fMRI. *Neuroimage* 94, 396–407. doi: 10.1016/j.neuroimage.2013.12.009

Friston, K. J., Williams, S., Howard, R., Frackowiak, R. S., and Turner, R. (1996). Movement-related effects in fMRI time-series. *Magn. Reson. Med.* 35, 346–355. doi: 10.1002/mrm.1910350312

Gu, H., Salmeron, J. B., Ross, J. T., Geng, X., Zhan, W., Stein, E. A., et al. (2010). Mesocorticolimbic circuits are impaired in chronic cocaine users as demonstrated by resting-state functional connectivity. *Neuroimage* 53, 593–601. doi: 10.1016/j.neuroimage.2010.06.066

Hanlon, C. A., Wesley, M. J., Stapleton, J. R., Laurienti, P. J., and Porrino, L. J. (2011). The association between frontal-striatal connectivity and sensorimotor control in cocaine users. *Drug Alcohol Depend.* 115, 240–243. doi: 10.1016/j.drugalcdep.2010.11.008

Jasinska, A. J., Stein, E. A., Kaiser, J., Naumer, M. J., and Yalachkov, Y. (2014). Factors modulating neural reactivity to drug cues in addiction: a survey of human neuroimaging studies. *Neurosci. Biobehav. Rev.* 38, 1–16. doi: 10.1016/j.neubiorev.2013.10.013

Jay, T. M. (2003). Dopamine: a potential substrate for synaptic plasticity and memory mechanisms. *Prog. Neurobiol.* 69, 375–390. doi: 10.1016/S0301-0082(03)00085-6

Kalivas, P. W., and O'Brien, C. (2008). Drug addiction as a pathology of staged neuroplasticity. *Neuropsychopharmacology* 33, 166–180. doi: 10.1038/sj.npp.1301564

Kelley, A. E. (2004). Memory and addiction: shared neural circuitry and molecular mechanisms. *Neuron* 44, 161–179. doi: 10.1016/j.neuron.2004.09.016

Liu, X., Zhu, X., and Chen, W. (2011). Baseline BOLD correlation predicts individuals' stimulus-evoked BOLD responses. *Neuroimage* 54, 2278–2286. doi: 10.1016/j.neuroimage.2010.10.001

Ma, L., Steinberg, J. L., Cunningham, K., Lane, S., Bjork, J., Neelakantan, H., et al. (2015). Inhibitory behavioral control: a stochastic dynamic causal modeling study comparing cocaine dependent subjects and controls. *Neuroimage* 7, 837–847. doi: 10.1016/j.nicl.2015.03.015

Ma, L., Steinberg, J. L., Hasan, K. M., Narayana, P. A., Kramer, L. A., and Moeller, F. G. (2014). Stochastic dynamic causal modeling of working memory connections in cocaine dependence. *Hum. Brain Mapp.* 35, 760–778. doi: 10.1002/hbm.22212

Nestler, E. J. (2005). Is there a common molecular pathway for addiction? *Nat. Neurosci.* 8, 1445–1449. doi: 10.1038/nn1578

Ramsey, J. D., Hanson, S. J., Hanson, C., Halchenko, Y. O., Poldrack, R. A., and Glymour, C. (2010). Six problems for causal inference from fMRI. *Neuroimage* 49, 1545–1558. doi: 10.1016/j.neuroimage.2009.08.065

Ray, S., Gohel, S., and Biswal, B. B. (2015a). Altered functional connectivity strength in abstinent chronic cocaine smokers compared to healthy controls. *Brain Connect.* 5, 476–486. doi: 10.1089/brain.2014.0240

Ray, S., Haney, M., Hanson, C., Biswal, B., and Hanson, S. J. (2015b). Modeling causal relationship between brain regions within the drug-cue processing network in chronic cocaine smokers. *Neuropsychopharmacology* 40, 2960–2968. doi: 10.1038/npp.2015.150

Razi, A., Kahan, J., Rees, G., and Friston, K. J. (2015). Construct validation of a DCM for resting state fMRI. *Neuroimage* 106, 1–14. doi: 10.1016/j.neuroimage.2014.11.027

Ridderinkhof, K. R., Ullsperger, M., Crone, E. A., and Nieuwenhuis, S. (2004). The role of the medial frontal cortex in cognitive control. *Science* 306, 443–447. doi: 10.1126/science.1100301

Robinson, T. E., and Berridge, K. C. (1993). The neural basis of drug craving: an incentive sensitization theory of addiction. *Brain Res. Rev.* 18, 247–291. doi: 10.1016/0165-0173(93)90013-P

Spaniol, J., Davidson, P. S., Kim, A. S., Han, H., Moscovitch, M., and Grady, C. L. (2009). Event-related fMRI studies of episodic encoding and retrieval: meta-analyses using activation likelihood estimation. *Neuropsychologia* 47, 1765–1779. doi: 10.1016/j.neuropsychologia.2009.02.028

Sussner, B. D., Smelson, D. A., Rodrigues, S., Kline, A., Losonczy, M., and Ziedonis, D. (2006). The validity and reliability of a brief measure of cocaine craving. *Drug Alcohol Depend.* 83, 233–237. doi: 10.1016/j.drugalcdep.2005.11.022

Tiffany, S. T. (1990). A cognitive model of drug urges and drug-use behavior: role of automatic and nonautomatic processes. *Psychol. Rev.* 97, 147–168. doi: 10.1037/0033-295X.97.2.147

Tomasi, D., Volkow, N. D., Wang, R., Carrillo, H. J., Maloney, T., Alia-Klien, N., et al. (2010). Disrupted functional connectivity with dopaminergic midbrain in cocaine abusers. *PLoS ONE* 5:e10815. doi: 10.1371/journal.pone.0010815

Volkow, N. D., Wang, G. J., Telang, F., Fowler, J. S., Logan, J., Childress, A. R., et al. (2006). Cocaine cues and dopamine in dorsal striatum: mechanism of craving in cocaine addiction. *J. Neurosci.* 26, 6583–6588. doi: 10.1523/JNEUROSCI.1544-06.2006

Volkow, N. D., Wang, G. J., Telang, F., Fowler, J. S., Logan, J., Childress, A. R., et al. (2008). Dopamine increases in striatum do not elicit craving in cocaine abusers unless they are coupled with cocaine cues. *Neuroimage* 39, 1266–1273. doi: 10.1016/j.neuroimage.2007.09.059

Wilcox, C. E., Teshiba, T. M., Merideth, F., Ling, J., and Mayer, A. R. (2011). Enhanced cue reactivity and fronto-striatal functional connectivity in cocaine use disorders. *Drug Alcohol Depend.* 115, 137–144. doi: 10.1016/j.drugalcdep.2011.01.009

Conflict of Interest Statement: The authors declare that the research was conducted in the absence of any commercial or financial relationships that could be construed as a potential conflict of interest.

frontiers in Human Neuroscience

HYPOTHESIS AND THEORY
published: 15 November 2016
doi: 10.3389/fnhum.2016.00550

Allostatic Self-efficacy: A Metacognitive Theory of Dyshomeostasis-Induced Fatigue and Depression

Klaas E. Stephan[1, 2, 3], Zina M. Manjaly[1, 4], Christoph D. Mathys[2], Lilian A. E. Weber[1], Saee Paliwal[1], Tim Gard[1, 5], Marc Tittgemeyer[3], Stephen M. Fleming[2], Helene Haker[1], Anil K. Seth[6] and Frederike H. Petzschner[1]*

[1] Translational Neuromodeling Unit, Institute for Biomedical Engineering, University of Zurich and ETH Zurich, Zurich, Switzerland, [2] Wellcome Trust Centre for Neuroimaging, University College London, London, UK, [3] Max Planck Institute for Metabolism Research, Cologne, Germany, [4] Department of Neurology, Schulthess Clinic, Zurich, Switzerland, [5] Center for Complementary and Integrative Medicine, University Hospital Zurich, Zurich, Switzerland, [6] Sackler Centre for Consciousness Science, School of Engineering and Informatics, University of Sussex, Brighton, UK

OPEN ACCESS

Edited by:
Adeel Razi,
Wellcome Trust Centre for Neuroimaging - UCL, UK

Reviewed by:
Sören Krach,
University of Lübeck, Germany
Xiaosi Gu,
University of Texas at Dallas, USA

***Correspondence:**
Klaas E. Stephan
stephan@biomed.ee.ethz.ch

Received: *15 June 2016*
Accepted: *14 October 2016*
Published: *15 November 2016*

Citation:
Stephan KE, Manjaly ZM, Mathys CD, Weber LAE, Paliwal S, Gard T, Tittgemeyer M, Fleming SM, Haker H, Seth AK and Petzschner FH (2016) Allostatic Self-efficacy: A Metacognitive Theory of Dyshomeostasis-Induced Fatigue and Depression. Front. Hum. Neurosci. 10:550. doi: 10.3389/fnhum.2016.00550

This paper outlines a hierarchical Bayesian framework for interoception, homeostatic/allostatic control, and meta-cognition that connects fatigue and depression to the experience of chronic dyshomeostasis. Specifically, viewing interoception as the inversion of a generative model of viscerosensory inputs allows for a formal definition of dyshomeostasis (as chronically enhanced surprise about bodily signals, or, equivalently, low evidence for the brain's model of bodily states) and allostasis (as a change in prior beliefs or predictions which define setpoints for homeostatic reflex arcs). Critically, we propose that the performance of interoceptive-allostatic circuitry is monitored by a metacognitive layer that updates beliefs about the brain's capacity to successfully regulate bodily states (allostatic self-efficacy). In this framework, fatigue and depression can be understood as sequential responses to the interoceptive experience of dyshomeostasis and the ensuing metacognitive diagnosis of low allostatic self-efficacy. While fatigue might represent an early response with adaptive value (cf. sickness behavior), the experience of chronic dyshomeostasis may trigger a generalized belief of low self-efficacy and lack of control (cf. learned helplessness), resulting in depression. This perspective implies alternative pathophysiological mechanisms that are reflected by differential abnormalities in the effective connectivity of circuits for interoception and allostasis. We discuss suitably extended models of effective connectivity that could distinguish these connectivity patterns in individual patients and may help inform differential diagnosis of fatigue and depression in the future.

Keywords: computational psychiatry, effective connectivity, dynamic causal modeling, homeostasis, allostasis, predictive coding, active inference, multiple sclerosis

INTRODUCTION

Fatigue is a prominent symptom of major clinical significance, not only in chronic fatigue syndrome (CFS) *per se*, but across a wide range of immunological and endocrine disorders, cancer and neuropsychiatric diseases (for overviews, see Wessely, 2001; Chaudhuri and Behan, 2004; Dantzer et al., 2014). For example, it is the most frequent (Stuke et al., 2009) symptom in Multiple Sclerosis (MS), with major impact on quality of life. It is strongly associated with depression (Wessely et al., 1996; Bakshi et al., 2000; Kroencke et al., 2000; Pittion-Vouyovitch et al., 2006), and longitudinal studies have demonstrated that fatigue represents a risk factor for depression (and vice versa; Skapinakis et al., 2004). Additionally, fatigue represents a core criterion for the diagnosis of major depression in standard psychiatric classification schemes (ICD-10 and DSM-5).

The clinical concept of fatigue is a heterogeneous construct, comprising at least two dimensions (Kluger et al., 2013): fatiguability of cognitive and motor processes, and subjective perception of fatigue. While the former can be measured objectively, the latter requires self-report via questionnaires. Given its clinical importance, it has been remarkably difficult to develop a theory of fatigue that is comprehensive, specific and allows for developing objective clinical tests (Wessely, 2001). Research on its pathophysiology has largely focused on molecular processes, particularly in the context of inflammation (Dantzer et al., 2014; Patejdl et al., 2016), but efforts to link these molecular processes to the physiology and computation (information processing) of cerebral circuits are rare. This paper attempts to address this challenge and outlines the foundations of a theory of fatigue that is grounded in interoception (Craig, 2002) and homeostatic/allostatic control (Sterling, 2012), offering a formal (hierarchical Bayesian) perspective on (some of) the computations involved. In particular, we propose a metacognitive mechanism that explains the sequential occurrence of fatigue and depression, given a state of prolonged dyshomeostasis.

This paper has the following structure. First, we discuss why disease theories of fatigue confined to the molecular/cellular level are not sufficient for a comprehensive understanding of fatigue, but need to be complemented by a computational perspective. Second, as a basis for developing this perspective, we review long-standing notions from systems theory and control theory and their implications for interoception as well as homeostatic and allostatic control. Third, we apply a hierarchical Bayesian view to fatigue and cast it as a meta-cognitive phenomenon: a belief of failure at one's most fundamental task—homeostatic/allostatic regulation—which arises from experiencing enhanced interoceptive surprise. We suggest that fatigue is a (possibly adaptive) initial allostatic response to a state of interoceptive surprise; if dyshomeostasis continues, the belief of low allostatic self-efficacy and lack of control may pervade all domains of cognition and manifests as a generalized sense of helplessness, with depression as a consequence. Fourth, we derive specific predictions against which this theory can be tested and outline the necessary methodological extensions of contemporary models of effective connectivity, such as DCM. Finally, we consider how such extended generative models might become useful for differential diagnosis of fatigue in the future.

THE NEED FOR A COMPUTATIONAL THEORY OF FATIGUE

Existing pathophysiological theories of fatigue mainly refer to inflammatory and metabolic processes at the molecular level. For example, a longstanding observation is that pro-inflammatory cytokines, resulting from peripheral (extra-cerebral) immunological processes, induce "sickness behavior" (Dantzer and Kelley, 2007) with fatigue as a key symptom. This may result from a range of different mechanisms, including reduced synthesis of monoaminergic transmitters or inflammation-induced shifts in the production of metabolites such as kynurenines, which impact on transmission at glutamatergic synapses (for a comprehensive recent review, see Dantzer et al., 2014).

While these hypotheses have been very influential and useful in suggesting potential future treatment avenues, they do not, on their own, allow for constructing a comprehensive theory of fatigue. First, as for any neuropsychiatric symptom, we eventually need a theory that unifies and links disease processes across molecular, cellular and circuit (systems) levels of description. This is important because a theory of fatigue that is confined to the molecular level does not explain how clinical symptoms arise; by contrast, a circuit-level description is the closest we can presently get to behavior and subjective experience. Moreover, neuropsychiatric disease processes can not only originate from the molecular level and spread "bottom-up," causing cellular and circuit-level disturbances; in addition, the reverse (top-down) direction and the ubiquitous existence of reciprocal brain-body interactions are well-established (Sapolsky, 2015). For example, seemingly maladaptive behavior can materialize as the (optimal) consequence of beliefs that form under exposure to specific environmental input statistics (Schwartenbeck et al., 2015b). That is, in the absence of any primary molecular or synaptic pathology, exposure to unusual environmental events can induce distorted beliefs about the causal structure of the world, e.g., that it is inherently unpredictable or uncontrollable (cf. learned helplessness; Abramson et al., 1978). Such beliefs engender misdirected coping behavior and have profound physiological consequences, including a dysregulation of cerebral control over endocrine and autonomic nervous system processes (e.g., aberrant activation of the hypothalamic-pituitary axis; HPA; Tsigos and Chrousos, 2002). Importantly, the ensuing immunological and metabolic disturbances in the body exert strong feedback effects on cerebral circuits. For example, stress-related increases in levels of cortisol and pro-inflammatory cytokines affect NMDA receptor (NMDAR) function (Nair and Bonneau, 2006; Gruol, 2015; Vezzani and Viviani, 2015). Importantly, NMDAR dependent signaling is thought to be essential for updating and encoding representations of beliefs (Corlett et al., 2010; Vinckier et al., 2016). This suggests

that peripheral inflammatory or endocrine disturbances could impede the adjustment of aberrant beliefs by which they were caused in the first place (i.e., a positive feedback loop). In brief, the existence of closed-loop interactions between cognitive and bodily processes implies that we require a wider theory of fatigue than one focusing on molecular events alone.

There is a second, more practical, reason why a purely molecular/cellular theory of fatigue cannot provide a clinically sufficient account of fatigue: molecular disease processes in brain tissue are not easily accessible for non-invasive diagnostics in humans. The relative separation of the brain from the body by the blood-brain barrier means that we only have indirect access to brain tissue, such as biochemical analyses of cerebrospinal fluid (CSF), and there are very few diagnostic questions (e.g., in neuro-oncology or epilepsy) where the risks of brain tissue biopsies or invasive recordings are justified by diagnostic benefits. However, provided we have a concrete model that specifies how a disease process at the molecular/cellular level leads to measurable changes in the activity of specific brain circuits, one can, in principle, infer the expression of this process from non-invasive neuroimaging and electrophysiological measurements, such as functional magnetic resonance imaging (fMRI) or magneto-/electroencephalography (M/EEG). Technically, this involves a so-called "generative model" m which specifies how the hidden (unobservable) state x of a neuronal circuit translates probabilistically into a measurement obtained y with fMRI or M/EEG, and which can be used to infer hidden states from measurements (**Figure 1**). Using a generative model of brain activity or behavioral measurements to address diagnostic questions amounts to a "computational assay" (Stephan and Mathys, 2014; Stephan et al., 2015). The application of generative models to clinical questions is presently beginning to take place across the whole range of neuropsychiatry, including applications to schizophrenia (Schlagenhauf et al., 2014), depression (Hyett et al., 2015), bipolar disorder (Breakspear et al., 2015), Parkinson's disease (Herz et al., 2014), channelopathies (Gilbert et al., 2016), or epilepsy (Cooray et al., 2015). One particular approach we return to below is the generative modeling of neurophysiological circuits. For example, dynamic causal models (DCMs; for reviews see Daunizeau et al., 2011; Friston et al., 2013) allow one to infer directed synaptic connections (effective connectivity) from neuroimaging or electrophysiological data.

Generative modeling is an attractive approach for establishing differential diagnostic procedures. However, given the myriad of possible disease processes, guidance by clinical theories is crucial for the development of computational assays. The framework outlined in this paper is meant to inform the development generative models that infer mechanisms of fatigue and depression from fMRI and MEG/EEG data. The predictions by this framework suggest that differential diagnosis could be decisively facilitated by model-based estimates of directed synaptic connectivity (effective connectivity) within interoceptive circuits and their interactions with regions potentially involved in meta-cognition.

TELEOLOGICAL BRAIN THEORIES AS FUNDAMENT FOR UNDERSTANDING FATIGUE

The diverse behavioral, cognitive and emotional facets of fatigue, its occurrence in numerous syndromatically defined diseases, and the multitude of findings from immunology, neurophysiology and psychology offer a large number of degrees of freedom for "bottom-up" explanations of this complex symptom (Dantzer et al., 2014; Patejdl et al., 2016). Given this complexity, investigating fatigue requires guidance by formal theories which provide top-down constraints on organizing and interpreting the diversity of experimental findings. These top-down constraints could be derived, for example, from theories about the purpose, structure and biophysical implementation of the brain's computations[1]. This strategy is at the heart of an emerging discipline, "Computational Psychiatry" (Montague et al., 2012; Stephan and Mathys, 2014; Friston et al., 2014b; Huys et al., 2016), and has shown promise in tackling other complex neuropsychiatric symptoms, such as delusions (Corlett et al., 2010).

Although its historical roots have rarely been discussed so far, Computational Psychiatry builds on seminal teleological theories of biological (and other) systems that provide fundamental constraints for any attempt of understanding brain function. These include, for example, general systems theory (Von Bertalanffy, 1969), cybernetics and control theory (Wiener, 1948; Ashby, 1954, 1956; Conant and Ashby, 1970; Powers, 1973; Carver and Scheier, 1982; von Foerster, 2003; Seth, 2015a,b,c) and constructivism (Richards and von Glasersfeld, 1979). Some core ideas from these general theories of inference and control in biological systems have laid the foundation for recent concepts of perception and action in computational neuroscience (e.g., Mumford, 1992; Dayan et al., 1995; Rao and Ballard, 1999; Friston, 2005, 2010; Friston et al., 2006; Doya et al., 2011). For example, the central notion of radical constructivism that the brain actively "constructs" a subjective reality from noisy and ambiguous sensory inputs (Richards and von Glasersfeld, 1979; von Foerster, 2003)—as opposed to the brain representing an objective outer reality that is reflected by sensory inputs—are expressed formally, using the language of probability theory, in hierarchical Bayesian models we encounter below. Other central ideas—such as the notion that cognitive systems are self-referential and monitor themselves (von Foerster, 2003) are yet to be exploited fully, e.g., for models of metacognition.

This paper represents a first attempt to use some of these principles for articulating a novel theory of fatigue and how it may transition to depression. In brief, our account views fatigue and depression as metacognitive phenomena: a set of beliefs held by the brain about its own functional capacity—specifically, a perceived lack of control over bodily states. This

[1]In the well-known framework by Marr (1982), these levels are referred to as the "computational," "algorithmic," and "implementational" levels of analysis, respectively. Considering the original definition of "computation" in theoretical computer science, these designations are partially confusing, and in the following we will therefore refer to the first level as the "teleological" (purpose) level of description.

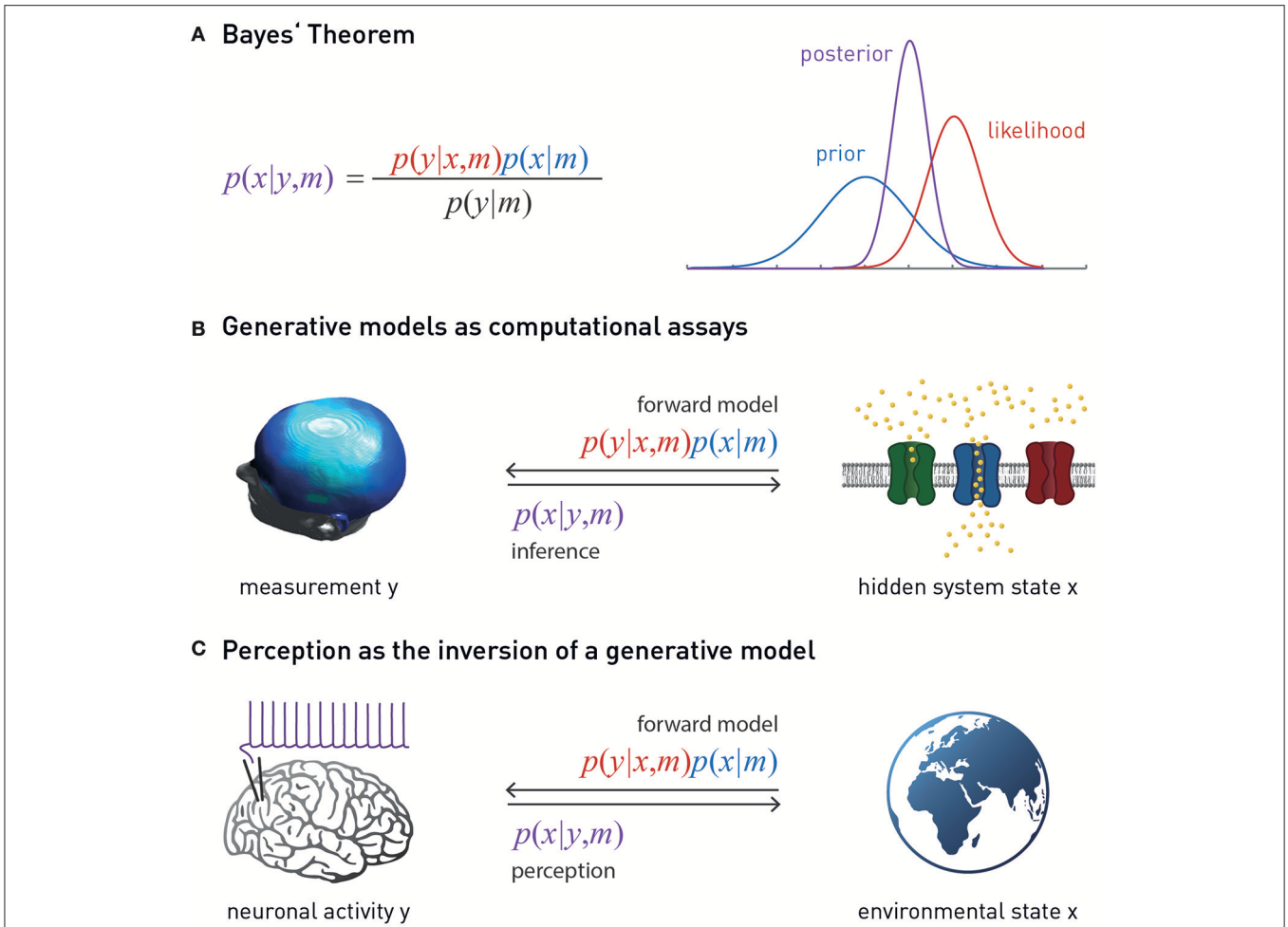

FIGURE 1 | (A) Bayes theorem provides the foundation for a generative model m. This combines the likelihood function $p(y|x,m)$ (a probabilistic mapping from hidden states of the world, x, to sensory inputs y) with the prior $p(x|m)$ (an *a priori* probability distribution of the world's states). Model inversion corresponds to computing the posterior $p(x|y,m)$, i.e., the probability of the hidden states, given the observed data y. The posterior is a "compromise" between likelihood and prior, weighted by their relative precisions. The model evidence $p(y|m)$ in the denominator of Bayes' theorem is a normalization constant that forms the basis for Bayesian model comparison—see main text. **(B)** Suitably specified and validated generative models with mechanistic (e.g., physiological or algorithmic) interpretability could be used as a computational assay for diagnostic purposes. The left graphics is reproduced, with permission, from Garrido et al. (2008). **(C)** Contemporary models of perception (the "Bayesian brain hypothesis") assume that the brain instantiates a generative model of its sensory inputs. Perception corresponds to inverting this model, yielding posterior beliefs about the causes of sensory inputs. The globe picture is freely available from http://www.vectortemplates.com/raster-globes.php.

belief arises when attempts of homeostatic regulation fail to reduce the experience of chronic dyshomeostasis: enduring deviations between expected and sensed bodily states. These persistent deviations or prediction errors signal interoceptive surprise or, equivalently, low evidence of the brain's model of bodily processes. Before we can turn to this notion in more detail, we review some ideas on the role of perception (inference) and prediction (action selection) for homeostasis which originate from the longstanding literature mentioned above and have resurfaced in more recent work in computational neuroscience.

The Brain As an Organ for Homeostatic Control

The brain is literally "embodied": its structural and functional integrity depends on mechanical support, energy supply, and the provision of a suitable biochemical milieu provided by the body. As a corollary, the selectionist pressures which act upon the brain during evolution cannot be uncoupled from those acting upon the body's *milieu intérieur* (Claude Bernard); i.e., control of bodily homeostasis must constitute a primary purpose of brain function (Cannon, 1929). This control has long been known to involve reflex-like actions (comprising motor, endocrine, immunological, and autonomic processes) that are driven by feedback and the resulting "prediction error"—the discrepancy between an expected bodily state (a homeostatic setpoint[2]) and its actual level as signaled by sensory inputs from the body (Modell et al., 2015); see **Figure 4**. Feedback- or

[2]Below, we will define homeostatic setpoints as the expectations (means) of prior beliefs about the states the body should inhabit, and homeostatic range as the variance of these prior beliefs.

error-based reactive control has been studied for many vitally important variables (such as blood acidity, body temperature, blood levels of glucose and calcium, plasma osmolality) (Woods and Wilson, 2013), and the anatomy and physiology of neuronal circuits involved have been mapped out in detail by physiologists over many decades.

While this reactive type of control dominates the classical literature on homeostasis, it likely only represents the lowest layer in a hierarchy of temporally extended control mechanisms, with most immediate consequences. By contrast, assuming that the brain maintains a model of bodily states and the external environment, higher levels enable prospective control, with two essential components: *inference* (on current bodily state) and *prediction* (of its future evolution, on its own and in response to chosen actions) (Sterling, 2012; Penny and Stephan, 2014; Pezzulo et al., 2015; Seth, 2015a). There are several reasons why homeostatic regulation requires a model that enables inference (perception) and prediction (action selection). First, control is "blind" without perceptual inference: the brain does not have direct access to either bodily or environmental states, but has to infer them from sensory inputs which are inherently noisy and ambiguous. Disentangling the many external states that could underlie any given sensory input is an ill-posed inverse problem that requires constraints or regularization (e.g., by the priors of a generative model; Lee and Mumford, 2003; Kersten et al., 2004). Second, numerous experimental observations indicate that the brain engages in regulatory responses *prior* to a homeostatic perturbation, provided it can be anticipated (Sterling, 2012). In other words, a predicted deviation from a homeostatic setpoint is avoided by choosing suitable actions in advance. Importantly, setpoints are hierarchically structured, and changes in hierarchically lower setpoints may be necessary to prevent departure of bodily state from higher setpoints (Powers, 1973). For example, a temporary change in (lower) setpoints for blood pressure and catecholamine levels may be elicited to engage in fight-flight behavior that is necessary to ensure bodily integrity (higher setpoint). As we will see below, this longstanding notion of hierarchically structured homeostatic setpoints fits nicely to hierarchical Bayesian architectures, where the prior belief at one level is constrained by the prior belief at the next higher level.

This anticipatory control or *allostasis* ("stability through change"; Sterling, 2014) necessarily requires a model capable of generating predictions. The notion of model-based allostatic regulation is a special case of the more general and long-standing view that the brain requires a model of the external world in order to implement optimal control. Specifically, seminal work by Conant and Ashby (1970) has resulted in an influential theorem "[...] which shows, under very broad conditions, that any regulator that is maximally both successful and simple must be isomorphic with the system being regulated. [...] The theorem has the interesting corollary that the living brain, so far as it is to be successful and efficient as a regulator for survival, must proceed, in learning, by the formation of a model (or models) of its environment."

This notion of anticipatory homeostatic control (allostatic control) has important ramifications. Significant perturbations of bodily states arise from the physical and social environments through which the brain navigates the body. For example, basic properties of the physical environment (e.g., ambient temperature, weather, physical activity required by geographical conditions, availability of food and water) have delayed but severe effects on key homeostatic variables (such as body temperature, blood glucose levels, plasma osmolality); these must be predicted in advance and incorporated into the selection of actions in order to avoid fatal effects (for some simple simulations, see Penny and Stephan, 2014). Similarly, in the social domain, learning about the (potentially hostile) intentions of other agents in a reactive way, by trial and error, is risky. Instead, a model or "theory of mind" of other agents' mental states (Frith and Frith, 2012), perhaps grounded in the prolonged interaction with early-life caregivers, is required to predict and avoid interactions with potentially deleterious consequences for social status, access to resources, and ultimately bodily integrity. This means that anticipatory control of bodily states would be drastically incomplete if the brain did not possess a model which enabled inference on current states of the physical and social environment and predicted their trajectories into the future. In brief, principles of anticipatory homeostatic control and the necessity of model-based prediction must generalize beyond the body and apply to physical and social domains of the external world. In the following, the term "external world" is used to refer to both the body and the physical and social world outside the body; this is for notational brevity only and not meant to disregard differences in how bodily, social and physical states can influence brain activity in general and the emergence of fatigue in particular; a topic we return to below.

Generative Models

The notion that the brain maintains and continuously updates a model of its external world for perceptual inference and anticipatory control has been around for a considerable period (Conant and Ashby, 1970). What could such a model look like? Across various proposals, two main design features re-occur and are supported by strong theoretical and empirical arguments. That is, (i) the brain's model is likely to follow principles of probability theory and hence represent a "generative" model; and (ii) structurally, it is plausible to assume that this has a hierarchical structure.

A so-called "generative model" directly follows from the basic laws of probability theory and essentially implements Bayes' theorem—a simple but fundamental statement about how uncertain sources of information (represented by conditional probabilities) can be combined (**Figure 1**). In the context of perception, a generative model m combines a "likelihood function" $p(y \mid x, m)$ (a probabilistic mapping from hidden states of the world, x, to sensory inputs y), with a "prior" $p(x \mid m)$ (an *a priori* probability distribution of the world's states) (**Figure 1**). The likelihood describes how any given state of the world causes a sensory input with a certain probability; the prior expresses the range of values environmental states inhabit *a priori* and thus encodes learned environmental statistics. One way to understand why this model is called "generative" is to note that it can be used to generate or simulate sensory inputs (data): this simply requires that one samples a value from the prior distribution and plugs it into the likelihood function. This process can be turned

around: that is, given some observed data (experienced sensory inputs), Bayes' theorem allows one to compute the probability of the hidden states (the "posterior" $p\left(x \mid y, m\right)$)—this is inference:

$$p\left(x \mid y, m\right) = \frac{p\left(y \mid x, m\right) p\left(x \mid m\right)}{p\left(y \mid m\right)} \quad (1)$$

As inference corresponds to inverting the process of data generation (from hidden states to sensory inputs), it is also referred to as "inversion" of the generative model, or solving the "inverse problem." Finally, an important component of a generative model is the model evidence $p\left(y \mid m\right)$ (the denominator from Bayes' theorem). The evidence represents a principled measure of the goodness of a generative model which trades-off accuracy and complexity (Stephan et al., 2009; Penny, 2012); notably, its logarithm relates to the information-theoretic concept of (Shannon) surprise, S (sometimes also referred to as surprisal or self-information to distinguish it from psychological notions of surprise). Specifically, the log evidence is identical to negative surprise about seeing the data under model m:

$$\log p\left(y \mid m\right) = -S\left(y \mid m\right) \quad (2)$$

In other words, a good model is one that minimizes the surprise about encountering the data. Conversely, persistent surprise is the hallmark of a bad model.

Generative models can be expressed in a hierarchical form, where each level provides a prediction (prior) for the state of the level below; this prediction can be compared against the actual state (likelihood), resulting in a prediction error which can be signaled upwards for updating the prior (**Figures 2**, **3**). This is an extremely general concept which not only underlies common models in statistics (Kass and Steffey, 1989), but provides a key metaphor for models of brain function (e.g., Rao and Ballard, 1999; Lee and Mumford, 2003; Friston, 2005, 2008; Petzschner et al., 2015), such as predictive coding described below.

The "Bayesian Brain"

The hierarchical form of generative models fits remarkably well to structural principles of cortical organization, where the sensory processing streams consist of hierarchically related cortical areas. This hierarchy is defined anatomically in terms of different cytoarchitectonic properties and types of synaptic connections (bottom-up/ascending/forward connections vs. top-down/descending/backward connections) (Felleman and Van Essen, 1991; Hilgetag et al., 2000). These connections are thought to have different functional properties which are compatible with hierarchical Bayesian inference. For example, in the visual system, anatomical and physiological studies suggest that descending connections convey predictions about activity in lower areas (e.g., Alink et al., 2010; Nassi et al., 2013; Vetter et al., 2015) and have largely inhibitory effects (e.g., Angelucci and Bressloff, 2006; Andolina et al., 2013), as required for "explaining away" in predictive coding (see the discussion in Nassi et al., 2013). Furthermore, pharmacological and computational studies of the auditory mismatch negativity (MMN) system have provided evidence for NMDA receptor dependent signaling of

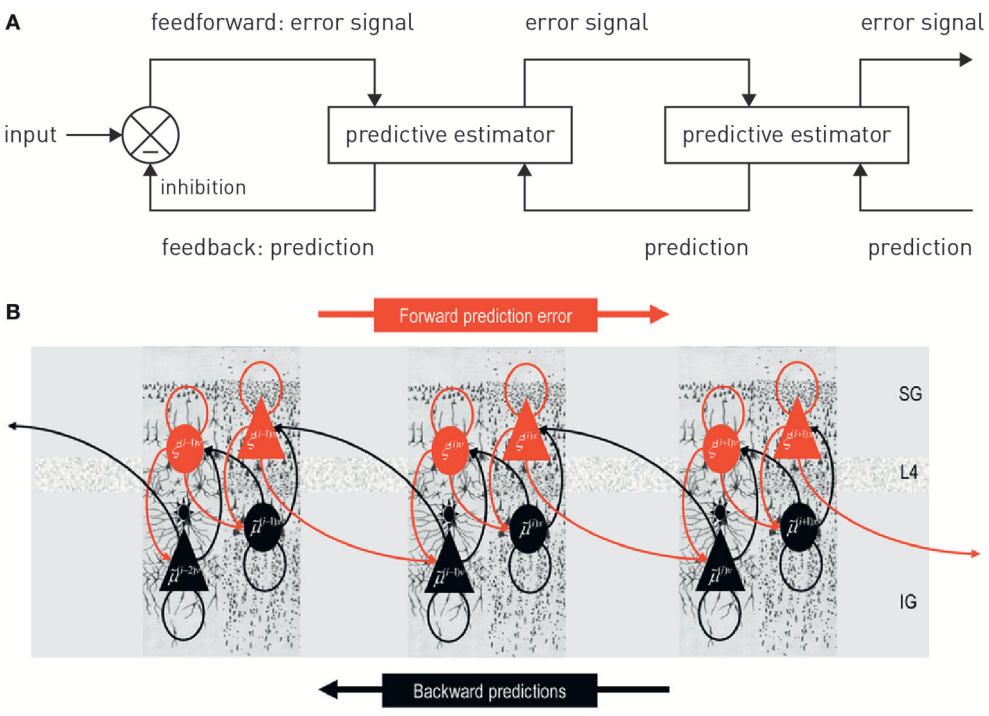

FIGURE 2 | (A) A graphical summary of predictive coding. See main text for details. Figure reproduced, with permission, from Rao and Ballard (1999). **(B)** A possible neuronal implementation of predictive coding. See main text for details. Figure reproduced, with permission, from Friston (2008).

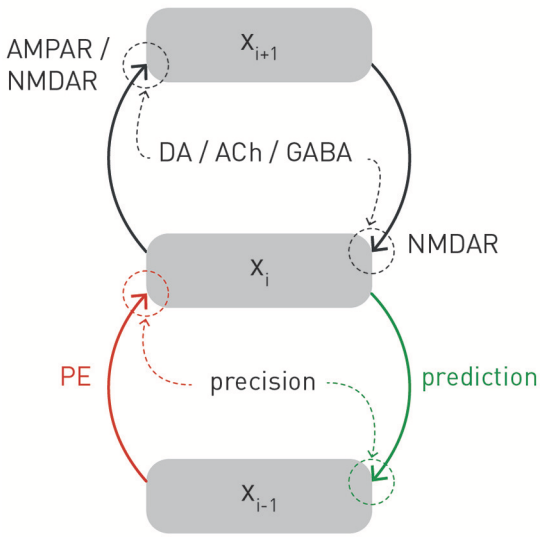

FIGURE 3 | A graphical summary of computational and physiological key components of hierarchical Bayesian inference. Computationally, prediction errors are conveyed by ascending or forward connections, while predictions are signaled via backward or descending connections. Critically, both experience a weighting by precision. Physiologically, the currently available evidence suggests that, in cortex, prediction errors are signaled via ionotropic glutamatergic receptors (AMPA and NMDA receptors), predictions via NMDA receptors, while precision-weighting is either implemented through neuromodulatory inputs (e.g., dopamine or acetylcholine) or by local GABAergic mechanisms. The figure is adapted, with permission, from Stephan et al. (2016b).

prediction errors via ascending connections (Wacongne et al., 2012; Schmidt et al., 2013). In summary, while definitive proof is outstanding, there is general consensus that ascending connections serve to signal prediction errors up the hierarchy, while predictions are communicated from higher to lower areas via descending connections (for reviews, see Friston, 2005; Corlett et al., 2009; **Figure 3** provides an overview).

In the past two decades, theories of perception have converged on the idea that perception corresponds to inverting a hierarchical generative model of sensory inputs (Dayan et al., 1995; Rao and Ballard, 1999; Friston, 2005). In some sense, this idea is not new: more than a century ago, the physiologist Helmholtz already suggested that the brain would have to invert the process of how a visual image was generated in order to infer the underlying physical cause (perception as "unconscious inference"; Helmholtz, 1860/1962). The more recent formalization of this notion under principles of probability theory is commonly referred to as the "Bayesian brain" hypothesis (Friston, 2010; Doya et al., 2011). In addition to the reasons given above, the general idea of perception as inversion of a hierarchical generative model derives from numerous empirical observations and theoretical arguments. Here, we briefly summarize a few central points and point the interested reader to more detailed literature. First, the sensory inputs the brain receives are noisy and often show a non-linear dependence on states in the world; this introduces the need for regularization by prior expectations or knowledge (Friston, 2003; Lee and Mumford, 2003; Kersten et al., 2004). Second, it can be shown that the integration of uncertain sources of information according to principles of probability theory (Bayesian inference) is optimal; this implies that the brain should have evolved to implement perceptual inference in the way such that Bayesian inference is approximated (Geisler and Diehl, 2002). Third, a large body of psychophysical experiments indicate that basic perceptual judgements and multi-sensory integration show clear evidence for the operation of Bayesian inference (for overviews, Knill and Richards, 1996; Geisler and Kersten, 2002; Petzschner et al., 2015). Finally, a generative model not only supports inference, but also allows for predictions. This can be achieved in several ways, for example, predictions about future sensory inputs can be derived from the model's posterior predictive density, and predictions about future states of the world under a chosen action or goal can be derived from the model's posterior dynamics (for example, see Penny and Stephan, 2014).

This link from inference to prediction is important because it provides a basis for coupling perception to action; a fundamental basis for homeostatic control, as described above. Generally, the challenge of control is framed by asking, informed by an estimate of the current state of the world (and possibly a prediction how it evolves), what action optimizes a particular criterion (a "utility function" or "cost function"). One framework to address this challenge is Bayesian decision theory (Körding, 2007; Dayan and Daw, 2008; Daunizeau et al., 2010). In a nutshell, this identifies an optimal action as one that maximizes the "expected utility" (where "expected" refers to a weighted average; i.e., the predicted outcomes are weighted by their relative uncertainty). The definition of utility, however, is not trivial. One common choice is to define utility in relation to "rewards." This, however, only shifts the problem and raises the question what constitutes "reward" for the brain (compare the discussion in Friston et al., 2012). From a homeostatic perspective, the utility or reward afforded by a particular action depends on four estimates based on inference and prediction:

- an estimate of the current bodily state (interoception);
- an estimate of the current environmental state (exteroception);
- a prediction of how these states would evolve in time (provided by a model of bodily and environmental dynamics);
- and a prediction to what degree the action considered will keep bodily state close to a homeostatic setpoint over time (allostatic control).

Current models of decision-making do not incorporate all of these aspects, and first attempts of accounting for homeostasis and allostasis in formal models of decision-making have only surfaced relatively recently (e.g., Keramati and Gutkin, 2014; Penny and Stephan, 2014; Pezzulo et al., 2015).

Importantly, perception and action do not operate in isolation, nor is there a unidirectional dependency of action on perception. Any chosen action changes the world (and/or the way

the brain samples it[3]) and hence the feedback the brain receives in terms of new sensory inputs. This sensory feedback (likelihood function) is combined with the current prior belief (prediction) held by the agent, resulting in a belief update about the state of the world (posterior probability) which, in turn, can inform new actions. This closes the loop from perception to action.

In summary, this section discussed homeostatic and allostatic control as fundamental objectives for the brain and reviewed long-standing concepts that highlight the importance of closed loops of perception and action. In particular, we have emphasized the notion that homeostatic control is not simply reactive, but proactive or anticipatory, and rests on a model of the external world which includes both the body and the influences it may receive from physical and social domains of the environment. Of course, these ideas raise the question how predictive models of this sort may actually be implemented by the brain. This question has been addressed by several recent theories, usually with a focus either on the body (Seth et al., 2011; Seth, 2013, 2015a; Feldman-Barrett and Simmons, 2015) or its environment (Rao and Ballard, 1999; Friston, 2005). In the next section, we review two classes of theories—predictive coding and active inference—which have recently begun to find application to questions of interoception and homeostasis.

Predictive Coding and Hierarchical Filtering

Predictive coding is a long-standing idea about neural computation that was initially formulated for information processing in the retina (Srinivasan et al., 1982). In its current form, predictive coding postulates that perception rests on the inversion of a hierarchical generative model of sensory inputs which reflects the hierarchical structure of the environment and predicts how sensory inputs are generated from (physical) causes in the world (Rao and Ballard, 1999; Friston, 2005). By inverting this model, the brain can infer the most likely cause (environmental state) underlying sensory input; this process of inference corresponds to perception. At any given level of the model, it is the (precision-weighted, see below) "prediction error" that is of interest—the deviation of the actual input from the expected input. Prediction errors signal that the model needs to be updated and thus drive inference and learning.

Anatomically, models of predictive coding are inspired by the remarkably hierarchical structure of sensory processing streams in cortex, where the laminar patterns of cortical-cortical connections define their function as ascending (forward or bottom-up) or descending (backward or top-down) connections and establish hierarchical relations between cortical areas (Felleman and Van Essen, 1991; Hilgetag et al., 2000). Computationally, the key idea of predictive coding is that cortical areas communicate in loops: Each area sends predictions about the activity in the next lower level of the hierarchy via backward connections; conversely, the lower level computes the difference or mismatch between this prediction and its actual activity and transmits the ensuing prediction error by forward connections to the higher level, where this error signal is used to update the prediction (**Figures 2**, **3**). This recurrent message passing takes place across all levels of the hierarchy until prediction errors are minimized throughout the network. In the words of Rao and Ballard (1999): "[...] neural networks learn the statistical regularities of the natural world, signaling deviations from such regularities to higher processing centers. This reduces redundancy by removing the predictable, and hence redundant, components of the input signal." This is a computationally attractive proposition because it satisfies information-theoretical criteria for a sparse code (Rao and Ballard, 1999).

In this scheme, minimizing prediction errors under the predictions encoded by the synaptic weights of backward connections in the hierarchy corresponds to hierarchical Bayesian inference and allows for computing the posterior probability of the causes, given the sensory data. Notably, plausible neuronal implementations exist which are compatible with known neuroanatomy and neurophysiology (Friston, 2005, 2008; Bastos et al., 2012); for a beautiful tutorial introduction (see Bogacz, in press).

A notion closely related to predictive coding is the idea that layers of hierarchical generative models may not predict the state of the next lower level, but its temporal evolution. This is known as hierarchical filtering and emphasizes the importance of taking into account the volatility of the environment, i.e., the temporal instability of its statistical structure, such as the probabilities by which one event causes another (Behrens et al., 2007; Mathys et al., 2011). Here, a hierarchical generative model combines a lower layer with value prediction errors about environmental variables with upper layers where volatility prediction errors drive inference and learning (Mathys et al., 2014). One concrete implementation of this idea is the hierarchical Gaussian filter (HGF; Mathys et al., 2011, 2014) which allows one to estimate subject-specific parameters encoding an individual's approximation to Bayes-optimal hierarchical learning.

One property of hierarchical Bayesian models deserves particular emphasis. This is the fact that under broad assumptions (i.e., for all distributions from the exponential family; Mathys, 2016), hierarchical Bayesian belief updates have a generic form with remarkably simple interpretability: at any given level i, belief updates $\Delta\mu_i$ are proportional to the prediction error (sent from the level below) but weighted by uncertainty or, more specifically, a precision ratio (**Figure 3**). This ratio denotes the relation between the estimated precision of the input from the level below (e.g., signal-to-noise ratio of a sensory input) and the precision of the prior belief. For example, in the case of the HGF, this takes the following form:

$$\Delta\mu_i \propto \frac{\hat{\pi}_{i-1}}{\pi_i} PE_{i-1} \quad (3)$$

Here, the numerator of this precision ratio represents the expected precision of the input from the level below (i.e., the agent's estimate of signal-to noise ratio of the input), whereas the denominator encodes the precision of the current belief. That is, the impact of prediction error on a belief update is smaller

[3]For example, eye movements do not influence the environment beyond the body (social interactions perhaps excepted), but determine sampling of visual information.

the more precise (less uncertain) the prior belief and larger the more precise (higher signal-to-noise) the input from the level below. Evidence from anatomical and physiological studies has established bridges between the computational and physiological components of this hierarchical precision-weighted message passing: prediction error signaling via forward connections likely rests on glutamatergic (AMPA and NMDA) receptors, prediction signaling via backward connections probably exclusively on NMDA receptors, while precision-weighting is assumed to draw on mechanisms which modulate postsynaptic gain, such as neuromodulatory (e.g., dopamine or acetylcholine) or local GABAergic inputs (Friston, 2009; Corlett et al., 2010; Adams et al., 2013b); for a summary, see **Figure 3**.

Perceptual Control Theory and Active Inference

Predictive coding represents one particular instantiation of the Bayesian brain hypothesis that represents an attractive foundation for studying interoception (Seth, 2013). However, predictive coding is limited to perception and does not directly speak to action selection and control, which is of fundamental importance for homeostasis. However, the link between perception and action can be studied in the framework of related theories which share the core ideas of predictive coding but generalize it to action selection; these include perceptual control theory (PCT; Powers, 1973, 1978; and active inference Friston, 2009; Friston K. J. et al., 2010).

PCT originated from the control theoretic principles of cybernetics (Wiener, 1948) and cognitive theories emphasizing the self-referential structure of the brain, such as radical constructivism (Richards and von Glasersfeld, 1979; von Foerster, 2003). The central premise is that any adaptive system tries to control certain quantities in the environment, q, that are essential for the system's existence and survival (**Figure 4A**). Critically, as it can only infer the value of q through perception, controlling q amounts to ensuring that the sensory inputs reflecting q remain at the desired (expected) level. In other words, the system will resist any external perturbations or disturbances by eliciting appropriate actions that restore the expected sensory input. This control can be exerted by the classical negative feedback loop of cybernetics (**Figure 4A**), where an internal reference (setpoint or goal signal) is compared to incoming sensory input reflecting the state of q. The resulting mismatch or prediction error serves to elicit actions which restore q to the expected value. In Powers' (1973) words: "The reference signal is a *model* [our emphasis] inside the behaving system against which the sensor signal is compared: behavior is always such as to keep the sensor signal close to the setting of this reference signal."

Critically, PCT postulates that control systems are, in many cases, structured hierarchically, where the "action" of higher systems consists of providing the reference or goal signal for lower systems. As a consequence, in order to reach a high-order goal, the relevant systems level (say i) does not need to directly access any actuators or specify a chain of commands; all it has to do is to alter the reference signal for the next lower system $i-1$. This will adjust the output from $i-1$ and thus the reference signal for the next lower system $i-2$, and so forth, until a level is reached whose output drives actuators and thus impacts on the environment. Intriguingly, nowhere in this chain of downward changes is the actual behavioral act specified; it is only the goals (expected sensory inputs) that are re-specified at each level of the hierarchy when the sensed environmental state does not correspond to the goal state (reference signal) at any levels of the hierarchy. In a nutshell, "... control systems control what they *sense*, not what they *do*." (Powers, 1973; his emphasis).

PCT was formulated at a time when neither the hierarchical structure of the human brain was well understood, nor when Bayesian ideas of perception had been well developed. These concepts have informed a more general framework—active inference (Friston, 2009; Friston K. J. et al., 2010)—which, although not directly building on PCT, shares its fundamental notion that control is hierarchically organized and directed toward sensory input, not motor output. Active inference derives

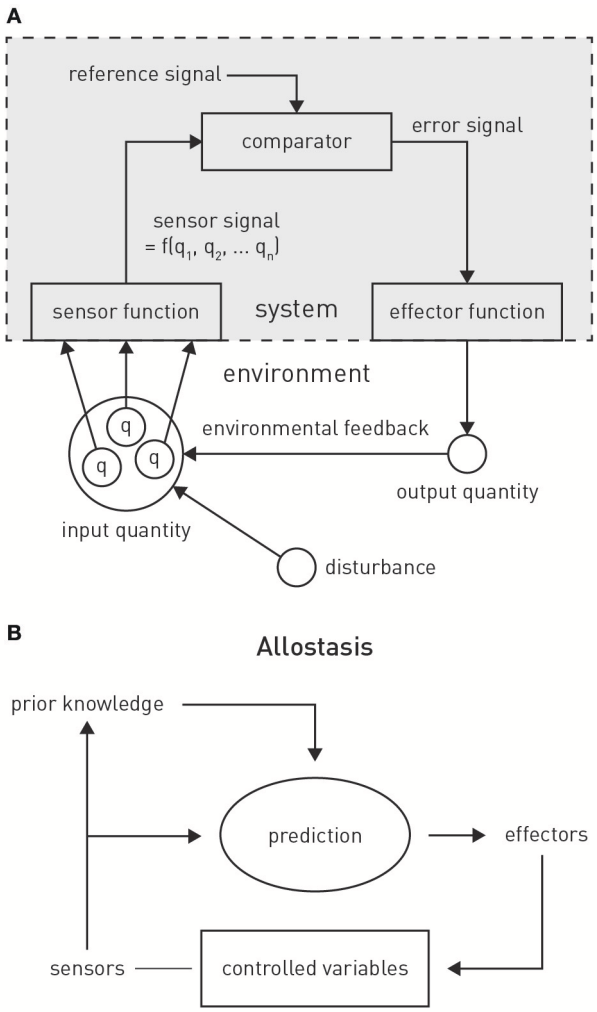

FIGURE 4 | (A) Principles of classical feedback control. Figure is reproduced, with permission, from Powers (1973). **(B)** A graphical summary of allostasis and its dependence on predictions about future bodily states. Figure is reproduced, with permission, from Sterling (2012).

from the free energy principle (Friston et al., 2006; Friston, 2009, 2010) which postulates that biological agents strive to minimize surprise about their sensory inputs. In the general case, however, this requires integrating over all possible hidden states of the world, a computationally intractable problem. A solution is provided by a more easily computable quantity called "free energy" which represents an upper bound on surprise. A free energy minimizing system thus corresponds to a system which experiences minimum surprise about its sensory inputs. This notion is similar to the functional principle underlying PCT, but is formulated in terms of probability theory and thus tied closely to inference and generative models. The free energy principle has found numerous applications to cognition, suggesting efficient algorithms for how perceptual inference and learning can be implemented by a hierarchical generative model that maps onto the known neuroanatomy and neurophysiology of the cortex (Friston et al., 2006; Friston, 2008, 2009; Bogacz, in press).

Notably, the brain could reduce free energy in two major ways (Friston, 2009): (i) by updating its beliefs or expectations; this corresponds to adjusting its generative model of sensory inputs, as postulated by predictive coding; or (ii) by selecting those actions which lead to sensory inputs that are in accordance with the brain's expectations; this is active inference. Simply speaking, active inference suggests that predictions (prior expectations) about sensory inputs define preferences or goals that engender behavior (Friston et al., 2015). Similar to PCT, prior expectations at a high-level in the hierarchy define a set point against which current sensory input is evaluated and actions are automatically elicited by lower levels initiated until any mismatch is eliminated. That is, actions arise from a hierarchical cascade of changes in expectations that eventually lead to reflex-like motor behavior at the lowest level in order to yield the expected sensory input (Adams et al., 2012, 2013a; Friston et al., 2015).

A HIERARCHICAL BAYESIAN VIEW ON FATIGUE AND DEPRESSION AS META-COGNITIVE PHENOMENA

Circuit Models of Interoception and Homeostatic Control

Hierarchical Bayesian theories have begun to play an influential role in the treatment of interoception and homeostatic control. Although not specifying a particular computational mechanism, a seminal paper by Paulus and Stein (2006) highlighted the importance of predictive processes for understanding interoception and its role in psychopathology, specifically anxiety. More recently, several proposals have linked interoception and homeostatic/allostatic control to predictive coding and active inference (Seth et al., 2011; Gu et al., 2013; Seth, 2013; Feldman-Barrett and Simmons, 2015).

While these proposals have remained unspecific about the exact implementation of active inference for allostatic control, they have incorporated anatomical and physiological knowledge about the neuronal circuits for interoception and homeostatic control (for reviews, see Saper, 2002; Craig, 2002, 2003; Critchley and Harrison, 2013). Viscerosensory information about a wide range of bodily states—including bodily integrity (pain, inflammatory mediators), cardiovascular (e.g., blood pressure, oxygenation), humoral (e.g., plasma osmolality), physical (e.g., body temperature), metabolic (e.g., levels of glucose and hormones like insulin, ghrelin, leptin), immunological (e.g., cytokines), or mechanical (e.g., dilation of internal organs) properties—reaches the brain via three main channels: visceral afferents that enter the spino-thalamic tract via spinal cord lamina 1, cranial nerves IX (glossopharyngeal) and X (vagus), and humoral information which is sensed by circumventricular organs and specialized hypothalamic neurons situated outside the blood-brain barrier. These channels reach the thalamus (ventroposterior and ventromedial nuclei)—either directly or indirectly via brain stem nuclei including the nucleus of the solitary tract, parabrachial nucleus, and periaqueductal gray—and eventually target the viscerosensory cortex. The latter essentially comprises posterior and mid-insular cortex which represent a viscerotopic map of bodily state with respect to numerous physiological variables (Cechetto and Saper, 1987; Allen et al., 1991; Craig, 2002). Their efferent connections convey information about bodily state to cortical visceromotor areas—such as anterior insular cortex (AIC), anterior cingulate cortex (ACC), subgenual cortex (SGC), and orbitofrontal cortex (OFC)—which, in turn, send projections to hypothalamus, brainstem and spinal cord nuclei (Mesulam and Mufson, 1982; Hurley et al., 1991; Carmichael and Price, 1995; Freedman et al., 2000; Chiba et al., 2001; Vogt, 2005; Hsu and Price, 2007) in order to control autonomic, endocrine and immunological reflex arcs.

Based on this general anatomical layout, several computationally inspired proposals have been put forward, although so far without mathematically concrete implementations. Seth et al. (2011) conceptualized interoception as a predictive coding process combined with corollary discharge. In their concept, the AIC was assigned a central role as comparator (Gray et al., 2007) receiving corollary discharges (efference copies) of autonomic control signals from visceromotor regions like the ACC. Subsequent formulations based on active inference no longer understood autonomic control signals originating from visceromotor regions as "commands," but as predictions of bodily states which are fulfilled by autonomic reflexes implemented by lower (hypothalamic and brainstem) centers (Gu et al., 2013; Seth, 2013; Feldman-Barrett and Simmons, 2015; Pezzulo et al., 2015).

In the following, we build on and extend the above models to formulate a theory of fatigue that connects hierarchical Bayesian inference to metacognition (cognition about cognition). Specifically, we unpack and extend a mechanism proposed recently as part of a list of priority problems for psychiatry: "With respect to fatigue, can we identify distinct patient subgroups in whom the brain's model of interoceptive inputs signal constant surprise because of persistent violation of fixed beliefs (homoeostatic setpoints) regarding metabolic states or bodily integrity and in whom this enduring dyshomoeostasis induces high-order beliefs about lack of control and low self-efficacy?" (Problem 8 in Stephan et al., 2016a). In the following, we describe how homeostatic regulation can be regarded as a problem of hierarchical Bayesian inference and control, not dissimilar to

previous accounts but with three novel aspects: (i) an explicit discussion of how conventional homeostatic concepts can be transformed into Bayesian counterparts, including an extremely simple but concrete illustration of how active inference could mediate homeostatic control; (ii) the extension of active inference to a formal definition of allostatic control; and (iii) the addition of a metacognitive layer to the interoceptive hierarchy.

Homeostatic Control through Active Inference As "Bayesian Reflexes"

The conventional cybernetic view of homeostasis regards the brain's task as ensuring that its carrier (the body) inhabits a limited number of states which are compatible with survival, for example, being within a narrow range of body temperature or blood oxygenation. From a control theory perspective, this amounts to keeping sensory signals of bodily state close to setpoints, which are defined by a reference signal that is provided to a comparator unit (compare the traditional cybernetic circuit implementing feedback control in **Figure 4A**).

We now formulate this circuit and its components in a way that provides a basis for extending homeostatic to allostatic control. Under a Bayesian perspective, homeostatic setpoints can be defined as the expectations (means) of prior beliefs about the states the body should inhabit. These prior beliefs are instantiated biophysically by "hard-wired" local circuits in "effector regions" that control homeostatic reflex arcs, such as the hypothalamus, brain stem nuclei like the periaqueductal gray (PAG), and autonomic cell columns in the spinal cord (Craig, 2003). The "homeostatic range" (of values compatible with life) are reflected by prior variance: priors of vitally important variables (such as blood oxygenation) are extremely tight (low variance), whereas other beliefs (e.g., about blood pressure) can afford being considerably wider (high prior variance). Notably, all of these beliefs are subject to evolutionary pressure: depending on how well they support homeostasis under the conditions of a given environment and thus maintain bodily integrity and survival, they (the neuronal structures encoding them, respectively) will be more or less likely selected out.

Given this notion of a homeostatic setpoint as a belief about physiological states the body should inhabit, one can now formulate a basic homeostatic reflex arc in Bayesian terms (**Figure 5**), including its control by higher-order centers (allostasis). Specifically, we consider how a particular physiological state x can be controlled by actions elicited by a neuronal homeostatic reflex arc, e.g., in the hypothalamus or a brain stem nucleus, ensuring that x is kept within a homeostatic range (prior belief about its value). A key property of this formulation is that corrective action is more vigorous or rapid the higher the deviation of bodily states from prior expectations *and* the more precise these expectations (the tighter the homeostatic range). For clarity and simplicity, we only consider a very basic scenario here. While our approach is inspired by more general and sophisticated treatments of active inference formulated under the free-energy principle (Friston K. J. et al., 2010), the following derivation presents, to our knowledge, a first mathematically concrete proposal of an active inference

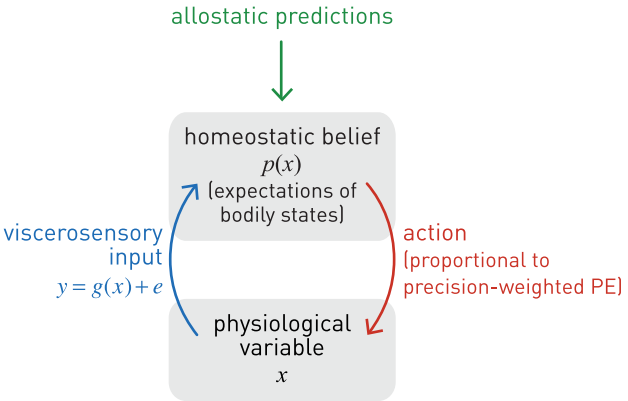

FIGURE 5 | A graphical summary of a homeostatic reflex arc and its modulation by allostatic predictions. Blue lines: sensory inputs; red lines: prediction errors; green lines: predictions.

mechanism for homeostatic reflexes under allostatic control. We emphasize that the following model is by no means complete, but should be seen as a mere starting point for developing generative models of allostatic control and metacognitive evaluation.

Let us initially begin from the perspective of perceptual inference as Bayesian belief updating, i.e., how one could determine the most likely value of bodily state x, given noisy sensory input which is sampled sequentially. Here, we examine the simplest case where x is assumed not to evolve or experience any perturbations over the period of observation. While, in this context, x is thus a constant state of the body, the brain's belief about x is updated sequentially, based on noisy sensory inputs (Because of this subtle difference, in the following few paragraphs on perception, we write the bodily state x as a time-invariant variable while mean and variance of the belief about x are time-dependent. In subsequent paragraphs on action, the opposite is the case). This belief can be described, for example, as a normal distribution with mean μ_t and precision (inverse variance) π_t at time t:

$$p(x) = N\left(x; \mu_t, \pi_t^{-1}\right) \tag{4}$$

At any time t, viscerosensory input y results from some form of neuronal coding (transformation) g of x and is affected by inherent noise of the sensory channel (with constant precision π_{data}):

$$p\left(y \mid x\right) = N\left(y; g(x), \pi_{data}^{-1}\right) \tag{5}$$

or, equivalently:

$$\begin{aligned} y_t &= g(x) + e_t \\ p(e_t) &= N\left(e_t; 0, \pi_{data}^{-1}\right) \end{aligned} \tag{6}$$

In this context, the goal of perceptual inference would be to infer on the value of x given repeated samples of the noisy viscerosensory signal y. This corresponds to updating ones' estimates of the sufficient statistics of x (μ_t and π_t), where

the estimate at time t serves as the prior for the next belief update ("today's posterior is tomorrow's prior"). That is, using Bayes' theorem, one can sequentially transform a prior belief $p\left(x;\mu_t,\pi_t^{-1}\right)$ into a posterior belief $p\left(x;\mu_{t+1},\pi_{t+1}^{-1}\right)$, based on new sensory data y_t. Specifically, this sequential belief update would obey the following simple rule (see Mathys, 2016 for details):

$$\begin{aligned}\mu_{t+1} &= \mu_t + \frac{\pi_{data}}{\pi_t + \pi_{data}}\left(y_t - g\left(\mu_t\right)\right)\\ \pi_{t+1} &= \pi_t + \pi_{data}\end{aligned} \tag{7}$$

Here, the posterior mean results from updating the current estimate (prediction or prior mean) with the precision-weighted prediction error—where the latter corresponds to the difference between the actual sensory signal y_t and its predicted value, $g\left(\mu_t\right)$. The precision-weighting is critical because it renders the correction or update sensitive to the properties of both the sensory channel and the prior belief: the belief update is more pronounced the higher the estimated precision of the sensory input and the lower the precision of the prior.

We can now use the same type of precision-weighted prediction error for influencing x, instead of inferring or sensing it. In other words, we turn the perceptual update rule of Equation 7 into a control rule, based on two simple considerations. First, to fix the setpoint for the homeostatic reflex, we clamp the prior belief: $\forall t : \mu_t = \mu_{prior}, \pi_t = \pi_{prior}$. This effectively corresponds to delta function (hyper)priors on the sufficient statistics of the prior belief (see Equation 8). Equation (7) shows that this can be achieved by simply ignoring the sensory information (more formally: setting the data precision to zero). Second, we define an action or effector function whose driving force is the prediction error under expected homeostasis; in other words, the difference between the actual sensory input y and the sensory input that would be expected at the homeostatic setpoint (μ_{prior}). This prediction error can be derived from the log evidence of a model m_H which expects bodily state to be in homeostasis [and therefore the viscerosensory input to equal $g\left(\mu_{prior}\right)$]. This is the case when the sufficient statistics of the marginal likelihood are given by the homeostatic setpoint μ_{prior} and homeostatic range π_{prior}^{-1} (where c absorbs constant terms):

$$\begin{aligned}p\left(y|m_H\right) &= \int p\left(y|\mu_t,\pi_t\right)p\left(\mu_t\right)p\left(\pi_t\right)d\mu_t\,d\pi_t\\ &= \int N\left(y;g\left(\mu_t\right),\pi_t^{-1}\right)\delta\left(\mu_t-\mu_{prior}\right)\\ &\quad\ \delta\left(\pi_t-\pi_{prior}\right)d\mu_t\,d\pi_t\\ &= N\left(y;g\left(\mu_{prior}\right),\pi_{prior}^{-1}\right)\\ L &= \ln p\left(y|m_H\right)\\ &= \frac{1}{2}\left(\ln\pi_{prior}-\pi_{prior}\left(y-g\left(\mu_{prior}\right)\right)^2\right)+c\\ &= \frac{1}{2}\left(\ln\pi_{prior}-\pi_{prior}\left(PE\left(y\right)\right)^2\right)+c\end{aligned} \tag{8}$$

Notably, this is the negative (Shannon) surprise S of seeing the data under the expectation of homeostasis (compare Equation 2):

$$S\left(y\,|\,m_H\right) = -L \tag{9}$$

According to Equation (8), minimizing the precision-weighted squared prediction error thus minimizes the interoceptive surprise S about the sensory inputs. This requires actions that make x maximally congruent with the homeostatic setpoint and hence maximize log evidence L. This can be achieved by defining action[4] as the gradient of the log likelihood with regard to x (under application of the chain rule and noting, from Equation (6), that $\frac{\partial y}{\partial x} = \frac{\partial g}{\partial x}$):

$$\begin{aligned}a\left(t\right) &= \frac{\partial L}{\partial x}\\ &= \frac{\partial\left[-\frac{1}{2}\pi_{prior}\left(y\left(x,t\right)-g\left(\mu_{prior}\right)\right)^2\right]}{\partial x}\\ &= \frac{\partial\left[-\frac{1}{2}\pi_{prior}PE\left(y\right)^2\right]}{\partial x}\\ &= -\frac{\pi_{prior}}{2}\frac{\partial\left[PE\left(y\right)^2\right]}{\partial y}\frac{\partial y}{\partial x}\\ &= -\pi_{prior}PE\left(y\right)\frac{\partial g}{\partial x}\end{aligned} \tag{10}$$

and using it to smoothly adjust the value of the physiological variable x:

$$\frac{\mathrm{d}x}{\mathrm{d}t} = \lambda^{-1}f\left(a\left(t\right)\right) \tag{11}$$

Put differently, the chosen action a induces a gradient descent of x on interoceptive surprise:

$$\frac{\mathrm{d}x}{\mathrm{d}t} = -\lambda^{-1}f\left(\frac{\partial S}{\partial x}\right) \tag{12}$$

Here, λ is a time constant matched to the time scale at which action can affect x (for example, a slow time constant for hormonal regulation by the hypothalamus, or a very fast time constant for cardiovascular regulation via the baroreceptor reflex). Furthermore, for generality, Equation (11) includes a mapping f from action to changes in x. This could be non-linear and probabilistic to account for noise in motor processes (compare the analogous sensory mapping g in Equation 6). The advantage of a probabilistic formulation is that it allows for considering "action precision," i.e., the confidence with which an action would have the desired effect on the physiological variable; this will be examined in future work. In the present simulation shown in **Figure 6**, we have kept f maximally simple (a deterministic identity function).

Equations (8)–(12) specify how the effector emits actions that move x toward its setpoint and minimize precision-weighted

[4]Here, we are pragmatically changing the notation of time (from index to argument) as we find it more natural to express the action signal in continuous time.

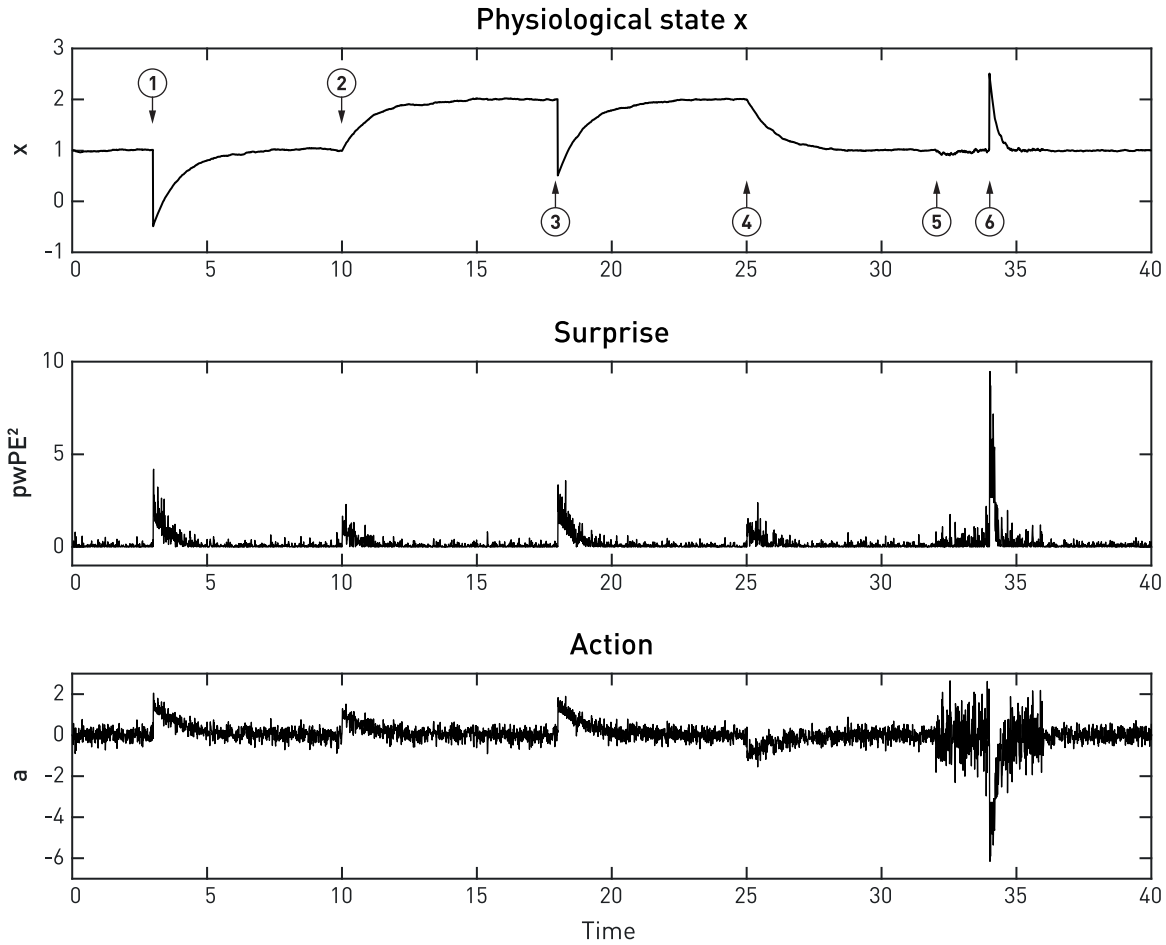

FIGURE 6 | A simulated example of allostatic regulation of homeostatic control, based on Equations (8)–(12). The upper panel shows the temporal evolution of a fictitious physiological state x (Equation 11) which is affected by environmental perturbations (❶,❸,❻; all with a magnitude of 1.5). The middle and lower panels display an approximation to interoceptive surprise—i.e., squared precision-weighted prediction error ($pwPE^2$; compare last line of Equation 8)—and the associated action signal (Equation 10), respectively. Following the timeline from left to right, the homeostatic setpoint or belief is initially specified with a prior mean and prior precision of 1 each. Please note that even before the first perturbation (❶) occurs, sensory noise (zero mean, 0.25 standard deviation) leads to ongoing actions of minute amplitude which lead to (very small) deviations of x from the setpoint. Following a first perturbation (❶), the homeostatic reflex arc emits corrective actions that are proportional to precision-weighted viscerosensory prediction error (middle panel). As the actions are successful, x returns to setpoint and viscerosensory prediction error decays. ❷ indicates the beginning of allostatic control: here, the prediction of imminent future perturbations (by some generative model not specified here) leads to an anticipatory rise in the homeostatic setpoint (a shift in the prior mean to 2). As a consequence, in the absence of any change in sensory input, actions are elicited to change the value of x to the new setpoint. This ensures that the following perturbation ❸ does not bring x anywhere near the critical threshold. At ❹, a safe period is predicted, and allostatic control resets the homeostatic setpoint (prior mean) to 1. At ❺, another perturbation in the near future is being predicted, however, this time the direction of the perturbation is uncertain. Therefore, changing the mean or setpoint is not a viable option and allostatic control takes a different form: instead of changing prior mean, the prior precision of the homeostatic belief is increased from 1 to 4. As a consequence, when a perturbation occurs at ❻, this yields a considerably larger precision-weighted prediction error and hence greater interoceptive surprise (see lower panel), leading to a significantly more rapid corrective action (compare the slope of signal rise between ❶ and ❻), putting the agent at less risk, should another perturbation occur shortly after ❻. It is also noteworthy that the increased prior precision enhances the effect of sensory noise (compare the roughness of the three signals just prior to ❶ and ❻, respectively).

prediction error and thus interoceptive surprise (see middle and lower panels in **Figure 6**). This makes the action signal progressively diminish toward zero as x asymptotes its setpoint. Notably, the vigor or speed of action depends on both the current prediction error (discrepancy between the sensory feedback signal and its desired/predicted level), and the precision of the prior homeostatic belief. This means that for vitally important physiological variables whose homeostatic ranges are very tight, corrective actions are necessarily rapid. Conversely, when physiological variables diverge from setpoints, the experience of dyshomeostasis (i.e., the magnitude of prediction error) is much more pronounced when prior homeostatic beliefs are tight. Both properties are illustrated by the simple simulation shown in **Figure 6**.

The above equations illustrate a key principle of active inference: the choice between reducing prediction error through changing predictions (updates of the generative model) or through action depends on precision. For example, reducing the

precision of sensory input (π_{data} in Equation 7) disables belief updates while action (Equation 10) remains unaffected. Similarly, increasing the precision of predictions or prior beliefs (π_t in Equation 7 or π_{prior} in Equation 8) abolishes belief updating while action is increased in proportion to the increase in precision. In other words, a modulation of precision of top-down predictions is sufficient to switch from learning to acting.

This section has outlined a Bayesian account of homeostatic control. Equations (8)–(12) illustrate the role of prior beliefs for implementing setpoints in homeostatic reflex arcs where actions minimize prediction errors (and hence interoceptive surprise) in order to fulfill a prior belief that physiological state x should be within a particular range. This represents a simple but concrete implementation of active inference in the context of homeostatic control. Perhaps most importantly, dyshomeostasis can now be defined formally as a persistent deviation from precise prior expectations about bodily state that is indexed by chronically elevated surprise about viscerosensory inputs; or equivalently, as high entropy (average surprise) of viscerosensory channels.

One might note that entropy minimization by homeostatic control might constitute a violation of the second law of thermodynamics (that all systems monotonically increase their entropy over time). However, the second law of thermodynamics only applies to closed systems; by contrast, biological organisms represent open systems which exchange energy and information with their environment and are capable of decreasing entropy—at least temporarily (Von Bertalanffy, 1969). This is the very nature of homeostatic regulation: to maintain the body in a highly particular (low entropy and hence unlikely) condition.

An Active Inference Perspective on Allostasis

A critical extension of the above scheme for homeostatic control is to allow higher-order goals or predictions to alter the homeostatic belief $p(x)$. This amounts to allostasis: the proactive deployment of behavior, guided by predictions from a model, in order to avoid dyshomeostatic future states (Sterling, 2012; **Figure 4B**). For example, prolonged exposure to intense sunlight will not only cause immediate (e.g., increase in body temperature) but also delayed (e.g., dehydration) perturbations of homeostasis. Provided the brain is equipped with a generative model for predicting the evolution of environmental and bodily states, based on previous experience, it can take proactive actions and avoid dyshomeostatic states before they arise. Importantly, these homeostatic goals often have a hierarchical structure, where temporary deviations from homeostatic setpoints are tolerated or even induced in order to ensure that higher-order homeostatic goals can be reached in the future. For example, under a model that predicts a possible encounter with a hostile agent in a specific context, anticipatory deviations from hormonal and cardiovascular setpoints are induced to prepare for future fight-flight behavior.

From the perspective of theories like PCT or active inference, an efficient way of accomplishing hierarchical control is to temporarily alter the setpoint or prior belief of the relevant homeostatic reflex arc (for example, changing the belief about desirable plasma osmolality elicits drinking behavior before dehydration reaches a critical level). This relies on higher brain structures with three properties: (i) access to estimates of bodily state (interoception), (ii) capable of generating predictions over longer time scales, and (iii) with anatomical connections that can modulate the homeostatic beliefs which reflex arcs in regions like the hypothalamus or brain stem serve to fulfill. Neuroanatomically, regions that are in a position to modulate homeostatic reflex arcs through allostatic predictions are likely situated at the top of the interoceptive hierarchy and include the AIC, ACC and subgenual cortex; this is discussed in more detail below.

The hierarchical (top-down) modulation of reflex arcs by predictions means that (homeostatic) beliefs about desirable bodily states in the present become dependent on (allostatic) beliefs about bodily states in the future. This essentially turns homeostatic beliefs into time-varying quantities under the influence of higher allostatic predictions $\phi_i(t)$. This belief transformation could affect either the mean and/or the precision of the homeostatic belief across time:

$$p(x(t)) = N\left(x(t); \mu_{prior}(\phi_1(t)), \pi_{prior}(\phi_2(t))^{-1}\right) \quad (13)$$

Figure 6 shows a very simple simulation which illustrates both types of allostatic control. Here, a physiological variable x is driven away from its setpoint (the agent's homeostatic belief) three times, due to environmental perturbations. Each time a "Bayesian reflex" restores homeostasis according to Equations (8)–(12). Critically, following the first incident (❶ in **Figure 6**), higher levels of the system (not modeled here) predict further perturbations of a particular direction and allostatic control is exerted by shifting the mean (setpoint) into the opposite direction while leaving the precision of the homeostatic belief unaffected (❷). As a consequence, x rises to the new expected level. Note that this occurs without specifying the action; instead, the action follows automatically once a new belief or setpoint has been adopted. At ❺, perturbations are predicted, but with uncertainty about their direction; hence shifting the setpoint or mean is not a viable option. Instead, the precision of the homeostatic belief is increased, leading to a smaller range of tolerated deviations in either direction. The subsequent response to a perturbation (❻) leads to a far swifter restorative response than after the first perturbation (❶).

Here, we only provide a general frame for implementing allostasis from an active inference perspective; the specific form for the modulation of homeostatic beliefs by allostatic predictions is likely to vary across physiological variables, as these are controlled on different time scales and may draw on predictions from different generative models. Generally, however, we note that the frame suggested by Equation (13) is consistent with the PCT notion of control where hierarchically higher levels set the reference points for lower levels (Powers, 1973). It is also similar in structure to active inference accounts of motor control where primary motor cortex is assumed to modulate spinal reflex arcs through ascending connections to α and γ motor neurons, "programming" motor trajectories via predictions about future proprioceptive input (Adams et al., 2013b).

In summary, under the hierarchical Bayesian view presented above, homeostatic and allostatic control, respectively, can be understood as active inference about bodily states on different time scales: actions (of a motor, autonomic, endocrine, or immunological sort) are selected which fulfill beliefs about current and future bodily states and reduce the average surprise (entropy) of viscerosensory channels over time (the time scale of the respective allostatic goal). Notably, this entropy-reducing principle may not only be in operation during the lifetime of an organism, but has also been suggested as the driving force behind the evolution of homeostatic mechanisms (Woods and Wilson, 2013).

A Neuroanatomical Circuit for Interoception, Homeostasis, and Allostasis

The extension from homeostatic to allostatic control highlights that interoception and homeostatic regulation are inevitably linked and form a closed loop: tuning the setpoints of homeostatic reflex arcs depends on accurate allostatic predictions about future bodily states; these predictions, in, turn depend on accurate inference about current bodily states. **Figure 7** summarizes the neuroanatomy of a proposed circuit for integrating the afferent (interoceptive) and efferent (control) branches of homeostatic/allostatic regulation. This anatomical layout is not dissimilar to a previous proposal by Feldman-Barrett and Simmons (2015) but introduces several novel aspects (e.g., a metacognitive layer) and distinguishes interoception, allostatic predictions and homeostatic reflex arcs more explicitly.

In our proposal, AIC, ACC, subgenual cortex (SGC), and orbitofrontal cortex (OFC)—regions we refer to as "visceromotor areas" (VMAs) as a set—are situated at the top of this circuit, embodying a generative model of (potentially different types of) viscerosensory inputs that enables a biological agent to infer on current bodily states and predict future states, as a basis for allostatic predictions. This assumption is supported by known anatomical connections and their hierarchical relations based on laminar patterns of origin and target: tract tracing studies in the Macaque monkey (Mesulam and Mufson, 1982; Mufson and Mesulam, 1982; Vogt and Pandya, 1987; Carmichael and Price, 1995) demonstrated that VMAs receive ascending projections from viscerosensory cortex (posterior and mid-insula). As in circuits supporting exteroception, these ascending connections are thought to signal prediction errors (Seth et al., 2011; Gu et al., 2013; Seth, 2013; Feldman-Barrett and Simmons, 2015). On the other hand, according to tract tracing studies in monkeys and rats (Mesulam and Mufson, 1982; Hurley et al., 1991; Carmichael and Price, 1995; Freedman et al., 2000; Chiba et al., 2001; Vogt, 2005; Hsu and Price, 2007), the visceromotor areas possess connections targeting hypothalamus, brain stem nuclei and spinal cord (partially relayed by amygdala, periaqueductal gray (PAG), and basal ganglia). These connections are thought to convey allostatic predictions which modulate the setpoints of homeostatic reflexes, as described above. Importantly, descending projections from visceromotor areas could send the same prediction to posterior and mid-insula; this effectively serves as efference copy or corollary discharge against which viscerosensory inputs can be compared. The resulting prediction errors are returned via ascending connections to visceromotor areas, allowing for (presumably slow) adjustment of allostatic predictions.

Several sources of uncertainty need to be highlighted here. First, the specific roles and division of labor amongst VMAs are largely unclear; for the moment, we have grouped them together without any differentiation. Second, non-trivial species differences in the neuroanatomy of interoceptive circuitry exist. For example, SGC targets different autonomic effector regions in rodents and monkeys (Hurley et al., 1991; Freedman et al., 2000), and it has been questioned whether AIC and ACC in monkeys and humans are functionally equivalent (Critchley and Harrison, 2013). Third, the present circuit model ignores the fact that AIC, ACC, and OFC each consist of several anatomically distinct subfields. For example, even within agranular insular cortex of the Macaque monkey, subareas exhibit differential connectivity and may possess a hierarchical relation amongst themselves (Carmichael and Price, 1996). Finally, our present model assumes that effector regions (hypothalamus, brain stem, spinal cord), which receive allostatic predictions from VMAs, do not return prediction errors via ascending connections. This serves to ensure that allostatic predictions are fulfilled by actions, instead of these predictions being revised by prediction errors. This fits well to the agranular cytoarchitectonic nature of VMAs, i.e., the absence of a well-formed layer IV which represents a key

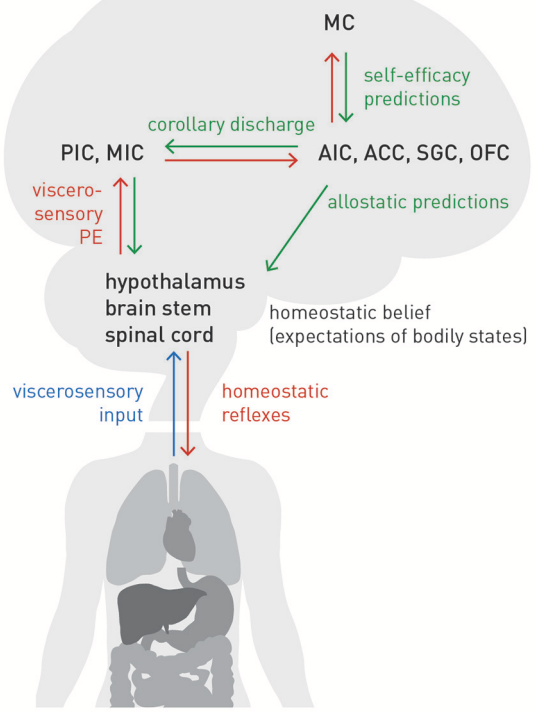

FIGURE 7 | A proposed circuit for interoception and allostatic regulation of homeostatic reflex arcs, together with a metacognitive layer (MC). See main text for details. Blue lines: sensory inputs; red lines: prediction errors; green lines: predictions.

target lamina for ascending connections conveying prediction errors in granular cortex (cf. Feldman-Barrett and Simmons, 2015). Alternatively, as suggested by analogous active inference schemes for motor control, this type of prediction error signal could temporarily "switched off" or attenuated during action execution by reducing precision (Adams et al., 2012, 2013a). It is questionable, however, whether this proposed mechanism could also apply to allostatic control, given the continuous presence of interoactions and the much longer time scales on they unfold (e.g., hormonal or immunological regulation).

Our Bayesian account of homeostatic control (see Equations 8–12 above) led to a definition of dyshomeostasis as a state of elevated interoceptive surprise, a deviation from precise prior expectations about bodily state that is indexed by increased precision-weighted prediction errors about viscerosensory inputs. The closed perception-action loop of homeostatic inference and control shown by **Figure 7** indicates that, in addition to peripheral causes residing in the body itself, structural lesions (e.g., due to demyelinating processes in MS) or functional impairments (e.g., due to inflammation in depression) in either afferent or efferent branches of this circuit could lead to chronic dyshomeostasis. We now turn to some implications of this view for specific domains of cognition and emotion: fatigue and depression.

Metacognition about Interoception and Allostatic Self-efficacy

Interoceptive surprise plausibly has general and major consequences for cognition and emotion—even in interoceptive domains that may be operating outside immediate awareness (e.g., levels of certain hormones, cytokines, or metabolites). As noted above, surprise is equivalent to negative log model evidence, and persistently high surprise is the hallmark of a bad model. A chronic state of perceived dyshomeostasis indicates that the brain's generative model of viscerosensory inputs has low evidence—either because it generates bad predictions or because it cannot transform them (with sufficient confidence) into homeostasis-restoring actions. In other words, persistently high interoceptive surprise represents a fundamental warning sign that the brain presently cannot adequately control perturbations of potential relevance for survival. This leads us to a key hypothesis of this paper—that "enduring dyshomoeostasis induces high-order beliefs about lack of control and low self-efficacy" (Stephan et al., 2016a).

Self-efficacy is a concept of self-evaluation and behavioral change which holds that humans not only have expectations with regard to the outcome of chosen actions, but also self-oriented expectations concerning whether they can successfully execute these actions (Bandura, 1977). Self-efficacy can be defined as an individual's expectation of personal mastery and control: an individual with high self-efficacy believes that he/she can successfully perform the cognitive and motor operations required to overcome negative situations (e.g., obstacles, adversaries, threats, and aversive experiences). The construct of self-efficacy is thus closely related to concepts of metacognition (for review, see Clark and Dumas, 2015). Theoretical and empirical work suggests that low levels of perceived self-efficacy prevent the deployment of adequate coping behavior and may constitute an important component in the pathogenesis of depression and anxiety (Rosenbaum and Hadari, 1985; Bandura et al., 1996, 1999; Arnstein et al., 1999).

While the importance of self-efficacy for adaptive behavior and general well-being has been examined in numerous cognitive domains, particularly with regard to learning, memory and other academically relevant cognitive skills, the possible link of self-efficacy to dyshomeostasis has received relatively little attention. One exception is the area of chronic pain research, where several studies demonstrated that perceived self-efficacy not only modulates pain perception (Bandura et al., 1987), but crucially determines coping behavior and quality of life, independently of and often more strongly than physical variables, such as pain intensity or duration (Arnstein et al., 1999; Denison et al., 2004; Burke et al., 2015).

Here, we suggest that the metacognitive evaluation of homeostatic/allostatic control during experienced dyshomoeostasis[5] has a major impact on self-efficacy beliefs and the ensuing choice of actions. Importantly, as we highlighted at the outset of this paper, this may proceed in two sequential stages. Initially, the metacognitive recognition that available homeostatic/allostatic control strategies fail to reduce interoceptive prediction error may materialize through fatigue as a subjective feeling. This resonates with the concept of "feeling states" in the interoception literature (i.e., re-representations of an image of bodily state; Craig, 2002) but highlights the evaluation of action outcomes and the experience of mastery. Importantly, this can be defined formally under our model above: if the gradient $\frac{\partial S}{\partial x}$ (Equations 8–12) indicates that interoceptive surprise is not decreasing but maintains constant or even increases as the action is performed, this indicates that homeostatic control fails and the available action does not control the dyshomeostasis-causing process. Fatigue may thus be understood as the metacognitive detection of an ongoing but fruitless effort of regulating bodily states that may manifest neurophysiologically as a failure to reduce incoming prediction errors to VMAs (**Figure 7**).

In this context, it is worth pointing out that, under our model, fatigue can be formally distinguished from tiredness. In case of tiredness, for example, from prolonged physical activity, interoceptive surprise arises from the concentration of metabolites such as lactic acid shifted away from their setpoints. In this case, however, a simple action is available: physical rest. This allows muscle metabolism to restore biochemical balance, which turns the gradient $\frac{\partial S}{\partial x}$ negative (Equations 8–12) and signals restoration of homeostasis by the chosen behavior. By contrast, in fatigue, physical rest does not have the same positive effect. From the view of our theory, where fatigue represents a metacognitive belief that arises from chronic experience of lack of mastery over bodily states, it is easy to explain why rest is not beneficial: when interoceptive surprise fails to decrease in the absence of actions, mastery cannot be experienced and the

[5]In principle, of any sort—although clearly some viscerosensory domains (e.g., about cardiac function) may exert greater impact on self-efficacy than others.

associated metacognitive beliefs cannot be adjusted. This may be a reason why, in some patients, graded exercise therapy can be helpful (Larun et al., 2016), perhaps because it gradually allows patients to experience mastery and restore self-efficacy.

Having said this, while rest is not directly effective against fatigue, it may not be the worst behavioral option as it prevents inefficient actions that do not target the origin of interoceptive surprise and would only require energy (something that in itself induces a positive gradient $\frac{\partial S}{\partial x}$). Put differently, fatigue could initially be an adaptive and functionally meaningful feeling state: if presently no homeostasis-restoring action strategies are (perceived to be) available, or the means for implementing these strategies are lacking, it may be a rational choice to reduce activity and save energy. Three cases may be worth distinguishing here, depending on whether the cause of dyshomeostasis resides in the body, the physical environment, or the social environment, respectively. First, in case of a bodily origin of dyshomeostasis, fatigue-driven passivity allows for saving and reallocating energy. An example of fatigue as an early and meaningful response to dyshomeostasis is "sickness behavior" during acute infections (Dantzer and Kelley, 2007), which is characterized by fatigue, lethargy, and social withdrawal. Sickness behavior is commonly interpreted as an adaptive response which promotes the conservation and reallocation of energy to immunological defense processes (for review, see Shattuck and Muehlenbein, 2015). Second, given a perceived lack of mastery over causes of dyshomeostasis in the physical environment, it may be a better choice to let the environment evolve and change by itself; with some probability, this may lead to more favorable conditions under which existing action plans can be implemented. Third, if the cause of dyshomeostasis resides in the social environment but cannot be influenced by actions, a passive "wait and watch" strategy may offer opportunities for extending the brain's generative model—and thus scope of possible actions—by observational learning from other agents' behavior.

However, if none of the three positive effects described above materialize and the experience of dyshomeostasis becomes chronic, this may initiate a second phase characterized by a generalization of low self-efficacy beliefs—akin to learned helplessness (Abramson et al., 1978)—and the onset of depression. More specifically, an agent's experience of enduring dyshomeostasis signals a fundamental lack of mastery and control (over bodily states and thus survival) which may generalize, from the allostatic domain to other cognitive domains that are crucial for self-evaluation, planning and action selection. This draws on previous empirical findings that subjective beliefs of low self-efficacy can generalize beyond the specific situation (Bandura, 1977; Burke et al., 2015) and might result in a domain-unspecific vulnerability: the self-fulfilling expectation that one generally lacks control and cannot deploy adequate coping behavior in response to adverse events. In other words, an agent's chronic experience of dyshomeostasis may induce a generalized sense of hopelessness, which makes any actions appear futile and which triggers the onset of depression.

To prevent misunderstandings, we would like to emphasize three things. First, we neither postulate a deterministic relation between chronic dyshomeostasis and depression nor do we claim that its aetiological importance is restricted to depression. Instead, we regard a dyshomeostasis-induced sense of low self-efficacy as weakening resilience to stress in general and thus a risk factor for many forms of psychopathology. While perceived low self-efficacy likely represents an inevitable consequence of persistent dyshomeostasis, various protective factors may prevent its spread to other cognitive domains and block the generalization to hopelessness. For example, intellectual abilities or social support may maintain a sense of mastery that shields against an all-encompassing feeling of loss of control. Additionally, the experience of dyshomeostasis is usually restricted to certain bodily states but not others, leaving the possibility of experiencing preserved allostatic mastery in some domains. Second, we do not claim that a dyshomeostasis-induced sense of low self-efficacy represents a single cause for the entire depression spectrum. Instead, we propose that it may play a particularly important role in melancholia, a subtype of depression with pronounced somatic symptoms and endocrine disturbances (Parker and Paterson, 2014) that differs physiologically from other forms of depression with respect to functional connectivity of visceromotor areas, including SGC and ACC (Guo et al., 2016). Indeed, model-based indices of individual interoception and allostatic control may provide a foundation for differential diagnosis and prognosis, a theme we return to below. Third, in its present form, our theory is not designed to explain the full spectrum of interactions between fatigue and depression. Longitudinal studies have shown that the causal relation between fatigue and depression is unlikely to be unidirectional, but that both act as independent risk factors for each other (Skapinakis et al., 2004). Focusing on patients with bodily conditions that cause chronic dyshomeostasis, our theory only considers one of these directions—from dyshomeostasis to fatigue to depression. It suggests a possible mechanism (a "learned helplessness"-like generalization of perceived low self-efficacy) for the progression from fatigue to depression and, as described below, points to neurophysiological markers (in terms of effective connectivity) that may distinguish "pure fatigue" from the combined presence of fatigue and depression. By contrast, our theory is less specific in offering a mechanistic explanation for the opposite direction, i.e., how fatigue may result from depression. However, our framework would not be incompatible with the possibility that external triggers of depression might instantiate false beliefs about self-efficacy that, once fulfilled and entrenched, lead to fatigue. In other words, in this case, the generalization of low self-efficacy believes would proceed in the opposite direction as discussed above, from various cognitive domains to homeostatic/allostatic control.

Viewing fatigue and depression as sequential consequences of the subjective belief of low self-efficacy with regard to homeostatic/allostatic control frames them as metacognitive phenomena. This implies that the hierarchical circuit for interoceptive inference and homeostatic/allostatic regulation discussed above likely represents only the lower level of a more complex system which includes a higher metacognitive layer for monitoring the performance of homeostatic/allostatic control

(**Figure 7**). What exactly, however, is being monitored, and what could be the anatomical basis of this metacognitive layer?

Anatomical and Computational Aspects of Metacognition

To our knowledge, there presently exist no specific computational models of a metacognitive system for interoception and homeostatis/allostasis. Here, we outline two ideas of how such a model could look like, without going into mathematical detail. One possibility, shown in **Figure 7**, is that the metacognitive level simply represents another layer on top of the hierarchical circuit for interoception and homeostatic/allostatic control and follows the same hierarchical Bayesian principles. Specifically, this metacognitive layer (metacognitive cortex "MC" in **Figure 7**) would encode high-order beliefs about allostatic mastery, for example, the belief that one is capable of responding adaptively to any perturbation one may possibly experience. These beliefs at the metacognitive level would then serve as predictions for the visceromotor regions, and the allostatic processes elicited by the latter would serve to fulfill these higher beliefs of self-efficacy. Conversely, beliefs about allostatic self-efficacy are updated by prediction errors communicated from the visceromotor regions.

Notably, while this type of metacognitive mechanism remains to be established for interoception and allostasis, it has been shown for other domains of cognition, including low-level processes such as visual discrimination performance (Zacharopoulos et al., 2014), that a prior belief of mastery enhances the actual performance (for reviews, see Bandura, 1977, 1989). Additionally, the proposed generalization of perceived low allostatic self-efficacy as a condition for the development from fatigue to depression requires that beliefs about allostatic mastery be broadcast beyond the circuit in **Figure 7**—for example, to areas involved in metacognition about other cognitive processes or circuits involved in regulation of mood—a process that should be detectable via differential effective connectivity of regions involved in metacognition about interoception and allostasis.

An alternative is that the metacognitive system not only receives prediction error signals from the visceromotor layer but has access to all levels in the hierarchy and monitors the performance of the interoceptive circuit as a whole, without influencing it. Since this circuit represents a generative model (of viscerosensory inputs), its performance or goodness would be indicated by the log evidence for the entire circuit (i.e., the cumulative negative surprise across all levels). A key question here is over what time window (into the past) this assessment takes place. Given a chosen time window, accumulated log evidence could be approximated by the integral of free energy, a quantity known as "free action" (Friston K. et al., 2010).

Turning to the neuroanatomy of metacognition, possible anatomical substrates have been investigated for several cognitive domains, in particular (extero)perceptual performance or memory (Shimamura and Squire, 1986; Schnyer et al., 2004; Fleming et al., 2010, 2012, 2014; McCurdy et al., 2013), but not, to our knowledge, for interoception or homeostasis/allostasis. Studies explicitly focused on metacognition of interoception are largely restricted to behavior (Garfinkel et al., 2015), with few neurophysiological investigations (but see Canales-Johnson et al., 2015). For other domains of cognition, such as exteroception or memory, the anterior prefrontal cortex (roughly corresponding to Brodmann's area 10) has been identified as a key area for metacognition by several neuroimaging and lesion studies (for review, see Fleming and Dolan, 2012). While the exact evaluative or monitoring mechanisms this region may perform are not well understood, the individual capacity for metacognition (of perceptual decision-making and memory) is reflected by functional connectivity (Baird et al., 2013).

By contrast, the involvement of anterior prefrontal cortex in metacognition of interoception has, to our knowledge, received little if any attention to date. Two empirical findings indicate that anterior prefrontal cortex is not an entirely implausible candidate region. First, it is known to exhibit functional connections with all key viscerosensory and visceromotor cortical regions of the circuit in **Figure 7** (Baird et al., 2013). Second, tract tracing studies in the monkey demonstrated the existence of many of the structural connections implied by the first option described above, including direct (and largely reciprocal) connections from AIC, ACC and SGC to medial prefrontal pole (area 10 m; Carmichael and Price, 1996). Further evidence for anatomical connections between anterior prefrontal cortex and ACC as well as OFC was provided by human diffusion-weighted imaging (Liu et al., 2013).

Alternatively, the metacognitive layer may be represented within one of the visceromotor regions such as AIC or ACC; more specifically, within the hierarchically highest of their various subfields (cf. Carmichael and Price, 1996). For the ACC in particular, this possibility draws support from neuroimaging investigations that have provided evidence for a role of ACC in metacognitive functions such as performance monitoring and conflict detection (Carter et al., 1998; Botvinick et al., 1999).

Empirical Support for the Hypothesis and Future Tests of Its Predictions

Above, we described our central clinical hypothesis with regard to the pathogenesis of fatigue and depression. In brief, we outlined how fatigue can be seen as an initial adaptive response to the metacognitive diagnosis of low allostatic self-efficacy; and how the chronic experience of dyshomeostasis may trigger a second phase in which beliefs about low self-efficacy generalize, inducing an abstract sense of lack of control and an all-encompassing sense of hopelessness. While direct tests of key predictions from this hypothesis remain to be performed, some empirical data support the plausibility of our proposal.

First, various studies indicate that the expression of fatigue and depression are associated with lesions or impairments of areas from our circuit model. For multiple sclerosis, (Hanken et al., 2014) reviewed neuroimaging studies relating fatigue to structural and functional properties of insula, ACC, and hypothalamus[6]. Additionally, neuropathological studies

[6]We would like to add the cautionary note that in MS research the literature on MRI-based morphometric studies shows striking variability (see Popescu et al., 2016).

reported a high proportion of patients with inflammatory and demyelinating lesions of the hypothalamus, with indices of altered HPA activity (Huitinga et al., 2001, 2004). Most convincingly, neuropathological work focusing on cortex showed that in multiple sclerosis gray matter lesions are present throughout the entire cortex, but particularly frequently in cingulate and insular cortex (Haider et al., 2016). Concerning depression, Avery et al. (2014) examined non-medicated patients with fMRI and found that mid-insula activity during an interoceptive attention task was negatively correlated with the severity of depression and somatic symptoms; additionally functional connectivity during unconstrained cognition (rest) between mid-insula and SGC, OFC and amygdala was increased in patients and correlated with depression severity. Beyond the insula, neuroimaging has long identified SGC as a candidate site of primary pathophysiological importance in depression (Drevets et al., 1997; Mayberg et al., 1999). This region has a key role for inhibiting the amygdala and the sympathetic nervous system (Gold, 2015), which may be compromised by inflammatory processes (Miller and Raison, 2016).

Evidence from interventional studies is particularly worth noting. For example, in several elegant studies using MRI and PET in conjunction with typhoid vaccination to induce a peripheral immunological response and inflammation, Harrison and colleagues provided compelling evidence for structural and functional changes in posterior insula, anterior insula, and ACC (Harrison et al., 2009a,b, 2015). Importantly, they showed that inflammation-induced activity changes in posterior insula and ACC were associated with subjectively perceived fatigue, while activity changes in SGC predicted mood changes. Additionally, an fMRI study of patients receiving interferon-α treatment for hepatitis reported an abnormal increase in ACC activity during visuo-spatial attention (Capuron et al., 2005).

Second, clinical studies have demonstrated a striking link between fatigue and the occurrence of dyshomeostasis-inducing autonomic nervous system disorders (e.g., Stewart, 2000). Specifically, in MS patients, various measures of autonomic dysfunction correlate strongly with individual fatigue levels (Flachenecker et al., 2003; Cortez et al., 2015). However, to our knowledge, none of these studies examined metacognition about interoception or homeostasis/allostasis. Maher-Edwards et al. (2011) showed that metacognitive factors (including need for control of thoughts) predict individual levels of fatigue symptoms in CFS; however, the metacognitive assessment did not specifically consider interoception. Delgado-Pastor et al. (2015) did focus on metacognition of interoception and showed that increasing metacognitive abilities about interoception (by mindfulness-based interoceptive training) reduced worry more than increasing metacognition about other cognitive processes; however, this study did not specifically examine fatigue.

Generally, research on metacognition of interoception and homeostasis/allostasis has been relatively sparse so far (but see Khalsa et al., 2008; Garfinkel et al., 2015), and our hypothesis will require testing by specifically designed future studies. These studies will need to span four domains: behavioral-physiological studies that (i) confirm the proposed mediating role of metacognition in the link between dyshomeostasis and fatigue/depression; and computational neuroimaging studies that (ii) verify the operation of hierarchical Bayesian principles in interoceptive circuitry, (iii) demonstrate the plausibility of a metacognitive layer on top of the established circuits for homeostatic control, and (iv) demonstrate the existence of subgroups of patients in which the expression of fatigue and depression is predicted by a disturbance in either the afferent (interoceptive), efferent (control) or metacognitive branches of this system.

Importantly, testing the last three implications of our hypothesis requires mathematical models that can infer, from individual neurophysiological data, trial-wise precision-weighted predictions and prediction errors about viscerosensory inputs and how they dynamically alter connection strengths in interoceptive circuits—while respecting the layer-specific patterns of ascending (prediction errors) and descending (predictions) connections in cortical hierarchies (cf. Friston, 2008; Feldman-Barrett and Simmons, 2015). This brings us to analyses of functional and effective connectivity and methodological extensions of existing methods that are required to test our hypotheses.

EXTENDING MODELS OF EFFECTIVE CONNECTIVITY

Functional connectivity refers to statistical dependencies between neurophysiological timeseries. It can be indexed by numerous statistical approaches, e.g., correlation analysis, autoregressive models, principal or independent component analysis (PCA, ICA) (Friston, 2011). Although advanced measures of functional connectivity can unearth directed influences (Friston et al., 2013; Seth et al., 2013), by itself functional connectivity does not disclose the mechanisms by which the measured signals were caused and may be vulnerable to confounds at the measurement level.

By contrast, other approaches are based on a forward model from hidden brain states to experimental measurements. These models do not strive for statistical characterizations of the data, but try to disambiguate alternative explanations of the data. Here, the focus is on effective connectivity, i.e., the "experiment- and time-dependent, simplest possible circuit diagram that would replicate the observed timing relationships between recorded neurons" (Aertsen and Preißl, 1999).

One approach to effective connectivity is provided by biophysical network models (BNMs; Honey et al., 2007; Jirsa et al., 2010; Woolrich and Stephan, 2013). BNMs consist of numerous (typically 10^2–10^3) neuronal network nodes, each of which is represented by a neural mass or mean field model of local neuronal populations. These nodes are connected by anatomical long-range connections (often informed by diffusion-weighted imaging data), and the resulting network activity is translated into node-specific measurements through an observation model. While their biological level of detail is attractive, a major limitation of BNMs is that their high degree of complexity renders the estimation of connection-specific parameters challenging (for review, see Stephan et al., 2015). Present BNMs only allow for a very limited number of parameters to be estimated, e.g., a single global scaling factor of

connection strength (Deco et al., 2013). By contrast, testing our hypotheses requires models that provide fine-grained inference on different connections in hierarchical circuits for interoception and allostatic control (e.g., signaling of prediction errors along ascending connections originating in supragranular layers). In the future, this may be overcome by ongoing efforts to turn BNMs into fully generative models, with priors for different types of parameters, and importing advanced methods for model inversion from other approaches (for a discussion of this trend, Deco and Kringelbach, 2014; Stephan et al., 2015).

Fortunately, fully generative models are already available which fulfill many (albeit not all) of the requirements for testing the implications of our hypothesis, for example, dynamic causal modeling (DCM). Introduced in 2003 for fMRI data (Friston et al., 2003), DCM rests on a state space formulation and partitions the likelihood function (forward model) into two hierarchically related layers: while bilinear differential equations describe the dynamics of hidden (unobservable) interacting neuronal populations, a static observation equation transforms the ensuing mass activity of each population separately into a measurable signal. Inverting this model allows for inference on the effective connectivity among regions of interest, and how it is modulated by experimentally controlled conditions. Subsequent extensions have considered non-linear (Stephan et al., 2008) and stochastic differential equations (Li et al., 2011), which enable DCM to account for dynamic gain effects at synapses and intrinsic fluctuations, respectively. Similarly, extensions to the frequency domain allow for inference on connectivity from measurements during unconstrained cognition (also known as "resting state") (Friston et al., 2014a).

The bilinear terms in DCM for fMRI allow for representing trial-wise modulation of connection strengths; this makes it well-suited for studying how connection strengths vary as a function of trial-by-trial prediction errors, where the latter are typically derived from a separate model applied to behavior or stimuli (e.g., den Ouden et al., 2010). However, extending this to interoceptive prediction errors and their role in hierarchically structured circuits faces several non-trivial challenges. First, while it is easy to induce prediction errors in exteroceptive paradigms, this is less trivial in the interoceptive domain, particularly in a way that is non-invasive and patient-friendly. With the exception of manipulations of inspiratory breathing load (Paulus et al., 2012), we presently lack non-invasive methods to do so, and new paradigms will need to be developed. An alternative option is to extract prediction errors from naturally occurring irregularities in bodily rhythms (e.g., variations in heartbeat intervals); this will be presented in future work. Second, existing formulations of DCM only consider a coarse representation of neuronal populations and do not, for example, differentiate between different layers and layer-specific connections. Thus, they lack the anatomical specificity required to fully test the above predictions. With the advent of high-field MRI, it is now possible, in principle, to obtain sufficiently high resolution that separate cortical layers can be imaged in humans (e.g., Koopmans et al., 2010; Olman et al., 2012). For example, consistent with predictive coding, a recent study was able to decode contextual information from superficial laminae of parts of primary visual cortex that did not receive direct "bottom up" input but which plausibly received top-down predictions from hierarchically higher regions (Muckli et al., 2015).

However, signals in upper cortical layers are contaminated by blood draining effects from lower layers. This confounds the identification of layer-specific activity and connections and requires adapting generative models of fMRI data. While a first model was recently developed to account for these layer-specific hemodynamic effects (Heinzle et al., 2016), this is so far restricted to the level of a single region, and further work is required to extend this to a network-level DCM.

DCM has also been formulated for M/EEG data, serving to explain a variety of data features such as event-related potentials (David et al., 2006), induced responses (Chen et al., 2008), or steady-state responses (Moran et al., 2009). The rich temporal information in M/EEG data allows for modeling far more detailed circuit architectures than DCM for fMRI. Specifically, DCM for M/EEG considers columnar cortical units which consist of different types of neurons (pyramidal cells, excitatory and inhibitory interneurons) and communicate through synaptic connections with laminar specificity. This allows for differentiating between the different type of connections (ascending and descending) in cortical hierarchies, as required to test for specific effects of predictions and prediction errors. However, existing formulations of DCM for M/EEG are fitted to averaged data (e.g., event-related potentials) and only consider modulatory effects across different experimental conditions. To test our hypotheses, extensions are needed which account for trial-wise prediction error effects on connections. The poor signal-to-noise ratio of single-trial recordings poses a serious challenge for modeling (Brodersen et al., 2011) and may require adapting hierarchical (empirical Bayesian) estimation schemes (Friston et al., 2016; Raman et al., 2016) to single-trial scenaria as well as sampling schemes for model inversion in DCM; the computational costs of the latter may require moving to GPU-based numerical schemes (Aponte et al., 2016).

A third extension of generative models could move beyond the current formulations of DCM altogether and consider models that are less directly connected to physiology, but are capable of modeling perceptual inference within trials and learning (belief updates) across trials. This could encompass generative models of trial-wise M/EEG responses where, for example, trial by trial amplitudes are predicted as a linear mixture of prediction errors (Lieder et al., 2013). Alternatively, hierarchically structured predictive coding circuits (Friston, 2005; Bogacz, in press) could be used to analyse trial-wise electrophysiological data, allowing for a closer connection to physiology.

In summary, while existing generative models of neuroimaging data provide a crucial platform for testing our hypothesis, no existing model fully meets the requirements and several extensions will be required.

DIFFERENTIAL DIAGNOSIS OF FATIGUE AND DEPRESSION

If the key predictions from our hypothesis are found to be correct and if a generative model of neuroimaging or electrophysiological

measurements of the interoceptive-allostatic circuit in **Figure 7** could be established, this might have important implications for the clinical management of fatigue and depression, in particular differential diagnosis. Specifically, comparing alternative models of effective connectivity could help disambiguate different origins of circuit dysfunction leading to fatigue and depression, respectively.

The circuit model displayed by **Figure 7** highlights that fatigue could result from functional disturbances or structural lesions—such as local inflammatory or demyelinating processes—in very different locations. According to our circuit model, the experience of chronic dyshomeostasis may be due to an initial pathology at the level of:

(i) "sensors" (viscerosensory areas)—corresponding to the "illusion" of dyshomeostasis,
(ii) "allostatic predictors" (visceromotor regions)—equivalent to flawed predictions of bodily states,
(iii) "effector" regions (hypothalamus, brainstem, spinal cord)—that is, at the level of homeostatic reflex arcs,
(iv) in the body itself—for example, a disease process that evades attempts of homeostatic regulation by (at least initially) intact cerebral circuits (e.g., autoimmunological processes or cancer),
(v) at the metacognitive level—in this case, insufficient regulation of bodily states would be the consequence, not the cause, of beliefs about low allostatic self-efficacy.

This suggests that patients with fatigue and depression, respectively, could be classified into several subgroups that differ in terms of the location as well as the type of disease mechanism. While a disturbance at any of the above locations will lead to compensatory changes throughout the entire circuit, the resulting patterns of effective connectivity might be distinguishable, particularly in the context of homeostatic perturbations. Notably, in internal medicine, differential diagnosis with regard to compensatory changes in feedback circuits is commonplace, such as distinguishing metabolic and respiratory origins of acidosis, or identifying hypothalamic, pituitary or peripheral causes for endocrine dysfunction. In our approach, such differential diagnosis could be implemented formally by model selection, i.e., evaluating the evidence of different models that assume a disturbance at different branches and are fitted to electrophysiological or fMRI data from an individual patient (cf. Stephan et al., 2016a). We will examine this possibility in future work, simulating circuit activity under different types of lesions and different perturbations[7].

The first of the cases described above deserves special consideration: when there is initially no real state of dyshomeostasis, but dyshomeostasis is only subjectively perceived due to damage to viscerosensory pathways. For example, in MS, lesions frequently affect insular cortex (Haider et al., 2016); this "broken sensor" would create PE signals (interoceptive surprise) that would be interpreted by visceromotor regions as bodily dyshomeostasis. As the emitted control actions cannot reduce interoceptive surprise, a metacognitive interpretation ensues that leads to the subjective feeling of fatigue, as discussed above. This case of an "illusion" of dyshomeostasis illustrates that fatigue is always an interpretation of perceived (not necessarily real) dyshomeostasis. This may apply beyond interoception in that fatigue could also result from other forms of surprise that are not reduced by adequate actions. For example, brain damage outside interoceptive pathways can invoke general changes in performance levels, for example, slowing of cognitive and motor acts due to demyelination and hence reduced conduction speed in MS. The metacognitive detection of such a general slowing of cognition and action, and the experience that adequate actions (in this case, rest) do not reduce surprise about performance levels (metacognitive surprise), may lead to a similar sensation of fatigue as when caused by bodily dyshomeostasis. This suggests that when primary brain diseases do not impair interoception or allostatic control (e.g., cases of stroke or MS outside viscerosensory/visceromotor regions) may also induce a subjective sensation of fatigue by means of a metacognitive mechanism.

An additional possible reason for dysfunction of the interoceptive-allostatic circuit must be highlighted: aberrant neuromodulatory input. Monoaminergic brain stem nuclei are in receipt of viscerosensory inputs and project to many, if not all, components of the interoceptive-allostatic circuit in **Figure 7** (Craig, 2003; Critchley and Harrison, 2013). There is now considerable evidence that one possible cause of fatigue is an impairment of these monoaminergic brainstem projections with reduced availability of dopamine, serotonin and noradrenaline at their (sub)cortical target sites (for review, see Dantzer et al., 2014). This can be caused by inflammatory processes—not only of intra-cerebral origin, but also due to chronic peripheral inflammatory processes which, through well understood biochemical cascades, lead to reduced synthesis of dopamine, serotonin and noradrenaline in brainstem neurons (Dantzer et al., 2014). In the context of the theory proposed in this paper, a reduced dopaminergic supply in particular may impact on the precision ratio which governs the weighting of prediction errors (compare Equations 3, 6). This is because various neurophysiological studies in humans and animals indicate that one of the computational quantities encoded by variations in dopamine release is uncertainty (inverse precision) (Fiorillo et al., 2003; de Lafuente and Romo, 2011; Hart et al., 2015; Schwartenbeck et al., 2015a; Tomassini et al., 2016). Notably, many if not all regions of the interoceptive circuit in **Figure 7**, are characterized by a high density of dopaminergic receptors and terminals across all cortical layers; this is particularly well-established for visceromotor regions like AIC, ACC, or OFC (Gaspar et al., 1989; Hurd et al., 2001; Lewis et al., 2001). The role of dopamine for viscerosensory (posterior insula) regions is less well established but *in situ* hybridisation studies point to the

[7] A separate potential subgroup is worth mentioning that also relates to a concept of homeostasis but is distinct from our hypothesis. In some patients, fatigue and/or depression may not result from a metacognitive reaction to a (perceived or real) chronic state of dyshomeostasis, as our hypothesis states, but represent the result of fulfilling a high-order belief (and thus represent a state of homeostasis)—for example, that one deserves a socially inferior position along with exhaustion and sadness.

existence of dopamine receptor mRNA in human posterior insula as well (Hurd et al., 2001).

An interesting corollary of our hypothesis is that, in principle, the chronic disturbance of *any* homeostatically critical physiological variable *in any direction* has the potential of inducing fatigue and depression. This is consistent with the fact that chronic diseases of very different nature that do not directly affect the brain are frequently accompanied by fatigue and depression (e.g., hepatitis, cancer, diabetes, fibromyalgia)—and may explain the counterintuitive observation that this includes endocrine and metabolic disorders which enhance (rather than decrease) the metabolic availability of energy und the activation/excitability levels of numerous tissues, e.g., hyperthyrodism, Cushing's syndrome, or hypercalcemia (Kaltsas et al., 2010).

Finally, while the present work has focused exclusively on interoception and bodily homeostasis/allostasis, it may be seen as a prelude to a wider concept of what one might call "generalized allostasis": the active inference notion that humans have setpoints (hold beliefs) with regard to many aspects of the physical, social and cognitive world; that they try to reach these setpoints (fulfill these beliefs) by adequate actions; and that they can, in principle, prospectively adjust these setpoints in order to elicit actions. Here, one key issue is that reaching one specific setpoint may compromise one's ability to reach another. For example, holding negative beliefs about states of the world (cf. "depressive realism"; Alloy and Abramson, 1988) could be seen as an allostatic change of setpoint that renders bad outcomes expected and should therefore lead to future homeostasis. However, this may come at the cost of violating higher setpoints, such as a belief that one expects to have a certain capacity for control, or that protective forces should exist in the world (e.g., caring other agents). Similarly, ensuring one's own bodily homeostasis can conflict with beliefs about other aspects of the world, and there are ample empirical demonstrations of humans' willingness to forego bodily homeostasis and sacrifice themselves in order to fulfill beliefs that transcend their own existence—for example, beliefs that loved ones should be protected or that certain religious principles must be upheld. This raises the interesting question what, ultimately, the highest setpoint or belief is that dictates the behavior of individual humans.

CONCLUSIONS

This paper contains three main contributions. First, we revisited how traditional homeostatic concepts can be merged with Bayesian perspectives on interoception, leading to formal definitions for dyshomeostasis (chronically enhanced interoceptive surprise, or, equivalently, low evidence for the brain's generative model of viscerosensory inputs) and allostasis (the change in prior beliefs which define setpoints of homeostatic reflex arcs). Second, these definitions allowed for a bridge to metacognition and the postulate that the performance of the interoceptive circuit is being monitored by a higher metacognitive layer, possibly located in anterior prefrontal cortex, which encodes and updates beliefs about the brain's capacity to successfully regulate bodily states (allostatic self-efficacy). Third, we suggested a two-stage process where fatigue might represent an initial adaptive response to the metacognitive diagnosis of low allostatic self-efficacy, while the enduring experience of dyshomeostasis may initiate a second phase in which low self-efficacy beliefs generalize, leading to an all-encompassing sense of lack of control and hopelessness.

The perspective offered by this paper may be useful to further our understanding of the pathogenesis of fatigue, and how it may be understood as a high-level interpretation of the brain in monitoring its own efforts to control a vital part of its environment, the body. We hope that this theoretical framework and the methodological extensions of models of effective connectivity it suggests will eventually lead to applications of diagnostic utility, in particular, for stratifying patients from spectrum diseases in whom fatigue and hopelessness are leading symptoms, such as multiple sclerosis or depression.

AUTHOR CONTRIBUTIONS

Conceptual discussions: KS, ZM, CM, LW, SP, TG, MT, SF, HH, AS, and FP. Derived mathematical theory: KS, CM. Implemented the simulations: KS. Wrote the manuscript: KS, ZM, CM, LW, SP, TG, MT, SF, HH, AS, and FP. Figures: HH and KS.

ACKNOWLEDGMENTS

We acknowledge support by the René and Susanne Braginsky Foundation (KS), the University of Zurich (KS), the Dr. Mortimer and Theresa Sackler Foundation (AS), and the UZH Clinical Research Priority Programs "Multiple Sclerosis" (CRPP MS) and "Molecular Imaging" (MINZ) (KS). KS and MT were supported by the German Research Foundation in the Transregional Collaborative Research Center 134.

REFERENCES

Abramson, L. Y., Seligman, M. E., and Teasdale, J. D. (1978). Learned helplessness in humans: critique and reformulation. *J. Abnorm. Psychol.* 87, 49–74. doi: 10.1037/0021-843X.87.1.49

Adams, R. A., Perrinet, L. U., and Friston, K. (2012). Smooth pursuit and visual occlusion: active inference and oculomotor control in schizophrenia. *PLoS ONE* 7:e47502. doi: 10.1371/journal.pone.0047502

Adams, R. A., Shipp, S., and Friston, K. J. (2013a). Predictions not commands: active inference in the motor system. *Brain Struct. Funct.* 218, 611–643. doi: 10.1007/s00429-012-0475-5

Adams, R. A., Stephan, K. E., Brown, H. R., Frith, C. D., and Friston, K. J. (2013b). The computational anatomy of psychosis. *Front. Psychiatry* 4:47. doi: 10.3389/fpsyt.2013.00047

Aertsen, A., and Preißl, H. (1999). "Dynamics of activity and connectivity in physiological neuronal networks," in *Nonlinear Dynamics and Neuronal Networks*, ed H. Schuster (New York, NY: Schuster VCH Publishers), 281–302.

Alink, A., Schwiedrzik, C. M., Kohler, A., Singer, W., and Muckli, L. (2010). Stimulus predictability reduces responses in primary visual cortex. *J. Neurosci.* 30, 2960–2966. doi: 10.1523/JNEUROSCI.3730-10.2010

Allen, G. V., Saper, C. B., Hurley, K. M., and Cechetto, D. F. (1991). Organization of visceral and limbic connections in the insular cortex of the rat. *J. Comp. Neurol.* 311, 1–16. doi: 10.1002/cne.903110102

Alloy, L. B., and Abramson, L. Y. (1988). "Depressive realism: four theoretical perspectives," in *Cognitive Processes in Depression,* ed L. B. Alloy (New York, NY: Guilford Press), 223–265.

Andolina, I. M., Jones, H. E., and Sillito, A. M. (2013). Effects of cortical feedback on the spatial properties of relay cells in the lateral geniculate nucleus. *J. Neurophysiol.* 109, 889–899. doi: 10.1152/jn.00194.2012

Angelucci, A., and Bressloff, P. C. (2006). Contribution of feedforward, lateral and feedback connections to the classical receptive field center and extra-classical receptive field surround of primate V1 neurons. *Prog. Brain Res.* 154, 93–120. doi: 10.1016/S0079-6123(06)54005-1

Aponte, E. A., Raman, S., Sengupta, B., Penny, W. D., Stephan, K. E., and Heinzle, J. (2016). mpdcm: a toolbox for massively parallel dynamic causal modeling. *J. Neurosci. Methods* 257, 7–16. doi: 10.1016/j.jneumeth.2015.09.009

Arnstein, P., Caudill, M., Mandle, C. L., Norris, A., and Beasley, R. (1999). Self efficacy as a mediator of the relationship between pain intensity, disability and depression in chronic pain patients. *Pain* 80, 483–491. doi: 10.1016/S0304-3959(98)00220-6

Ashby, W. R. (1954). *Design for a Brain*. New York, NY: John Wiley & Sons.

Ashby, W. R. (1956). *An Introduction to Cybernetics*. London: Chapman & Hall.

Avery, J. A., Drevets, W. C., Moseman, S. E., Bodurka, J., Barcalow, J. C., and Simmons, W. K. (2014). Major depressive disorder is associated with abnormal interoceptive activity and functional connectivity in the insula. *Biol. Psychiatry* 76, 258–266. doi: 10.1016/j.biopsych.2013.11.027

Baird, B., Smallwood, J., Gorgolewski, K. J., and Margulies, D. S. (2013). Medial and lateral networks in anterior prefrontal cortex support metacognitive ability for memory and perception. *J. Neurosci.* 33, 16657–16665. doi: 10.1523/JNEUROSCI.0786-13.2013

Bakshi, R., Shaikh, Z. A., Miletich, R. S., Czarnecki, D., Dmochowski, J., Henschel, K., et al. (2000). Fatigue in multiple sclerosis and its relationship to depression and neurologic disability. *Mult. Scler.* 6, 181–185. doi: 10.1177/135245850000600308

Bandura, A. (1977). Self-efficacy: toward a unifying theory of behavioral change. *Psychol. Rev.* 84, 191–215. doi: 10.1037/0033-295X.84.2.191

Bandura, A. (1989). Human agency in social cognitive theory. *Am. Psychol.* 44, 1175–1184. doi: 10.1037/0003-066X.44.9.1175

Bandura, A., Barbaranelli, C., Caprara, G. V., and Pastorelli, C. (1996). Multifaceted impact of self-efficacy beliefs on academic functioning. *Child Dev.* 67, 1206–1222. doi: 10.2307/1131888

Bandura, A., O'Leary, A., Taylor, C. B., Gauthier, J., and Gossard, D. (1987). Perceived self-efficacy and pain control: opioid and nonopioid mechanisms. *J. Pers. Soc. Psychol.* 53, 563–571. doi: 10.1037/0022-3514.53.3.563

Bandura, A., Pastorelli, C., Barbaranelli, C., and Caprara, G. V. (1999). Self-efficacy pathways to childhood depression. *J. Pers. Soc. Psychol.* 76, 258–269. doi: 10.1037/0022-3514.76.2.258

Bastos, A. M., Usrey, W. M., Adams, R. A., Mangun, G. R., Fries, P., and Friston, K. J. (2012). Canonical microcircuits for predictive coding. *Neuron* 76, 695–711. doi: 10.1016/j.neuron.2012.10.038

Behrens, T. E., Woolrich, M. W., Walton, M. E., and Rushworth, M. F. (2007). Learning the value of information in an uncertain world. *Nat. Neurosci.* 10, 1214–1221. doi: 10.1038/nn1954

Bogacz, R. (in press). A tutorial on the free-energy framework for modelling perception and learning. *J. Math. Psychol.* doi: 10.1016/j.jmp.2015.11.003

Botvinick, M., Nystrom, L. E., Fissell, K., Carter, C. S., and Cohen, J. D. (1999). Conflict monitoring versus selection-for-action in anterior cingulate cortex. *Nature* 402, 179–181. doi: 10.1038/46035

Breakspear, M., Roberts, G., Green, M. J., Nguyen, V. T., Frankland, A., Levy, F., et al. (2015). Network dysfunction of emotional and cognitive processes in those at genetic risk of bipolar disorder. *Brain* 138, 3427–3439. doi: 10.1093/brain/awv261

Brodersen, K. H., Haiss, F., Ong, C. S., Jung, F., Tittgemeyer, M., Buhmann, J. M., et al. (2011). Model-based feature construction for multivariate decoding. *Neuroimage* 56, 601–615. doi: 10.1016/j.neuroimage.2010.04.036

Burke, A. L., Mathias, J. L., and Denson, L. A. (2015). Psychological functioning of people living with chronic pain: a meta-analytic review. *Br. J. Clin. Psychol.* 54, 345–360. doi: 10.1111/bjc.12078

Canales-Johnson, A., Silva, C., Huepe, D., Rivera-Rei, A., Noreika, V., Garcia Mdel, C., et al. (2015). Auditory feedback differentially modulates behavioral and neural markers of objective and subjective performance when tapping to your heartbeat. *Cereb. Cortex* 25, 4490–4503. doi: 10.1093/cercor/bhv076

Cannon, W. B. (1929). Organization for physiological homeostasis. *Physiol. Rev.* 9, 399–431.

Capuron, L., Pagnoni, G., Demetrashvili, M., Woolwine, B. J., Nemeroff, C. B., Berns, G. S., et al. (2005). Anterior cingulate activation and error processing during interferon-alpha treatment. *Biol. Psychiatry* 58, 190–196. doi: 10.1016/j.biopsych.2005.03.033

Carmichael, S. T., and Price, J. L. (1995). Limbic connections of the orbital and medial prefrontal cortex in macaque monkeys. *J. Comp. Neurol.* 363, 615–641. doi: 10.1002/cne.903630408

Carmichael, S. T., and Price, J. L. (1996). Connectional networks within the orbital and medial prefrontal cortex of macaque monkeys. *J. Comp. Neurol.* 371, 179–207.

Carter, C. S., Braver, T. S., Barch, D. M., Botvinick, M. M., Noll, D., and Cohen, J. D. (1998). Anterior cingulate cortex, error detection, and the online monitoring of performance. *Science* 280, 747–749. doi: 10.1126/science.280.5364.747

Carver, C. S., and Scheier, M. F. (1982). Control theory: a useful conceptual framework for personality-social, clinical, and health psychology. *Psychol. Bull.* 92, 111–135. doi: 10.1037/0033-2909.92.1.111

Cechetto, D. F., and Saper, C. B. (1987). Evidence for a viscerotopic sensory representation in the cortex and thalamus in the rat. *J. Comp. Neurol.* 262, 27–45. doi: 10.1002/cne.902620104

Chaudhuri, A., and Behan, P. O. (2004). Fatigue in neurological disorders. *Lancet* 363, 978–988. doi: 10.1016/S0140-6736(04)15794-2

Chen, C. C., Kiebel, S. J., and Friston, K. J. (2008). Dynamic causal modelling of induced responses. *Neuroimage* 41, 1293–1312. doi: 10.1016/j.neuroimage.2008.03.026

Chiba, T., Kayahara, T., and Nakano, K. (2001). Efferent projections of infralimbic and prelimbic areas of the medial prefrontal cortex in the Japanese monkey, Macaca fuscata. *Brain Res.* 888, 83–101. doi: 10.1016/S0006-8993(00)03013-4

Clark, I., and Dumas, G. (2015). The regulation of task performance: a trans-disciplinary review. *Front. Psychol.* 6:1862. doi: 10.3389/fpsyg.2015.01862

Conant, R. C., and Ashby, W. R. (1970). Every good regulator of a system must be a model of that system. *Int. J. Syst. Sci.* 1, 89–97. doi: 10.1080/00207727008920220

Cooray, G. K., Sengupta, B., Douglas, P., Englund, M., Wickstrom, R., and Friston, K. (2015). Characterising seizures in anti-NMDA-receptor encephalitis with dynamic causal modelling. *Neuroimage* 118, 508–519. doi: 10.1016/j.neuroimage.2015.05.064

Corlett, P. R., Frith, C. D., and Fletcher, P. C. (2009). From drugs to deprivation: a Bayesian framework for understanding models of psychosis. *Psychopharmacology (Berl).* 206, 515–530. doi: 10.1007/s00213-009-1561-0

Corlett, P. R., Taylor, J. R., Wang, X. J., Fletcher, P. C., and Krystal, J. H. (2010). Toward a neurobiology of delusions. *Prog. Neurobiol.* 92, 345–369. doi: 10.1016/j.pneurobio.2010.06.007

Cortez, M. M., Nagi Reddy, S. K., Goodman, B., Carter, J. L., and Wingerchuk, D. M. (2015). Autonomic symptom burden is associated with MS-related fatigue and quality of life. *Mult. Scler. Relat. Disord.* 4, 258–263. doi: 10.1016/j.msard.2015.03.007

Craig, A. D. (2002). How do you feel? Interoception: the sense of the physiological condition of the body. *Nat. Rev. Neurosci.* 3, 655–666. doi: 10.1038/nrn894

Craig, A. D. (2003). Interoception: the sense of the physiological condition of the body. *Curr. Opin. Neurobiol.* 13, 500–505. doi: 10.1016/S0959-4388(03)00090-4

Critchley, H. D., and Harrison, N. A. (2013). Visceral influences on brain and behavior. *Neuron* 77, 624–638. doi: 10.1016/j.neuron.2013.02.008

Dantzer, R., Heijnen, C. J., Kavelaars, A., Laye, S., and Capuron, L. (2014). The neuroimmune basis of fatigue. *Trends Neurosci.* 37, 39–46. doi: 10.1016/j.tins.2013.10.003

Dantzer, R., and Kelley, K. W. (2007). Twenty years of research on cytokine-induced sickness behavior. *Brain Behav. Immun.* 21, 153–160. doi: 10.1016/j.bbi.2006.09.006

Daunizeau, J., David, O., and Stephan, K. E. (2011). Dynamic causal modelling: a critical review of the biophysical and statistical foundations. *Neuroimage* 58, 312–322. doi: 10.1016/j.neuroimage.2009.11.062

Daunizeau, J., den Ouden, H. E., Pessiglione, M., Kiebel, S. J., Stephan, K. E., and Friston, K. J. (2010). Observing the observer (I): meta-bayesian models of learning and decision-making. *PLoS ONE* 5:e15554. doi: 10.1371/journal.pone.0015554

David, O., Kiebel, S. J., Harrison, L. M., Mattout, J., Kilner, J. M., and Friston, K. J. (2006). Dynamic causal modeling of evoked responses in EEG and MEG. *Neuroimage* 30, 1255–1272. doi: 10.1016/j.neuroimage.2005.10.045

Dayan, P., and Daw, N. D. (2008). Decision theory, reinforcement learning, and the brain. *Cogn. Affect. Behav. Neurosci.* 8, 429–453. doi: 10.3758/CABN.8.4.429

Dayan, P., Hinton, G. E., Neal, R. M., and Zemel, R. S. (1995). The Helmholtz machine. *Neural Comput.* 7, 889–904. doi: 10.1162/neco.1995.7.5.889

Deco, G., and Kringelbach, M. L. (2014). Great expectations: using whole-brain computational connectomics for understanding neuropsychiatric disorders. *Neuron* 84, 892–905. doi: 10.1016/j.neuron.2014.08.034

Deco, G., Ponce-Alvarez, A., Mantini, D., Romani, G. L., Hagmann, P., and Corbetta, M. (2013). Resting-state functional connectivity emerges from structurally and dynamically shaped slow linear fluctuations. *J. Neurosci.* 33, 11239–11252. doi: 10.1523/JNEUROSCI.1091-13.2013

de Lafuente, V., and Romo, R. (2011). Dopamine neurons code subjective sensory experience and uncertainty of perceptual decisions. *Proc. Natl. Acad. Sci. U.S.A.* 108, 19767–19771. doi: 10.1073/pnas.1117636108

Delgado-Pastor, L. C., Ciria, L. F., Blanca, B., Mata, J. L., Vera, M. N., and Vila, J. (2015). Dissociation between the cognitive and interoceptive components of mindfulness in the treatment of chronic worry. *J. Behav. Ther. Exp. Psychiatry* 48, 192–199. doi: 10.1016/j.jbtep.2015.04.001

Denison, E., Asenlof, P., and Lindberg, P. (2004). Self-efficacy, fear avoidance, and pain intensity as predictors of disability in subacute and chronic musculoskeletal pain patients in primary health care. *Pain* 111, 245–252. doi: 10.1016/j.pain.2004.07.001

den Ouden, H. E., Daunizeau, J., Roiser, J., Friston, K. J., and Stephan, K. E. (2010). Striatal prediction error modulates cortical coupling. *J. Neurosci.* 30, 3210–3219. doi: 10.1523/JNEUROSCI.4458-09.2010

Doya, K., Ishii, S., Pouget, A., and Rao, R. P. (2011). *Bayesian Brain: Probabilistic Approaches to Neural Coding*. Cambridge, MA: MIT Press.

Drevets, W. C., Price, J. L., Simpson, J. R. Jr., Todd, R. D., Reich, T., Vannier, M., et al. (1997). Subgenual prefrontal cortex abnormalities in mood disorders. *Nature* 386, 824–827. doi: 10.1038/386824a0

Feldman-Barrett, L. F., and Simmons, W. K. (2015). Interoceptive predictions in the brain. *Nat. Rev. Neurosci.* 16, 419–429. doi: 10.1038/nrn3950

Felleman, D. J., and Van Essen, D. C. (1991). Distributed hierarchical processing in the primate cerebral cortex. *Cereb. Cortex* 1, 1–47. doi: 10.1093/cercor/1.1.1

Fiorillo, C. D., Tobler, P. N., and Schultz, W. (2003). Discrete coding of reward probability and uncertainty by dopamine neurons. *Science* 299, 1898–1902. doi: 10.1126/science.1077349

Flachenecker, P., Rufer, A., Bihler, I., Hippel, C., Reiners, K., Toyka, K. V., et al. (2003). Fatigue in MS is related to sympathetic vasomotor dysfunction. *Neurology* 61, 851–853. doi: 10.1212/01.WNL.0000080365.95436.B8

Fleming, S. M., and Dolan, R. J. (2012). The neural basis of metacognitive ability. *Philos. Trans. R. Soc. Lond. B. Biol. Sci.* 367, 1338–1349. doi: 10.1098/rstb.2011.0417

Fleming, S. M., Huijgen, J., and Dolan, R. J. (2012). Prefrontal contributions to metacognition in perceptual decision making. *J. Neurosci.* 32, 6117–6125. doi: 10.1523/JNEUROSCI.6489-11.2012

Fleming, S. M., Ryu, J., Golfinos, J. G., and Blackmon, K. E. (2014). Domain-specific impairment in metacognitive accuracy following anterior prefrontal lesions. *Brain* 137, 2811–2822. doi: 10.1093/brain/awu221

Fleming, S. M., Weil, R. S., Nagy, Z., Dolan, R. J., and Rees, G. (2010). Relating introspective accuracy to individual differences in brain structure. *Science* 329, 1541–1543. doi: 10.1126/science.1191883

Freedman, L. J., Insel, T. R., and Smith, Y. (2000). Subcortical projections of area 25 (subgenual cortex) of the macaque monkey. *J. Comp. Neurol.* 421, 172–188. doi: 10.1002/(SICI)1096-9861(20000529)421:2<172::AID-CNE4>3.0.CO;2-8

Friston, K. (2003). Learning and inference in the brain. *Neural Netw.* 16, 1325–1352. doi: 10.1016/j.neunet.2003.06.005

Friston, K. (2005). A theory of cortical responses. *Philos. Trans. R. Soc. Lond. B. Biol. Sci.* 360, 815–836. doi: 10.1098/rstb.2005.1622

Friston, K. (2008). Hierarchical models in the brain. *PLoS Comput. Biol.* 4:e1000211. doi: 10.1371/journal.pcbi.1000211

Friston, K. (2009). The free-energy principle: a rough guide to the brain? *Trends Cogn. Sci.* 13, 293–301. doi: 10.1016/j.tics.2009.04.005

Friston, K. (2010). The free-energy principle: a unified brain theory? *Nat. Rev. Neurosci.* 11, 127–138. doi: 10.1038/nrn2787

Friston, K., Adams, R., and Montague, R. (2012). What is value-accumulated reward or evidence? *Front. Neurorobot.* 6:11. doi: 10.3389/fnbot.2012.00011

Friston, K. J. (2011). Functional and effective connectivity: a review. *Brain Connect.* 1, 13–36. doi: 10.1089/brain.2011.0008

Friston, K. J., Daunizeau, J., Kilner, J., and Kiebel, S. J. (2010). Action and behavior: a free-energy formulation. *Biol. Cybern.* 102, 227–260. doi: 10.1007/s00422-010-0364-z

Friston, K. J., Harrison, L., and Penny, W. (2003). Dynamic causal modelling. *Neuroimage* 19, 1273–1302. doi: 10.1016/S1053-8119(03)00202-7

Friston, K. J., Kahan, J., Biswal, B., and Razi, A. (2014a). A DCM for resting state fMRI. *Neuroimage* 94, 396–407. doi: 10.1016/j.neuroimage.2013.12.009

Friston, K. J., Litvak, V., Oswal, A., Razi, A., Stephan, K. E., van Wijk, B. C., et al. (2016). Bayesian model reduction and empirical Bayes for group (DCM) studies. *Neuroimage* 128, 413–431. doi: 10.1016/j.neuroimage.2015.11.015

Friston, K. J., Stephan, K. E., Montague, R., and Dolan, R. J. (2014b). Computational psychiatry: the brain as a phantastic organ. *Lancet Psychiatry* 1, 148–158. doi: 10.1016/S2215-0366(14)70275-5

Friston, K., Kilner, J., and Harrison, L. (2006). A free energy principle for the brain. *J. Physiol. Paris* 100, 70–87. doi: 10.1016/j.jphysparis.2006.10.001

Friston, K., Moran, R., and Seth, A. K. (2013). Analysing connectivity with Granger causality and dynamic causal modelling. *Curr. Opin. Neurobiol.* 23, 172–178. doi: 10.1016/j.conb.2012.11.010

Friston, K., Rigoli, F., Ognibene, D., Mathys, C., Fitzgerald, T., and Pezzulo, G. (2015). Active inference and epistemic value. *Cogn. Neurosci.* 6, 187–214. doi: 10.1080/17588928.2015.1020053

Friston, K., Stephan, K. E., Li, B., and Daunizeau, J. (2010). Generalised filtering. *Math. Prob. Eng.* 2010:621670. doi: 10.1155/2010/621670

Frith, C. D., and Frith, U. (2012). Mechanisms of social cognition. *Annu. Rev. Psychol.* 63, 287–313. doi: 10.1146/annurev-psych-120710-100449

Garfinkel, S. N., Seth, A. K., Barrett, A. B., Suzuki, K., and Critchley, H. D. (2015). Knowing your own heart: distinguishing interoceptive accuracy from interoceptive awareness. *Biol. Psychol.* 104, 65–74. doi: 10.1016/j.biopsycho.2014.11.004

Garrido, M. I., Friston, K. J., Kiebel, S. J., Stephan, K. E., Baldeweg, T., and Kilner, J. M. (2008). The functional anatomy of the MMN: a DCM study of the roving paradigm. *Neuroimage* 42, 936–944. doi: 10.1016/j.neuroimage.2008.05.018

Gaspar, P., Berger, B., Febvret, A., Vigny, A., and Henry, J. P. (1989). Catecholamine innervation of the human cerebral cortex as revealed by comparative immunohistochemistry of tyrosine hydroxylase and dopamine-beta-hydroxylase. *J. Comp. Neurol.* 279, 249–271. doi: 10.1002/cne.902790208

Geisler, W. S., and Diehl, R. L. (2002). Bayesian natural selection and the evolution of perceptual systems. *Philos. Trans. R. Soc. Lond. B. Biol. Sci.* 357, 419–448. doi: 10.1098/rstb.2001.1055

Geisler, W. S., and Kersten, D. (2002). Illusions, perception and Bayes. *Nat. Neurosci.* 5, 508–510. doi: 10.1038/nn0602-508

Gilbert, J. R., Symmonds, M., Hanna, M. G., Dolan, R. J., Friston, K. J., and Moran, R. J. (2016). Profiling neuronal ion channelopathies with non-invasive brain imaging and dynamic causal models: case studies of single gene mutations. *Neuroimage* 124, 43–53. doi: 10.1016/j.neuroimage.2015.08.057

Gold, P. W. (2015). The organization of the stress system and its dysregulation in depressive illness. *Mol. Psychiatry* 20, 32–47. doi: 10.1038/mp.2014.163

Gray, M. A., Harrison, N. A., Wiens, S., and Critchley, H. D. (2007). Modulation of emotional appraisal by false physiological feedback during fMRI. *PLoS ONE* 2:e546. doi: 10.1371/journal.pone.0000546

Gruol, D. L. (2015). IL-6 regulation of synaptic function in the CNS. *Neuropharmacology* 96, 42–54. doi: 10.1016/j.neuropharm.2014.10.023

Gu, X., Hof, P. R., Friston, K. J., and Fan, J. (2013). Anterior insular cortex and emotional awareness. *J. Comp. Neurol.* 521, 3371–3388. doi: 10.1002/cne.23368

Guo, C. C., Hyett, M. P., Nguyen, V. T., Parker, G. B., and Breakspear, M. J. (2016). Distinct neurobiological signatures of brain connectivity in depression

subtypes during natural viewing of emotionally salient films. *Psychol. Med.* 46, 1535–1545. doi: 10.1017/S0033291716000179

Haider, L., Zrzavy, T., Hametner, S., Hoftberger, R., Bagnato, F., Grabner, G., et al. (2016). The topograpy of demyelination and neurodegeneration in the multiple sclerosis brain. *Brain* 139, 807–815. doi: 10.1093/brain/awv398

Hanken, K., Eling, P., and Hildebrandt, H. (2014). The representation of inflammatory signals in the brain - a model for subjective fatigue in multiple sclerosis. *Front. Neurol.* 5:264. doi: 10.3389/fneur.2014.00264

Harrison, N. A., Brydon, L., Walker, C., Gray, M. A., Steptoe, A., and Critchley, H. D. (2009a). Inflammation causes mood changes through alterations in subgenual cingulate activity and mesolimbic connectivity. *Biol. Psychiatry* 66, 407–414. doi: 10.1016/j.biopsych.2009.03.015

Harrison, N. A., Brydon, L., Walker, C., Gray, M. A., Steptoe, A., Dolan, R. J., et al. (2009b). Neural origins of human sickness in interoceptive responses to inflammation. *Biol. Psychiatry* 66, 415–422. doi: 10.1016/j.biopsych.2009.03.007

Harrison, N. A., Cooper, E., Dowell, N. G., Keramida, G., Voon, V., Critchley, H. D., et al. (2015). Quantitative magnetization transfer imaging as a biomarker for effects of systemic inflammation on the brain. *Biol. Psychiatry* 78, 49–57. doi: 10.1016/j.biopsych.2014.09.023

Hart, A. S., Clark, J. J., and Phillips, P. E. (2015). Dynamic shaping of dopamine signals during probabilistic Pavlovian conditioning. *Neurobiol. Learn. Mem.* 117, 84–92. doi: 10.1016/j.nlm.2014.07.010

Heinzle, J., Koopmans, P. J., den Ouden, H. E., Raman, S., and Stephan, K. E. (2016). A hemodynamic model for layered BOLD signals. *Neuroimage* 125, 556–570. doi: 10.1016/j.neuroimage.2015.10.025

Helmholtz, H. (1860/1962). *Handbuch der Physiologischen Optik*, ed J. P. C. Southall. New York, NY: Dover.

Herz, D. M., Florin, E., Christensen, M. S., Reck, C., Barbe, M. T., Tscheuschler, M. K., et al. (2014). Dopamine replacement modulates oscillatory coupling between premotor and motor cortical areas in Parkinson's disease. *Cereb. Cortex* 24, 2873–2883. doi: 10.1093/cercor/bht140

Hilgetag, C. C., O'Neill, M. A., and Young, M. P. (2000). Hierarchical organization of macaque and cat cortical sensory systems explored with a novel network processor. *Philos. Trans. R. Soc. Lond. B. Biol. Sci.* 355, 71–89. doi: 10.1098/rstb.2000.0550

Honey, C. J., Kotter, R., Breakspear, M., and Sporns, O. (2007). Network structure of cerebral cortex shapes functional connectivity on multiple time scales. *Proc. Natl. Acad. Sci. U.S.A.* 104, 10240–10245. doi: 10.1073/pnas.0701519104

Hsu, D. T., and Price, J. L. (2007). Midline and intralaminar thalamic connections with the orbital and medial prefrontal networks in macaque monkeys. *J. Comp. Neurol.* 504, 89–111. doi: 10.1002/cne.21440

Huitinga, I., De Groot, C. J., Van der Valk, P., Kamphorst, W., Tilders, F. J., and Swaab, D. F. (2001). Hypothalamic lesions in multiple sclerosis. *J. Neuropathol. Exp. Neurol.* 60, 1208–1218. doi: 10.1093/jnen/60.12.1208

Huitinga, I., Erkut, Z. A., van Beurden, D., and Swaab, D. F. (2004). Impaired hypothalamus-pituitary-adrenal axis activity and more severe multiple sclerosis with hypothalamic lesions. *Ann. Neurol.* 55, 37–45. doi: 10.1002/ana.10766

Hurd, Y. L., Suzuki, M., and Sedvall, G. C. (2001). D1 and D2 dopamine receptor mRNA expression in whole hemisphere sections of the human brain. *J. Chem. Neuroanat.* 22, 127–137. doi: 10.1016/S0891-0618(01)00122-3

Hurley, K. M., Herbert, H., Moga, M. M., and Saper, C. B. (1991). Efferent projections of the infralimbic cortex of the rat. *J. Comp. Neurol.* 308, 249–276. doi: 10.1002/cne.903080210

Huys, Q. J., Maia, T. V., and Frank, M. J. (2016). Computational psychiatry as a bridge from neuroscience to clinical applications. *Nat. Neurosci.* 19, 404–413. doi: 10.1038/nn.4238

Hyett, M. P., Breakspear, M. J., Friston, K. J., Guo, C. C., and Parker, G. B. (2015). Disrupted effective connectivity of cortical systems supporting attention and interoception in melancholia. *JAMA Psychiatry* 72, 350–358. doi: 10.1001/jamapsychiatry.2014.2490

Jirsa, V. K., Sporns, O., Breakspear, M., Deco, G., and McIntosh, A. R. (2010). Towards the virtual brain: network modeling of the intact and the damaged brain. *Arch. Ital. Biol.* 148, 189–205. Available online at: http://www.architalbiol.org/aib/article/view/148189/21175008

Kaltsas, G., Vgontzas, A., and Chrousos, G. (2010). Fatigue, endocrinopathies, and metabolic disorders. *PM R* 2, 393–398. doi: 10.1016/j.pmrj.2010.04.011

Kass, R. E., and Steffey, D. (1989). Approximate Bayesian inference in conditionally independent hierarchical models (parametric empirical Bayes models). *J. Am. Stat. Assoc.* 84, 171–726. doi: 10.1080/01621459.1989.10478825

Keramati, M., and Gutkin, B. (2014). Homeostatic reinforcement learning for integrating reward collection and physiological stability. *Elife* 3:e04811. doi: 10.7554/eLife.04811

Kersten, D., Mamassian, P., and Yuille, A. (2004). Object perception as Bayesian inference. *Annu. Rev. Psychol.* 55, 271–304. doi: 10.1146/annurev.psych.55.090902.142005

Khalsa, S. S., Rudrauf, D., Damasio, A. R., Davidson, R. J., Lutz, A., and Tranel, D. (2008). Interoceptive awareness in experienced meditators. *Psychophysiology* 45, 671–677. doi: 10.1111/j.1469-8986.2008.00666.x

Kluger, B. M., Krupp, L. B., and Enoka, R. M. (2013). Fatigue and fatigability in neurologic illnesses: proposal for a unified taxonomy. *Neurology* 80, 409–416. doi: 10.1212/WNL.0b013e31827f07be

Knill, D., and Richards, W. (1996). *Perception as Bayesian Inference*. Cambridge: Cambridge University Press.

Koopmans, P. J., Barth, M., and Norris, D. G. (2010). Layer-specific BOLD activation in human V1. *Hum. Brain Mapp.* 31, 1297–1304. doi: 10.1002/hbm.20936

Körding, K. (2007). Decision theory: what "should" the nervous system do? *Science* 318, 606–610. doi: 10.1126/science.1142998

Kroencke, D. C., Lynch, S. G., and Denney, D. R. (2000). Fatigue in multiple sclerosis: relationship to depression, disability, and disease pattern. *Mult. Scler.* 6, 131–136. doi: 10.1177/135245850000600213

Larun, L., Brurberg, K. G., Odgaard-Jensen, J., and Price, J. R. (2016). Exercise therapy for chronic fatigue syndrome. *Cochrane Database Syst. Rev.* 2:CD003200. doi: 10.1002/14651858.CD003200.pub4

Lee, T. S., and Mumford, D. (2003). Hierarchical Bayesian inference in the visual cortex. *J. Opt. Soc. Am. A Opt. Image Sci. Vis.* 20, 1434–1448. doi: 10.1364/JOSAA.20.001434

Lewis, D. A., Melchitzky, D. S., Sesack, S. R., Whitehead, R. E., Auh, S., and Sampson, A. (2001). Dopamine transporter immunoreactivity in monkey cerebral cortex: regional, laminar, and ultrastructural localization. *J. Comp. Neurol.* 432, 119–136. doi: 10.1002/cne.1092

Li, B., Daunizeau, J., Stephan, K. E., Penny, W., Hu, D., and Friston, K. (2011). Generalised filtering and stochastic DCM for fMRI. *Neuroimage* 58, 442–457. doi: 10.1016/j.neuroimage.2011.01.085

Lieder, F., Daunizeau, J., Garrido, M. I., Friston, K. J., and Stephan, K. E. (2013). Modelling trial-by-trial changes in the mismatch negativity. *PLoS Comput. Biol.* 9:e1002911. doi: 10.1371/journal.pcbi.1002911

Liu, H., Qin, W., Li, W., Fan, L., Wang, J., Jiang, T., et al. (2013). Connectivity-based parcellation of the human frontal pole with diffusion tensor imaging. *J. Neurosci.* 33, 6782–6790. doi: 10.1523/JNEUROSCI.4882-12.2013

Maher-Edwards, L., Fernie, B. A., Murphy, G., Wells, A., and Spada, M. M. (2011). Metacognitions and negative emotions as predictors of symptom severity in chronic fatigue syndrome. *J. Psychosom. Res.* 70, 311–317. doi: 10.1016/j.jpsychores.2010.09.016

Marr, D. (1982). *Vision: A Computational Investigation into the Human Representation and Processing of Visual Information.* New York, NY: Freeman.

Mathys, C. (2016). "How could we get nosology from computation?," in *Computational Psychiatry: New Perspectives on Mental Illness*, eds D. Reddish and J. Gordon (Boston, MA: MIT Press).

Mathys, C., Daunizeau, J., Friston, K. J., and Stephan, K. E. (2011). A Bayesian foundation for individual learning under uncertainty. *Front. Hum. Neurosci.* 5:39. doi: 10.3389/fnhum.2011.00039

Mathys, C. D., Lomakina, E. I., Daunizeau, J., Iglesias, S., Brodersen, K. H., Friston, K. J., et al. (2014). Uncertainty in perception and the Hierarchical Gaussian Filter. *Front. Hum. Neurosci.* 8:825. doi: 10.3389/fnhum.2014.00825

Mayberg, H. S., Liotti, M., Brannan, S. K., McGinnis, S., Mahurin, R. K., Jerabek, P. A., et al. (1999). Reciprocal limbic-cortical function and negative mood: converging PET findings in depression and normal sadness. *Am. J. Psychiatry* 156, 675–682.

McCurdy, L. Y., Maniscalco, B., Metcalfe, J., Liu, K. Y., de Lange, F. P., and Lau, H. (2013). Anatomical coupling between distinct metacognitive systems for memory and visual perception. *J. Neurosci.* 33, 1897–1906. doi: 10.1523/JNEUROSCI.1890-12.2013

Mesulam, M. M., and Mufson, E. J. (1982). Insula of the old world monkey. III: efferent cortical output and comments on function. *J. Comp. Neurol.* 212, 38–52. doi: 10.1002/cne.902120104

Miller, A. H., and Raison, C. L. (2016). The role of inflammation in depression: from evolutionary imperative to modern treatment target. *Nat. Rev. Immunol.* 16, 22–34. doi: 10.1038/nri.2015.5

Modell, H., Cliff, W., Michael, J., McFarland, J., Wenderoth, M. P., and Wright, A. (2015). A physiologist's view of homeostasis. *Adv. Physiol. Educ.* 39, 259–266. doi: 10.1152/advan.00107.2015

Montague, P. R., Dolan, R. J., Friston, K. J., and Dayan, P. (2012). Computational psychiatry. *Trends Cogn. Sci.* 16, 72–80. doi: 10.1016/j.tics.2011.11.018

Moran, R. J., Stephan, K. E., Seidenbecher, T., Pape, H. C., Dolan, R. J., and Friston, K. J. (2009). Dynamic causal models of steady-state responses. *Neuroimage* 44, 796–811. doi: 10.1016/j.neuroimage.2008.09.048

Muckli, L., De Martino, F., Vizioli, L., Petro, L. S., Smith, F. W., Ugurbil, K., et al. (2015). Contextual feedback to superficial layers of V1. *Curr. Biol.* 25, 2690–2695. doi: 10.1016/j.cub.2015.08.057

Mufson, E. J., and Mesulam, M. M. (1982). Insula of the old world monkey. II: afferent cortical input and comments on the claustrum. *J. Comp. Neurol.* 212, 23–37. doi: 10.1002/cne.902120103

Mumford, D. (1992). On the computational architecture of the neocortex. II. The role of cortico-cortical loops. *Biol. Cybern.* 66, 241–251. doi: 10.1007/BF00198477

Nair, A., and Bonneau, R. H. (2006). Stress-induced elevation of glucocorticoids increases microglia proliferation through NMDA receptor activation. *J. Neuroimmunol.* 171, 72–85. doi: 10.1016/j.jneuroim.2005.09.012

Nassi, J. J., Lomber, S. G., and Born, R. T. (2013). Corticocortical feedback contributes to surround suppression in V1 of the alert primate. *J. Neurosci.* 33, 8504–8517. doi: 10.1523/JNEUROSCI.5124-12.2013

Olman, C. A., Harel, N., Feinberg, D. A., He, S., Zhang, P., Ugurbil, K., et al. (2012). Layer-specific fMRI reflects different neuronal computations at different depths in human V1. *PLoS ONE* 7:e32536. doi: 10.1371/journal.pone.0032536

Parker, G., and Paterson, A. (2014). Melancholia: definition and management. *Curr. Opin. Psychiatry* 27, 1–6. doi: 10.1097/YCO.0000000000000024

Patejdl, R., Penner, I. K., Noack, T. K., and Zettl, U. K. (2016). Multiple sclerosis and fatigue: a review on the contribution of inflammation and immune-mediated neurodegeneration. *Autoimmun. Rev.* 15, 210–220. doi: 10.1016/j.autrev.2015.11.005

Paulus, M. P., Flagan, T., Simmons, A. N., Gillis, K., Kotturi, S., Thom, N., et al. (2012). Subjecting elite athletes to inspiratory breathing load reveals behavioral and neural signatures of optimal performers in extreme environments. *PLoS ONE* 7:e29394. doi: 10.1371/journal.pone.0029394

Paulus, M. P., and Stein, M. B. (2006). An insular view of anxiety. *Biol. Psychiatry* 60, 383–387. doi: 10.1016/j.biopsych.2006.03.042

Penny, W. D. (2012). Comparing dynamic causal models using AIC, BIC and free energy. *Neuroimage* 59, 319–330. doi: 10.1016/j.neuroimage.2011.07.039

Penny, W., and Stephan, K. E. (2014). A dynamic Bayesian model of homeostatic control. *Lecture Notes Comput. Sci.* 8779, 60–69. doi: 10.1007/978-3-319-11298-5_7

Petzschner, F. H., Glasauer, S., and Stephan, K. E. (2015). A Bayesian perspective on magnitude estimation. *Trends Cogn. Sci.* 19, 285–293. doi: 10.1016/j.tics.2015.03.002

Pezzulo, G., Rigoli, F., and Friston, K. (2015). Active Inference, homeostatic regulation and adaptive behavioural control. *Prog. Neurobiol.* 134, 17–35. doi: 10.1016/j.pneurobio.2015.09.001

Pittion-Vouyovitch, S., Debouverie, M., Guillemin, F., Vandenberghe, N., Anxionnat, R., and Vespignani, H. (2006). Fatigue in multiple sclerosis is related to disability, depression and quality of life. *J. Neurol. Sci.* 243, 39–45. doi: 10.1016/j.jns.2005.11.025

Popescu, V., Schoonheim, M. M., Versteeg, A., Chaturvedi, N., Jonker, M., de Menezes, R. X., et al. (2016). Grey matter atrophy in multiple sclerosis: clinical interpretation depends on choice of analysis method. *PLoS One* 11:e0143942. doi: 10.1371/journal.pone.0143942

Powers, W. T. (1973). Feedback: beyond behaviorism. *Science* 179, 351–356. doi: 10.1126/science.179.4071.351

Powers, W. T. (1978). Quantitative analysis of purposive systems: some spadework at the foundations of scientific psychology. *Psychol. Rev.* 85, 417–435. doi: 10.1037/0033-295X.85.5.417

Raman, S., Deserno, L., Schlagenhauf, F., and Stephan, K. E. (2016). A hierarchical model for integrating unsupervised generative embedding and empirical Bayes. *J. Neurosci. Methods* 269, 6–20. doi: 10.1016/j.jneumeth.2016.04.022

Rao, R. P., and Ballard, D. H. (1999). Predictive coding in the visual cortex: a functional interpretation of some extra-classical receptive-field effects. *Nat. Neurosci.* 2, 79–87. doi: 10.1038/4580

Richards, J., and von Glasersfeld, E. (1979). The control of perception and the construction of reality: epistemological aspects of the feedback-control system. *Dialectica* 33, 37–58. doi: 10.1111/j.1746-8361.1979.tb01519.x

Rosenbaum, M., and Hadari, D. (1985). Personal efficacy, external locus of control, and perceived contingency of parental reinforcement among depressed, paranoid, and normal subjects. *J. Pers. Soc. Psychol.* 49, 539–547. doi: 10.1037/0022-3514.49.2.539

Saper, C. B. (2002). The central autonomic nervous system: conscious visceral perception and autonomic pattern generation. *Annu. Rev. Neurosci.* 25, 433–469. doi: 10.1146/annurev.neuro.25.032502.111311

Sapolsky, R. M. (2015). Stress and the brain: individual variability and the inverted-U. *Nat. Neurosci.* 18, 1344–1346. doi: 10.1038/nn.4109

Schlagenhauf, F., Huys, Q. J., Deserno, L., Rapp, M. A., Beck, A., Heinze, H. J., et al. (2014). Striatal dysfunction during reversal learning in unmedicated schizophrenia patients. *Neuroimage* 89, 171–180. doi: 10.1016/j.neuroimage.2013.11.034

Schmidt, A., Diaconescu, A. O., Kometer, M., Friston, K. J., Stephan, K. E., and Vollenweider, F. X. (2013). Modeling ketamine effects on synaptic plasticity during the mismatch negativity. *Cereb. Cortex* 23, 2394–2406. doi: 10.1093/cercor/bhs238

Schnyer, D. M., Verfaellie, M., Alexander, M. P., LaFleche, G., Nicholls, L., and Kaszniak, A. W. (2004). A role for right medial prefontal cortex in accurate feeling-of-knowing judgements: evidence from patients with lesions to frontal cortex. *Neuropsychologia* 42, 957–966. doi: 10.1016/j.neuropsychologia.2003.11.020

Schwartenbeck, P., FitzGerald, T. H., Mathys, C., Dolan, R., and Friston, K. (2015a). The dopaminergic midbrain encodes the expected certainty about desired outcomes. *Cereb. Cortex* 25, 3434–3445. doi: 10.1093/cercor/bhu159

Schwartenbeck, P., FitzGerald, T. H., Mathys, C., Dolan, R., Wurst, F., Kronbichler, M., et al. (2015b). Optimal inference with suboptimal models: addiction and active Bayesian inference. *Med. Hypotheses* 84, 109–117. doi: 10.1016/j.mehy.2014.12.007

Seth, A. K. (2013). Interoceptive inference, emotion, and the embodied self. *Trends Cogn. Sci.* 17, 565–573. doi: 10.1016/j.tics.2013.09.007

Seth, A. K. (2015a). "The cybernetic Bayesian brain: from interoceptive inference to sensorimotor contingencies," in *Open MIND*, eds T. Metzinger and J. Windt (Frankfurt: MIND Group), 1–24. doi: 10.15502/9783958570108

Seth, A. K. (2015b). "Inference to the best prediction," in *Open MIND*, eds T. Metzinger and J. Windt (Frankfurt: MIND Group), 1–8. doi: 10.15502/9783958570986

Seth, A. K. (2015c). Presence, objecthood, and the phenomenology of predictive perception. *Cogn. Neurosci.* 6, 111–117. doi: 10.1080/17588928.2015.1026888

Seth, A. K., Chorley, P., and Barnett, L. C. (2013). Granger causality analysis of fMRI BOLD signals is invariant to hemodynamic convolution but not downsampling. *Neuroimage* 65, 540–555. doi: 10.1016/j.neuroimage.2012.09.049

Seth, A. K., Suzuki, K., and Critchley, H. D. (2011). An interoceptive predictive coding model of conscious presence. *Front. Psychol.* 2:395. doi: 10.3389/fpsyg.2011.00395

Shattuck, E. C., and Muehlenbein, M. P. (2015). Human sickness behavior: ultimate and proximate explanations. *Am. J. Phys. Anthropol.* 157, 1–18. doi: 10.1002/ajpa.22698

Shimamura, A. P., and Squire, L. R. (1986). Memory and metamemory: a study of the feeling-of-knowing phenomenon in amnesic patients. *J. Exp. Psychol. Learn. Mem. Cogn.* 12, 452–460. doi: 10.1037/0278-7393.12.3.452

Skapinakis, P., Lewis, G., and Mavreas, V. (2004). Temporal relations between unexplained fatigue and depression: longitudinal data from an international study in primary care. *Psychosom. Med.* 66, 330–335. doi: 10.1097/01.psy.0000124757.10167.b1

Srinivasan, M. V., Laughlin, S. B. and Dubs, A. (1982). Predictive coding: a fresh view of inhibition in the retina. *Proc. R. Soc. Lond. B Biol. Sci.* 216, 427–459. doi: 10.1098/rspb.1982.0085

Stephan, K. E., Bach, D. R., Fletcher, P. C., Flint, J., Frank, M. J., Friston, K. J., et al. (2016a). Charting the landscape of priority problems in psychiatry, part 1: classification and diagnosis. *Lancet Psychiatry* 3, 77–83. doi: 10.1016/S2215-0366(15)00361-2

Stephan, K. E., Diaconescu, A. O., and Iglesias, S. (2016b). Bayesian inference, dysconnectivity and neuromodulation in schizophrenia. *Brain* 139, 1874–1876. doi: 10.1093/brain/aww120

Stephan, K. E., Iglesias, S., Heinzle, J., and Diaconescu, A. O. (2015). Translational perspectives for computational neuroimaging. *Neuron* 87, 716–732. doi: 10.1016/j.neuron.2015.07.008

Stephan, K. E., Kasper, L., Harrison, L. M., Daunizeau, J., den Ouden, H. E., Breakspear, M., et al. (2008). Nonlinear dynamic causal models for fMRI. *Neuroimage* 42, 649–662. doi: 10.1016/j.neuroimage.2008.04.262

Stephan, K. E., and Mathys, C. (2014). Computational approaches to psychiatry. *Curr. Opin. Neurobiol.* 25, 85–92. doi: 10.1016/j.conb.2013.12.007

Stephan, K. E., Penny, W. D., Daunizeau, J., Moran, R. J., and Friston, K. J. (2009). Bayesian model selection for group studies. *Neuroimage* 46, 1004–1017. doi: 10.1016/j.neuroimage.2009.03.025

Sterling, P. (2012). Allostasis: a model of predictive regulation. *Physiol. Behav.* 106, 5–15. doi: 10.1016/j.physbeh.2011.06.004

Sterling, P. (2014). Homeostasis vs. allostasis: implications for brain function and mental disorders. *JAMA Psychiatry* 71, 1192–1193. doi: 10.1001/jamapsychiatry.2014.1043

Stewart, J. M. (2000). Autonomic nervous system dysfunction in adolescents with postural orthostatic tachycardia syndrome and chronic fatigue syndrome is characterized by attenuated vagal baroreflex and potentiated sympathetic vasomotion. *Pediatr. Res.* 48, 218–226. doi: 10.1203/00006450-200008000-00016

Stuke, K., Flachenecker, P., Zettl, U. K., Elias, W. G., Freidel, M., Haas, J., et al. (2009). Symptomatology of MS: results from the German MS Registry. *J. Neurol.* 256, 1932–1935. doi: 10.1007/s00415-009-5257-5

Tomassini, A., Ruge, D., Galea, J. M., Penny, W., and Bestmann, S. (2016). The role of dopamine in temporal uncertainty. *J. Cogn. Neurosci.* 28, 96–110. doi: 10.1162/jocn_a_00880

Tsigos, C., and Chrousos, G. P. (2002). Hypothalamic-pituitary-adrenal axis, neuroendocrine factors and stress. *J. Psychosom. Res.* 53, 865–871. doi: 10.1016/S0022-3999(02)00429-4

Vetter, P., Grosbras, M. H., and Muckli, L. (2015). TMS over V5 disrupts motion prediction. *Cereb. Cortex* 25, 1052–1059. doi: 10.1093/cercor/bht297

Vezzani, A., and Viviani, B. (2015). Neuromodulatory properties of inflammatory cytokines and their impact on neuronal excitability. *Neuropharmacology* 96, 70–82. doi: 10.1016/j.neuropharm.2014.10.027

Vinckier, F., Gaillard, R., Palminteri, S., Rigoux, L., Salvador, A., Fornito, A., et al. (2016). Confidence and psychosis: a neuro-computational account of contingency learning disruption by NMDA blockade. *Mol. Psychiatry* 21, 946–955. doi: 10.1038/mp.2015.73

Vogt, B. A. (2005). Pain and emotion interactions in subregions of the cingulate gyrus. *Nat. Rev. Neurosci.* 6, 533–544. doi: 10.1038/nrn1704

Vogt, B. A., and Pandya, D. N. (1987). Cingulate cortex of the rhesus monkey: II. Cortical afferents. *J. Comp. Neurol.* 262, 271–289. doi: 10.1002/cne.902620208

Von Bertalanffy, L. (1969). *General System Theory*. New York, NY: George Braziller.

von Foerster, H. (2003). *Understanding Understanding: Essays on Cybernetics and Cognition*. New York, NY: Springer.

Wacongne, C., Changeux, J. P., and Dehaene, S. (2012). A neuronal model of predictive coding accounting for the mismatch negativity. *J. Neurosci.* 32, 3665–3678. doi: 10.1523/JNEUROSCI.5003-11.2012

Wessely, S. (2001). Chronic fatigue: symptom and syndrome. *Ann. Intern. Med.* 134, 838–843. doi: 10.7326/0003-4819-134-9_Part_2-200105011-00007

Wessely, S., Chalder, T., Hirsch, S., Wallace, P., and Wright, D. (1996). Psychological symptoms, somatic symptoms, and psychiatric disorder in chronic fatigue and chronic fatigue syndrome: a prospective study in the primary care setting. *Am. J. Psychiatry* 153, 1050–1059. doi: 10.1176/ajp.153.8.1050

Wiener, N. (1948). *Cybernetics*. New York, NY: Wiley.

Woods, H. A., and Wilson, J. K. (2013). An information hypothesis for the evolution of homeostasis. *Trends Ecol. Evol.* 28, 283–289. doi: 10.1016/j.tree.2012.10.021

Woolrich, M. W., and Stephan, K. E. (2013). Biophysical network models and the human connectome. *Neuroimage* 80, 330–338. doi: 10.1016/j.neuroimage.2013.03.059

Zacharopoulos, G., Binetti, N., Walsh, V., and Kanai, R. (2014). The effect of self-efficacy on visual discrimination sensitivity. *PLoS ONE* 9:e109392. doi: 10.1371/journal.pone.0109392

Conflict of Interest Statement: The handling Editor declared a shared affiliation, though no other collaboration, with several of the authors KS, CM, SF and states that the process nevertheless met the standards of a fair and objective review.

The other authors declare that the research was conducted in the absence of any commercial or financial relationships that could be construed as a potential conflict of interest.

frontiers in Human Neuroscience

ORIGINAL RESEARCH
published: 27 July 2016
doi: 10.3389/fnhum.2016.00383

Anterior Cingulate Cortico-Hippocampal Dysconnectivity in Unaffected Relatives of Schizophrenia Patients: A Stochastic Dynamic Causal Modeling Study

*Yi-Bin Xi[1†], Chen Li[1†], Long-Biao Cui[1†], Jian Liu[2], Fan Guo[1], Liang Li[3], Ting-Ting Liu[1], Kang Liu[1], Gang Chen[1], Min Xi[4], Hua-Ning Wang[4] and Hong Yin[1]**

[1] Department of Radiology, Xijing Hospital, Fourth Military Medical University, Xi'an, Shaanxi, China, [2] Network Center, Fourth Military Medical University, Xi'an, Shaanxi, China, [3] School of Biomedical Engineering, Fourth Military Medical University, Xi'an, Shaanxi, China, [4] Department of Psychiatry, Xijing Hospital, Fourth Military Medical University, Xi'an, Shaanxi, China

Familial risk plays a significant role in the etiology of schizophrenia (SZ). Many studies using neuroimaging have demonstrated structural and functional alterations in relatives of SZ patients, with significant results found in diverse brain regions involving the anterior cingulate cortex (ACC), caudate, dorsolateral prefrontal cortex (DLPFC), and hippocampus. This study investigated whether unaffected relatives of first episode SZ differ from healthy controls (HCs) in effective connectivity measures among these regions. Forty-six unaffected first-degree relatives of first episode SZ patients—according to the DSM-IV—were studied. Fifty HCs were included for comparison. All subjects underwent resting state functional magnetic resonance imaging (fMRI). We used stochastic dynamic causal modeling (sDCM) to estimate the directed connections between the left ACC, right ACC, left caudate, right caudate, left DLPFC, left hippocampus, and right hippocampus. We used Bayesian parameter averaging (BPA) to characterize the differences. The BPA results showed hyperconnectivity from the left ACC to right hippocampus and hypoconnectivity from the right ACC to right hippocampus in SZ relatives compared to HCs. The pattern of anterior cingulate cortico-hippocampal connectivity in SZ relatives may be a familial feature of SZ risk, appearing to reflect familial susceptibility for SZ.

Keywords: schizophrenia, first-degree relatives, functional magnetic resonance imaging, effective connectivity, stochastic dynamic causal modeling

OPEN ACCESS

Edited by:
Adeel Razi,
Wellcome Trust Centre for Neuroimaging (WT), UK

Reviewed by:
Sahil Bajaj,
The Houston Methodist Research Institute, USA
Wei Qin,
Xidian University, China

****Correspondence:***
Hong Yin
yinhong@fmmu.edu.cn

[†]These authors have contributed equally to this work.

Received: *05 May 2016*
Accepted: *14 July 2016*
Published: *27 July 2016*

Citation:
Xi Y-B, Li C, Cui L-B, Liu J, Guo F, Li L, Liu T-T, Liu K, Chen G, Xi M, Wang H-N and Yin H (2016) Anterior Cingulate Cortico-Hippocampal Dysconnectivity in Unaffected Relatives of Schizophrenia Patients: A Stochastic Dynamic Causal Modeling Study. Front. Hum. Neurosci. 10:383. doi: 10.3389/fnhum.2016.00383

INTRODUCTION

It is well established that familial risk plays a significant role in the etiology of schizophrenia (SZ) through family, adoption, twin, and sibling studies. SZ as a hereditary component affects 0.3% to 0.7% of the general population globally according to American Psychiatric Association (APA, 2013), whereas first-degree relatives have a higher risk of developing SZ, with an actual prevalence of approximate 10% (Lim and Sim, 1992). In genetic epidemiology studies, a 31% to 58% concordance rate of SZ exists in monozygotic twins (Tsuang, 2000). It has been demonstrated that genetic

liability to SZ was 81% (95% confidence interval (CI): 73%, 90%) based on results from 12 twin studies of SZ (Sullivan et al., 2003). The individual's heritability in liability just partly mediates family history of SZ (Agerbo et al., 2015). Furthermore, brain structural deficits in twins discordant for SZ were more pronounced in monozygotic than in dizygotic twins (Baare et al., 2001; Hulshoff Pol et al., 2004, 2006), suggesting association of cerebral abnormalities with genetic factors for SZ. In our previous studies, we have detected altered brain structure and function in first episode drug-naïve SZ patients (Chang et al., 2015; Cui et al., 2015, 2016; Huang et al., 2015). Thus the question is whether their first-degree relatives present specific alterations of the brain.

During the past 5 years, many structural magnetic resonance imaging (MRI) studies have revealed that gray matter volume, cortical morphological features, and white matter integrity in individuals at high risk of SZ differ from controls, but usually to a lesser extent than in SZ patients, indicating that structural aberrancies may form markers of susceptibility and transition to this disease (Bois et al., 2015b), despite not absolutely consistent findings. For the cerebral morphology, an interrupted cingulate sulcus pattern and paracingulate morphology are associated with increased genetic risk of SZ (Meredith et al., 2012). In the Edinburgh High Risk Study by Lawrie et al. cortical thinning pronounced in the left middle temporal gyrus (Sprooten et al., 2013), as well as longitudinal reductions for volume of the whole brain and bilateral prefrontal and temporal lobes (McIntosh et al., 2011) and cortical surface area prominently in the frontal, cingulate, and occipital lobes (Bois et al., 2015a) were detected in individuals at familial high risk of SZ compared with controls. Also, young relatives of SZ patients showed reduced bilateral hippocampal volume (Thermenos et al., 2013). As reported in a meta-analysis by Cooper et al. (2014), the gray matter volume increased in the left middle frontal gyrus, and decreased in the left thalamus/putamen, insula, and right superior frontal gyrus in high-risk individuals.

With the exception of diverse structural abnormalities, overall, a series of studies have demonstrated functional alterations in relatives of SZ patients at resting state (McIntosh et al., 2006; Hao et al., 2009; Jang et al., 2011; Liao et al., 2012; Su et al., 2013; Zhou et al., 2015) or task state (Whitfield-Gabrieli et al., 2009; Woodward et al., 2009; Rasetti et al., 2011; Stolz et al., 2012), with significant results found in several specific brain regions involving the dorsolateral prefrontal cortex (DLPFC), anterior cingulate cortex (ACC), caudate, and hippocampus.

Notably, the left DLPFC is a featured brain area in SZ relatives. It has been found that familial liability to SZ was associated with decreased gray matter volume of the left DLPFC (McIntosh et al., 2006). Furthermore, healthy siblings of SZ patients showed reduced white matter fractional anisotropy (FA) in the left DLPFC, without significant difference between SZ patients and their siblings (Hao et al., 2009). DLPFC dysfunction has been implicated in the familial susceptibility for SZ (Li and Funahashi, 2015). Aberrant regional function of the left DLPFC was detected by a resting state MRI study on the first-degree relatives of SZ patients (Liao et al., 2012). When identifying familial vulnerability markers by examining default mode network (DMN) connectivity, posterior cingulate cortex (PCC) seed region connectivity analysis showed reduced functional connectivity in the bilateral DLPFC of relatives (Jang et al., 2011). Unaffected relatives also had impaired connectivity from the left DLPFC to its coordinated regions, distributed in the bilateral caudate, left middle frontal gyrus, and right cerebellum (Su et al., 2013). However, few studies examined connectivity between some of these brain regions in unaffected relatives of SZ patients (Meda et al., 2012; Su et al., 2013), to date, leaving the open question of brain connectivity among these areas in familial high risk individuals.

Although previous studies have identified brain structural and functional abnormalities in frontal and temporal regions, it is still unclear how these regions interacts with each other differently in relatives of SZ patients compared with healthy controls (HCs). In the current study, we used stochastic dynamic causal modeling (sDCM) to investigate directed brain connectivity within a brain network encompasses ACC, caudate, DLPFC and hippocampus. DCM is a technique to investigate brain effective connectivity which refers to the causal influence of one brain region exerts over another or itself (Friston et al., 2003). Compared with functional connectivity analysis which simply measures the correlations between the blood-oxygen-level-dependent (BOLD) signals of different brain regions, effective connectivity analysis is able to further provide us information on how the signals are propagated within a brain network. Understanding the information flow within a brain network is crucial for understanding the neural mechanism of familial susceptibility for SZ. DCM was first invented to model the interactions between brain regions during task performance (Friston et al., 2003). Dauvermann et al. (2013) found decreased thalamo-cortical connectivity in first- or second-degree relatives of SZ patients using nonlinear deterministic DCM during verbal fluency processing. Recently, traditional deterministic DCM has been extended to stochastic DCM (Daunizeau et al., 2009; Li et al., 2011, 2014) which is also able to model brain effective connectivity at rest (Li et al., 2012). Here we used sDCM to identify changes in brain effective connectivity in unaffected first-degree relatives of SZ patients using resting-state fMRI (rsfMRI) data. On the basis of existing evidence that familial risk for SZ appears along with aberrant brain structural and functional alterations involving DLPFC, ACC, caudate, and hippocampus, we hypothesized that effective connectivity among them would also be disrupted in relatives, and provide more accurate parameter estimates (Li et al., 2011) compared with conventional deterministic DCM.

MATERIALS AND METHODS

Subjects

We assessed 53 HCs and 48 unaffected first-degree relatives of patients with first episode SZ (age- and gender-matched to HCs). The Diagnostic and Statistic Manual of Mental Disorders, 4th

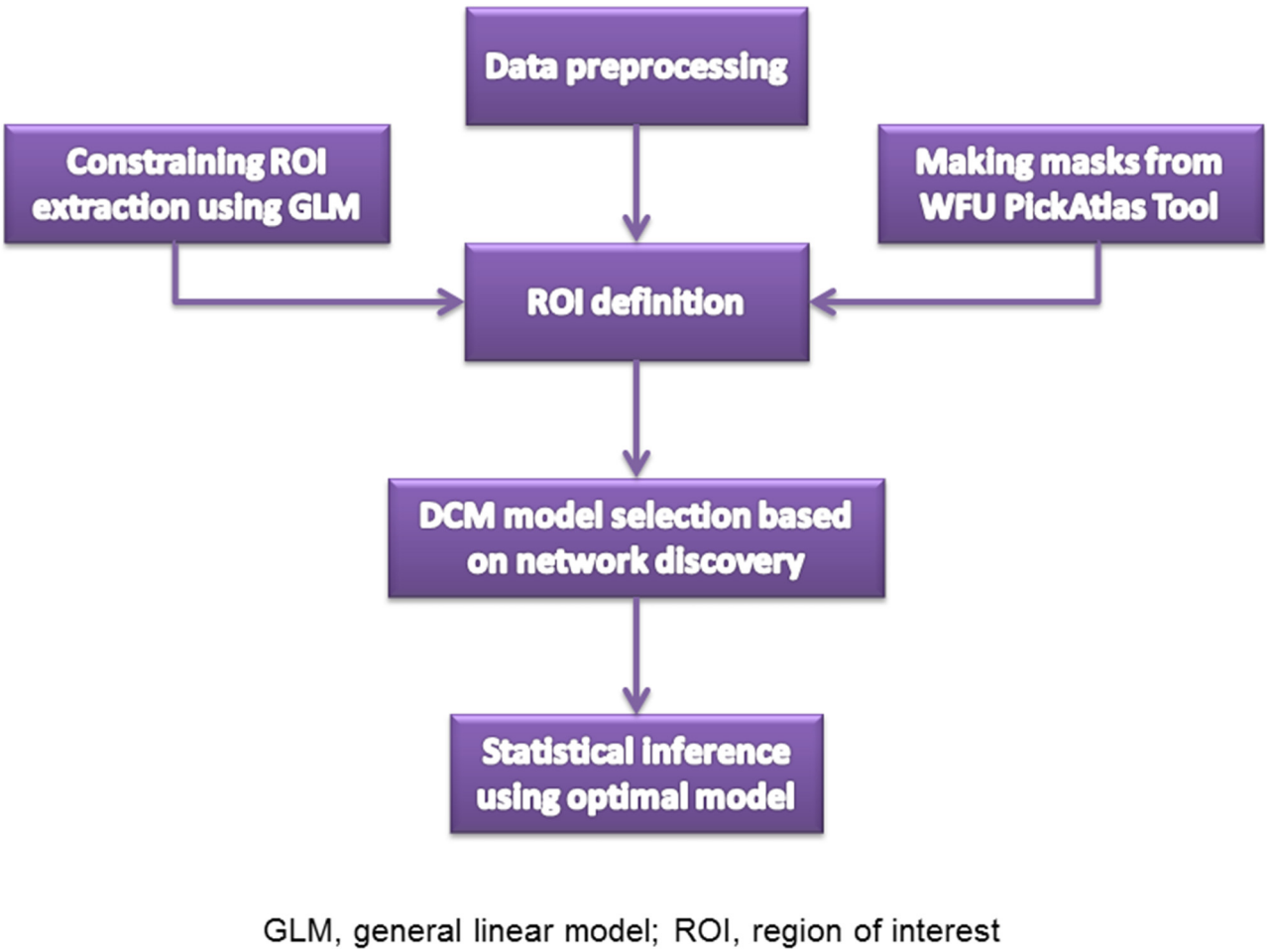

FIGURE 1 | Steps for data analysis.

edition (DSM-IV), revised criteria (Mittal and Walker, 2011) consensus diagnoses were established by two trained senior clinical psychiatrists with all clinical data and Structured Clinical Interviews for DSM Diagnoses interviews: inter-rater reliability was higher than 90% among raters. Relatives of probands were free of Axis 1 psychopathology and not taking psychoactive medications. Participants were recruited via word of mouth and advertisements at the Fourth Military Medical University; all provided written informed consent approved by the institutional review board of Xijing Hospital.

Data Acquisition and Preprocessing

The resting state fMRI images were collected on the 3.0-T Siemens Magnetom Trio Tim scanner. High-resolution T1-weighted 3D anatomical data were acquired using the 3D magnetization-prepared rapid gradient echo (3D MPRAGE) sequence (repetition time (TR): 2530 ms; echo time (TE): 3.5 ms; flip angle: 7°; field of view (FOV): 256 × 256 mm^2; matrix: 256 × 256; slice thickness: 1 mm; section gap: 0 mm; number of slices: 192). The image resolution was 1 mm × 1 mm × 1 mm. The echo planar imaging (EPI) sequence (TR: 2000 ms; TE: 30 ms; flip angle: 90°; FOV: 220 × 220 mm^2; matrix: 64 × 64; slice thickness: 4 mm; section gap: 0.6 mm) effectively covered the entire brain. Head motion was restricted with a custom-built head-coil foam cushion. During scanning, participants were asked to remain alert with eyes closed and head still. These instructions aided reducing head motion and prevented subjects from falling asleep. All participants were judged as awake and alert at the start and conclusion of the fMRI session. **Figure 1** is the flowchart for each step. Images were reconstructed offline, and realigned with statistical parametric mapping (SPM8[1]). The translation/rotation corrections of each participant were examined to exclude excessive head motion (>2.5 mm translation and/or >2.5° rotation), resulting in that eventual 46 first-degree relatives of SZ patients and 50 HCs were included. A mean functional image volume was constructed for each session from the realigned image volumes to determine parameters for spatial

[1]http://www.fil.ion.ucl.ac.uk/spm/software/spm8/

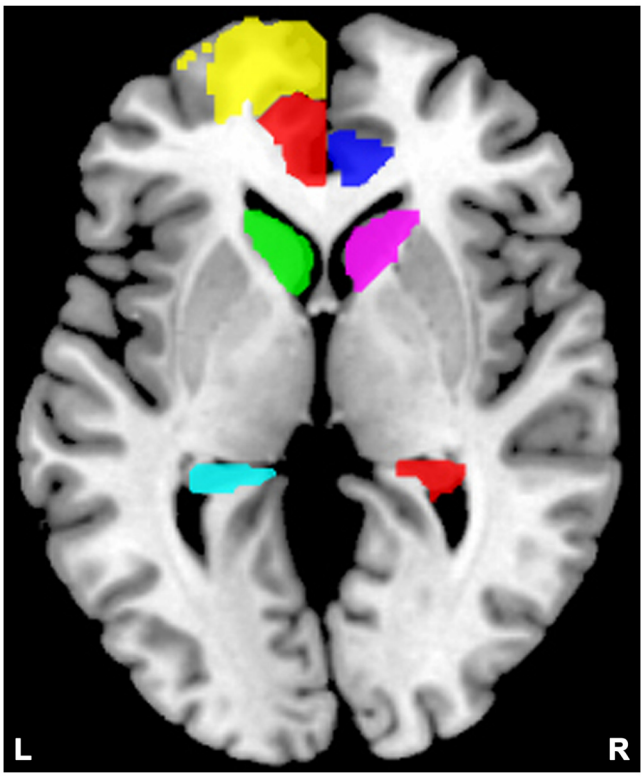

FIGURE 2 | Locations of the masks. Yellow indicates the left dorsolateral prefrontal cortex (DLPFC); semitransparent red indicates the left anterior cingulate cortex (ACC), and blue indicates the right ACC; green indicates the left caudate, and violet indicates the right caudate; cyan indicates the left hippocampus, and red indicates the right hippocampus.

normalization into Montreal Neurological Institute standardized space[2]. Normalization parameters determined for the mean functional volume were applied to the corresponding functional image volumes of each participant, which were smoothed with an 8 mm full width half maximum (FWHM) Gaussian kernel.

General Linear Model

In the first-level (within subject) analyses, participant-specific responses were modeled using a general linear model (GLM). The six motion parameters were included to model the movement correlated effects. One constant regressor was used to model the baseline, and cosine basis functions were included in the GLM. The resulting contrast images were then used to constrain the region of interest (ROI) extraction step in the sDCM.

Stochastic Dynamic Causal Modeling

Regions of Interest

For each subject, we studied the effective connectivity among seven ROIs including the left DLPFC (consists of Frontal_Sup_L and Frontal_Sup_Medial_L), and the bilateral ACC (Cingulum_Ant_L and Cingulum_Ant_R), caudate nuclei (Caudate_L and Caudate_R), and hippocampi (Hippocampus_L and Hippocampus_R). The left rather than the right DLPFC showed alterations in most studies of SZ relatives during rest condition (McIntosh et al., 2006; Hao et al., 2009; Liao et al., 2012; Su et al., 2013) thereby being chosen as the ROI. For each region, a ROI mask of that region was created by the WFU PickAtlas Tool (Version 3.0.4[3]) and the automated anatomical labeling (AAL) atlas template (**Figure 2**; Tzourio-Mazoyer et al., 2002; Maldjian et al., 2003, 2004). Subject-specific time series were then extracted based on the ROI mask and the contrast image generated by first-level (within subject) analyses. We then extracted time series from the voxels within the ROI that also showed activation in the contrast image. The first principle component of these time series was finally used to summarize the BOLD response to the ROI.

Model Specification and Parameter Estimation

In the current study, we aimed to search over all possible models generated from the connections among the seven ROIs. In this case, we did not limit our analysis to simply compare a few competing hypothesis (models). In contrast, we used a data-driven approach to search over all possible models. Specifically, a fully connected model (full model) with bidirectional connections between any pair of regions was constructed for each subject (**Figure 3**). Parameter estimates and model evidence of the full model was obtained using generalized filtering which is a recently developed scheme for sDCM model inversion and parameter estimation (Friston et al., 2010). After the full model was inverted, we employed a network discovery procedure (Friston et al., 2011) to search for the best reduced model which has the highest model evidence. A reduced model has the same group of ROIs as the full model, but only a subgroup of the connections in the full model (i.e., some of the connections are absent in the reduced model). The network discovery scheme provides approximation of the model evidences of all the possible reduced models without inverting every reduced model. The reduced models and the full model are then scored according to their model evidence. Model which has the highest model evidence was chosen as the winning model. Parameter estimates of the winning model were also obtained using the network discovery scheme and used for group analysis and making inferences on effective connectivity between brain regions.

Group Analysis

On the basis of sDCM analysis, the strength of connection described the coupling strength according to the rate at which neuronal responses were triggered in the target area (connection strengths are effectively rate constants in 1/s, Hz; Friston et al., 2003). To see whether these differences could be estimated and detected reliably, we characterized the differences using Bayesian parameter averaging (BPA; Friston et al., 2014; Razi et al., 2015). We used BPA for each group separately after network discovery procedure. We can then go on to discuss the results based on largest two or three connection differences, thereby being as a

[2]http://www.mni.mcgill.ca/

[3]http://www.nitrc.org/projects/wfu_pickatlas/

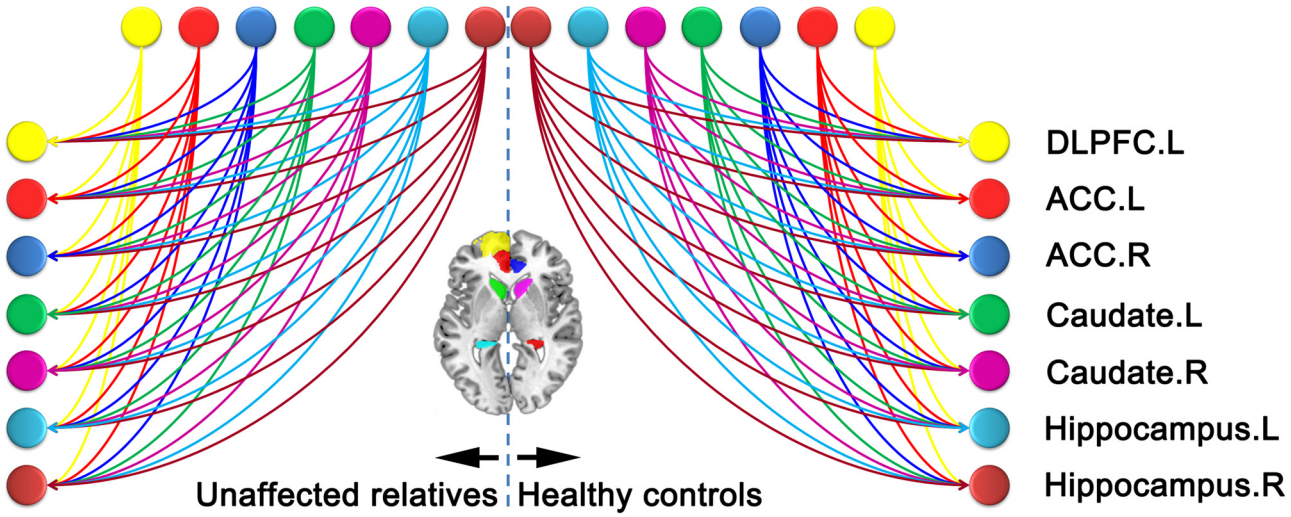

FIGURE 3 | Fully connected model constructed. The lines with arrowheads between distinct region of interests (ROIs) refer to the connections in the left panel for relatives of schizophrenia (SZ) patients and right panel for healthy controls (HCs). The color of each node is in line with that of **Figure 2**. ACC, anterior cingulate cortex; DLPFC, dorsolateral prefrontal cortex.

TABLE 1 | Demographical data of the participants.

Variables	First-degree relatives of SZ patients	HCs	Statistics	*P* value
Age (years)	28 ± 5	27 ± 4	$t = -0.35$	0.73
Gender (M/F)	22/24	31/19	$\chi^2 = 1.95$	0.22
Ethnicity	Han (Chinese)	Han (Chinese)	—	—
Handedness (R/L)	46/0	50/0	—	—
Education (years)	15 ± 1	15 ± 2	$t = 0.23$	0.82
Smoking status (S/N)	11/35	18/32	$\chi^2 = 1.66$	0.27

M, male; F, female; R, right; L, left; S, smoker; N, nonsmoker.

guiding principle to set the threshold (strength of connections measured in Hz).

RESULTS

Demographical Characteristics

No significant differences were present between SZ patients' first-degree relatives and HCs on any demographic variables (**Table 1**).

Network Discovery-Based Model Selection Results

The evidence of all reduced models was compared by the network discovery procedure for each group (**Figure 4**). The left panel is for first-degree relatives of SZ patients and right panel refers to HCs. The procedure selected the fully connected model as the best model with a posterior probability of almost 1. The fully connected model had 49 parameters describing the extrinsic connections between nodes and the intrinsic (self-connections) within nodes. In **Figure 4**, the profiles of model evidences are shown with the posterior probability for each model. In both groups, the full model had a log-probability of almost 0 and probability of 1. Therefore, they shared the identical winning model.

Effectivity Connectivity

BPA results of the effective connectivity can be seen in **Figure 5**. When using BPA, in the context of uncovering the group differences, as a guiding principle it would be best to choose top two or three connections and then we set the threshold to 0.06 Hz. SZ patients' relatives exerted increased connection from the left ACC to right hippocampus, but decreased connection from the right ACC to right hippocampus as compared to HCs.

DISCUSSION

Our study presents sDCM-based effective connectivity outcomes contrasted between first-degree relatives of first episode SZ patients and HCs. As compared with HCs, first-degree relatives who did not show any psychiatric symptoms revealed abnormal connectivity primarily localized to the connections from the bilateral ACC to right hippocampus.

Cognitive deficits are a core characteristic of SZ (Elvevag and Goldberg, 2000), which has been previously observed in biological relatives of SZ patients (Snitz et al., 2006; Bove, 2008; Keshavan et al., 2010; Liao et al., 2012). As well, impaired neural circuitry within the emotion processing has been reported in unaffected siblings of SZ patients (van Buuren et al., 2011; Hanssen et al., 2015). The neural basis of impaired cognition, including emotion processing, in SZ patients and their relatives remains uncertain, thus leaving an open question of whether presence of cognitive and emotional deficits in unaffected first-degree relatives at high risk for developing SZ suggests genetic basis of SZ symptoms. Determining the neural correlates of

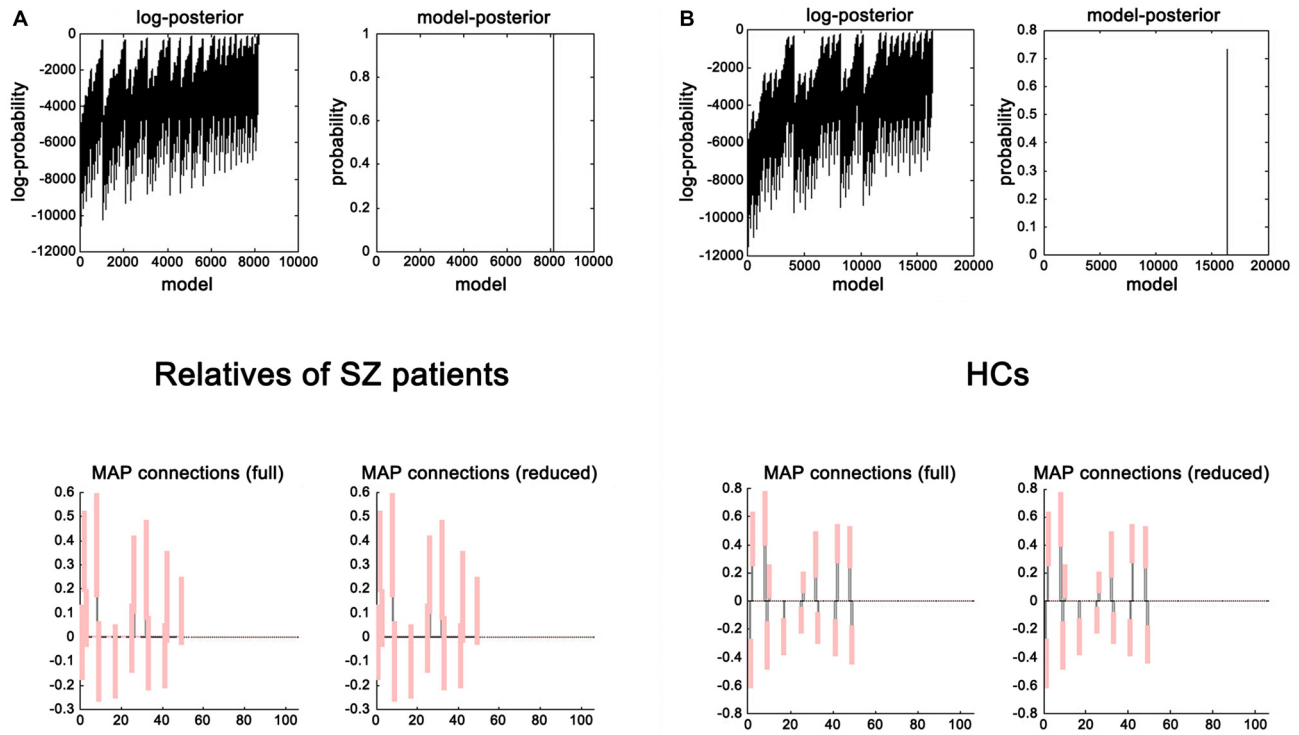

FIGURE 4 | Results of the *post hoc* optimization. The corresponding conditional parameter estimates were shown over the 49 (extrinsic and intrinsic) connections in relatives of SZ patients **(A)** and HCs **(B)**. This figure suggested that the fully connected model was the best explanation for the data.

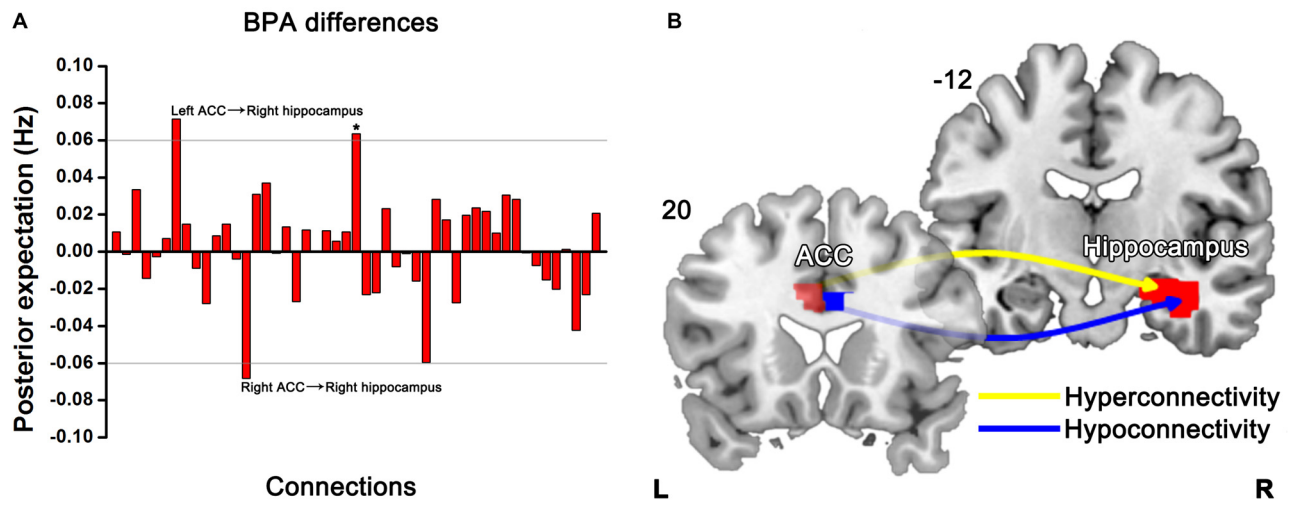

FIGURE 5 | Significant effective connectivity (between the group level) among ROIs in the first-degree relatives of SZ patients and HCs. Bayesian parameter averaging (BPA) of the differences for stochastic dynamic causal modeling (sDCM) shows only those edges on the graph that survive the threshold of 0.06 Hz, i.e., the increased (left ACC-right hippocampus) and decreased (right ACC-right hippocampus) connections in relatives compared to HCs **(A)**. Schematic illustration showing connectivity patterns in first-degree relatives of SZ patients **(B)**. *Indicates self-connection of the left caudate. The slice location (coordinate) is marked in the upper-left.

familial risk for SZ is essential to elucidate the neurobiology for SZ that may aid in the development of novel targeted treatment.

For one thing, relatives of SZ patients exhibited bilateral anterior cingulate cortical dysconnectivity in our present study. Previous studies have demonstrated the important role of the dorsal ACC in cognitive control (Carter and van Veen, 2007) consistently. For these regions, these are association of aberrant activation patterns with deficient

behavioral performance in SZ (Minzenberg et al., 2009). Most recently, we found altered effective connectivity related to ACC in SZ patients using spectral DCM, indicating anterior cingulate cortico-prefrontal-hippocampal hyperconnectivity (Cui et al., 2015). The effective connectivity and white matter connectivity analysis provides some evidence that weaker connectivity involved in ACC may be the neural basis of specific cognitive impairments in SZ (Wagner et al., 2015). Furthermore, using a regional homogeneity approach, Liao et al. (2012) reported decreased local neural activity in ACC in first-degree relatives of SZ patients along cognitive deficits. When taken with these previous results, our findings in unaffected relatives point to the possibility of altered functional interplay between ACC and hippocampus as the unit responsible for cognition and initial sign for developing SZ.

For another, we detect abnormal connection from ACC to the right hippocampus in relatives of SZ patients. Reduced bilateral hippocampal volume has been observed in young relatives of SZ patients (Keshavan et al., 2002; Thermenos et al., 2013). It has been found smaller hippocampi in relatives of SZ patients (Seidman et al., 2002, 2014; Francis et al., 2013). Furthermore, patients with SZ and their healthy siblings shared disrupted white matter integrity in the hippocampus that may be related to higher risk of healthy siblings to develop SZ (Hao et al., 2009). The hippocampus is part of the hippocampal formation that is comprised of subfields namely the dentate gyrus, subiculum, and pre-subiculum. By means of Van Leemput et al. (2009) method enabling quantification of elusive subfields, reduction in volume of the left and right subicula was observed in familial high risk persons with first-degree relatives suffering from SZ or schizoaffective disorder (Francis et al., 2013). The subibulum could mediate hippocampal-cortical interaction, and is purportedly involved in spatial information processing and memory (O'Mara et al., 2009). In the aforementioned study, verbal memory was impaired and significantly correlated with the subicular volume within the relatives of SZ patients (Francis et al., 2013). Dysconnectivity between DLPFC and hippocampal formation has also been reported in SZ patients (Liu et al., 2014). Accordingly, compromised anterior cingulate cortico-hippocampal connection links with the risk of developing SZ in individuals at familial high risk.

Moreover, aberrant DLPFC connectivity and familial risk for SZ are closely related in SZ pathophysiology (Hao et al., 2009; Whitfield-Gabrieli et al., 2009; Woodward et al., 2009; Jang et al., 2011; Rasetti et al., 2011; Su et al., 2013). The prefrontal cortex (PFC) is a compartment of the human brain involved in highly diverse processes, ranging from cognition, motivation, emotion, working memory and complex motor activity to social interactions (Ku et al., 2015; Zhou et al., 2015). These aforementioned results in SZ patients and their relatives suggest that neuro-integrative deficits from the DLPFC to other brain regions are likely to be involved in cognitive function and the familial risk for SZ. However, we did not detect significantly different DLPFC-related connectivity in the sample of relatives of SZ patients in our current study. Last but not least, altered caudate nucleus-related connections were not observed in SZ relatives compared to HCs, either. Unaffected relatives from mixed families (with at least one relative with SZ and one with bipolar disorder) showed reductions in bilateral caudate gray matter density (McIntosh et al., 2004). Paradoxically, our results did not show aberrant connections involving caudate nucleus in relatives of SZ patients. This divergence in findings (i.e., the failure to observe anomalies of connections involved in DLPFC and caudate) could be due to differences in subject selection. In our present study, individuals at high risk for SZ were unaffected first-degree relatives of first episode drug-naïve patients with this illness, rather than mixed first- and second-degree relatives of treated patients commonly used previously. A possible interpretation is the heritable characteristics of SZ and featured effects of facing patients with diverse symptoms before receiving therapy on these subjects in the current study.

We acknowledge that there were several limitations. First, we enrolled a not so large sample size of subjects in this study. Larger sample is desirable to confirm our present findings. Second, the present study did not involve any behavioral data, i.e., we did not measure the severity of cognitive impairment in the relatives. Currently, we are collecting the behavioral data to clarify the relationship between neuroimaging findings and altered cognition. Third, although a recent study demonstrated both noisy and neural effect of head motion on functional connectivity analysis (Zeng et al., 2014), the current study did not examine the difference of head motion between these two groups. This factor should be taken into account in future research.

Our findings show the pattern of effective connectivity among DLPFC, ACC, hippocampus, and caudate in the familial high risk population of SZ patients, which may be tied to a familial risk of SZ. Specifically, we found that increased effective connectivity from the left ACC to right hippocampus and decreased effective connectivity from the right ACC to right hippocampus in unaffected first-degree relatives of first episode SZ patients. The anterior cingulate cortico-hippocampal dysconnectivity may therefore serve as a potential sign of a general vulnerability to develop SZ.

AUTHOR CONTRIBUTIONS

HY had full access to all the data in the study and take responsibility for the integrity of the data and the accuracy of the data analysis. Y-BX, CL and L-BC contributed equally to this work. Study concept and design: H-NW, HY. Acquisition, analysis, or interpretation of data: Y-BX, CL, L-BC, JL, FG, LL, T-TL, KL, GC, MX, H-NW, HY. Drafting of the manuscript: Y-BX, CL, L-BC. Critical revision of the manuscript for important intellectual content: Y-BX, CL, L-BC, FG, H-NW, HY. Statistical analysis: CL, L-BC. Administrative, technical, or material support: CL, L-BC, MX. Study supervision: HY.

ACKNOWLEDGMENTS

This work was supported by the National Key Basic Research and Development Program (973; Grant No. 2011CB707805), National Natural Science Foundation of China (Grant Nos.

81571651, 81171278 and 81301199), and Fund for the Dissertation Submitted to Fourth Military Medical University for the Academic Degree of Doctor (Grant No. 2014D07). We are truly grateful to Baojuan Li from School of Biomedical Engineering, Fourth Military Medical University for her help about the technical guidance and revision.

REFERENCES

Agerbo, E., Sullivan, P. F., Vilhjálmsson, B. J., Pedersen, C. B., Mors, O., Borglum, A. D., et al. (2015). Polygenic risk score, parental socioeconomic status, family history of psychiatric disorders and the risk for schizophrenia: a danish population-based study and meta-analysis. *JAMA Psychiatry* 72, 635–641. doi: 10.1001/jamapsychiatry.2015.0346

APA. (2013). *Diagnostic and Statistical Manual of Mental Disorders.* 5th Edn. Washington, DC: American Psychiatric Association.

Baare, W. F., van Oel, C. J., Hulshoff Pol, H. E., Schnack, H. G., Durston, S., Sitskoorn, M. M., et al. (2001). Volumes of brain structures in twins discordant for schizophrenia. *Arch. Gen. Psychiatry* 58, 33–40. doi: 10.1001/archpsyc.58.1.33

Bois, C., Ronan, L., Levita, L., Whalley, H. C., Giles, S., McIntosh, A. M., et al. (2015a). Cortical surface area differentiates familial high risk individuals who go on to develop schizophrenia. *Biol. Psychiatry* 78, 413–420. doi: 10.1016/j.biopsych.2014.12.030

Bois, C., Whalley, H. C., McIntosh, A. M., and Lawrie, S. M. (2015b). Structural magnetic resonance imaging markers of susceptibility and transition to schizophrenia: a review of familial and clinical high risk population studies. *J. Psychopharmacol.* 29, 144–154. doi: 10.1177/0269881114541015

Bove, E. A. (2008). Cognitive performance and basic symptoms in first-degree relatives of schizophrenic patients. *Compr. Psychiatry* 49, 321–329. doi: 10.1016/j.comppsych.2008.01.001

Carter, C. S., and van Veen, V. (2007). Anterior cingulate cortex and conflict detection: an update of theory and data. *Cogn. Affect. Behav. Neurosci.* 7, 367–379. doi: 10.3758/cabn.7.4.367

Chang, X., Xi, Y. B., Cui, L. B., Wang, H. N., Sun, J. B., Zhu, Y. Q., et al. (2015). Distinct inter-hemispheric dysconnectivity in schizophrenia patients with and without auditory verbal hallucinations. *Sci. Rep.* 5:11218. doi: 10.1038/srep11218

Cooper, D., Barker, V., Radua, J., Fusar-Poli, P., and Lawrie, S. M. (2014). Multimodal voxel-based meta-analysis of structural and functional magnetic resonance imaging studies in those at elevated genetic risk of developing schizophrenia. *Psychiatry Res.* 221, 69–77. doi: 10.1016/j.pscychresns.2013.07.008

Cui, L. B., Liu, K., Li, C., Wang, L. X., Guo, F., Tian, P., et al. (2016). Putamen-related regional and network functional deficits in first-episode schizophrenia with auditory verbal hallucinations. *Schizophr. Res.* 173, 13–22. doi: 10.1016/j.schres.2016.02.039

Cui, L. B., Liu, J., Wang, L. X., Li, C., Xi, Y. B., Guo, F., et al. (2015). Anterior cingulate cortex-related connectivity in first-episode schizophrenia: a spectral dynamic causal modeling study with functional magnetic resonance imaging. *Front. Hum. Neurosci.* 9:589. doi: 10.3389/fnhum.2015.00589

Daunizeau, J., Friston, K. J., and Kiebel, S. J. (2009). Variational Bayesian identification and prediction of stochastic nonlinear dynamic causal models. *Physica D* 238, 2089–2118. doi: 10.1016/j.physd.2009.08.002

Dauvermann, M. R., Whalley, H. C., Romaniuk, L., Valton, V., Owens, D. G., Johnstone, E. C., et al. (2013). The application of nonlinear dynamic causal modelling for fMRI in subjects at high genetic risk of schizophrenia. *Neuroimage* 73, 16–29. doi: 10.1016/j.neuroimage.2013.01.063

Elvevag, B., and Goldberg, T. E. (2000). Cognitive impairment in schizophrenia is the core of the disorder. *Crit. Rev. Neurobiol.* 14, 1–21. doi: 10.1615/critrevneurobiol.v14.i1.10

Francis, A. N., Seidman, L. J., Tandon, N., Shenton, M. E., Thermenos, H. W., Mesholam-Gately, R. I., et al. (2013). Reduced subicular subdivisions of the hippocampal formation and verbal declarative memory impairments in young relatives at risk for schizophrenia. *Schizophr. Res.* 151, 154–157. doi: 10.1016/j.schres.2013.10.002

Friston, K. J., Harrison, L., and Penny, W. (2003). Dynamic causal modelling. *Neuroimage* 19, 1273–1302. doi: 10.1016/s1053-8119(03)00202-7

Friston, K. J., Kahan, J., Biswal, B., and Razi, A. (2014). A DCM for resting state fMRI. *Neuroimage* 94, 396–407. doi: 10.1016/j.neuroimage.2013.12.009

Friston, K. J., Li, B., Daunizeau, J., and Stephan, K. E. (2011). Network discovery with DCM. *Neuroimage* 56, 1202–1221. doi: 10.1016/j.neuroimage.2010.12.039

Friston, K. J., Stephan, K., Li, B. J., and Daunizeau, J. (2010). Generalised filtering. *Math. Probl. Eng.* 2010:621670. doi: 10.1155/2010/621670

Hanssen, E., van der Velde, J., Gromann, P. M., Shergill, S. S., de Haan, L., Bruggeman, R., et al. (2015). Neural correlates of reward processing in healthy siblings of patients with schizophrenia. *Front. Hum. Neurosci.* 9:504. doi: 10.3389/fnhum.2015.00504

Hao, Y., Yan, Q., Liu, H., Xu, L., Xue, Z., Song, X., et al. (2009). Schizophrenia patients and their healthy siblings share disruption of white matter integrity in the left prefrontal cortex and the hippocampus but not the anterior cingulate cortex. *Schizophr. Res.* 114, 128–135. doi: 10.1016/j.schres.2009.07.001

Huang, P., Xi, Y., Lu, Z. L., Chen, Y., Li, X., Li, W., et al. (2015). Decreased bilateral thalamic gray matter volume in first-episode schizophrenia with prominent hallucinatory symptoms: a volumetric MRI study. *Sci. Rep.* 5:14505. doi: 10.1038/srep14505

Hulshoff Pol, H. E., Brans, R. G., van Haren, N. E., Schnack, H. G., Langen, M., Baare, W. F., et al. (2004). Gray and white matter volume abnormalities in monozygotic and same-gender dizygotic twins discordant for schizophrenia. *Biol. Psychiatry* 55, 126–130. doi: 10.1016/s0006-3223(03)00728-5

Hulshoff Pol, H. E., Schnack, H. G., Mandl, R. C., Brans, R. G., van Haren, N. E., Baare, W. F., et al. (2006). Gray and white matter density changes in monozygotic and same-sex dizygotic twins discordant for schizophrenia using voxel-based morphometry. *Neuroimage* 31, 482–488. doi: 10.1016/j.neuroimage.2005.12.056

Jang, J. H., Jung, W. H., Choi, J. S., Choi, C. H., Kang, D. H., Shin, N. Y., et al. (2011). Reduced prefrontal functional connectivity in the default mode network is related to greater psychopathology in subjects with high genetic loading for schizophrenia. *Schizophr. Res.* 127, 58–65. doi: 10.1016/j.schres.2010.12.022

Keshavan, M. S., Dick, E., Mankowski, I., Harenski, K., Montrose, D. M., Diwadkar, V., et al. (2002). Decreased left amygdala and hippocampal volumes in young offspring at risk for schizophrenia. *Schizophr. Res.* 58, 173–183. doi: 10.1016/s0920-9964(01)00404-2

Keshavan, M. S., Kulkarni, S., Bhojraj, T., Francis, A., Diwadkar, V., Montrose, D. M., et al. (2010). Premorbid cognitive deficits in young relatives of schizophrenia patients. *Front. Hum. Neurosci.* 3:62. doi: 10.3389/neuro.09.062.2009

Ku, Y., Bodner, M., and Zhou, Y. D. (2015). Prefrontal cortex and sensory cortices during working memory: quantity and quality. *Neurosci. Bull.* 31, 175–182. doi: 10.1007/s12264-014-1503-7

Li, B., Daunizeau, J., Stephan, K. E., Penny, W., Hu, D., and Friston, K. (2011). Generalised filtering and stochastic DCM for fMRI. *Neuroimage* 58, 442–457. doi: 10.1016/j.neuroimage.2011.01.085

Li, B., Friston, K. J., Liu, J., Liu, Y., Zhang, G., Cao, F., et al. (2014). Impaired frontal-basal ganglia connectivity in adolescents with internet addiction. *Sci. Rep.* 4:5027. doi: 10.1038/srep05027

Li, B. M., and Funahashi, S. (2015). A step forward in the understanding of prefrontal cortical functions. *Neurosci. Bull.* 31, 161–163. doi: 10.1007/s12264-015-1516-2

Li, B., Wang, X., Yao, S., Hu, D., and Friston, K. (2012). Task-dependent modulation of effective connectivity within the default mode network. *Front. Psychol.* 3:206. doi: 10.3389/fpsyg.2012.00206

Liao, H., Wang, L., Zhou, B., Tang, J., Tan, L., Zhu, X., et al. (2012). A resting-state functional magnetic resonance imaging study on the first-degree relatives of persons with schizophrenia. *Brain Imaging Behav.* 6, 397–403. doi: 10.1007/s11682-012-9154-7

Lim, L. C., and Sim, L. P. (1992). The prevalence of schizophrenia in relatives of schizophrenic patients. *Singapore Med. J.* 33, 645–647.

Liu, B., Zhang, X., Hou, B., Li, J., Qiu, C., Qin, W., et al. (2014). The impact of MIR137 on dorsolateral prefrontal-hippocampal functional connectivity in healthy subjects. *Neuropsychopharmacology* 39, 2153–2160. doi: 10.1038/npp.2014.63

Maldjian, J. A., Laurienti, P. J., and Burdette, J. H. (2004). Precentral gyrus discrepancy in electronic versions of the Talairach atlas. *Neuroimage* 21, 450–455. doi: 10.1016/j.neuroimage.2003.09.032

Maldjian, J. A., Laurienti, P. J., Kraft, R. A., and Burdette, J. H. (2003). An automated method for neuroanatomic and cytoarchitectonic atlas-based interrogation of fMRI data sets. *Neuroimage* 19, 1233–1239. doi: 10.1016/s1053-8119(03)00169-1

McIntosh, A. M., Job, D. E., Moorhead, T. W., Harrison, L. K., Forrester, K., Lawrie, S. M., et al. (2004). Voxel-based morphometry of patients with schizophrenia or bipolar disorder and their unaffected relatives. *Biol. Psychiatry* 56, 544–552. doi: 10.1016/j.biopsych.2004.07.020

McIntosh, A. M., Job, D. E., Moorhead, W. J., Harrison, L. K., Whalley, H. C., Johnstone, E. C., et al. (2006). Genetic liability to schizophrenia or bipolar disorder and its relationship to brain structure. *Am. J. Med. Genet. B Neuropsychiatr. Genet.* 141B, 76–83. doi: 10.1002/ajmg.b.30254

McIntosh, A. M., Owens, D. C., Moorhead, W. J., Whalley, H. C., Stanfield, A. C., Hall, J., et al. (2011). Longitudinal volume reductions in people at high genetic risk of schizophrenia as they develop psychosis. *Biol. Psychiatry* 69, 953–958. doi: 10.1016/j.biopsych.2010.11.003

Meda, S. A., Gill, A., Stevens, M. C., Lorenzoni, R. P., Glahn, D. C., Calhoun, V. D., et al. (2012). Differences in resting-state functional magnetic resonance imaging functional network connectivity between schizophrenia and psychotic bipolar probands and their unaffected first-degree relatives. *Biol. Psychiatry* 71, 881–889. doi: 10.1016/j.biopsych.2012.01.025

Meredith, S. M., Whyler, N. C., Stanfield, A. C., Chakirova, G., Moorhead, T. W., Job, D. E., et al. (2012). Anterior cingulate morphology in people at genetic high-risk of schizophrenia. *Eur. Psychiatry* 27, 377–385. doi: 10.1016/j.eurpsy.2011.11.004

Minzenberg, M. J., Laird, A. R., Thelen, S., Carter, C. S., and Glahn, D. C. (2009). Meta-analysis of 41 functional neuroimaging studies of executive function in schizophrenia. *Arch. Gen. Psychiatry* 66, 811–822. doi: 10.1001/archgenpsychiatry.2009.91

Mittal, V. A., and Walker, E. F. (2011). Diagnostic and statistical manual of mental disorders. *Psychiatry Res.* 189, 158–159. doi: 10.1016/j.psychres.2011.06.006

O'Mara, S. M., Sanchez-Vives, M. V., Brotons-Mas, J. R., and O'Hare, E. (2009). Roles for the subiculum in spatial information processing, memory, motivation and the temporal control of behaviour. *Prog. Neuropsychopharmacol. Biol. Psychiatry* 33, 782–790. doi: 10.1016/j.pnpbp.2009.03.040

Rasetti, R., Sambataro, F., Chen, Q., Callicott, J. H., Mattay, V. S., and Weinberger, D. R. (2011). Altered cortical network dynamics: a potential intermediate phenotype for schizophrenia and association with ZNF804A. *Arch. Gen. Psychiatry* 68, 1207–1217. doi: 10.1001/archgenpsychiatry.2011.103

Razi, A., Kahan, J., Rees, G., and Friston, K. J. (2015). Construct validation of a DCM for resting state fMRI. *Neuroimage* 106, 1–14. doi: 10.1016/j.neuroimage.2014.11.027

Seidman, L. J., Faraone, S. V., Goldstein, J. M., Kremen, W. S., Horton, N. J., Makris, N., et al. (2002). Left hippocampal volume as a vulnerability indicator for schizophrenia: a magnetic resonance imaging morphometric study of nonpsychotic first-degree relatives. *Arch. Gen. Psychiatry* 59, 839–849. doi: 10.1001/archpsyc.59.9.839

Seidman, L. J., Rosso, I. M., Thermenos, H. W., Makris, N., Juelich, R., Gabrieli, J. D., et al. (2014). Medial temporal lobe default mode functioning and hippocampal structure as vulnerability indicators for schizophrenia: a MRI study of non-psychotic adolescent first-degree relatives. *Schizophr. Res.* 159, 426–434. doi: 10.1016/j.schres.2014.09.011

Snitz, B. E., Macdonald, A. W. 3rd, and Carter, C. S. (2006). Cognitive deficits in unaffected first-degree relatives of schizophrenia patients: a meta-analytic review of putative endophenotypes. *Schizophr. Bull.* 32, 179–194. doi: 10.1093/schbul/sbi048

Sprooten, E., Papmeyer, M., Smyth, A. M., Vincenz, D., Honold, S., Conlon, G. A., et al. (2013). Cortical thickness in first-episode schizophrenia patients and individuals at high familial risk: a cross-sectional comparison. *Schizophr. Res.* 151, 259–264. doi: 10.1016/j.schres.2013.09.024

Stolz, E., Pancholi, K. M., Goradia, D. D., Paul, S., Keshavan, M. S., Nimgaonkar, V. L., et al. (2012). Brain activation patterns during visual episodic memory processing among first-degree relatives of schizophrenia subjects. *Neuroimage* 63, 1154–1161. doi: 10.1016/j.neuroimage.2012.08.030

Su, T. W., Lan, T. H., Hsu, T. W., Biswal, B. B., Tsai, P. J., Lin, W. C., et al. (2013). Reduced neuro-integration from the dorsolateral prefrontal cortex to the whole brain and executive dysfunction in schizophrenia patients and their relatives. *Schizophr. Res.* 148, 50–58. doi: 10.1016/j.schres.2013.05.005

Sullivan, P. F., Kendler, K. S., and Neale, M. C. (2003). Schizophrenia as a complex trait: evidence from a meta-analysis of twin studies. *Arch. Gen. Psychiatry* 60, 1187–1192. doi: 10.1001/archpsyc.60.12.1187

Thermenos, H. W., Keshavan, M. S., Juelich, R. J., Molokotos, E., Whitfield-Gabrieli, S., Brent, B. K., et al. (2013). A review of neuroimaging studies of young relatives of individuals with schizophrenia: a developmental perspective from schizotaxia to schizophrenia. *Am. J. Med. Genet. B Neuropsychiatr. Genet.* 162B, 604–635. doi: 10.1002/ajmg.b.32170

Tsuang, M. (2000). Schizophrenia: genes and environment. *Biol. Psychiatry* 47, 210–220. doi: 10.1016/s0006-3223(99)00289-9

Tzourio-Mazoyer, N., Landeau, B., Papathanassiou, D., Crivello, F., Etard, O., Delcroix, N., et al. (2002). Automated anatomical labeling of activations in SPM using a macroscopic anatomical parcellation of the MNI MRI single-subject brain. *Neuroimage* 15, 273–289. doi: 10.1006/nimg.2001.0978

van Buuren, M., Vink, M., Rapcencu, A. E., and Kahn, R. S. (2011). Exaggerated brain activation during emotion processing in unaffected siblings of patients with schizophrenia. *Biol. Psychiatry* 70, 81–87. doi: 10.1016/j.biopsych.2011.03.011

Van Leemput, K., Bakkour, A., Benner, T., Wiggins, G., Wald, L. L., Augustinack, J., et al. (2009). Automated segmentation of hippocampal subfields from ultra-high resolution *in vivo* MRI. *Hippocampus* 19, 549–557. doi: 10.1002/hipo.20615

Wagner, G., De la Cruz, F., Schachtzabel, C., Gullmar, D., Schultz, C. C., Schlosser, R. G., et al. (2015). Structural and functional dysconnectivity of the fronto-thalamic system in schizophrenia: a DCM-DTI study. *Cortex* 66, 35–45. doi: 10.1016/j.cortex.2015.02.004

Whitfield-Gabrieli, S., Thermenos, H. W., Milanovic, S., Tsuang, M. T., Faraone, S. V., McCarley, R. W., et al. (2009). Hyperactivity and hyperconnectivity of the default network in schizophrenia and in first-degree relatives of persons with schizophrenia. *Proc. Natl. Acad. Sci. U S A* 106, 1279–1284. doi: 10.1073/pnas.0809141106

Woodward, N. D., Waldie, B., Rogers, B., Tibbo, P., Seres, P., and Purdon, S. E. (2009). Abnormal prefrontal cortical activity and connectivity during response selection in first episode psychosis, chronic schizophrenia and unaffected siblings of individuals with schizophrenia. *Schizophr. Res.* 109, 182–190. doi: 10.1016/j.schres.2008.11.028

Zeng, L. L., Wang, D., Fox, M. D., Sabuncu, M., Hu, D., Ge, M., et al. (2014). Neurobiological basis of head motion in brain imaging. *Proc. Natl. Acad. Sci. U S A* 111, 6058–6062. doi: 10.1073/pnas.1317424111

Zhou, Y., Fan, L., Qiu, C., and Jiang, T. (2015). Prefrontal cortex and the dysconnectivity hypothesis of schizophrenia. *Neurosci. Bull.* 31, 207–219. doi: 10.1007/s12264-014-1502-8

Conflict of Interest Statement: The authors declare that the research was conducted in the absence of any commercial or financial relationships that could be construed as a potential conflict of interest.

frontiers in Human Neuroscience

ORIGINAL RESEARCH
published: 31 March 2016
doi: 10.3389/fnhum.2016.00141

Aging into Perceptual Control: A Dynamic Causal Modeling for fMRI Study of Bistable Perception

Ehsan Dowlati[1†], Sarah E. Adams[2†], Alexandra B. Stiles[3] and Rosalyn J. Moran[1,2,4]*

[1] Virginia Tech Carilion School of Medicine, Roanoke, VA, USA, [2] Virginia Tech Carilion Research Institute, Roanoke, VA, USA, [3] Virginia Commonwealth University School of Medicine, Richmond, VA, USA, [4] Bradley Department of Electrical and Computer Engineering, Virginia Tech, Blacksburg, VA, USA

Aging is accompanied by stereotyped changes in functional brain activations, for example a cortical shift in activity patterns from posterior to anterior regions is one hallmark revealed by functional magnetic resonance imaging (fMRI) of aging cognition. Whether these neuronal effects of aging could potentially contribute to an amelioration of or resistance to the cognitive symptoms associated with psychopathology remains to be explored. We used a visual illusion paradigm to address whether aging affects the cortical control of perceptual beliefs and biases. Our aim was to understand the effective connectivity associated with volitional control of ambiguous visual stimuli and to test whether greater top-down control of early visual networks emerged with advancing age. Using a bias training paradigm for ambiguous images we found that older participants (n = 16) resisted experimenter-induced visual bias compared to a younger cohort (n = 14) and that this resistance was associated with greater activity in prefrontal and temporal cortices. By applying Dynamic Causal Models for fMRI we uncovered a selective recruitment of top-down connections from the middle temporal to Lingual gyrus (LIN) by the older cohort during the perceptual switch decision following bias training. In contrast, our younger cohort did not exhibit any consistent connectivity effects but instead showed a loss of driving inputs to orbitofrontal sources following training. These findings suggest that perceptual beliefs are more readily controlled by top-down strategies in older adults and introduce age-dependent neural mechanisms that may be important for understanding aberrant belief states associated with psychopathology.

Keywords: visual illusion, visual processing, aging, dynamic causal modeling, fMRI

OPEN ACCESS

Edited by:
Adeel Razi,
University College London, UK

Reviewed by:
Kamen Atanasov Tsvetanov,
University of Camrbidge, UK
Gerald Cooray,
Karolinska Institute, Sweden

***Correspondence:**
Rosalyn J. Moran
rosalynj@vtc.vt.edu

[†]These authors have contributed equally to this work.

***Received:** 18 January 2016*
***Accepted:** 15 March 2016*
***Published:** 31 March 2016*

Citation:
Dowlati E, Adams SE, Stiles AB and Moran RJ (2016) Aging into Perceptual Control: A Dynamic Causal Modeling for fMRI Study of Bistable Perception. Front. Hum. Neurosci. 10:141. doi: 10.3389/fnhum.2016.00141

INTRODUCTION

Several studies have demonstrated that later patient age-at-onset is a predictor of greater remission rates and better outcome prognosis in psychopathologies including schizophrenia (Häfner et al., 1998; Ho et al., 2000; Jeste et al., 2003), first-episode psychosis (Malla et al., 2006) and bipolar disorder (Carlson et al., 2002; Carter et al., 2003), independent of other contributing factors such as illness duration. Age also influences the relative symptom spectrum in these psychopathologies (Gur et al., 1996; Topor et al., 2013). In schizophrenia, for example the trajectories of positive, negative and thought-disorder symptom dimensions have been shown to display differential age effects, with advancing age associated with decreases in positive symptoms including hallucinations, delusions and bizarre behavior

(Schultz et al., 1997). However, the putative neural mechanisms underlying adaptive effects of aging have been relatively unexplored in the neuroimaging and neuropsychiatric literature.

For this special issue on psychopathology, we aimed to address the basic mechanisms of brain networks that underlie age-dependent changes in constructive perception. A method of examining conscious perception is to take advantage of the visual system by instigating bistable perception. This allows us to study the underlying neural networks related to perception formation rather than stimulus-driven visual processing. Illusory visual paradigms have proved useful in probing the neural mechanisms associated with impaired perceptual inference and aberrant beliefs in psychosis and schizophrenia (Foxe et al., 2005; Dima et al., 2009, 2010; Notredame et al., 2014). Ambiguous visual stimuli such as the Necker's cube, Rubin's face-vase, or Boring's Old-Young lady, where images have two distinct interpretations (Leopold and Logothetis, 1999), in particular lend themselves to the study of volitional inference and subjective perception (Sundareswara and Schrater, 2008; Wang et al., 2013). Moreover, these paradigms are often designed to illicit activations across distributed cortical networks or hierarchies. Earlier theories of switching perceptions focused on neuronal adaptation as a key mediator (Blake, 1989) however these have been superseded by connectivity analyses which demonstrate that bottom-up and top-down connections to early visual cortices (Cardin et al., 2011; Wang et al., 2013) and endogenous neuronal oscillations (Kloosterman et al., 2015) also contribute to the bistability of a percept. Bayesian decision theory, used to construct models of perception (Kersten and Schrater, 2002) support the role of networked cortical communication. In these accounts, reverses in perception between competing alternatives are posed as an active process that involves multiple regions of the brain seeking to understand the stimulus, where one particular perception emerges as the result of bottom-up and top-down interplay that suppresses one interpretation in favor of the other (Dayan, 1998). Modeling accounts have also demonstrated a potential impact from noisy neuronal firing as a possible bottom-up influence in perceptual switches (Shapiro et al., 2009). These computational accounts appeal to priors on what might be perceived—on our visual beliefs (Cardin et al., 2011).

In terms of the prior beliefs that encourage perceptual switching and image stability, opposing behaviors have been observed which support both bottom-up and top-down neuronal mediators. Some studies reveal that the most prevalent percept in the recent past is the one that is most likely favored when the ambiguous image is shown (Leopold et al., 2002), suggesting that implicit perceptual memory may affect perception of ambiguous figures (de Jong et al., 2014). Other studies have shown that prolonged viewing of an ambiguous stimuli leads to preference of the novel perception vs. past perceptual experience (de Jong et al., 2012). Importantly, these images can also be manipulated to induce stability of a particular percept, for example moving bistable stimuli can be stabilized by motion of background elements (Kramer and Yantis, 1997) and the Necker cube, which elicits viewpoint ambiguity, can be manipulated with color enhancement of particular sides so that one viewpoint is predominantly perceived (Wang et al., 2013). This enables the investigation of perceptual priors and their volitional control.

We have previously shown that alterations in perceptual priors by short-term changes in environmental statistics are linked to adjusted ratios of bottom-up to top-down signal propagation in neural hierarchies that exhibit a pronounced age effect, with older adults less likely to adjust their beliefs (Moran et al., 2014). In the current study, we build upon these findings to test whether advanced age is associated with greater control of what is perceived.

The aim of the study was to establish a perceptual preference based on external stimulus manipulations and to use dynamic causal modeling (DCM) to assess changes in effective connectivity that arise from bias training. Our training consisted of a modified Rubin vase as a non-ambiguous image used to induce bias within subjects. We intended to elicit this effect to observe a change in percept duration in the younger individuals behaviorally. For older adults, we hypothesized that they would resist biasing by the training stimulus (Moran et al., 2014) and more actively control perceptual states when viewing bistable images. We were interested specifically in whether there was an age-dependence in post-training constructive perception.

MATERIALS AND METHODS

Participants

A total of 30 participants (16 females) partook in our fMRI experiment. The average age of the participants was 44.9, ranging from 18–76. Participants were divided into two groups: a young cohort with an average age of 23.9 (n = 14, 18–29 years, 7 females) and an older cohort with an average age of 63.7 (n = 16, 54–76 years, 9 females). All were screened for MRI contraindication and psychiatric or neurological disorders, had normal or corrected-to-normal visual acuity, and were fluent in English. Study protocols were approved by the Virginia Tech Institutional Review Board and written informed consent was obtained from each participant. Participants were compensated for their time.

Experimental Protocol

Each participant received task instructions and completed an instruction quiz prior to the scanning session. The fMRI task consisted of three blocks: ambiguous Block 1, "Biasing" Non-ambiguous Block 2, and ambiguous Block 3 (**Figure 1A**). In ambiguous Block 1, the Rubin vase was presented for 60 s, followed by a fixation cross displayed for 6 s (Rubin, 1921). Participants were instructed to indicate via button press whether they perceived two faces or a vase initially as well as every time their perception switched over the 60-s trial. This experimental design was similar to that employed in Sterzer et al. (2009) in that participants were not given instructions to focus on one perception over the other. All button presses were recorded and this was repeated for a total of six trials. Participants were then shown a modified, non-ambiguous stimulus during the "Biasing"

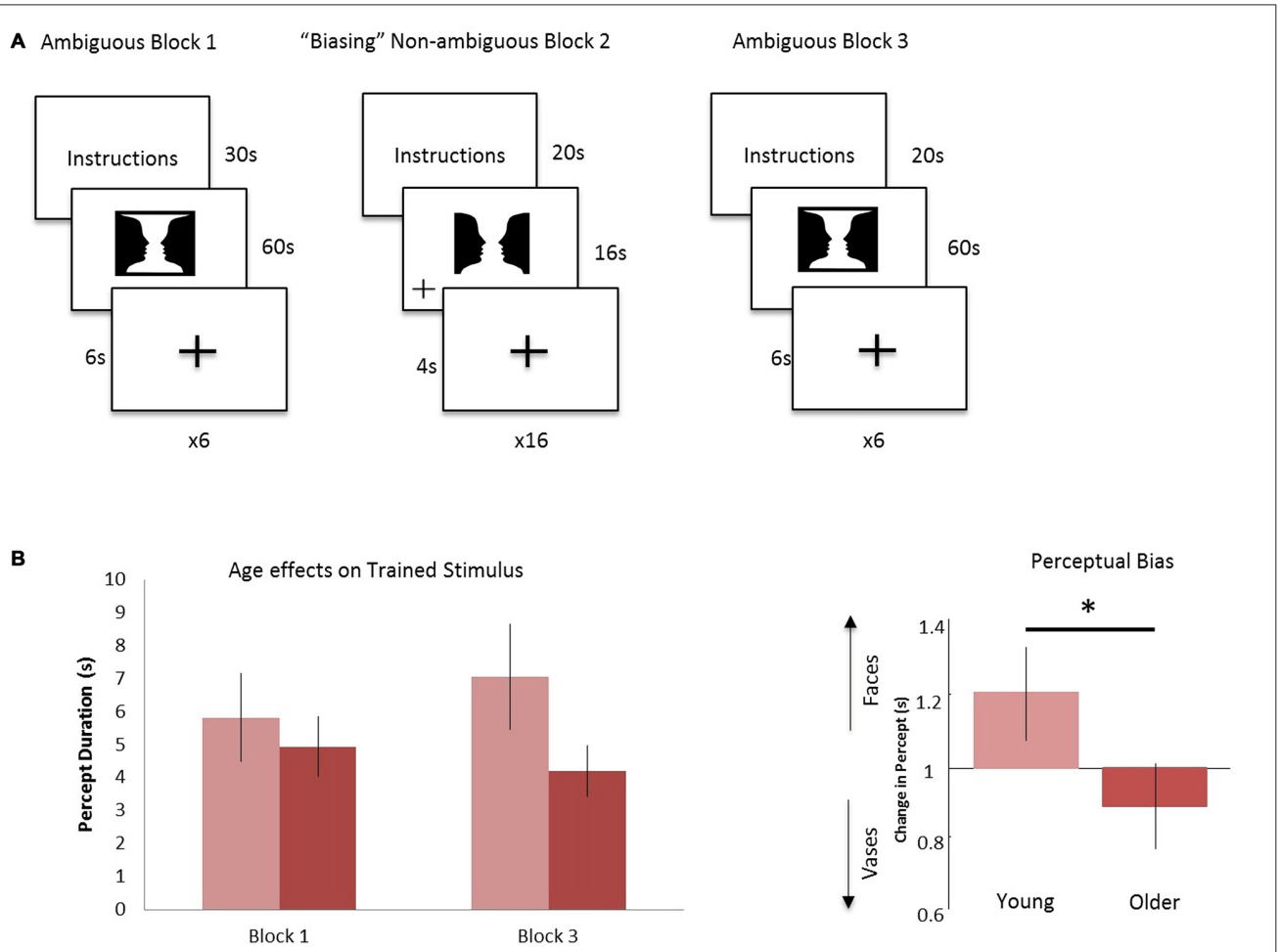

FIGURE 1 | Experimental design and age effects on trained stimulus. (A) Block 1: the ambiguous Rubin vase was shown for 60 s, where participants indicated their perception, faces or vase, with a button press. This was repeated 6 times and each trial was separated by a 6 s fixation cross. Block 2: a non-ambiguous, modified Rubin vase was shown for 16 s, where participants indicated when the fixation-cross appeared on either the left or right of the image. This was repeated 16 times and each trial was separated by a 4 s fixation cross. Block 3 was identical in design to Block 1. **(B)** Left: the average duration in viewing faces (the biased percept) in Block 3 compared to Block 1 for the young cohort (light red) and older cohort (dark red). Right: the ratio of these durations—i.e., the perceptual biasing effect, was significantly different between the younger and older groups $^*p < 0.05$.

Non-ambiguous Block 2. This non-ambiguous stimulus was intended to explicitly portray two faces by modifying it in a way that the two faces was the most likely perception gained from looking at the stimulus. By presenting such an image, we intended to "train" or "bias" participants toward the perception of the faces vs. a vase when they viewed the ambiguous figure. The non-ambiguous stimulus was presented for a total of 16 s, followed by a fixation cross displayed for 4 s. This was repeated for a total of 16 trials. When the non-ambiguous stimuli were presented, a fixation cross would appear at random to either the left or right of the screen and participants were instructed to indicate via button press when the fixation cross appeared. In Ambiguous Block 3, participants were again presented the ambiguous Rubin vase image for 60 s, followed by a fixation cross displayed for 6 s and instructed to indicate via button press their initial perception and their subsequent perceptual switches. This repeated for a total of six trials. To summarize: in two blocks (Blocks 1 and 3), we showed participants a non-modified ambiguous Rubin vase figure. The non-ambiguous block (block 2) was the "training" block in which the participant was shown a modified version of the Rubin vase diagram eliciting a stable perception showing two faces, where the top and bottom borders were removed. This was a similar modification to the image as presented in Wang et al. (2013). The non-ambiguous image was also chosen as a result of pilot data (not reported) which suggested the Rubin image modified to elicit a face-bias was a stronger non-ambiguous image than the Rubin image modified to elicit a vase-bias.

Button presses indicating percept switches, their times, and perceptual durations were recorded for behavioral data analysis. Total percept duration throughout the trials and average percept duration for each perception, i.e., face or vase, was analyzed across age and block (pre- vs. post-training).

fMRI Data Acquisition

Anatomical and functional images were acquired using a 3-T Siemens MAGNETOM Trio scanner. High-resolution T1-weighted structural images were collected using MPRAGE sequence with a repetition time (TR) = 1200 ms, echo time (TE) = 2.66 ms, field of view (FOV) = 245 mm, 1.0 mm slice thickness. Echo planar image data were acquired with a TR of 2000 ms, TE = 25 ms, field of view (FOV) = 220 mm, with 37 slices acquired at a slice thickness of 4.0 mm. Slices were oriented 30° superior-caudal to the plane through the anterior and posterior commissures to reduce signal drop-out. Headphones were used to reduce scanner noise. Participants used a mirror to view the stimuli projected behind them in the scanner. Participants were provided with additional items such as blankets and noise-cancelling ear plugs upon request.

fMRI Data Analysis

Preprocessing and data analysis were performed using statistical parametric mapping software implemented in Matlab (SPM12b beta; Wellcome Trust Centre for Neuroimaging, London, UK). The first five functional images of the acquisition were discarded to allow for equilibrium magnetization. The mean scan was used as the reference for EPI blood-oxygen-level dependent (BOLD) images which were realigned with a six parameter spatial transformation. The structural image was co-registered to the mean resliced image. The unified segmentation routine was then used to perform segmentation bias correction and spatial normalization. Images were normalized to MNI space using the ICBM template. Then, the data was smoothed using a kernel with 8 mm full-width at half maximum (FWHM).

Individual participant BOLD responses were analyzed using a General Linear Model (GLM). There were nine total regressors: (1) ambiguous stimuli presentation Ambiguous Block 1; (2) ambiguous stimuli presentation Ambiguous Block 3; (3) non-ambiguous image presentation Non-ambiguous Block 2; (4) button press responses for Block 1; (5) pre-switch event, a 2000 ms time period immediately prior to button press, during Block 1; (6) button press responses for Block 3; (7) pre-switch event, a 2000 ms time period immediately prior to button press, during Block 3; (8) button press responses in Block 2; and (9) pre-press, 2000 ms prior to button press, during the Block 2. All regressors were convolved with a canonical hemodynamic response function. In the first level GLM, estimated motion parameters were used as nuisance regressors. Once all regressors for all individual GLMs had been created, contrasts were created at the first-level to identify activation differences between ambiguous and non-ambiguous stimuli and between the pre- and post-training ambiguous stimuli. We assigned 2000 ms prior to the button press as the "pre-switch" event. This was motivated by previous research suggesting that subjective decisions can be observed in fMRI activity up to 10 s prior to a motor report (Soon et al., 2008).

We then used a summary statistic approach to assess group-level whole-brain peak activations to identify regions of interest. An F-contrast was used to identify positive or negative responses to the ambiguous stimuli compared to non-ambiguous stimuli (**Table 1**). An F-contrast was also applied to identify training effects—examining positive or negative response differences to ambiguous stimuli before (Block 1) and after biasing (Block 3; **Table 1**). A 2 × 2 analysis of variance (ANOVA) was preformed to test interactions between age and training effects as well.

Dynamic Causal Modeling

DCM for fMRI provides a model-based investigation of effective connectivity (Friston et al., 2003), where effective connectivity represents directional and modulatory interactions between multiple brain regions using separate neuronal and hemodynamic parameterizations. At the neuronal level the DCMs comprise a set of differential equations with parameters that control the drive of external inputs and of inter-regional neuronal influences. Given our interests in endogenous drivers of perceptual switches, we applied stochastic DCM for fMRIs which explicitly parameterizes non-stimulus linked fluctuations in neuronal activity (Li et al., 2011). We chose this over the alternative counterpart, deterministic DCM, due to its ability to parameterize and formally incorporate random neuronal fluctuations (Friston et al., 2014). Bayesian Model Selection was applied to find the best—most probable—model to explain the observed hemodynamics (Stephan et al., 2007). Our aim was to identify the neuronal connections associated with perceptual changes—i.e., pre-switch events.

We used our second-level summary statistics to identify regions of interest which responded differentially to ambiguous and non-ambiguous stimuli. We further used two age covariates to identify within these regions, specific nodes that exhibited positive and negative correlations with age. The regions of interest (ROIs) were identified around the group peak coordinates of the Lingual gyrus (LIN) [−6 −68 −2] and the Precuneus (PRE) [−12 −70 36]-these regions exhibited a negative correlation with age. ROIs were identified around the group peak coordinates of the Middle Temporal gyrus (MTG) [50 30 −6] and Inferior Orbitofrontal Cortex (IOF) [62 −22 −6]-with a positive correlation with age (group peaks are summarized in **Table 1**).

Given these coordinates, we extracted BOLD time series from each participant's fMRI data individually. Time series were extracted using an F-contrast mask that tested for differences between ambiguous and non-ambiguous stimuli with a p-value threshold of $p < 0.05$, uncorrected with a sphere radius of 8 mm (note: p-values here are used to define the voxel cluster from which the principal eigenvariate will be extracted, they are not involved in the final DCM statistics). The principal eigenvariate within a sphere of 8 mm was extracted for the model-based analysis. To correct for confounding motion and button-press contributions to our ROI time series, these extractions were corrected for "effects of interest" using an F contrast to partition data variance in order to incorporate effects from just four regressors including: (1) "Ambiguous Block 1", (2) "Ambiguous Block 3", (5) "Pre-Switch Block 1" and (7) "Pre-Switch Block 3". By using this F contrast, we are partitioning out any effects that could be due to all the other regressors, which include head motion and button presses.

TABLE 1 | fMRI second level group statistics: effects of ambiguity and age correlations.

Peak activation region (MNI)	X	Y	Z	F statistic	$P_{uncorrected}$	$P_{FWE-corrected}$
(A) Significant voxels with positive or negative response to onset of ambiguous vs. non-ambiguous images, unmasked, extended threshold 10 voxels						
R Lingual	6	−68	−4	6.26	0	0
R Sup occipital	14	−96	18	5.99	0	0
L Cerebelum	−25	−58	−25	5.92	0	0
L Mid temporal	−52	−48	14	5.81	0	0
L Angular	−42	−64	36	5.47	0	0.001
(B) Significant voxels with positive or negative response to onset of ambiguous images Block 1 vs. Block 3, unmasked, extended threshold 10 voxels						
L Lingual	−6	−68	−2	5.88	0	0
R Lingual	6	−64	−2	5.85	0	0
R Cuneus	14	−96	16	5.83	0	0
L Precentral	−60	2	28	5.83	0	0
L Mid temporal	−50	−60	−2	5.78	0	0
(C) Significant voxels with positive or negative response to onset of ambiguous vs. non-ambiguous images, masked inclusively with a negative correlation contrast of age, extended threshold 10 voxels: Lingual gyrus and Precuneus						
Lingual	−6	−68	−2	5.90	0	0
L Precuneus	−12	−70	36	5.17	0	0.004
Significant voxels with positive or negative response to onset of ambiguous vs. non-ambiguous images, masked inclusively with a positive correlation contrast of age, extended threshold 10 voxels: Mid Temporal gyrus and Inferior Orbitofrontal cortex						
R Mid temp	50	30	−6	4.94	0	0.011
R Inf orb	62	−22	−6	4.85	0	0.016

(A) The peak activations were identified as positive or negative response to the onset of ambiguous compared to non-ambiguous images and image onsets of ambiguous images before and after biasing. Both comparisons were unmasked and extended thresholds were at 20 voxels. (B) The effects of perceptual biases—comparing post and pre-training responses to ambiguous stimuli. (C) The peak activations with positive or negative response to onset of ambiguous compared to non-ambiguous images were used to mask age covariation. Lingual and precuneus activations were found when testing for decreasing with age. Right middle temporal gyrus and right inferior orbitofrontal cortex activations were found with a covariate of increasing age.

To test the effective connections across the network we constructed four models of potential interactions among our four regions of interest. There were intrinsic connections within all regions and between all regions (DCM's A matrix), except for the IOF and MTG. Inputs from ambiguous stimuli onsets drove all regions (DCM's C matrix). Modulatory connections (DCM's B matrix) were used to test network connections associated with pre-switch events. In model 1 we placed these modulations only on bottom-up connections for block 1 (LIN to MTG, LIN to IOF, PRE to MTG, and PRE to IOF) and only on top-down connections for post-training block 3 (MTG to LIN, MTG to PRE, IOF to LIN, IOF to PRE). For model 2 we allowed modulation of pre-switch events for pre and post training blocks on both sets of bottom-up and top-down connections. For model 3 we allowed modulation of pre-switch events only on bottom-up connections. Finally, for model 4 we allowed modulation of pre-switch events only on top-down connections.

RESULTS

Behavioral Effects of Biasing

Behavioral data were analyzed to test for perceptual biasing effects. For this we compared the average duration of perception of trained stimulus (i.e., two faces, see **Figure 1A**) between pre- and post-training blocks. All percepts throughout the six 60-s trials were examined, regardless of number of switches made within the trial and of the initial percept. Furthermore, we ensured that all participants had at least three or more switches within a single trial of 60 s. From these data we established a simple bias ratio—the ratio of average time durations for perceptions where the stimulus was viewed as two faces for post-training (block 3) relative to pre-training (block 1; **Figure 1**). Although we were not interested in the initial percept at each trial during the ambiguous blocks, it is important to note that there was no significant difference on the effect of training or age in the initial percept.

Overall, our hypothesized effects of age on biasing were evidenced. Average percept duration of the trained stimuli was similar between the young and older group (**Figure 1B**), however, during the post-training block, the average duration of the "faces" percept significantly differed between the young and older cohort (young (n = 14): 7064 ms; older (n = 16): 4209 ms) showing a positive bias for the trained stimulus for the young relative to older cohort ($p < 0.05$, **Figure 1B**). There was a medium effect size in this comparison (Cohen's d = 0.6). In addition, analysis of total percept duration for vases compared to faces post-training showed preference in older individuals towards the novel, non-trained percept significantly

($p < 0.001$). These data demonstrate a preference toward the novel or untrained percept in block 3 for the older cohort relative to a trained or biased prior in the younger cohort.

SPM Analysis

First, we identified brain regions that exhibited significant effects of ambiguity; that is, we tested ambiguous relative to non-ambiguous blocks over the whole brain using an F-contrast. Comparing the responses to these stimuli we observed significant activation across a distributed brain network, with large activations in visual and parietal cortices—voxel peak in the LIN [6 −68 −4; *x*, *y*, *z* MNI coordinates] ($p < 0.05$, Family Wise Error (FWE) corrected, **Table 1**, **Figure 2A**). We then used this contrast as a mask to test for age dependencies within the regions that exhibited ambiguity effects and found negative correlations with ambiguity-related activations in visual and parietal cortices, with a peak in the LIN at [−6, −68, −2], ($p < 0.05$ FWE, **Figure 2C**). In contrast, positive correlations with age were found in frontal and temporal cortices with a peak in the anterior middle temporal gyrus [50, 30, −6] ($p < 0.05$, FWE, **Table 1**, **Figure 2C**).

We assessed group level interactions between training and age using a 2 × 2 ANOVA. An interaction of age and

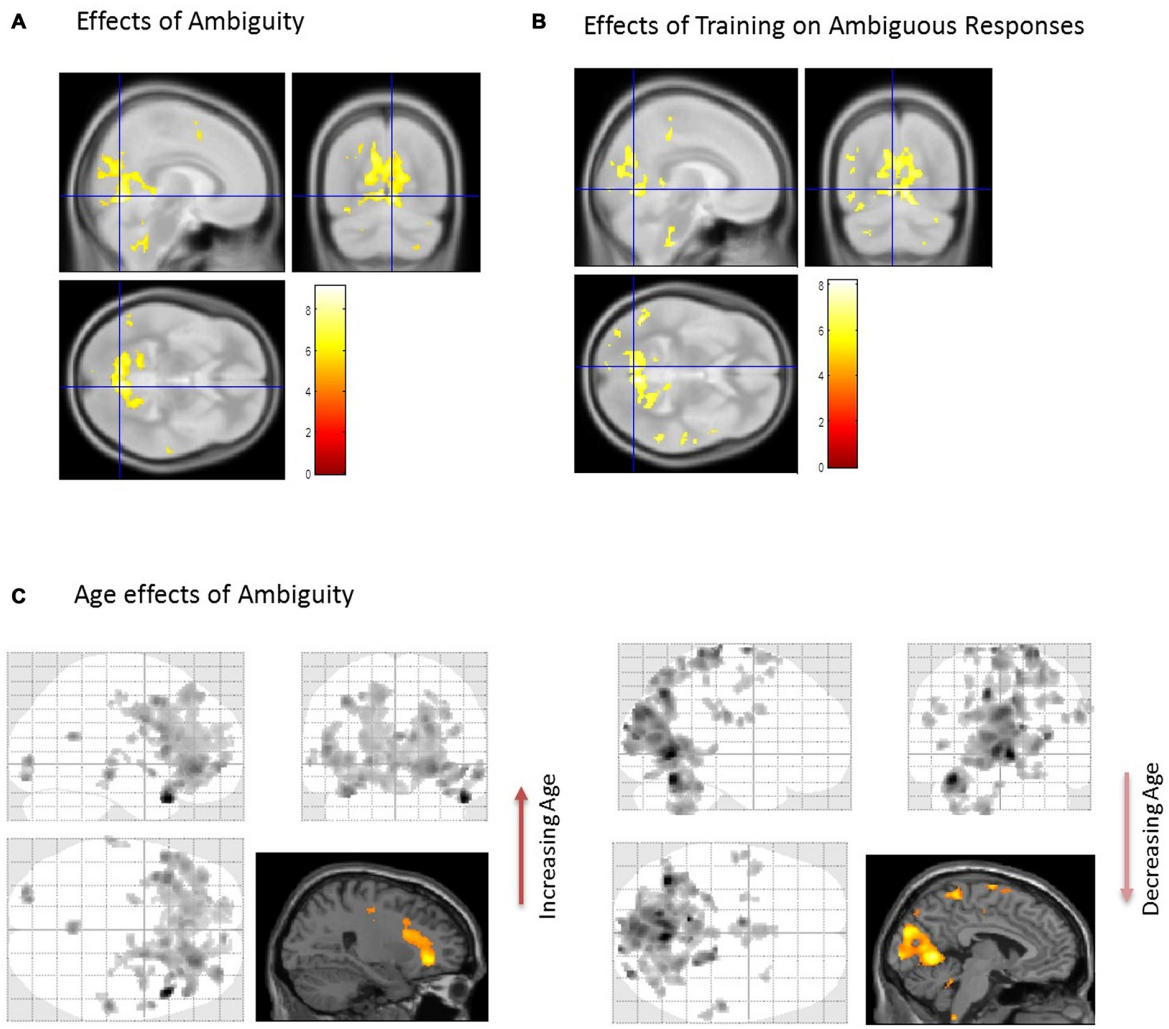

FIGURE 2 | Brain activations associated with the perception of ambiguous stimulus. (A) When comparing Ambiguous and non-Ambiguous stimuli the overall effect was seen with a group peak activation in the R Lingual [6 −68 −4] ($p < 0.05$, family wise error (FWE) corrected). **(B)** Comparison of ambiguous stimuli before (Block 1) and after training (Block 3). When comparing the two ambiguous blocks (1 and 3) to measure the effect of the "biasing" block. Here, similar regions in parietal and visual cortices predominated with significant effects also observed in the right anterior temporal cortex ($p < 0.05$ *FWE* corrected, **Table 1**). **(C)** Using the regions differentially active to ambiguous vs. non-ambiguous stimuli as a mask **(A)** we then found activations that positively correlated with age in anterior regions (Right orbitofrontal and anterior temporal lobe, top image, $p < 0.001$, uncorrected, **Table 1**). In contrast regions negatively correlated with age were observed posteriorly (cluster peaks in lingual gyrus and precuneus, bottom image, $p < 0.001$, uncorrected, **Table 1**). For extracting our ROIs, application of F-contrasts as inclusive masks and these regions were present at $p < 0.05$, *FWE* corrected (image not shown).

training was seen in posterior regions with peak activation in the right LIN [4 −64 6] ($p < 0.05$, FWE). To unpack this result we performed a "simple main effects" analysis specifically for training in **Figure 2B**. Here, we tested only for the effects of the non-ambiguous training block we compared ambiguous responses pre and post training. This contrast showed that similar regions exhibited the biasing effects as previous seen for ambiguous processing generally (ambiguous pre-trained vs. ambiguous post-training), including LIN, PRE and middle temporal cortices ($p < 0.05$, FWE, **Table 1**). Furthermore, we tested for other covariates that may be implicated in the context of psychopathology, including gender and education. These covariates did not show any significant effects in activation between male or female participants or in terms of education level categorized by some high school, high school graduate, some college, college graduate (data not shown).

DCM of Ambiguous Visual Processing and Age-Related Connectivity Effects

We used those activations associated with ambiguous compared to non-ambiguous stimuli to study perceptual belief networks using DCM (see "Materials and Methods" Section, **Figure 3A**). We were particularly interested in the mechanisms subtending switches in subjective perceptual beliefs and the effects bias training had on the network. To analyze switch responses we defined "pre-switch events", a 2000 ms period immediately prior to a button press indicating the percept had switched. We chose this timing due to the possibility of active networks present before the action of a button press, without overlapping button press responses. This was motivated by previous research suggesting that subjective decisions can be observed in fMRI activity up to 10 s prior to a motor report (Soon et al., 2008). Our network comprised four regions including LIN, PRE, mid-temporal gyrus (MTG) and IOF, with intrinsic connections arranged reciprocally among these regions (with the exception of IOF to MTG). The percent variances explained by our fMRI data in the four extracted principal eigenvariates over an 8 mm-radius sphere were determined and averages across all subjects were calculated (**Table 2**).

TABLE 2 | Average percent variation explained in regions of interest (ROIs).

	Average percent variance ± SEM
LIN	79.00% ± 1.91
PRE	79.18% ± 1.89
MTG	74.75% ± 2.06
IOF	77.58% ± 2.32

For our DCMs, we extracted the principal eigenvariate for an 8 mm-radius sphere around a group peak at the four regions of interest (LIN: [−6, −68, −2]; PRE: [−12, −70, 36]; MTG: [50, 30, −6]; IOF: [62, −22, −6]) at p < 0.05, uncorrected. This principal eigenvariates explain the above percent variances on average over each region for all subjects. The table shows average ± standard error mean of these regions across all 30 subjects.

We constructed four models to test for training-related differences in top-down vs. bottom-up perceptual control. In model 1, pre-switch modulations during the pre-training block were confined to bottom-up connections and pre-switch modulations during the post-training block were confined to top-down connections. In model 2, we allowed for both bottom-up and top-down pre-switch modulations in both pre- and post-training blocks (**Figure 3B**). In model 3, only bottom-up pre-switch modulations were present in both pre- and post-training blocks. In contrast, in model 4, only top-down pre-switch modulations were present in both pre- and post-training blocks. We show the equations representing the models (**Figure 3C**). Using a random-effects Bayesian model comparison across participants and within each cohort separately we found that both the young and older cohorts preferred model 1 (with a model exceedance probability (MEP) of 0.9993 for all subjects, **Figure 3D**, MEP = 0.9882 in the young cohort, and MEP = 0.9494 in the older cohort). The effect across individuals was consistent with 11 participants in the younger cohort preferring model 1, and the other three preferring model 3. Nine participants in the older cohort preferred model 1, five preferred model 4, and two preferred model 3.

Equipped with this winning model we tested for training or biasing effects within each cohort. To test for effect size, the average coefficients of determination for the model fit were determined in each cohort. There is a medium effect size for the lingual region in the young cohort, a medium effect size for the middle temporal regions in both cohorts, and a small effect size for PRE and inferior orbitofrontal regions (**Table 3**). Interestingly, we observed that the young cohort exhibited no significant modulations in connections related to training. Rather, we found that the arrangement of driving inputs differed between pre- and post-training. Specifically, the initial pre-training block was associated with a negative driving input to both lingual (student's t test; $p = 0.0016$) and PRE sources ($p = 0.014$), while in the post-training block these negative driving inputs were confined to the lingual source only ($p = 0.0017$). These negative driving inputs will suppress endogenous noise in each region under the stochastic DCM. In the older cohort however significant effects of training were observed—with the emergence of a significant top-down connection from the middle temporal gyrus to LIN on the post-training block ($p < 0.05$; **Figure 4A**). This cohort also exhibited negative input drive into lingual and frontal sources post training ($p < 0.05$). Within both cohorts, the DCMs adequately recapitulated the measured data features (**Figure 4B**).

Hemodynamic changes with age may alter BOLD activity and contribute to second-level group statistics (Tsvetanov et al., 2015). With DCM we were able to separate the hemodynamic parameters and test whether they exhibited age-dependent effects. However no effects of age on hemodynamic parameters were observed where we tested decay and transit time differences between the two age groups for all four regions ($p > 0.1$ uncorrected for eight tests).

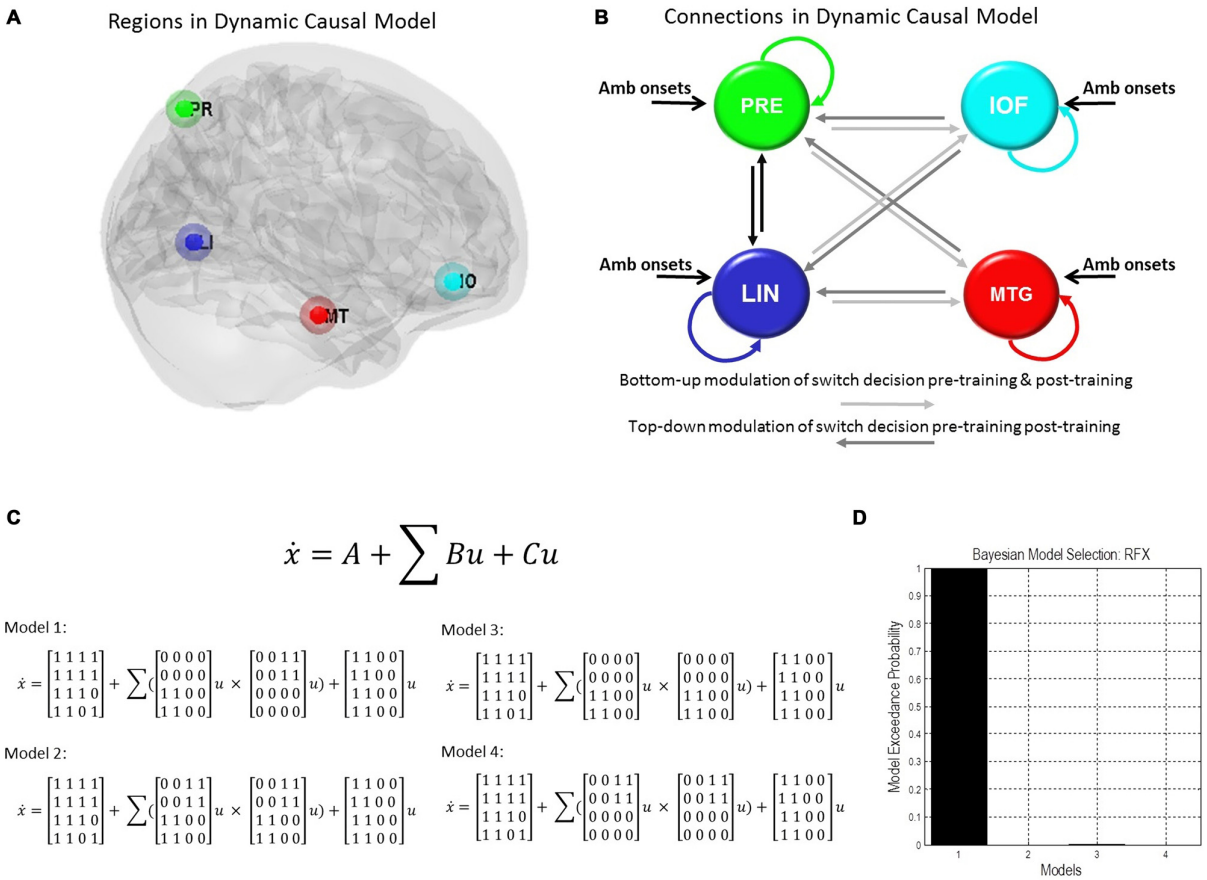

FIGURE 3 | Dynamic causal model and Bayesian model selection. (A) Sources for the Dynamic Causal Modelings (DCMs) were obtained from the second level analysis, displayed here. Regions of interest were identified around the group peak coordinates for Lingual [−6 −68 −2], Precuneus [−12 −70 36], Mid Temporal [50 30 −6], and Inf Orbitofrontal [62 −22 −6]. **(B)** The four regions of interest (ROIs) were used to create a stochastic DCM. There were intrinsic connections within all regions and between all regions, except for the inferior orbitofrontal cortex (IOF) and middle temporal gyrus (MTG). **(B)** Inputs from ambiguous image onsets entered all regions. The modulations in connections associated with pre-switch events were tested using Bayesian model comparison. In model 1 pre-switch connections in the pre-training block were confined to bottom-up connections (light gray), i.e., from Lingual and PRE to Inferior Orbitofrontal and Mid Temporal Lobe. While in model 1 post-training switches were modeled via top-down connection modulations only (dark gray), i.e., from Inferior Orbitofrontal and Mid Temporal Lobe to Lingual and PRE. Model 2 comprised pre-switch, pre- and post-training modulations in both directions. Model 3 consisted of bottom-up pre-switch modulations for both pre- and post-training modulations. Finally, model 4 involved of top-down pre-switch modulations for both pre- and post-training modulations. **(C)** We also display the equations used to define each of these models. A is the intrinsic connection parameters matrix. B is the input-dependent or modulatory connection parameter matrix. z denotes the regions. C is the extrinsic influences or input connection parameter matrix. u Represents the inputs. **(D)** Bayesian model comparison revealed that both younger and older cohorts preferred model 1 (see "Results" Section) and these fixed effects were consistent across most subjects. Here, we illustrate the exceedance probabilities for a comparison including all models from both age groups.

TABLE 3 | Average coefficient of determination for DCM fits in ROIs.

	Average coefficient of determination (R^2) ± SEM			
	LIN	**PRE**	**MTG**	**IOF**
Young (n = 14)	0.30 ± 0.03	0.12 ± 0.02	0.29 ± 0.04	0.076 ± 0.02
Older (n = 16)	0.20 ± 0.02	0.11 ± 0.03	0.28 ± 0.03	0.073 ± 0.02
Overall	0.24 ± 0.02	0.12 ± 0.02	0.29 ± 0.02	0.074 ± 0.01

Coefficients of determination for DCM fits were calculated for all 30 subjects for the winning model. We present these as effect size for our DCM data extraction and model fit. We compared predicted response with observed response. Coefficients of determination show a medium effect size for the LIN region in the young cohort, a medium effect size for the MTG region in both cohorts, and a small effect size for PRE and IOF regions.

DISCUSSION

Despite theoretical and imaging-driven advances in understanding bistable perception, its interaction with an aging neurobiology has received little attention. Motivated by the ubiquitous role age plays in psychopathological status (Häfner et al., 1998; Ho et al., 2000; Jeste et al., 2003; Topor et al., 2013; Lin et al., 2006), the present study addresses the age-dependency of neuronal connectivity underlying volitional control of perceptual beliefs. In our study, we investigated the brain regions associated with fluctuating perceptual content, whether these brain regions interact during perceptual rivalry, and how stimulus-driven biasing can affect subsequent subjective perceptual beliefs and neuronal

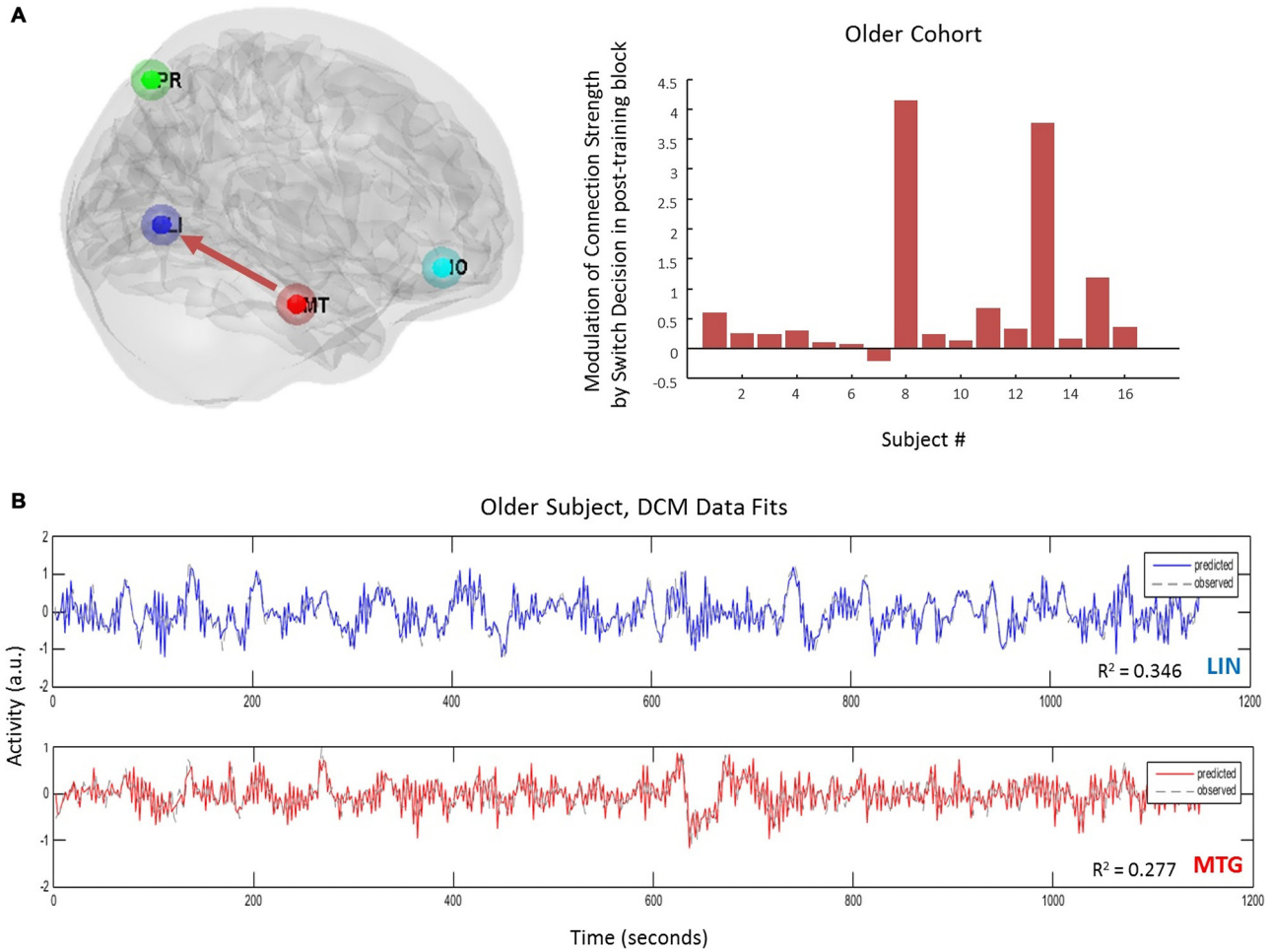

FIGURE 4 | Age-effects on connectivity mediating volitional perception. (A) Only in the older cohort did we see pre-switch modulations of effective connectivity. Specifically we observed an emergence of a top-down control connection (MTG → LIN) following the bias or training block. **(B)** DCM fits here from one subject and displayed for two regions accurately recapitulate the extracted time-series.

connectivity. In our study, we used the Rubin vase diagram and manipulated the image in order to bias perception and tested the underlying processing networks using fMRI and DCM. In summary our findings reveal that consistent with our hypothesized training effect, older cohorts exhibited a resistance to perceptual biasing compared to the younger cohort and these effects were found to be mediated by an increase in top-down connections from temporal to visual cortical sources post training.

Our study was motivated by predictive coding theories of cortico-cortical interactions which has been explored recently in the context of visual illusory processing (Brown and Friston, 2012; Chopin and Mamassian, 2012). Our aim was to determine whether prior beliefs could resist external manipulation in an age-dependent manner. Our paradigm was suited to this connectivity hypothesis given recent work by Kok et al. (2016) who show that top-down connections selectively activate early visual regions during the perception of illusory figures such as the Kanizsa stimulus. In our study, we used the non-ambiguous block for training to test whether inference networks within the brain became more robust to environmental perturbations as we age. This fits within larger theoretical frameworks such as the Free-energy principle (Brown and Friston, 2012), which appeals to the Bayesian brain hypothesis and laminar specific connectivity which optimizes to better predict future sensory inputs (Moran et al., 2014). With this in mind, we suggest that perceptual switches in the aging population can be described as changes in connectivity between regions, generated by an internal predictive model. In the context of visual processing and perceptual competition, binocular rivalry is another phenomenon explained in the framework of a brain that is engaged in Bayesian inference (Hohwy et al., 2008). Furthermore our motivation for this framework relates to psychopathology where studies such as Shergill et al. (2005) have implicated predictive coding abnormalities in diseases such as schizophrenia.

Whole-brain analysis from the fMRI study identified a network of cortical regions involved in viewing the ambiguous figures that included the LIN and precuneus, regions typically associated with perceptual changes in ambiguous figures (Sterzer and Kleinschmidt, 2007; Wang et al., 2013). Within these activated regions we found a striking correlation with aging, as age increases the ambiguity-associated activations predominated in anterior regions, while younger age was associated with greater posterior activity. This is consistent with general aging effects observed in fMRI-neurocognitive experiments which demonstrate a posterior to anterior shift in activation (PASA) patterns (Cabeza, 2001; Davis et al., 2008). With regards to PASA, there is reduced neural specialization in the visual cortex with age as well as an increase in distributed processing in frontal areas (Cabeza, 2001), with these anterior shifts noted in visual processing tasks (Ansado et al., 2012). However, such a paradigm has not been considered in bistable perception visual processing, making our study unique in that matter. In our study, we show that this shift to anterior regions of the brain can be associated with visual processing and perceptual control and not attributed to any specific default network, which has been shown to undergo reallocation with aging as a compensatory mechanism (Davis et al., 2008). We are unable to provide evidence for or against a compensatory mechanism in our study since we do not have a metric of "good" or "poor" performance. Instead, we are interested in Bayesian predictive coding leading to differences in connectivity. Exploring our activations using DCM we found that younger participants did recruit frontal regions during ambiguous stimulus processing but that this dropped offline following a biasing session. In contrast, our older cohorts resisted biasing and furthermore recruited top-down connections to control their perceptual beliefs following training. In the context of psychopathology it may be useful to control perceptual beliefs internally and to resist model updating based on spurious environmental stimuli. An inaccurate assignment of one's environmental experiences may contribute to the underlying pathology in diseases such as schizophrenia (Kapur, 2003).

Previous behavioral studies using binocular rivalry have shown that perceptual stability increases with increasing age (Ukai et al., 2003; Beers et al., 2013). However, binocular rivalry, compared to bistable perception with ambiguous figures, involves a more automatic and stimulus driven form of visual competition occurring at the lower levels of the visual pathway (Tong et al., 2006). We do not assume that our findings extend to studies of binocular rivalry. Bistable perception with ambiguous figures occurs at a higher level in the visual pathway (Tong and Engel, 2001). This provides a method of intentional control, making it more suitable for the larger goal of our analysis, which is the study of the active process of perception. Using multisensory sound flash-illusions, studies have also demonstrated that aging presents with stronger illusory percepts compared to younger adults (DeLoss et al., 2013), but that training to avoid the temporal overlap illusion can be accomplished by older cohorts (Setti et al., 2014). Few studies however have sought to establish the neural correlates of these effects. In our study we used stochastic DCM for fMRI (Daunizeau et al., 2011; Li et al., 2011) in order to account for the internally-generated dynamics that cause endogenous percept fluctuations as well as task-dependent changes (deterministic effects; Friston et al., 2014). This is in contradistinction to other spectral DCMs which may present a more accurate and parsimonious account of connectivity in studies examining complete resting or stationary states (Razi et al., 2015). The optimized parameter sets of our stochastic models revealed interesting dynamics particularly in the driving inputs (Friston et al., 2003). We found that negative driving inputs were observed in posterior and frontal sources for the older subjects post-training whereas for the younger subjects these patterns were seen pre-training with a dropout of frontal inhibitory drive post-training. The polarity of these driving inputs are reasonable in the setting of stochastic DCMs since they would dampen endogenous noisy fluctuations in their respective regions and in the case of the older cohort enable top-down control via long-range connections.

Our results complement previous studies involving bistable perception, which have shown a decline in attentional selection of low-salient stimuli (Tsvetanov et al., 2013). Additionally, Aydin et al. (2013) examined perceptual switching of the Rubin vase showing that older individuals are less likely to attend to visual stimuli after holding a specific percept. In fact, the older group prefers the novel percept. However, we do not use distractors or perceptual holding in our experiment but rather assess control in the context of biasing effects.

Overall, our analysis provides a holistic account of bistable perceptual processing in aging given the combination of fMRI and stochastic DCMs. Our observed network involving the frontal and temporal regions was derived from our whole brain analysis. Our regions in these models are supported by previous research suggesting significant modulation of inferior frontal cortex to medial temporal regions during the perceptual transitions of the ambiguous rotating Lissajous figure (Weilnhammer et al., 2013). All of our four ROIs have been shown to respond to bistable percepts in previous studies (Wang et al., 2013). An electroencephalogram (EEG) study on bistable perception using ambiguous images showed activity in the posterior visual regions in addition to higher-order fronto-parietal and temporal regions of the brain (Britz et al., 2009). In terms of psychopathology, frontal and temporal cortices, specifically the inferior frontal gyrus and superior temporal gyrus, is implicated in schizophrenia showing altered connectivity in resting state fMRI study (Zaytseva et al., 2015). Orbitofrontal cortices and middle temporal gyrus are furthermore areas of disruption in perspective-taking tasks in schizophrenia (Eack et al., 2013). Brain networks such as the default network or salience network may play a role in bistable perception and show differences in age. Future work can use task-based independent component analysis (ICA; Hyett et al., 2015; Tsvetanov et al., 2015) to characterize the network topology in control to better understand perceptual changes.

Limitations of the study include other covariates that are affected with normal aging. For example, potential time

differences may exist in the pre-switch event with age. In our study, we allotted the same pre-switch period duration for both the younger and older group. Given that our analysis relies on subjective recording of perceptual switches, this is an inherent limitation in the study of bistable perception since the only objective marker to assume a change in perception is the button press. Other limitations of the study include putative effects on bistability not accounted for in our design including eye position (Einhäuser et al., 2004) or attention (van Ee et al., 2005). Future studies could address these and more fine-grained features of aging control dynamics, using electrophysiological DCMs (Legon et al., 2015). For example, GABA levels in the visual cortex have been linked to bistable perception, with higher concentrations resulting in slower perceptual dynamics (van Loon et al., 2013)-an effect used to simulate aging differences in computational modeling studies of multistable perception (Hoshino, 2013). These simple visual paradigms may uncover further neurobiological correlates of perceptual control, and provide important clues for developmental and aging dependencies in psychopathology.

AUTHOR CONTRIBUTIONS

ED and RJM designed the experiment, performed analysis. ED, SEA and ABS collected the data. ED, SEA, ABS and RJM prepared the manuscript.

FUNDING

This work was supported by a start-up grant from VTCRI to RJM.

REFERENCES

Ansado, J., Monchi, O., Ennabil, N., Faure, S., and Joanette, Y. (2012). Load-dependent posterior-anterior shift in aging in complex visual selective attention situations. *Brain Res.* 1454, 14–22. doi: 10.1016/j.brainres.2012.02.061

Aydin, S., Strang, N. C., and Manahilov, V. (2013). Age-related deficits in attentional control of perceptual rivalry. *Vision Res.* 77, 32–40. doi: 10.1016/j.visres.2012.11.010

Beers, A. M., Bennett, P. J., and Sekuler, A. B. (2013). Age-related effects of size and contrast on binocular rivalry. *J. Vis.* 13, 546–546. doi: 10.1167/13.9.546

Blake, R. (1989). A neural theory of binocular rivalry. *Psychol. Rev.* 96, 145–167. doi: 10.1037/0033-295x.96.1.145

Britz, J., Landis, T., and Michel, C. M. (2009). Right parietal brain activity precedes perceptual alternation of bistable stimuli. *Cereb. Cortex* 19, 55–65. doi: 10.1093/cercor/bhn056

Brown, H., and Friston, K. J. (2012). Free-energy and illusions: the cornsweet effect. *Front. Psychol.* 3:43. doi: 10.3389/fpsyg.2012.00043

Cabeza, R. (2001). Cognitive neuroscience of aging: contributions of functional neuroimaging. *Scand. J. Psychol.* 42, 277–286. doi: 10.1111/1467-9450.00237

Cardin, V., Friston, K. J., and Zeki, S. (2011). Top-down modulations in the visual form pathway revealed with dynamic causal modeling. *Cereb. Cortex* 21, 550–562. doi: 10.1093/cercor/bhq122

Carlson, G. A., Bromet, E. J., Driessens, C., Mojtabai, R., and Schwartz, J. E. (2002). Age at onset, childhood psychopathology and 2-year outcome in psychotic bipolar disorder. *Am. J. Psychiatry* 159, 307–309. doi: 10.1176/appi.ajp.159.2.307

Carter, T. D. C., Mundo, E., Parikh, S. V., and Kennedy, J. L. (2003). Early age at onset as a risk factor for poor outcome of bipolar disorder. *J. Psychiatr. Res.* 37, 297–303. doi: 10.1016/s0022-3956(03)00052-9

Chopin, A., and Mamassian, P. (2012). Predictive properties of visual adaptation. *Curr. Biol.* 22, 622–626. doi: 10.1016/j.cub.2012.02.021

Daunizeau, J., David, O., and Stephan, K. E. (2011). Dynamic causal modelling: a critical review of the biophysical and statistical foundations. *Neuroimage* 58, 312–322. doi: 10.1016/j.neuroimage.2009.11.062

Davis, S. W., Dennis, N. A., Daselaar, S. M., Fleck, M. S., and Cabeza, R. (2008). Qué PASA? the posterior-anterior shift in aging. *Cereb. Cortex* 18, 1201–1209. doi: 10.1093/cercor/bhm155

Dayan, P. (1998). A hierarchical model of binocular rivalry. *Neural Comput.* 10, 1119–1135. doi: 10.1162/089976698300017377

de Jong, M. C., Brascamp, J. W., Kemner, C., van Ee, R., and Verstraten, F. A. (2014). Implicit perceptual memory modulates early visual processing of ambiguous images. *J. Neurosci.* 34, 9970–9981. doi: 10.1523/JNEUROSCI.2413-13.2014

de Jong, M. C., Knapen, T., and van Ee, R. (2012). Opposite influence of perceptual memory on initial and prolonged perception of sensory ambiguity. *PLoS One* 7:e30595. doi: 10.1371/journal.pone.0030595

DeLoss, D. J., Pierce, R. S., and Andersen, G. J. (2013). Multisensory integration, aging and the sound-induced flash illusion. *Psychol. Aging* 28, 802–812. doi: 10.1037/a0033289

Dima, D., Roiser, J. P., Dietrich, D. E., Bonnemann, C., Lanfermann, H., Emrich, H. M., et al. (2009). Understanding why patients with schizophrenia do not perceive the hollow-mask illusion using dynamic causal modelling. *Neuroimage* 46, 1180–1186. doi: 10.1016/j.neuroimage.2009.03.033

Dima, D., Dietrich, D. E., Dillo, W., and Emrich, H. M. (2010). Impaired top-down processes in schizophrenia: a DCM study of ERPs. *Neuroimage* 52, 824–832. doi: 10.1016/j.neuroimage.2009.12.086

Eack, S. M., Wojtalik, J. A., Newhill, C. E., Keshavan, M. S., and Phillips, M. L. (2013). Prefrontal cortical dysfunction during visual perspective-taking in schizophrenia. *Schizophr. Res.* 150, 491–497. doi: 10.1016/j.schres.2013.08.022

Einhäuser, W., Martin, K. A., and König, P. (2004). Are switches in perception of the Necker cube related to eye position? *Eur. J. Neurosci.* 20, 2811–2818. doi: 10.1111/j.1460-9568.2004.03722.x

Foxe, J. J., Murray, M. M., and Javitt, D. C. (2005). Filling-in in schizophrenia: a high-density electrical mapping and source-analysis investigation of illusory contour processing. *Cereb. Cortex* 15, 1914–1927. doi: 10.1093/cercor/bhi069

Friston, K. J., Harrison, L., and Penny, W. (2003). Dynamic causal modelling. *Neuroimage* 19, 1273–1302. doi: 10.1016/s1053-8119(03)00202-7

Friston, K. J., Kahan, J., Biswal, B., and Razi, A. (2014). A DCM for resting state fMRI. *Neuroimage* 94, 396–407. doi: 10.1016/j.neuroimage.2013.12.009

Gur, R. E., Petty, R. G., Turetsky, B. I., and Gur, R. C. (1996). Schizophrenia throughout life: sex differences in severity and profile of symptoms. *Schizophr. Res.* 21, 1–12. doi: 10.1016/0920-9964(96)00023-0

Häfner, H., Hambrecht, M., Löffler, W., Munk-Jørgensen, P., and Riecher-Rössler, A. (1998). Is schizophrenia a disorder of all ages? A comparison of first episodes and early course across the life-cycle. *Psychol. Med.* 28, 351–365. doi: 10.1017/s0033291797006399

Ho, B. C., Andreasen, N. C., Flaum, M., Nopoulos, P., and Miller, D. (2000). Untreated initial psychosis: its relation to quality of life and symptom remission in first-episode schizophrenia. *Am. J. Psychiatry* 157, 808–815. doi: 10.1176/appi.ajp.157.5.808

Hohwy, J., Roepstorff, A., and Friston, K. (2008). Predictive coding explains binocular rivalry: an epistemological review. *Cognition* 108, 687–701. doi: 10.1016/j.cognition.2008.05.010

Hoshino, O. (2013). Ambient GABA responsible for age-related changes in multistable perception. *Neural Comput.* 25, 1164–1190. doi: 10.1162/NECO_a_00431

Hyett, M. P., Breakspear, M. J., Friston, K. J., Guo, C. C., and Parker, G. B. (2015). Disrupted effective connectivity of cortical systems supporting attention and interoception in melancholia. *JAMA Psychiatry* 72, 350–358. doi: 10.1001/jamapsychiatry.2014.2490

Jeste, D. V., Twamley, E. W., Eyler Zorrilla, L. T., Golshan, S., Patterson, T. L., and Palmer, B. W. (2003). Aging and outcome in schizophrenia. *Acta Psychiatr. Scand.* 107, 336–343. doi: 10.1034/j.1600-0447.2003.01434.x

Kapur, S. (2003). Psychosis as a state of aberrant salience: a framework linking biology, phenomenology and pharmacology in schizophrenia. *Am. J. Psychiatry* 160, 13–23. doi: 10.1176/appi.ajp.160.1.13

Kersten, D., and Schrater, P. R. (2002). "Pattern inference theory: a probabilistic approach to vision," in *Perception and the Physical World*, eds R. Mausfeld and D. Heyer (Chichester: John Wiley & Sons), 191–228.

Kloosterman, N. A., Meindertsma, T., Hillebrand, A., van Dijk, B. W., Lamme, V. A., and Donner, T. H. (2015). Top-down modulation in human visual cortex predicts the stability of a perceptual illusion. *J. Neurophysiol.* 113, 1063–1076. doi: 10.1152/jn.00338.2014

Kok, P., Bains, L. J., van Mourik, T., Norris, D. G., and de Lange, F. P. (2016). Selective activation of the deep layers of the human primary visual cortex by top-down feedback. *Curr. Biol.* 26, 371–376. doi: 10.1016/j.cub.2015.12.038

Kramer, P., and Yantis, S. (1997). Perceptual grouping in space and time: evidence from the ternus display. *Percept. Psychophys.* 59, 87–99. doi: 10.3758/bf03206851

Legon, W., Punzell, S., Dowlati, E., Adams, S. E., Stiles, A. B., and Moran, R. J. (2015). Altered prefrontal excitation/inhibition balance and prefrontal output: markers of aging in human memory networks. *Cereb. Cortex*. doi: 10.1093/cercor/bhv200 [Epub ahead of print].

Leopold, D. A., and Logothetis, N. K. (1999). Multistable phenomena: changing views in perception. *Trends Cogn. Sci.* 3, 254–264. doi: 10.1016/s1364-6613(99)01332-7

Leopold, D. A., Wilke, M., Maier, A., and Logothetis, N. K. (2002). Stable perception of visually ambiguous patterns. *Nat. Neurosci.* 5, 605–609. doi: 10.1038/nn851

Li, B., Daunizeau, J., Stephan, K. E., Penny, W., Hu, D., and Friston, K. (2011). Generalised filtering and stochastic DCM for fMRI. *Neuroimage* 58, 442–457. doi: 10.1016/j.neuroimage.2011.01.085

Lin, P. I., McInnis, M. G., Potash, J. B., Willour, V., MacKinnon, D. F., DePaulo, J. R., et al. (2006). Clinical correlates and familial aggregation of age at onset in bipolar disorder. *Am. J. Psychiatry* 163, 240–246. doi: 10.1176/appi.ajp.163.2.240

Malla, A., Norman, R., Schmitz, N., Manchanda, R., BÉChard-Evans, L., Takhar, J., et al. (2006). Predictors of rate and time to remission in first-episode psychosis: a two-year outcome study. *Psychol. Med.* 36, 649–658. doi: 10.1017/s0033291706007379

Moran, R. J., Symmonds, M., Dolan, R. J., and Friston, K. J. (2014). The brain ages optimally to model its environment: evidence from sensory learning over the adult lifespan. *PLoS Comput. Biol.* 10:e1003422. doi: 10.1371/journal.pcbi.1003422

Notredame, C. E., Pins, D., Deneve, S., and Jardri, R. (2014). What visual illusions teach us about schizophrenia. *Front. Integr. Neurosci.* 8:63. doi: 10.3389/fnint.2014.00063

Razi, A., Kahan, J., Rees, G., and Friston, K. J. (2015). Construct validation of a DCM for resting state fMRI. *Neuroimage* 106, 1–14. doi: 10.1016/j.neuroimage.2014.11.027

Rubin, E. (1921). *Visuell Wahrgenommene Figuren: Studien in Psychologischer Analyse*. Copenhagen: Gyldendalske boghandel.

Schultz, S. K., Miller, D. D., Oliver, S. E., Arndt, S., Flaum, M., and Andreasen, N. C. (1997). The life course of schizophrenia: age and symptom dimensions. *Schizophr. Res.* 23, 15–23. doi: 10.1016/s0920-9964(96)00087-4

Setti, A., Stapleton, J., Leahy, D., Walsh, C., Kenny, R. A., and Newell, F. N. (2014). Improving the efficiency of multisensory integration in older adults: audio-visual temporal discrimination training reduces susceptibility to the sound-induced flash illusion. *Neuropsychologia* 61, 259–268. doi: 10.1016/j.neuropsychologia.2014.06.027

Shapiro, A., Moreno-Bote, R., Rubin, N., and Rinzel, J. (2009). Balance between noise and adaptation in competition models of perceptual bistability. *J. Comput. Neurosci.* 27, 37–54. doi: 10.1007/s10827-008-0125-3

Shergill, S. S., Samson, G., Bays, P. M., Frith, C. D., and Wolpert, D. M. (2005). Evidence for sensory prediction deficits in schizophrenia. *Am. J. Psychiatry* 162, 2384–2386. doi: 10.1176/appi.ajp.162.12.2384

Soon, C. S., Brass, M., Heinze, H. J., and Haynes, J. D. (2008). Unconscious determinants of free decisions in the human brain. *Nat. Neurosci.* 11, 543–545. doi: 10.1038/nn.2112

Stephan, K. E., Weiskopf, N., Drysdale, P. M., Robinson, P. A., and Friston, K. J. (2007). Comparing hemodynamic models with DCM. *Neuroimage* 38, 387–401. doi: 10.1016/j.neuroimage.2007.07.040

Sterzer, P., and Kleinschmidt, A. (2007). A neural basis for inference in perceptual ambiguity. *Proc. Natl. Acad. Sci. U S A* 104, 323–328. doi: 10.1073/pnas.0609006104

Sterzer, P., Kleinschmidt, A., and Rees, G. (2009). The neural bases of multistable perception. *Trends Cogn. Sci.* 13, 310–318. doi: 10.1016/j.tics.2009.04.006

Sundareswara, R., and Schrater, P. R. (2008). Perceptual multistability predicted by search model for Bayesian decisions. *J. Vis.* 8, 12.1–12.19. doi: 10.1167/8.5.12

Tong, F., and Engel, S. A. (2001). Interocular rivalry revealed in the human cortical blind-spot representation. *Nature* 411, 195–199. doi: 10.1038/35075583

Tong, F., Meng, M., and Blake, R. (2006). Neural bases of binocular rivalry. *Trends Cogn. Sci.* 10, 502–511. doi: 10.1016/j.tics.2006.09.003

Topor, D. R., Swenson, L., Hunt, J. I., Birmaher, B., Strober, M., Yen, S., et al. (2013). Manic symptoms in youth with bipolar disorder: factor analysis by age of symptom onset and current age. *J. Affect. Disord.* 145, 409–412. doi: 10.1016/j.jad.2012.06.024

Tsvetanov, K. A., Henson, R. N. A., Tyler, L. K., Davis, S. W., Shafto, M. A., Taylor, J. R., et al. (2015). The effect of ageing on fMRI: correction for the confounding effects of vascular reactivity evaluated by joint fMRI and MEG in 335 adults. *Hum. Brain Mapp.* 36, 2248–2269. doi: 10.1002/hbm.22768

Tsvetanov, K. A., Mevorach, C., Allen, H., and Humphreys, G. W. (2013). Age-related differences in selection by visual saliency. *Atten. Percept. Psychophys* 75, 1382–1394. doi: 10.3758/s13414-013-0499-9

Ukai, K., Ando, H., and Kuze, J. (2003). Binocular rivalry alternation rate declines with age. *Percept. Mot. Skills* 97, 393–397. doi: 10.2466/pms.97.5.393-397

van Ee, R., van Dam, L. C. J., and Brouwer, G. J. (2005). Voluntary control and the dynamics of perceptual bi-stability. *Vision Res.* 45, 41–55. doi: 10.1016/j.visres.2004.07.030

van Loon, A. M., Knapen, T., Scholte, H. S., St. John-Saaltink, E. , Donner, T. H., and Lamme, V. A. (2013). GABA shapes the dynamics of bistable perception. *Curr. Biol.* 23, 823–827. doi: 10.1016/j.cub.2013.03.067

Wang, M., Arteaga, D., and He, B. (2013). Brain mechanisms for simple perception and bistable perception. *Proc. Natl. Acad. Sci. U S A* 10, E3350–E3359. doi: 10.1073/pnas.1221945110

Weilnhammer, V. A., Ludwig, K., Hesselmann, G., and Sterzer, P. (2013). Frontoparietal cortex mediates perceptual transitions in bistable perception. *J. Neurosci.* 33, 16009–16015. doi: 10.1523/JNEUROSCI.1418-13.2013

Zaytseva, Y., Chan, R. C., Pöppel, E., and Heinz, A. (2015). Luria revisited: cognitive research in schizophrenia, past implications and future challenges. *Philos. Ethics Humanit. Med.* 10:4. doi: 10.1186/s13010-015-0026-9

Conflict of Interest Statement: The authors declare that the research was conducted in the absence of any commercial or financial relationships that could be construed as a potential conflict of interest.

frontiers in Human Neuroscience

ORIGINAL RESEARCH
published: 04 May 2016
doi: 10.3389/fnhum.2016.00195

Mapping Smoking Addiction Using Effective Connectivity Analysis

*Rongxiang Tang[1], Adeel Razi[2,3], Karl J. Friston[2] and Yi-Yuan Tang[4]**

[1] Department of Psychology, Washington University in St. Louis, St. Louis, MO, USA, [2] The Wellcome Trust Centre for Neuroimaging, University College London, London, UK, [3] Department of Electronic Engineering, NED University of Engineering and Technology, Karachi, Pakistan, [4] Department of Psychological Sciences, Texas Tech University, Lubbock, TX, USA

Prefrontal and parietal cortex, including the default mode network (DMN; medial prefrontal cortex (mPFC), and posterior cingulate cortex, PCC), have been implicated in addiction. Nonetheless, it remains unclear which brain regions play a crucial role in smoking addiction and the relationship among these regions. Since functional connectivity only measures correlations, addiction-related changes in effective connectivity (directed information flow) among these distributed brain regions remain largely unknown. Here we applied spectral dynamic causal modeling (spDCM) to resting state fMRI to characterize changes in effective connectivity among core regions in smoking addiction. Compared to nonsmokers, smokers had reduced effective connectivity from PCC to mPFC and from RIPL to mPFC, a higher self-inhibition within PCC and a reduction in the amplitude of endogenous neuronal fluctuations driving the mPFC. These results indicate that spDCM can differentiate the functional architectures between the two groups, and may provide insight into the brain mechanisms underlying smoking addiction. Our results also suggest that future brain-based prevention and intervention in addiction should consider the amelioration of mPFC-PCC-IPL circuits.

Keywords: dynamic causal modeling (DCM), smoking addiction, medial prefrontal cortex (mPFC), posterior cingulate cortex (PCC), effective connectivity analysis

OPEN ACCESS

Edited by:
Yong He,
Beijing Normal University, China

Reviewed by:
Xia Liang,
National Institute on Drug Abuse, USA
Lirong Yan,
Wuhan General Hospital, China

****Correspondence:***
Yi-Yuan Tang
yiyuan.tang@ttu.edu

Received: *25 August 2015*
Accepted: *18 April 2016*
Published: *04 May 2016*

Citation:
Tang R, Razi A, Friston KJ and Tang Y-Y (2016) Mapping Smoking Addiction Using Effective Connectivity Analysis. Front. Hum. Neurosci. 10:195. doi: 10.3389/fnhum.2016.00195

INTRODUCTION

Tobacco use is a leading preventable cause of death. However, over 90% of smokers try repeatedly to quit but often fail (Centers for Disease Control and Prevention, 2006; Hajek et al., 2009). Nicotine, a component of tobacco, is the primary reason that tobacco is addictive. From the perspective of public health, there is an urgent need to address these serious issues in smoking addiction. Prefrontal and parietal cortex, including the default mode network (DMN); medial prefrontal cortex (mPFC), and posterior cingulate cortex (PCC), anterior cingulate cortex and limbic areas have been shown to involve in addiction (Baler and Volkow, 2006; Hong et al., 2009; Jarraya et al., 2010; Goldstein and Volkow, 2011; Tang et al., 2013, 2015a; Leech and Sharp, 2014; Liang et al., 2015; Weiland et al., 2015). Nonetheless, it remains unclear which brain regions play a crucial role in smoking addiction and the relationship among these regions.

Functional connectivity has been used to examine the intrinsic brain networks related to smoking addiction (Hu et al., 2015; Weiland et al., 2015). However, functional connectivity does not support inferences about causal or directed connectivity. Therefore, any changes in information flow among the brain areas implicated in smoking remain unclear. This limitation calls for a new solution that can characterize causal interactions. Dynamic causal modeling (DCM)

has the capacity to identify the causal (directed) connections among distributed brain areas—known as effective connectivity. Spectral DCM (Friston et al., 2014a,b) is especially suited for resting state Functional magnetic resonance imaging or functional MRI (fMRI) that can be summarized with cross spectra. In other words, spectral dynamic causal modeling (spDCM) estimates the effective connectivity among coupled brain regions, which subtends the observed functional connectivity in the frequency domain. Crucially, spectral DCM not only furnishes an efficient estimation of DCM parameters but also enables the detection of group differences in effective connectivity, the amplitude of endogenous neuronal fluctuations or both. It has been shown that spDCM is not only more accurate but also more sensitive to group differences, when compared to stochastic DCM (Razi et al., 2015).

In the current study, we focused on the differences of effective connectivity using spectral DCM at rest between the groups of smokers and non-smokers. We recruited 30 adults (15 smokers and 15 nonsmokers) and applied spectral DCM to resting state fMRI data to quantify the effective connectivity among core regions implicated in smoking addiction. We hypothesized that—in comparison with nonsmokers—smokers would show a disrupted equilibrium between intrinsic (within region) excitatory and inhibitory connectivity—and abnormalities in extrinsic (between region) connectivity, associated with mPFC-PCC-IPL circuits.

The default mode and its connectivity has provided a useful focus for many studies of dysconnectivity in normal subjects and psychopathology. In this work, we characterized coupling within the nodes of the default mode to establish its predictive validity in relation to addictive traits. Our motivation for examining the DMN was two-fold. First, many of the constituent nodes in the DMN have been implicated in addiction. Second, the resting state paradigm is simple and reproducible. In other words, establishing the predictive validity of resting state effective connectivity—as a biomarker in addiction research—may have useful implications for neurogenetic and clinical studies. However, the shortcomings of resting state fMRI studies should be acknowledged. This follows from the fact that endogenous fluctuations in the resting state do not necessarily engage those areas implicated in the functional anatomy of interest. In other words, by restricting our focus to an intrinsic brain network, we cannot guarantee that key connections responsible for executive control and decision making are estimated efficiently. Put simply, studying resting state functional connectivity is a little like "looking for keys under the lamppost". With this qualification in mind, we now turn to the evidence that many of DMN nodes have a direct relevance for impulsive behavior, attentional deployment and addiction.

Here we have focused on cardinal regions that constitute key nodes of DMN, where these regions have been previously implicated in addiction. The default mode has been implicated in introspective cognition and perspective taking (Amft et al., 2015; Konishi et al., 2015). Crucially, the integration between the salience system and default mode may play a key role in addiction and the moderation of impulsive behavior—as has been demonstrated in the context of cocaine addiction (Liang et al., 2015). This integration between internal and externally directed processing is further substantiated by recently reported reductions in executive and default network functional connectivity in smokers (Weiland et al., 2015). Furthermore, the addictive behavior may be related to a suspension of—or aberrant—reality testing, recent evidence points to the key role of the default mode (in particular, the medial prefrontal cortex) in reality monitoring, relative to source monitoring (Metzak et al., 2015). Clearly, this subset of regions does not provide an exhaustive characterization of the distributed networks implicated in addiction and behavioral control. A pragmatic reason we focused on nodes within the default mode is that these are the regions that were engaged during our resting state study. This is an important aspect of effective connectivity in the following sense: effective connectivity is inherently context sensitive. In other words, it can change with experimental condition, cognitive set and many other factors. This means that the effective connectivity assessed in the current report is specific to the resting state—and is only meaningfully evaluated among regions that show (endogenous) fluctuations in coupled neuronal activity. This is why we focused on components of the default mode that are implicated in addiction. The alternative approach would be to selectively engage regions known to be involved in addiction (and smoking) using a task-based paradigm that selectively activates key regions and implicitly engages effective connectivity among these regions. We will pursue this approach in subsequent work. Comparing the results of effective connectivity analyses between resting state and tasks based studies will be an interesting endeavor and will, hopefully, establish the construct validity of one in terms of the other.

MATERIALS AND METHODS

Subjects

Healthy college students, including smokers and nonsmokers, were recruited through campus advertisements. Among those who responded, we randomly assigned 15 cigarette smokers to one group and 15 nonsmokers to another group (mean ages, 21.30 ± 2.43 years, 20 men), there is no significant difference in age, gender and education between two randomized groups (all $p > 0.05$). We used the widely used Fagerström Test for Nicotine Dependence and carbon monoxide monitor to measure smoking addiction and severity (Heatherton et al., 1991; Deveci et al., 2004). The smokers used tobacco without other drugs, with an average of 10 cigarettes per day. The experiment was approved by the local institutional review board at Texas Tech University, and informed consent was obtained from each participant.

Neuroimaging

All data were collected using a 3-Telsa Siemens Skyra MRI scanner at the Texas Tech University. A 3D T1-weighted anatomical images were acquired using the MPRAGE sequence (Repetition time (TR) = 1, 780 ms; Echo time (TE) = 2.36 ms;

slice thickness = 1.0 mm). A 6-min resting-state functional scan (T2*-weighted images) was obtained for each participant using a gradient echo planar sequence (TR = 2000 ms; TE = 27 ms; flip angle = 80°; field of view (FOV) = 256 mm × 256 mm; matrix size = 64 × 64; slice thickness = 4 mm; Axial direction, 36 slices). Participants looked at a crosshair shown on a screen and were instructed not think of anything in particular. Head movement was minimized with individually custom-made foam padding (Fox and Raichle, 2007). We obtained 28 usable imaging time-series with 14 smokers and 14 nonsmokers for DCM analysis.

Functional data were processed using the Data processing assistant for resting-state fMRI[1], which is based on SPM[2] and resting-state fMRI data analysis toolkit (Song et al., 2011). For each participant, the subsequent standard procedures included slice timing, motion correction, regression of WM/CSF signals, and spatial normalization of images into the Montreal Neurological Institute template with a resampling voxel size of 3 × 3 × 3 mm. Finally, a Gaussian filter of 5 mm full-width at half-maximum (FWHM) was applied to the dataset for spatial smoothing (Tang et al., 2013). Our main analysis used spectral DCM as implemented in SPM12.

ROI Selection

Based on previous literature in addiction fields (Goldstein and Volkow, 2011; Volkow et al., 2012; Tang et al., 2015a), we identified four ROIs including the mPFC, PCC, left and right inferior parietal lobule (L-IPL and R-IPL) as key nodes for effective connectivity analysis. These analyses assess the causal interactions across these regions, as well as the amplitude of endogenous neuronal fluctuations within each region (Di and Biswal, 2014; Razi et al., 2015). To identify nodes of the DMN, the resting state was modeled using a GLM containing a discrete cosine basis set with frequencies ranging from 0.0078 to 0.1 Hz (Fransson, 2005; Kahan et al., 2014), in addition to the nuisance regressors that include the six head motion parameters, CSF and WM regressors. Six head motion parameters were also added into the model to remove potential confounding variances caused by head motion. Data were high-pass filtered to remove any slow frequency drifts (< 0.0078 Hz) in the normal manner. An F-contrast was specified across the discrete cosine transforms (DCT), producing an SPM that identified regions exhibiting blood oxygen level-dependent (BOLD) fluctuations within the frequency band. Our DMN graph comprised of four nodes; the PCC, the LIPL and RIPL), and the mPFC. The PCC node was identified using this GLM: the principal eigenvariate of a (8 mm radius) sphere was computed (adjusted for aforementioned confounds: six head motion parameters and CSF/WM regressors), centered on the peak voxel of the aforementioned F-contrast. The ensuing region of interest was masked by a (8 mm radius) sphere centered on previously reported MNI coordinates for the PCC [0, −52, 26; Di and Biswal, 2014; Razi et al., 2015]. The remaining DMN nodes were identified using a standard seed-based functional connectivity analysis, using the PCC as the reference time series in an independent GLM containing the same confounds. A *t*-contrast on the PCC time series was specified, and the resulting SPM was masked by spheres centered on previously reported coordinates for the RIPC [48, −69, 35], LIPC [−50, −63, 32], and mPFC [3, 54, −2; Di and Biswal, 2014; Razi et al., 2015]. The principal eigenvariate from a (8 mm radius) sphere centered on the peak *t*-value from each region was computed for each region and corrected for confounds. **Figure 1** (left panel) shows the 4 nodes of the connectivity model or subgraph. The time series extracted from each of the four regions—for typical subject—are shown in **Figure 1** (right panel).

Dynamic Causal Modeling

We used spectral DCM to analyze the resting state fMRI data. A standard DCM analysis involves a specification of plausible models, which are then allows the model parameters (and subsequent group differences) to be estimated following Bayesian model selection (Friston et al., 2014a; Razi et al., 2015). The first step is to specify a model space. Because there is no previous literature on information transfer within DMN in addiction, we adopted and exploratory approach, starting with a fully connected model. This means that all four ROIs were connected to each other hence there were 16 connectivity parameters (including the recurrent self-connections). It is important to note that the spectral DCM also furnishes parameters that characterize the form of endogenous neuronal fluctuations. These additional parameters model the amplitude and exponent of the neural fluctuations—modeled as power law—for each ROI in the model. Hence, there were 16 connectivity and eight neuronal parameters in our model. Having specified the model, the next step is to estimate or invert the DCM. Model inversion is based on standard variational Bayes procedures (variational Laplace). This approximate Bayesian inference method uses Free Energy as a proxy for (log) model evidence, while optimizing the posterior probabilities (under Laplace approximation) over the model parameters (Friston et al., 2014b).

Bayesian Model Reduction

In the absence of a particular hypothesis or model space we used the fully connected model for an exploratory analysis of all possible reduced models, without one or more connections: after the full DCM for each participant was inverted, we employed a network discovery procedure using Bayesian model reduction (BMR) (Friston and Penny, 2011) to find the best model that explains the data. This procedure tests every possible model nested within the fully connected model. The model with the highest posterior probability is chosen as the winning model during this procedure. This BMR procedure is an efficient way to score a large model space without having to invert every reduced model. This procedure is based on an approximation, using Savage Dickey

[1]www.restfmri.net
[2]www.fil.ion.ucl.ac.uk/spm

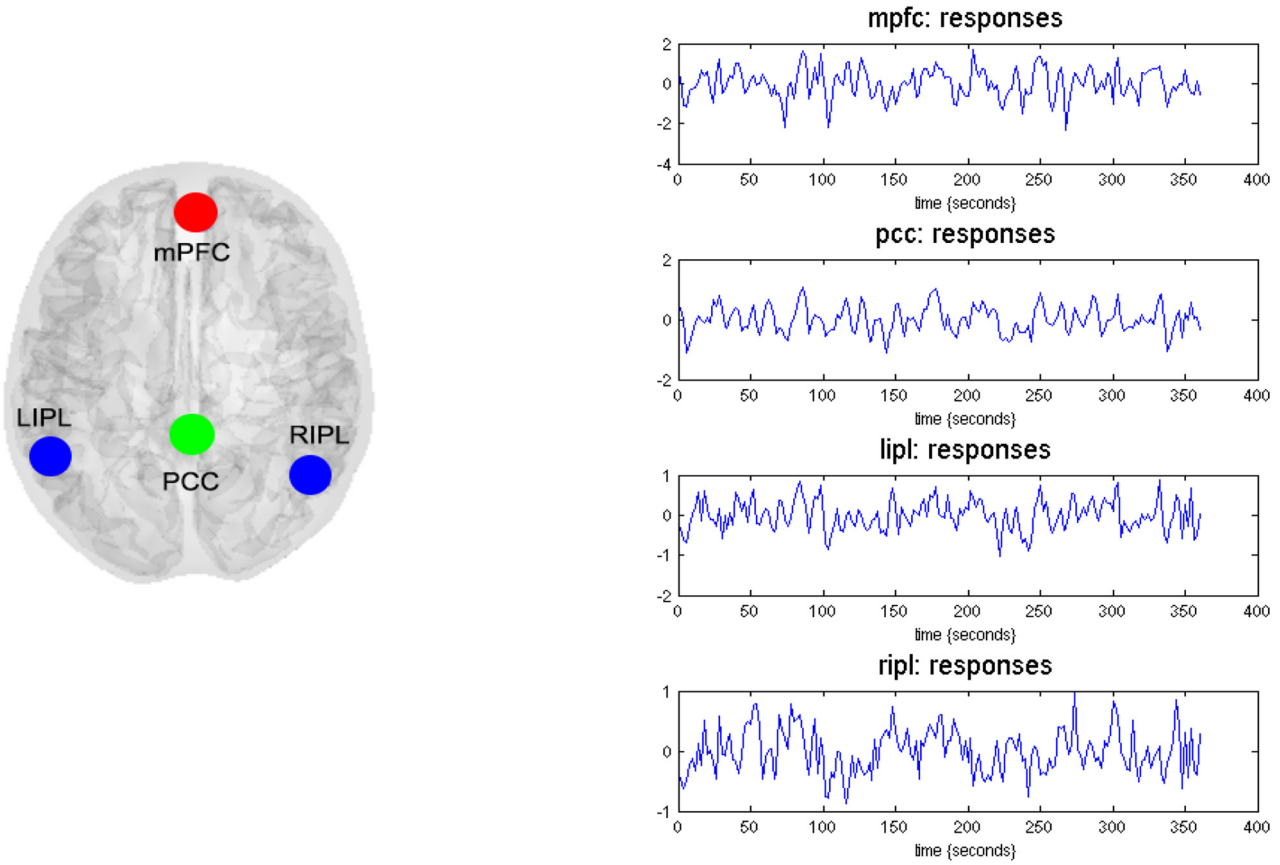

FIGURE 1 | Four nodes of dynamic causal modeling (DCM) model. The left panel shows the medial frontal cortex (MFC), the posterior cingulate cortex (PCC), the left inferior parietal lobule (LIPL), and the right inferior parietal lobule (RIPL). The time series (right-hand panels) from four regions are the principal eigenvariates of regions identified using seed connectivity analyses for a typical subject. These time series we used to invert the spectral DCM with the (fully-connected) architecture.

density ratio, which allows the computation of the log-evidence of any reduced model, nested within the full model, from the conditional density over the parameters of the full model.

Inference

Once the winning models for each population are established we can use the parameter estimates from these models to make inference about any group differences. In this work we used Bayesian parameter averaging (BPA; Razi et al., 2015) to quantify group differences in effective connectivity—for each parameter separately: i.e., ignoring posterior correlations (these correlations were subsequently accommodated in a classical multivariate analysis—please see below). This average was calculated for smokers and non-smokers separately. Finally, to test for group differences we used a classical multivariate test—canonical variate analysis (CVA)—to identify significant differences in (mixtures of) model parameters. This multivariate test is inclusive in a sense that it considers all the connections collectively alleviating any need for corrections for multiple corrections.

RESULTS

Bayesian Model Reduction

BMR compared the evidence of all reduced models for each group. The results are shown in **Figure 2** where left column A is for non-smokers and right column B is for smokers. In both groups, the procedure selected the fully connected model as the best model with a posterior probability of almost 1. The fully connected model had 24 parameters describing the extrinsic connections between nodes, the intrinsic (self-connections) within nodes and neuronal parameters describing the neuronal fluctuations within each node (note that BMR only optimses the connectivity parameter and not neuronal fluctuation parameters). In **Figure 2**, the profiles of model evidences are shown with the posterior probability for each model. In both groups, the full model had a probability of almost 1 and a log-probability of almost 0. The lower panel of column A (resp. B) shows the Bayesian parametric average for the non-smokers (resp. smokers) of the optimized (full) model. On the horizontal scale, we have the 16 connectivity parameters (which were optimized) and eight neuronal parameters

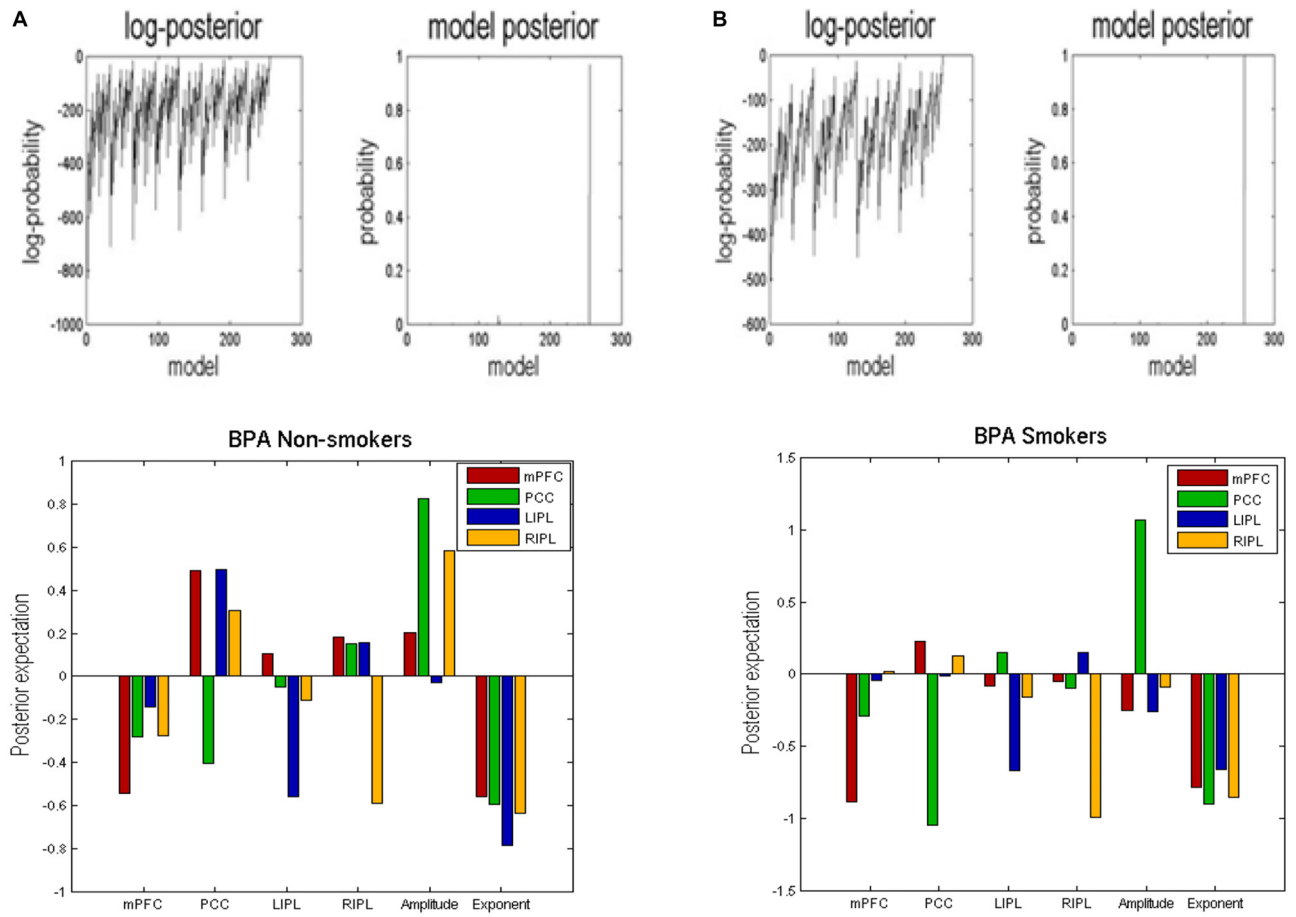

FIGURE 2 | Bayesian model reduction (BMR). This figure shows the results of applying BMR procedure. Here column **(A)** is for non-smokers while column **(B)** is for smokers. The upper two panels of column **(A)** (resp. column **B**) show the log-posterior and posterior probability for every model nested within the full model for non-smokers (resp. smokers). The lower panel of column **(A)** (resp. column **B**) shows the Bayesian parametric average (BPA) for the non-smokers (resp. smokers). The horizontal axis show the source region for the 16 connectivity parameters whereas the colors refer to the target regions. We also plotted the eight neuronal parameters showing the amplitude and exponents of the neural fluctuations.

reflecting the amplitude and power law exponent of the neuronal oscillations. The horizontal axis indicates the source regions for the 16 connectivity parameters, while the color indicates the target region. Extrinsic connections have units of hertz (c.f., rate constants), while intrinsic connections and the neuronal estimates are log scaling parameters; in other words, a value of 0.1 corresponds roughly to a 10% increase.

Bayesian Parametric Averaging

We used BPA to summarize the group differences between the smokers and non-smokers. Please note that we used BPA to quantify group differences in effective connectivity– for each parameter separately: i.e., ignoring posterior correlations (these correlations were accommodated in BPA shown in **Figure 2** and were also subsequently accommodated in the classical multivariate test). This average was calculated for smokers and non-smokers separately. In **Figure 3**, we show the difference by subtracting the BPA of non-smokers from the smokers. This means that the positive values on this plot reflects that the connectivity in smokers is greater than non-smokers and *vice versa*. It is in the same format as the lower panels on **Figure 3**.

In terms of the four self-connections, we see that inhibitory self-connection of PCC showed the largest difference. Since the self-connections in DCM are always inhibitory, this means the responses of the PCC in smokers are disinhibited when compared to non-smokers (by about 30%). We further identified two extrinsic connections—both involving mPFC—that show large differences in connectivity. One is from PCC to mPFC and the other is from RIPL to mPFC. The connection from PCC to mPFC is excitatory for both smokers and non-smokers (see **Figure 2**) and suggests that smokers have reduced connectivity for these connections as compared to non-smokers. The connection from RIPL to mPFC is inhibitory for smokers and excitatory for non-smokers (see **Figure 2**) and again shows reduction in connectivity for smokers as compared to controls. The overall profile of extrinsic and

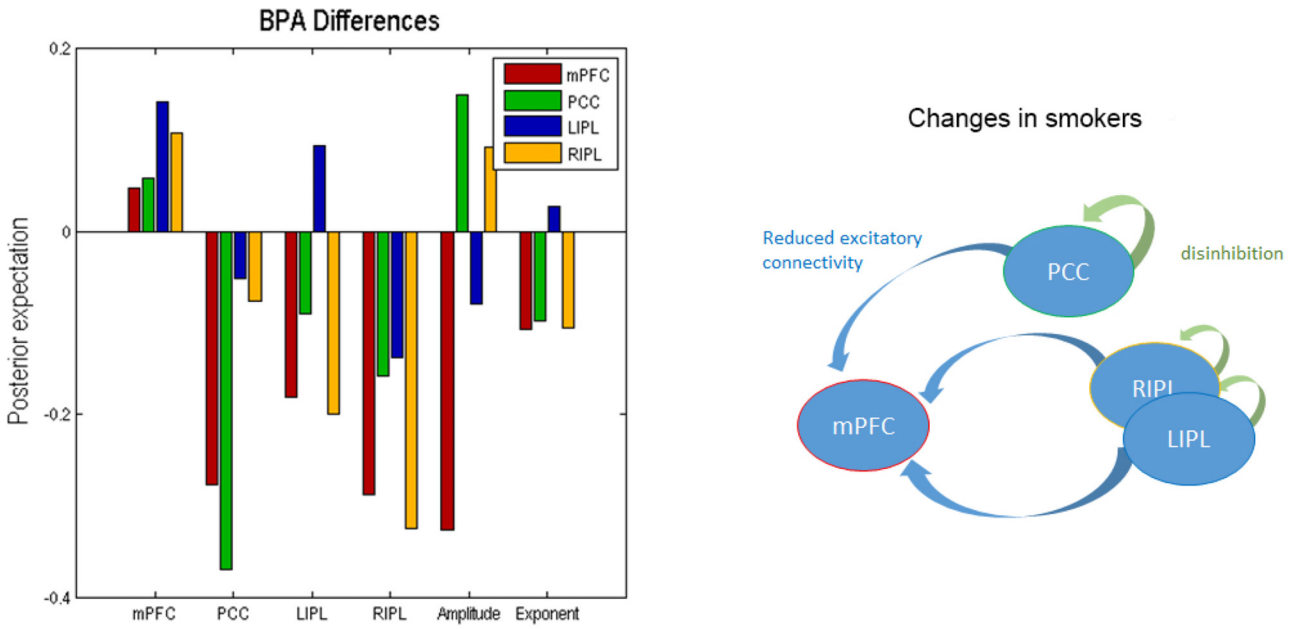

FIGURE 3 | Bayesian parametric averaging. This figure shows the Bayesian parametric average (BPA) differences of the two groups. The left panel shows the difference by subtracting the BPA of non-smokers from the smokers. This panel is in the same format as the lower panels of **Figure 2**. The right panel shows the overall profile of extrinsic and intrinsic differences schematically in the smokers.

intrinsic differences is shown schematically in the right panel of **Figure 3**. This suggests a functional disconnection of the medial prefrontal cortex from a parietal nodes, which themselves become disinhibited.

In terms of the neuronal parameters, **Figure 3** shows that mPFC has the largest (negative) difference. It should to be noted that smokers had negative and non-smokers had positive amplitude scaling for the driving neuronal fluctuations (not shown in **Figure 3** as we only show the difference). This means that smokers have reduced neuronal fluctuations in mPFC, as compared to non-smokers. We further note that mPFC also has the largest difference in terms of the power law exponent of the neural fluctuations, suggesting that mPFC may have faster oscillations in smokers as compared to the non-smokers. In other words, the endogenous fluctuations became more slowly as frequency increases. A preponderance of higher frequencies usually indicates more excitable intrinsic neuronal dynamics, which is consistent with a loss of extrinsic entrainment by extrinsic inputs from parietal regions.

Multivariate Analysis

The profile of connectivity changes, using BPA, above is purely quantitative. To establish that these differences are significant, in relation to intersubject variability, we used classical tests based on subject specific parameter estimates. **Figure 4** shows the results of a classical multivariate test—CVA. We used this analysis to test for any differences over all connections between the groups. The results of CVA include canonical vectors and variates—and their significance. These are plotted on the left and the right panels respectively. First, we see that this test is significant with a *p*-value of 0.032 and a strong canonical correlation *(r)* of 0.702. Note that because there is only one multivariate test, there is no need to correct for multiple comparisons. The canonical variate (shown on the left panel) expresses the degree to which a pattern of differences—encoded by the canonical vector (shown on the right panel)—is expressed in each subject. The left panel shows that, with the exception of couple of subjects in each group, the corresponding canonical variate can reliably discriminate between the two groups. The right panel shows the pattern of weights assigned by CVA to each parameter. It is pleasing to note a very similar pattern here to the one shown in **Figure 3**. We see that PCC self-connection is the largest difference, which is agreement with BPA results. Also, the connection from PCC to mPFC is given the largest (negative) weight. As for the amplitude and exponent of the neural fluctuations, we again see very similar pattern: the mPFC has the largest differences in smokers (compared to controls), which is consistent with the BPA differences in **Figure 3**.

DISCUSSION

In this work, we focused on the implication of DMN on addiction (Posner et al., 2007; Hong et al., 2009; Tang et al., 2010, 2013, 2015b; Goldstein and Volkow, 2011; Petersen and Posner, 2012; Liang et al., 2015; Weiland et al., 2015), and modeled the effective connectivity underlying low frequency BOLD fluctuations in the resting smoker's brain network. This analysis disclosed the causal and distributed

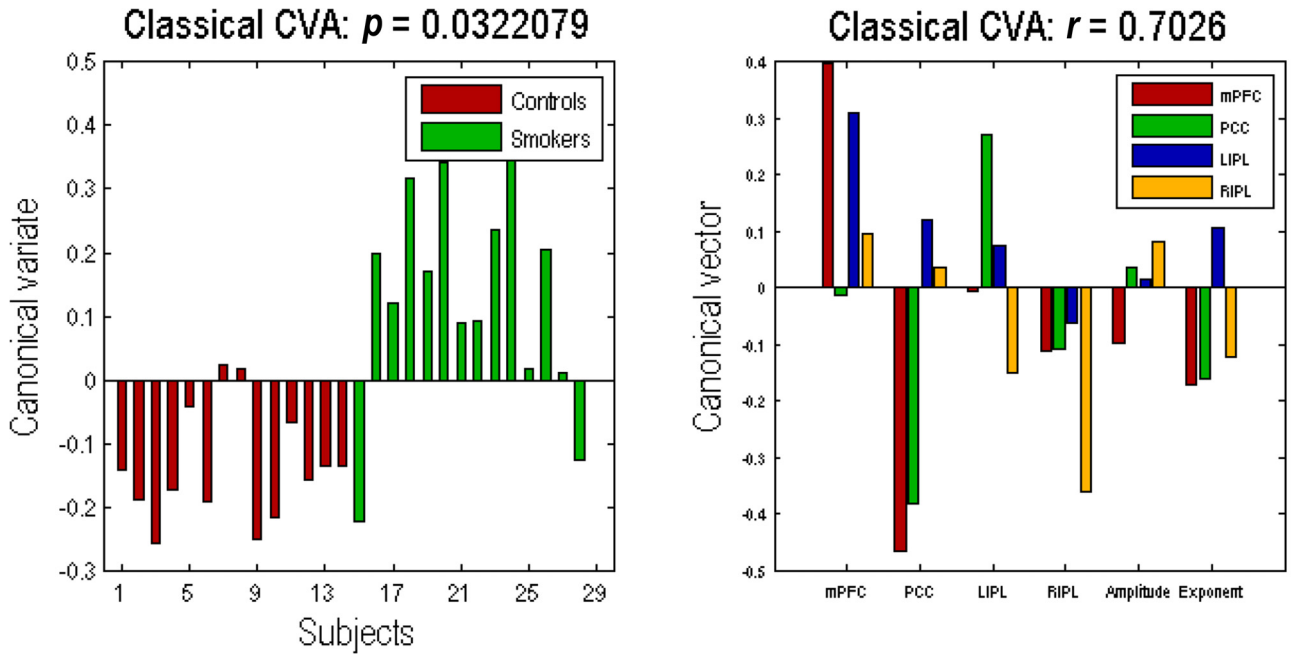

FIGURE 4 | Canonical variate analysis (CVA). This figure shows the results of a canonical variates analysis (the multivariate classical inference) using the same summary statistics used in **Figure 3**. The canonical variate shows reliable group discrimination on the left panel, while the canonical vector shows weights assigned to each parameter by CVA on the right panel (the format of this panel is same as the **Figures 2**, **3**). The effect of group difference was significant with a canonical correlation of $r = 0.7026$; $p = 0.0322$.

effects of smoking addiction on four core brain regions and their prefrontal-parietal connections. Our results suggest differences in functional integration among brain DMNs between nonsmokers and smokers.

Compared to nonsmokers, smokers showed a reduced excitatory coupling from PCC to mPFC, a reduced coupling from RIPL to mPFC, and disinhibition of both PCC and RIPL. These results suggest smokers lose equilibrium between excitatory and inhibitory connectivity, especially in the mPFC-PCC-IPL circuits. Overall, the results suggest that the medial prefrontal cortex becomes less sensitive to extrinsic afferents from parietal nodes, which themselves are disinhibited. Our findings are consistent with previous neuroscientific research in smoking addiction; for example, smokers often show reduced brain activity in the prefrontal-parietal networks (Hong et al., 2009; Goldstein and Volkow, 2011; Tang et al., 2013, 2015a; Weiland et al., 2015), and after intervention, the brain activity of these networks increases (Tang et al., 2013, 2015a). mPFC and PCC are key nodes of the human default network (Raichle, 2015) which orchestrates the brain's ongoing or endogenous activity in the resting-state. Previous research has shown that endogenous activity plays a major role in the human brain in health and neurological and psychiatric disorders (Zhang and Raichle, 2010).

Our study reveals changes in the dynamic interplay among mPFC and PCC—two key brain regions involved in smoking addiction (Jarraya et al., 2010; Goldstein and Volkow, 2011), in which smokers have reduced connectivity from PCC to mPFC as compared to non-smokers. Given that PCC has been shown as the brain connector hubs that link all major structural modules and play an important role in functional integration (Hagmann et al., 2008; Zuo et al., 2012), the dysregulation from PCC to mPFC in smoking addiction may be a crucial biomarker. The addicts such as nicotine, cocaine and methamphetamine users show functional and structural abnormalities in the PFC and IPL (Bustamante et al., 2011; Luijten et al., 2013; Hall et al., 2015). For example, the RIPL is often less activated in cocaine-dependent groups during conditions requiring attention and cognitive control (Barrós-Loscertales et al., 2011; Bustamante et al., 2011). However, these studies did not address the directed and dynamic interactions among the brain regions involved. In the current study, we applied spectral DCM to first show a reduced excitatory coupling from RIPL to mPFC, reflecting the directed connectivity and abnormalities of information flow from one area to another, consistent with previous empirical findings. These results may shed light on the potential biomarkers of diagnosis and the target of effective treatment in smoking addiction. Furthermore, they suggest that future brain based prevention and intervention could consider the amelioration of interactions in mPFC-PCC-IPL circuits. Future work should also explore cortico-subcortical interactions in smoking addiction.

In terms of the functional anatomy suggested by our dynamic causal modeling, a key region appears to be the mPFC. This region was unique in showing a reduction in extrinsic afferents from other areas. This finding is particularly

interesting given the role of the mPFC in evaluation, reality monitoring, decision-making and choice behavior (Rushworth et al., 2004; Metzak et al., 2015). For example, it has been proposed that the function of the mPFC "is to learn associations between context, locations, events, and corresponding adaptive responses, particularly emotional responses" (Euston et al., 2012). Furthermore, functional connectivity analyses have suggested "that the value signal in VMPFC might integrate inputs from networks, including the anterior insula and posterior superior temporal cortex that are thought to be involved in social cognition" (Hare et al., 2010). To the extent that addictive behavior may be related to a suspension of—or aberrant—reality testing, recent evidence points to the key role of the default mode (in particular, the mPFC) in reality monitoring, relative to source monitoring (Metzak et al., 2015). The particular profile of effective connectivity changes that characterize addicted smokers are also remarkably similar to the decrease in effective connectivity between parietal and mPFC regions in schizophrenia. In a recent stochastic DCM study of the default mode in first episode schizophrenia, the authors found reduced effective connectivity to the anterior frontal node of the default mode—"reflecting a reduced postsynaptic efficacy of prefrontal afferents" (Bastos-Leite et al., 2015).

Does smoking severity correlate with connectivity? We conducted an analysis but did not find the correlation between smoking severity and effective connectivity, possibly because of the small sample size in the current study. Nonetheless, our data indicate the use of spectral DCM on resting-state fMRI data can differentiate the directed connections between two groups, and provide insight into the brain mechanisms underlying smoking addiction; namely, abnormalities of effective connectivity in the brain. Our findings are in accord with our hypothesis that in—comparison with nonsmokers—smokers show a disrupted equilibrium between excitatory and inhibitory connectivity (mPFC-PCC-IPL circuits). This disrupted functional integration can be summarized as a functional disconnection of the medial prefrontal cortex from posterior parietal nodes.

In summary, many psychiatric (and neurological) conditions such as major depressive disorder and schizophrenia can be understood as functional disconnection syndromes (Menon, 2011; Sylvester et al., 2012): effective connectivity can tell us how brain regions interact with each other in terms of context sensitive changes in directed coupling—and even address the relationship between persistent changes in effective connectivity and relapse.

AUTHOR CONTRIBUTIONS

All authors listed, have made substantial, direct and intellectual contribution to the work, and approved it for publication.

ACKNOWLEDGMENTS

This work was supported by the Office of Naval Research. We thank lab members for assistance with data collection.

REFERENCES

Amft, M., Bzdok, D., Laird, A. R., Fox, P. T., Schilbach, L., and Eickhoff, S. B. (2015). Definition and characterization of an extended social-affective default network. *Brain Struct. Funct.* 220, 1031–1049. doi: 10.1007/s00429-013-0698-0

Baler, R. D., and Volkow, N. D. (2006). Drug addiction: the neurobiology of disrupted self-control. *Trends Mol. Med.* 12, 559–566. doi: 10.1016/j.molmed.2006.10.005

Barrós-Loscertales, A., Bustamante, J. C., Ventura-Campos, N., Llopis, J. J., Parcet, M. A., and Avila, C. (2011). Lower activation in the right frontoparietal network during a counting Stroop task in a cocaine-dependent group. *Psychiatry Res.* 194, 111–118. doi: 10.1016/j.pscychresns.2011.05.001

Bastos-Leite, A. J., Ridgway, G. R., Silveira, C., Norton, A., Reis, S., and Friston, K. J. (2015). Dysconnectivity within the default mode in first-episode schizophrenia: a stochastic dynamic causal modeling study with functional magnetic resonance imaging. *Schizophr. Bull.* 41, 144–153. doi: 10.1093/schbul/sbu080

Bustamante, J. C., Barrós-Loscertales, A., Ventura-Campos, N., Sanjuán, A., Llopis, J. J., Parcet, M. A., et al. (2011). Right parietal hypoactivation in a cocaine-dependent group during a verbal working memory task. *Brain Res.* 1375, 111–119. doi: 10.1016/j.brainres.2010.12.042

Centers for Disease Control and Prevention. (2006). Sustaining state programs for tobacco control: State data highlights (Office on Smoking and Health, Atlanta).

Deveci, S. E., Deveci, F., Açik, Y., and Ozan, A. T. (2004). The measurement of exhaled carbon monoxide in healthy smokers and non-smokers. *Respir Med.* 98, 551–556. doi: 10.1016/j.rmed.2003.11.018

Di, X., and Biswal, B. B. (2014). Identifying the default mode network structure using dynamic causal modeling on resting-state functional magnetic resonance imaging. *Neuroimage* 86, 53–59. doi: 10.1016/j.neuroimage.2013.07.071

Euston, D. R., Gruber, A. J., and McNaughton, B. L. (2012). The role of medial prefrontal cortex in memory and decision making. *Neuron* 76, 1057–1070. doi: 10.1016/j.neuron.2012.12.002

Fox, M. D., and Raichle, M. E. (2007). Spontaneous fluctuations in brain activity observed with functional magnetic resonance imaging. *Nat. Rev. Neurosci.* 8, 700–711. doi: 10.1038/nrn2201

Fransson, P. (2005). Spontaneous low-frequency BOLD signal fluctuations: an fMRI investigation of the resting-state default mode of brain function hypothesis. *Hum. Brain Mapp.* 26, 15–29. doi: 10.1002/hbm.20113

Friston, K. J., Kahan, J., Biswal, B., and Razi, A. (2014a). A DCM for resting state fMRI. *Neuroimage* 94, 396–407. doi: 10.1016/j.neuroimage.2013.12.009

Friston, K. J., Kahan, J., Razi, A., Stephan, K. E., and Sporns, O. (2014b). On nodes and modes in resting state fMRI. *Neuroimage* 99, 533–547. doi: 10.1016/j.neuroimage.2014.05.056

Friston, K., and Penny, W. (2011). *Post hoc* Bayesian model selection. *Neuroimage* 56, 2089–2099. doi: 10.1016/j.neuroimage.2011.03.062

Goldstein, R. Z., and Volkow, N. D. (2011). Dysfunction of the prefrontal cortex in addiction: neuroimaging findings and clinical implications. *Nat. Rev. Neurosci.* 12, 652–669. doi: 10.1038/nrn3119

Hagmann, P., Cammoun, L., Gigandet, X., Meuli, R., Honey, C. J., Wedeen, V. J., et al. (2008). Mapping the structural core of human cerebral cortex. *PLoS Biol.* 6:e159. doi: 10.1371/journal.pbio.0060159

Hajek, P., Stead, L. F., West, R., Jarvis, M., and Lancaster, T. (2009). Relapse prevention interventions for smoking cessation. *Cochrane Database Syst. Rev.* 1:CD003999. doi: 10.1002/14651858.CD003999

Hall, M. G., Alhassoon, O. M., Stern, M. J., Wollman, S. C., Kimmel, C. L., Perez-Figueroa, A., et al. (2015). Gray matter abnormalities in cocaine versus methamphetamine-dependent patients: a neuroimaging meta-analysis. *Am. J. Drug Alcohol Abuse.* 41, 290–299. doi: 10.3109/00952990.2015.1044607

Hare, T. A., Camerer, C. F., Knoepfle, D. T., and Rangel, A. (2010). Value computations in ventral medial prefrontal cortex during charitable decision

making incorporate input from regions involved in social cognition. *J. Neurosci.* 30, 583–590. doi: 10.1523/JNEUROSCI.4089-09.2010

Heatherton, T. F., Kozlowski, L. T., Frecker, R. C., and Fagerström, K. O. (1991). The fagerström test for nicotine dependence: a revision of the fagerström tolerance questionnaire. *Br. J. Addict.* 86, 1119–1127. doi: 10.1111/j.1360-0443.1991.tb01879.x

Hong, L. E., Gu, H., Yang, Y., Ross, T. J., Salmeron, B. J., Buchholz, B., et al. (2009). Association of nicotine addiction and nicotine's actions with separate cingulate cortex functional circuits. *Arch. Gen. Psychiatry* 66, 431–441. doi: 10.1001/archgenpsychiatry.2009.2

Hu, Y., Salmeron, B. J., Gu, H., Stein, E. A., and Yang, Y. (2015). Impaired functional connectivity within and between frontostriatal circuits and its association with compulsive drug use and trait impulsivity in cocaine addiction. *JAMA Psychiatry* 72, 584–592. doi: 10.1001/jamapsychiatry.2015.1

Jarraya, B., Brugières, P., Tani, N., Hodel, J., Grandjacques, B., Fénelon, G., et al. (2010). Disruption of cigarette smoking addiction after posterior cingulate damage. *J. Neurosurg.* 113, 1219–1221. doi: 10.3171/2010.6.JNS10346

Kahan, J., Urner, M., Moran, R., Flandin, G., Marreiros, A., Mancini, L., et al. (2014). Resting state functional MRI in Parkinson's disease: the impact of deep brain stimulation on 'effective' connectivity. *Brain* 137, 1130–1144. doi: 10.1093/brain/awu027

Konishi, M., McLaren, D. G., Engen, H., and Smallwood, J. (2015). Shaped by the past: the default mode network supports cognition that is independent of immediate perceptual input. *PLoS One* 10:e0132209. doi: 10.1371/journal.pone.0132209

Leech, R., and Sharp, D. J. (2014). The role of the posterior cingulate cortex in cognition and disease. *Brain* 137, 12–32. doi: 10.1093/brain/awt162

Liang, X., He, Y., Salmeron, B. J., Gu, H., Stein, E. A., and Yang, Y. (2015). Interactions between the salience and default-mode networks are disrupted in cocaine addiction. *J. Neurosci.* 35, 8081–8090. doi: 10.1523/JNEUROSCI.3188-14.2015

Luijten, M., O'Connor, D. A., Rossiter, S., Franken, I. H., and Hester, R. (2013). Effects of reward and punishment on brain activations associated with inhibitory control in cigarette smokers. *Addiction* 108, 1969–1978. doi: 10.1111/add.12276

Menon, V. (2011). Large-scale brain networks and psychopathology: a unifying triple network model. *Trends Cogn. Sci.* 15, 483–506. doi: 10.1016/j.tics.2011.08.003

Metzak, P. D., Lavigne, K. M., and Woodward, T. S. (2015). Functional brain networks involved in reality monitoring. *Neuropsychologia* 75, 50–60. doi: 10.1016/j.neuropsychologia.2015.05.014

Petersen, S. E., and Posner, M. I. (2012). The attention system of the human brain: 20 years after. *Annu. Rev. Neurosci.* 35, 73–89. doi: 10.1146/annurev-neuro-062111-150525

Posner, M. I., Rothbart, M. K., Sheese, B. E., and Tang, Y. Y. (2007). The anterior cingulate gyrus and the mechanism of self-regulation. *Cogn. Affect. Behav. Neurosci.* 7, 391–395. doi: 10.3758/cabn.7.4.391

Raichle, M. E. (2015). The brain's default mode network. *Annu. Rev. Neurosci.* 38, 433–447. doi: 10.1146/annurev-neuro-071013-014030

Razi, A., Kahan, J., Rees, G., and Friston, K. J. (2015). Construct validation of a DCM for resting state fMRI. *Neuroimage* 106, 1–14. doi: 10.1016/j.neuroimage.2014.11.027

Rushworth, M. F., Walton, M. E., Kennerley, S. W., and Bannerman, D. M. (2004). Action sets and decisions in the medial frontal cortex. *Trends Cogn. Sci.* 8, 410–417. doi: 10.1016/j.tics.2004.07.009

Song, X. W., Dong, Z. Y., Long, X. Y., Li, S. F., Zuo, X. N., Zhu, C. Z., et al. (2011). REST: a toolkit for resting-state functional magnetic resonance imaging data processing. *PLoS One* 6:e25031. doi: 10.1371/journal.pone.0025031

Sylvester, C. M., Corbetta, M., Raichle, M. E., Rodebaugh, T. L., Schlaggar, B. L., Sheline, Y. I., et al. (2012). Functional network dysfunction in anxiety and anxiety disorders. *Trends Neurosci.* 35, 527–535. doi: 10.1016/j.tins.2012.04.012

Tang, Y. Y., Hölzel, B. K., and Posner, M. I. (2015b). The neuroscience of mindfulness meditation. *Nat. Rev. Neurosci.* 16, 213–225. doi: 10.1038/nrn3916

Tang, Y. Y., Lu, Q., Geng, X., Stein, E. A., Yang, Y., and Posner, M. I. (2010). Short-term meditation induces white matter changes in the anterior cingulate. *Proc. Natl. Acad. Sci. U S A* 107, 15649–15652. doi: 10.1073/pnas.1011043107

Tang, Y. Y., Posner, M. I., Rothbart, M. K., and Volkow, N. D. (2015a). Circuitry of self-control and its role in reducing addiction. *Trends Cogn. Sci.* 19, 439–444. doi: 10.1016/j.tics.2015.06.007

Tang, Y. Y., Tang, R., and Posner, M. I. (2013). Brief meditation training induces smoking reduction. *Proc. Natl. Acad. Sci. U S A* 110, 13971–13975. doi: 10.1073/pnas.1311887110

Volkow, N. D., Wang, G. J., Fowler, J. S., and Tomasi, D. (2012). Addiction circuitry in the human brain. *Annu. Rev. Pharmacol. Toxicol.* 52, 321–336. doi: 10.1146/annurev-pharmtox-010611-134625

Weiland, B. J., Sabbineni, A., Calhoun, V. D., Welsh, R. C., and Hutchison, K. E. (2015). Reduced executive and default network functional connectivity in cigarette smokers. *Hum. Brain Mapp.* 36, 872–882. doi: 10.1002/hbm.22672

Zhang, D., and Raichle, M. E. (2010). Disease and the brain's dark energy. *Nat. Rev. Neurol.* 6, 15–28. doi: 10.1038/nrneurol.2009.198

Zuo, X. N., Ehmke, R., Mennes, M., Imperati, D., Castellanos, F. X., Sporns, O., et al. (2012). Network centrality in the human functional connectome. *Cereb. Cortex* 22, 1862–1875. doi: 10.1093/cercor/bhr269

Conflict of Interest Statement: The authors declare that the research was conducted in the absence of any commercial or financial relationships that could be construed as a potential conflict of interest.

frontiers in Human Neuroscience

ORIGINAL RESEARCH
published: 25 November 2015
doi: 10.3389/fnhum.2015.00634

Detection of Motor Changes in Huntington's Disease Using Dynamic Causal Modeling

Lora Minkova[1, 2, 3], Elisa Scheller[1, 2], Jessica Peter[1, 2], Ahmed Abdulkadir[2, 4], Christoph P. Kaller[2, 5, 6], Raymund A. Roos[7], Alexandra Durr[8], Blair R. Leavitt[9], Sarah J. Tabrizi[10], Stefan Klöppel[1, 2, 5] and TrackOn-HD Investigators*

[1] Department of Psychiatry and Psychotherapy, University Medical Center Freiburg, Freiburg, Germany, [2] Freiburg Brain Imaging Center, University Medical Center Freiburg, Freiburg, Germany, [3] Laboratory for Biological and Personality Psychology, Department of Psychology, University of Freiburg, Freiburg, Germany, [4] Department of Computer Science, University of Freiburg, Freiburg, Germany, [5] Department of Neurology, University Medical Center Freiburg, Freiburg, Germany, [6] BrainLinks-BrainTools Cluster of Excellence, University of Freiburg, Freiburg, Germany, [7] Department of Neurology, Leiden University Medical Centre, Leiden, Netherlands, [8] Department of Genetics and Cytogenetics, Pitié-Salpêtrière University Hospital, Paris, France, [9] Centre for Molecular Medicine and Therapeutics, Department of Medical Genetics, University of British Columbia, Vancouver, Canada, [10] Department of Neurodegenerative Disease, Institute of Neurology, University College London, London, UK

Deficits in motor functioning are one of the hallmarks of Huntington's disease (HD), a genetically caused neurodegenerative disorder. We applied functional magnetic resonance imaging (fMRI) and dynamic causal modeling (DCM) to assess changes that occur with disease progression in the neural circuitry of key areas associated with executive and cognitive aspects of motor control. Seventy-seven healthy controls, 62 pre-symptomatic HD gene carriers (preHD), and 16 patients with manifest HD symptoms (earlyHD) performed a motor finger-tapping fMRI task with systematically varying speed and complexity. DCM was used to assess the causal interactions among seven pre-defined regions of interest, comprising primary motor cortex, supplementary motor area (SMA), dorsal premotor cortex, and superior parietal cortex. To capture heterogeneity among HD gene carriers, DCM parameters were entered into a hierarchical cluster analysis using Ward's method and squared Euclidian distance as a measure of similarity. After applying Bonferroni correction for the number of tests, DCM analysis revealed a group difference that was not present in the conventional fMRI analysis. We found an inhibitory effect of complexity on the connection from parietal to premotor areas in preHD, which became excitatory in earlyHD and correlated with putamen atrophy. While speed of finger movements did not modulate the connection from caudal to pre-SMA in controls and preHD, this connection became strongly negative in earlyHD. This second effect did not survive correction for multiple comparisons. Hierarchical clustering separated the gene mutation carriers into three clusters that also differed significantly between these two connections and thereby confirmed their relevance. DCM proved useful in identifying group differences that would have remained undetected by standard analyses and may aid in the investigation of between-subject heterogeneity.

Keywords: Huntington's disease, motor network, sequential finger tapping, fMRI, DCM, cluster analysis

OPEN ACCESS

Edited by:
Baojuan Li,
Fourth Military Medical University, China

Reviewed by:
Graham J. Galloway,
The University of Queensland, Australia
Ling Wang,
South China Normal University, China

****Correspondence:***
Lora Minkova
lora.minkova@uniklinik-freiburg.de

Received: *13 August 2015*
Accepted: *06 November 2015*
Published: *25 November 2015*

Citation:
Minkova L, Scheller E, Peter J, Abdulkadir A, Kaller CP, Roos RA, Durr A, Leavitt BR, Tabrizi SJ, Klöppel S and TrackOn-HD Investigators (2015) Detection of Motor Changes in Huntington's Disease Using Dynamic Causal Modeling. Front. Hum. Neurosci. 9:634. doi: 10.3389/fnhum.2015.00634

INTRODUCTION

Huntington's disease (HD) is a genetic neurodegenerative disorder characterized by a devastating combination of motor, cognitive, and psychiatric symptoms, with a typical clinical onset around the age of 40. Advances in genetic testing have offered the opportunity to reliably diagnose the fully penetrant genetic mutation many years before the onset of first symptoms.

A substantial body of research, including large-scale multimodal and multicenter studies, such as PADDINGTON (Hobbs et al., 2013), PREDICT-HD (Biglan et al., 2013), and TRACK-HD (Tabrizi et al., 2009), have revealed a complex pattern of structural and functional abnormalities in diverse subcortical and cortical regions in both pre-clinical (preHD) and early manifest (earlyHD) gene mutation carriers. HD disease-specific effects have been observed in fronto-striatal and fronto-parietal networks (Klöppel et al., 2008, 2010; Rosas et al., 2008; Wolf et al., 2008, 2011, 2012; Tabrizi et al., 2009), affecting essential cognitive, motor and executive domains. Specifically, deficits in motor functioning are a clinical hallmark of HD, as indicated by previous functional magnetic resonance imaging (fMRI) studies (Biglan et al., 2009; Klöppel et al., 2009), and are possibly caused by striatal atrophy as well as volume loss in prefrontal areas (Lawrence, 1998; Rosas et al., 2003). Furthermore, diffusion tensor imaging (DTI) studies have indicated disease-specific changes in overall white matter diffusivity, correlated with caudate and white matter volume loss (Novak et al., 2014), as well as alterations in striatal projection pathways and their associations with clinical motor data (Poudel et al., 2014) in earlyHD and to varying extent in preHD. Moreover, neuronal loss progressively affecting frontal, sensorimotor, and parietal regions appears to be remarkably variable both within and between HD gene carrier sub-populations (Nana et al., 2014).

Despite structural changes, behavioral performance during motor tasks remains relatively intact in individuals far from clinical onset, possibly as the result of compensatory mechanisms, but starts to deteriorate at early stages of manifest HD and during more demanding motor tasks (Farrow et al., 2006; Feigin et al., 2006; Georgiou-Karistianis et al., 2014). Functional MRI has proven to be a promising candidate for studying functional decline as well as neural compensatory reorganization in both preHD and earlyHD. Previous neuroimaging data, including PET studies, have identified HD disease-specific abnormalities in key brain areas involved in motor control, such as the primary motor cortex, supplementary motor area (SMA), premotor cortex, and parietal regions (Bartenstein et al., 1997; Gavazzi et al., 2007; Klöppel et al., 2009). However, findings vary across studies, suggesting that the nature of changes in brain activations is still not well understood. Furthermore, studying distinct, spatially segregated brain areas in isolation may not necessarily provide insights into the inter-regional interactions within functional networks and how connectivity becomes abnormal in clinical conditions in general and specifically in HD.

Functional integration, as opposed to functional segregation, allows us to focus on the dynamic causal interactions between distinct brain regions (i.e., effective connectivity) and how they depend on the task that the brain is performing. One of the most widely used methods for assessing effective connectivity is dynamic causal modeling (DCM) (Friston et al., 2003). DCM is a hypothesis-driven Bayesian approach that has been successfully used to study causal interactions between regions sub-serving the same functional network, as well as the way experimental manipulation influences connectivity in both healthy individuals and clinical populations (for a review of DCM studies in patients see Seghier et al., 2010). In a previous DCM study in preHD (Scheller et al., 2013), we identified an excitatory effect from bilateral dorsal premotor cortex (PMd) to parietal regions as critical for compensation, an effect that was restricted to conditions with high cognitive demand and was most pronounced in individuals closer to clinical onset of first motor symptoms. To our knowledge, this is the only task-based DCM study in HD published in the literature, so far.

Here, we collected motor task fMRI data from 155 participants from the large-scale, multi-centric TrackOn-HD study (Klöppel et al., 2015; http://hdresearch.ucl.ac.uk/completed-studies/trackon-hd/). We used DCM, based on task fMRI, to assess abnormal effective connectivity of the motor network in HD. The aim of the current study was twofold: first, we sought to extend on our previous DCM findings using a much larger and clinically heterogeneous sample. Specifically, previous results (Scheller et al., 2013) indicated the crucial role of the dorsal premotor cortex for the maintenance of motor functioning in preHD. Furthermore, research has shown that impairment in the striatum and its frontal motor projection areas in manifest HD, including the premotor cortex, may induce a compensatory recruitment of parietal cortices (Bartenstein et al., 1997). A differential involvement of the SMA has also been reported (Klöppel et al., 2009), expressed by the over-recruitment of caudal SMA during faster finger-tapping movements with approaching clinical onset in preHD, possibly indicative of its compensatory role, as well as a monotonic attenuation in task-related activity in pre-SMA during complex finger-tapping movements, most likely indicating disease-specific changes. Thus, we here expected to provide further evidence for the compensatory role of premotor and parietal areas, associated with approaching clinical onset and increasing cognitive demand.

Second, and more importantly, we aimed to demonstrate the use of an exploratory cluster analysis based on DCM parameters as a classification method in identifying sub-groups among the HD gene mutation carriers that may benefit from targeted interventions. Furthermore, we investigated to what extent the DCM parameters differed among the identified sub-groups and how differential neural coupling strengths were associated with behavioral performance during the finger-tapping task and clinical markers of disease progression. We hypothesized that effective connectivity would not be homogeneously altered across the group of HD gene carriers but may depend on the task demand and the disease progression in some individuals more than in others.

MATERIALS AND METHODS

Study Population

A total of 241 participants were recruited within the large-scale, multimodal TrackOn-HD study at four different sites (Paris, London, Vancouver, and Leiden). Out of them, only 155 right-handers completed a sequential finger-tapping motor task. In addition to left-handedness ($n = 16$), further exclusion criteria included technical issues ($n = 11$), corrupt or missing fMRI data ($n = 9$), poor task performance and missing activations ($n = 15$), as well as failed DCM quality check ($n = 35$). A detailed summary of excluded participants is provided in the **Table S1**.

For the current study, data were available for a total of 155 participants scanned between April and November 2013, comprising the following three groups: 77 age- and gender-matched controls (HC: 45 females, mean age ± SD: 48.53 ± 9.56), 62 individuals without HD but carrying the mutant huntingtin (HTT) gene (preHD: 30 females, mean age ± SD: 41.89 ± 8.58), and 16 early manifest HD patients (earlyHD: 6 females, mean age ± SD: 46.18 ± 8.59). PreHD required a disease burden of pathology score greater than 250 and a total of total motor score of 5 or less in the motor assessment of the Unified Huntington's Disease Rating Scale (UHDRS 99), indicating no substantial motor signs. EarlyHD were required to have motor symptoms consistent with HD, and a diagnostic confidence score of 4, according to the UHDRS, as well as to be within the Shoulson and Fahn stage I or II (Shoulson and Fahn, 1979) assessed according to UHDRS total functional capacity (TFC ≥ 7) (Tabrizi et al., 2009). Demographic and clinical information is provided in **Table 1**. Putamen volume (adjusted for total intracranial volume), disease burden score (DBS; Penney et al., 1997), and cumulative probability of clinical onset (CPO; Langbehn et al., 2004) were used as markers of HD disease progression.

The study was approved by the Ethics Committees of the Institute of Neurology, UCL (London), the University of British Columbia (Vancouver), Pierre and Marie Curie University (Paris), and the University of Leiden (Leiden). All participants gave a written informed consent according to the Declaration of Helsinki (World Medical Association, 2013).

fMRI Paradigm

The experimental design of the motor task fMRI was adopted from a previous study (Klöppel et al., 2009) and consisted of a sequential finger-tapping task probing for both executive (movement speed) and cognitive (movement complexity) aspects of motor control (**Figure S1**). The successful reproducibility of the finger-tapping paradigm across scanning sites has been shown elsewhere (Gountouna et al., 2010).

The task involved metronome-paced sequential finger tapping with their right dominant hand, using the (1) index, (2) middle, (3) ring, and (4) small fingers. Tapping sequences were either simple (i.e., 1-2-3-4) or complex (i.e., 4-2-3-1). With respect to speed, each sequence was paced by metronome clicks presented to the participant via headphones at a rate of either 0.5 or 1.5 Hz, resulting in slow or fast sequences, respectively. In addition to the task condition, a rest condition was used in which the metronome clicks were presented to the participants but no movement was required. Thus, the experimental paradigm consisted of six types of different blocks, each lasting for 20 s (i.e., simple-slow, simple-fast, complex-slow, complex-fast, rest-slow, and rest-fast). Each block type was presented five times in a pseudo-randomized order.

Button presses during the task were recorded using Current Designs button boxes (http://www.curdes.com). Similarly to our previous study (Klöppel et al., 2009), single omitted or wrongly added button presses were counted as one mistake. In sections with more complex errors, only sequences of three or more buttons in the appropriate order were counted as correct. Participants who scored low in performance (<50% accuracy across all blocks) or performed a completely wrong condition (e.g., simple instead of complex sequence or pressed during the whole rest condition) were excluded from subsequent analyses. It was furthermore examined whether exclusions were dictated by group affiliation using Pearson's chi-square test in SPSS.

Performance from the tapping conditions, measured by the mean timing inaccuracies (i.e., cue-response intervals) and their standard deviations (SD) were compared among the three groups. The timing inaccuracies were calculated from the intervals between each sound click (i.e., cue) and the actual button click (i.e., response) for each participant. Statistical analysis was conducted in SPSS using a $3 \times 2 \times 2$ repeated measures analysis of covariance (ANCOVA), with group (HC, preHD, and earlyHD) as a between-subject factor and complexity (simple and complex) as well as speed (slow and fast) as within-subject factors, adjusting for age, gender, education, and site. Additionally, we investigated the association between

TABLE 1 | Demographic and clinical information.

	HC ($n = 77$)	preHD ($n = 62$)	earlyHD ($n = 16$)
Age (years)	48.53 ± 9.56 (27:67)	41.89 ± 8.58 (24:61)	46.18 ± 8.59 (34:67)
Gender (F/M)	45/32	30/32	6/10
CAG length	–	43.19 ± 2.55 (39:50)	43.25 ± 1.73 (41:48)
CPO	–	0.22 ± 0.15 (0.02:0.62)	0.41 ± 0.21 (0.03:0.83)
Disease burden score*	–	304 ± 58 (182:457)	347 ± 48 (224:429)
Putamen (TIV-adjusted)	0.58 ± 0.07 (0.40:0.75)	0.50 ± 0.08 (0.29:0.75)	0.42 ± 0.12 (0.24:0.66)

*DBS = age × (CAG length-35.5) (Penney et al., 1997). Values are given in means ± SD (range), where applicable. HC, healthy controls; preHD, pre-symptomatic HD; earlyHD, early manifest HD; F, female; M, male; CAG, trinucleotide; CPO, cumulative probability of clinical onset; TIV, total intracranial volume.

performance and CPO among the gene carriers using Pearson's partial correlation, correcting for the covariates.

Mean timing inaccuracies and their SD were chosen as indices for motor performance based on previous literature (Hinton et al., 2007; Klöppel et al., 2009), which showed that motor timing variability, but not accuracy, increased in preHD with approaching clinical onset. Timing inaccuracies, rather than reaction time, reflect the ability of patients to anticipate the next click. However, for reasons of completeness, between-group differences were also investigated for accuracies (percentage of correct responses) for each condition using non-parametric Kruskal-Wallis H test in SPSS.

MRI Data Acquisition and Preprocessing

Scanning was performed on a 3T Siemens MAGNETOM TimTrio MR scanner at Paris and London and on a 3T Philips Achieva MR scanner at Vancouver and Leiden, both using a 12-channel head coil. High-resolution three-dimensional T1-weighted structural scans were acquired for all participants with a magnetization-prepared rapid gradient echo (3D MPRAGE) sequence for Siemens and a fast-field echo (FFE) sequence for Philips, using standardized protocols with the following parameters for the two scanner systems, respectively (Siemens / Philips): TR = 2200/7.7 ms, TE = 2.9/3.5 ms, TI = 900/875 ms, FA = 10/8°, FOV = 28/24 cm, matrix size of 256 × 256 × 208/224 × 224 × 164, zero-filled in the 3rd dimension to give an isotropic resolution of 1.1 mm. Two T1-weighted scans were acquired for each participant if time allowed and the one with the best quality was used for the analysis. Image quality of the anatomical scans was ensured after visual inspection. For the fMRI motor task, 225 whole-brain volumes were acquired using a T2*-weighted single-shot gradient echo planar imaging (GE-EPI) sequence with the following parameters: TR = 3 s, TE = 30 ms, FOV = 212 mm, flip angle = 80°, 48 slices in ascending order (slice thickness: 2.8 mm, gap: 1.5 mm, in plane resolution 3.3 × 3.3 mm), matrix size of 64 × 64, and bandwidth of 1906 Hz/Px. Rigorous inspection of the functional image quality was conducted using the FBIRN QC protocol (Greve et al., 2011; Glover et al., 2012). FBIRN's standardized ratings were based on two summary variables: (1) the number of volumes with mean intensity more than 3 SD away from intensity of overall mean image, and (2) number of volumes with mean volume difference (volume minus overall mean image) of more than 1%. Datasets with more than 20% outlier volumes in at least one variable were excluded from subsequent analyses.

Data preprocessing was performed in SPM8 (Statistical Parametric Mapping, r5638, Welcome Trust Centre for Neuroimaging, http://www.fil.ion.ucl.ac.uk/spm), using MATLAB R2012a (Mathworks, Natick, MA, USA). Each participant's T1 scan was segmented into gray and white matter using the VBM8 (r435) toolbox (http://dbm.neuro.uni-jena.de/vbm/). Segmented images were used to create an improved anatomical scan for co-registration of the functional scans. Using the DARTEL extension (Ashburner, 2007) for high-dimensional registration within the VBM8 toolbox, deformation parameters were extracted for later normalization of contrast images prior to second-level analysis.

The first four functional volumes were discarded prior to data preprocessing to allow for the equilibration of T1 signal effects. The remaining images were realigned to the mean image using a rigid body transformation and co-registered to the improved anatomical scan. Volumes with significant artifacts were detected using the ArtRepair software (http://cibsr.stanford.edu/tools/human-brain-project/artrepair-software.html). Those scans with more than 1.3% variation in global intensity and 1.0 mm/TR scan-to-scan motion were identified as outliers and replaced by interpolation from the nearest unaffected volumes. On average, <3% of all slices for all participants were corrected by this procedure. Following a histogram-based approach for outlier identification, participants with more than 13% of bad volumes were excluded from the subsequent analysis. The co-registered and repaired functional scans were then spatially smoothed with an isotropic Gaussian kernel of 6 mm FWHM.

GLM Analysis

Statistical analysis at the first (within-subject) level was carried out using the General Linear Model (GLM) as implemented in SPM8 (Friston et al., 1994). Task-related changes of BOLD signals were estimated at each voxel by modeling each block separately for each of the conditions (simple-slow, simple-fast, complex-slow, complex-fast, rest-slow, and rest-fast) after convolving with the canonical hemodynamic response function (HRF). High-pass filter with a cut-off at 152 s was applied to the data to remove low frequency artifacts. The instruction screen and the blocks during which participants performed a wrong condition (i.e., accuracy was below 50%) were modeled as separate regressors of no interest. Similarly, single button presses during the rest conditions were modeled as separate regressors. Six additional regressors containing the absolute values of the first derivative of the respective realignment parameters (Power et al., 2012) were included to regress out variance caused by translational and rotational head movements in x-, y-, and z-direction.

Subject-specific contrasts of interest were created from the beta estimates coding the effect of complexity (complex vs. simple sequence), as well as the effect of speed (fast vs. slow sequence). These contrasts were normalized to standard Montreal Neurological Institute (MNI) space using the DARTEL deformation parameters and taken forward to random-effects group analyses, treating participants as a random variable. To reduce inter-subject variability and allow for group analyses, the contrasts were additionally smoothed, resulting in total spatial smoothing of 8 mm FWHM.

Main effects of experimental task were characterized in SPM8 using one-sample *t*-tests, separately for complexity and speed, including age, gender, education, and site as confounding covariates. All participants were included in the one-sample *t*-tests as one group to ensure that regions of interests (ROIs) for the subsequent DCM analysis were commonly activated across all groups. Task-specific activations were identified at $p < 0.05$ FWE-corrected. Additionally, between-group comparisons were implemented in the GLM Flex tool (http://mrtools.mgh.harvard.edu/index.php/GLM_Flex) using a 3 × 2 × 2 ANCOVA design, including group (HC, preHD, and HD) as a between-group factor, as well as complexity (complex and simple) and speed

(fast and slow) as within-group factors, while correcting for age, gender, site, and education. In contrast to classical SPM8 analysis, which has a pooled error term across all within-subject factors, GLM Flex uses partitioned error terms and can be used to run full-factorial models with more factors than SPM8 allows.

DCM Analysis

Effective connectivity analysis was conducted using DCM (Friston et al., 2003), a hypothesis-driven Bayesian approach that describes the biophysical nature of directed interactions among distinct brain regions by incorporating two forward models: one at the neural and one at the hemodynamic level. At the neural level, DCM is expressed by the following equation:

$$\frac{dz}{dt} = \left(A + \sum u_j B^j\right) z + Cu$$

where vector z represents the time series of the neural behavior, vector u contains the time course(s) $(1, \ldots, j, \ldots, n)$ of the external perturbation (i.e., the experimental paradigm), as well as the task-independent endogenous couplings denoted by A, modulatory effects on these connections by stimulus u_j given by B, and experimental input to the system that drives regional activity, modeled by C. The hemodynamic model, on the other hand, is based on a biophysical forward model (Balloon model; Buxton et al., 1998) and comprises parameters characterizing blood flow and oxygenation change, measured by the actual BOLD response. By combining a priori knowledge of a biologically plausible neural model (input) with the measured BOLD response (output), it is possible to infer on underlying hidden states such as regional causal interactions. Further reading on the DCM approach can be found elsewhere (e.g., Penny et al., 2004; Friston, 2009; Stephan et al., 2010; Daunizeau et al., 2011; Kahan and Foltynie, 2013).

Here, we used deterministic, bilinear, one-state DCM to assess the effective connectivity among seven regions activated by the motor task (see **Table 2** for results) and in agreement with previously published data (Klöppel et al., 2009; Scheller et al., 2013). These regions comprised the left motor cortex (lM1), SMA, divided in pre- (pSMA) and caudal (cSMA), as well as bilateral dorsal premotor cortex (lPMd, rPMd), and bilateral superior parietal cortex (lSPC, rSPC). For each participant, time series from each of the seven ROIs were extracted using the fixed coordinates from the second-level activations identified in the one-sample *t*-test and adjusted for the effect of interest (F-contrast). No statistical threshold was used within each ROI, which allowed for the time series extraction of the same set of voxels in all participants. The motivation for this approach is based on previous literature (Parker Jones et al., 2013) and is advantageous for the current study because it ensured that there was no overlap of subject-specific spheres in neighboring brain regions, which would have otherwise been problematic in the case of pre- and caudal SMA. Furthermore, participants having ROIs with weak activations do not have to be excluded but at the expense of potentially including condition-independent noise (Parker Jones et al., 2013). This is an issue particularly in small sample sizes but potentially less so in our relatively large study.

TABLE 2 | Imaging results: task-specific regions of interest.

Regions	Hemi-sphere	MNI coords (mm)			T	$p_{FWE-corr}$
		x	y	z		
Pre-supplementary motor area (pSMA)	L	−8	11	45	12.10	<0.001
Caudal supplementary motor area (cSMA)	L	−5	−5	51	15.54	<0.001
Primary motor cortex (lM1)	L	−38	−12	53	16.46	<0.001
Dorsal premotor cortex (lPMd)	L	−24	−4	46	15.07	<0.001
Dorsal premotor cortex (rPMd)	R	26	−3	47	13.76	<0.001
Superior parietal cortex (lSPC)	L	−16	−63	58	12.93	<0.001
Superior parietal cortex (rSPC)	R	15	−66	58	16.65	<0.001

The extracted time series of all seven ROIs were included in one DCM, based on our previous study (Scheller et al., 2013). Intrinsic connections were modeled among all seven regions (represented with white arrows in **Figure 1A**). SMA was divided in pre-SMA and caudal SMA, the former involved in more cognitively challenging conditions (thus more strongly activated by the complex finger tapping condition) and interconnected with the premotor and associative cortices, while the latter strongly interconnected with M1 and activated by the speed conditions (thus representing the motoric executive part of SMA). No direct connection was modeled between pre-SMA and M1, but an indirect influence was assumed via left PMd and M1. Modulatory connections were specified in the B-matrix, separately for the complex (**Figure 1B**) and the speed conditions (**Figure 1C**). Based on the previously reported activations (Klöppel et al., 2009), modulatory effects of speed were included for cSMA, left M1, right PMd, and right SPC, while modulation by complexity was specified for M1, pSMA, right PMd, and bilateral SPC. Modulatory effects were expected only for the right PMd because of its involvement during auditorially paced finger-tapping sequences (Witt et al., 2008), as well as its higher recruitment during more demanding tasks (Bartenstein et al., 1997; Klöppel et al., 2009). All experimental inputs entered the model via the associative sensory regions in the parietal cortex. A more detailed discussion about the choice of connections can be found elsewhere (Scheller et al., 2013).

The fully connected DCMs were then reduced using the *post-hoc* optimization procedure for approximating model evidence, proposed by Friston and Penny (2011). This approach optimizes only the large model, while the evidence for any sub-model is obtained using generalization of the Savage-Dickey density ratio (Dickey, 1971; for more detailed discussion readers may refer to Rosa et al., 2012, Friston and Penny, 2011, and Seghier and Friston, 2013). Additionally, *post-hoc* diagnostics of each participant's DCM were conducted using in-house MATLAB routines to ensure that model inversion has converged, requiring at least 10% of variance explained.

DCM model specification, estimation and *post-hoc* optimization were carried out with DCM12, as implemented in SPM12b. Statistical inference on model parameters was

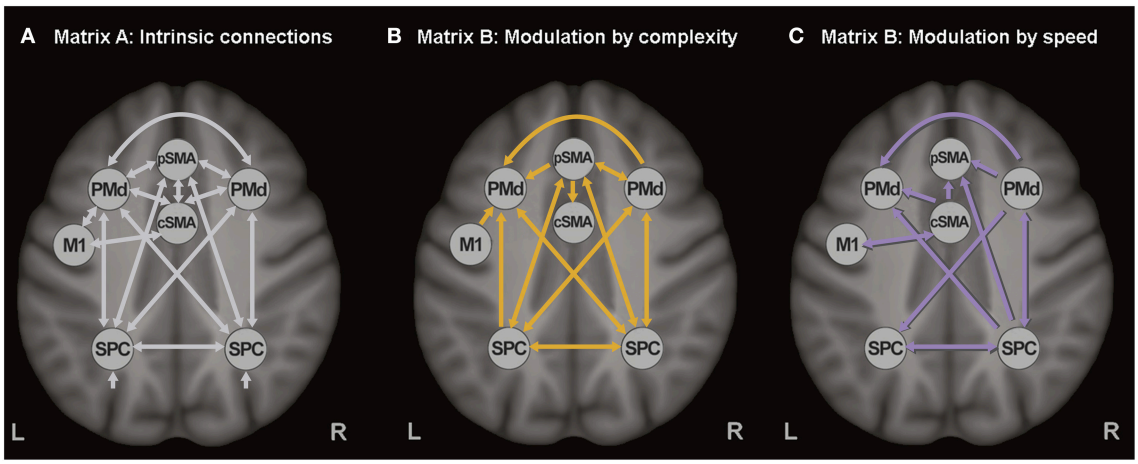

FIGURE 1 | Dynamic causal model. (A) Task-independent, intrinsic connections, **(B)** Modulatory connections (complexity), and **(C)** Modulatory connections (speed).

conducted in SPSS, Version 20.0 (IBM Corp., 2011). Random-effects inference at the connection level was assessed using ANCOVA analysis after covariate adjustment. Between-group differences were considered significant at a threshold of $p < 0.001$ after accounting for the number of connections (i.e., 30 intrinsic and 17 modulatory). Two-sample *t*-tests were used for *post-hoc* analyses of significant between-group differences, with applying Bonferroni correction for the three groups.

Cluster Analysis

To identify sub-groups differing in connectivity pattern, DCM intrinsic and modulatory parameters across all HD gene mutation carriers were entered into a hierarchical agglomerative cluster analysis, as implemented in SPSS (Burns, 2009). Ward's clustering linkage method (Ward, 1963) was performed on all parameters with squared Euclidean distance as a measure of proximity. We used the agglomeration schedule (i.e., the change in agglomeration coefficients as the number of clusters increase) to determine the optimum number of clusters. Afterwards, each HD mutation gene carrier was assigned to one of the identified sub-groups by repeating the cluster analysis using the optimal number of clusters. Finally, we used Pearson's partial correlation analysis, including age, gender, site, and education as covariates of no interest, to examine how sub-group membership was correlated with behavioral performance and putamen volume as a marker of disease progression. Bonferroni correction was used to account for the number of correlation tests.

RESULTS

Behavioral Data

Fifteen participants scored low in performance (<50% accuracy) or performed a wrong condition and were thus excluded from the subsequent analysis (**Table S1**). It was furthermore examined whether this exclusion was dictated by group affiliation, which was not the case [$\text{chi}^2(2, N = 200) = 1.28, p = 0.53$].

Descriptive information of the motor performance is provided in the **Table S2**. Between-group differences were assessed using factorial ANCOVA analysis. Significant performance differences were found among the groups only for the speed conditions [$F_{(2,\ 148)} = 4.19$, $p = 0.017$], as measured by the standard deviation of timing inaccuracy (i.e., the time between a button press and closest click). No between-group differences were observed for complexity [$F_{(2,\ 148)} = 1.691$, $p = 0.181$] or for the interaction between complexity and speed [$F_{(2,\ 148)} = 1.734$, $p = 0.180$]. To further investigate the significant between-group effects in speed, *post-hoc t*-tests (Bonferroni-corrected) were conducted for each pair of groups separately. Between-group differences in timing inaccuracy (SD) were observed for the two slow speed conditions (simple slow and complex slow) and only between HC and earlyHD ($p < 0.05$, Bonferroni-corrected). No significant differences were found between HC vs. preHD and between preHD vs. earlyHD. Groups did not differ in accuracy (i.e., percentage of correct responses), neither for the main effect of complexity, nor for the main effect of speed (both with $p > 0.1$).

Similarly to our previous study (Klöppel et al., 2009), a positive correlation was found in HD gene carriers between CPO and performance in both complex conditions (complex slow: $r = 0.242$, $n = 78$, $p = 0.047$, and complex fast: $r = 0.289$, $n = 78$, $p = 0.017$) as well as during simple slow ($r = 0.252$, $n = 78$, $p = 0.038$), as measured by the absolute values of the timing inaccuracies (SD). This suggests that HD gene carriers performed worse (i.e., became less accurate during tapping) with disease progression.

GLM Results

Main effects of experimental task resulted in activations of left primary motor cortex (lM1), left pre-SMA (pSMA), left caudal SMA (cSMA), bilateral dorsal premotor cortex (lPMd, rPMd) and bilateral superior parietal cortex (lSPC, rSPC), which is in agreement with previous findings (Klöppel et al., 2009). Increased complexity of sequential movements resulted in

stronger activations in the pSMA, bilateral PMd, and bilateral SPC, while increased speed of sequential movements led to stronger activation in cSMA and lM1 areas. Activation results are shown in **Figure 2** and the corresponding regions of interest and their coordinates can be found in **Table 2**. No significant main effects of group or interactions between group and the two task conditions (i.e., complexity and speed) were found at $p < 0.05$ (FWE-corrected) using the GLM Flex tool.

DCM Results

The diagnostics of each participant's DCM with regard to variance explained by the model and parameter estimability led to the exclusion of 35 participants (17 HC, 14 preHD, and 4 earlyHD). *Post-hoc* analysis revealed the same winning model across the three groups with the highest probability of (almost) 1. In the winning model (**Figure 3**), only a small number of modulatory connections were removed, such as the connections from the rPMd cortex toward the other regions, as well as the modulatory effects of complexity on the neural coupling from pSMA toward both bilateral SPC and cSMA. In an exploratory manner, the *post-hoc* optimization procedure was repeated for controls and HD gene carriers separately to ensure that the same winning model was identified for the patient group, which was the case. The posterior probabilities resulting from the *post-hoc* optimization across all subjects were further examined in quantitative terms using frequentist inference. Descriptive statistics of all intrinsic and modulatory parameters can be found in the (**Table S3**).

Differences in effective connectivity between HC and HD gene mutation carriers were found only for the task-dependent, modulatory neural coupling from lSPC toward lPMd during complex conditions [$F_{(2,\ 148)} = 4.43$, $p < 0.001$; **Figure 4A**], but not for the endogenous connectivity (i.e., coupling that is constant across all experimental conditions). Specifically, *post-hoc* Bonferroni tests showed that effects of complexity from lSPC toward lPMd were inhibitory in preHD, which is in line with previous findings (Scheller et al., 2013), but became excitatory in earlyHD ($p < 0.001$, Bonferroni-corrected). Interestingly, a negative correlation was also found in all mutation carriers between lSPC-lPMd coupling and TIV-adjusted putamen volume ($r = -0.302$, $n = 78$, $p = 0.007$), suggesting that complex conditions led to increasingly excitatory neural coupling associated with decreasing putamen volume (**Figure 4B**). However, this effect was not correlated with any of the behavioral data. Still, this could partly be explained by the fact that our complex condition comprised a 4-item sequence (i.e., 4-2-3-1, see **Figure S1**), which might have not been too cognitively demanding.

Furthermore, modulatory effects during speed conditions significantly differed among the groups for the connections from rSPC to pSMA [$F_{(2,\ 148)} = 4.10$, $p = 0.001$], as well as from cSMA to pSMA [$F_{(2,\ 148)} = 2.58$, $p = 0.021$]. *Post-hoc* Bonferroni tests showed that these modulatory effects were expressed by excitatory rSPC to pSMA coupling in earlyHD as opposed to inhibitory in preHD and HC ($p = 0.001$), which, however, was not correlated to either putamen volume or behavioral performance. A trend of increased inhibitory coupling from cSMA toward pSMA, modulated by speed, was observed in earlyHD, relative to preHD and HC ($p = 0.002$), but this effect did not survive Bonferroni correction after accounting for the number of tests. Of note, the stronger inhibitory cSMA to pSMA connections were associated with decreased putamen volume ($r = 0.632$, $n = 16$, $p = 0.032$) and worse behavioral performance during both fast conditions (simple fast: $r = -0.522$, $n = 16$, $p = 0.045$, and complex fast: $r = -0.724$, $n = 16$, $p = 0.018$) in earlyHD, but not in preHD ($n = 62$;

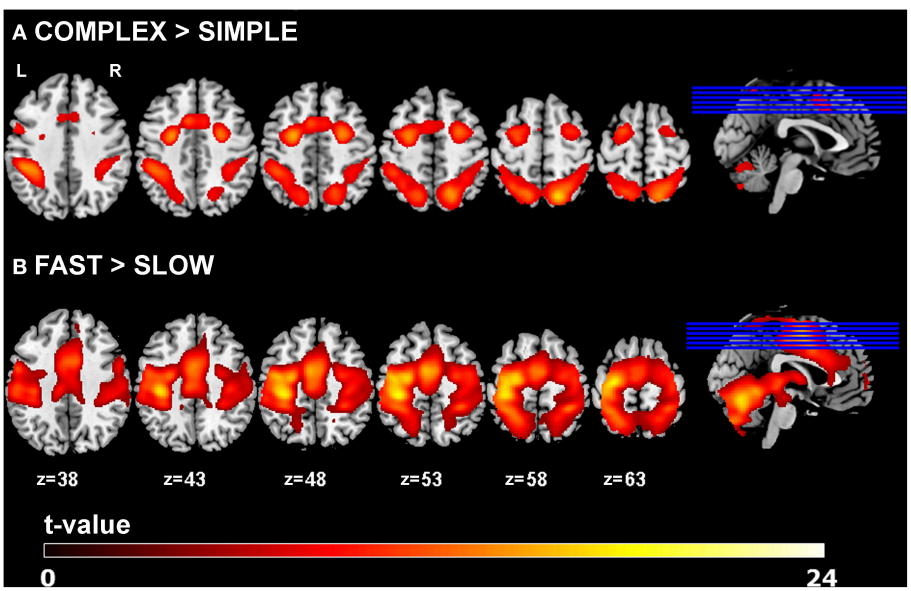

FIGURE 2 | GLM results. Main effects of task for **(A)** complexity and **(B)** speed across all participants ($p < 0.05$ FWE-corrected, minimum cluster size $k = 100$).

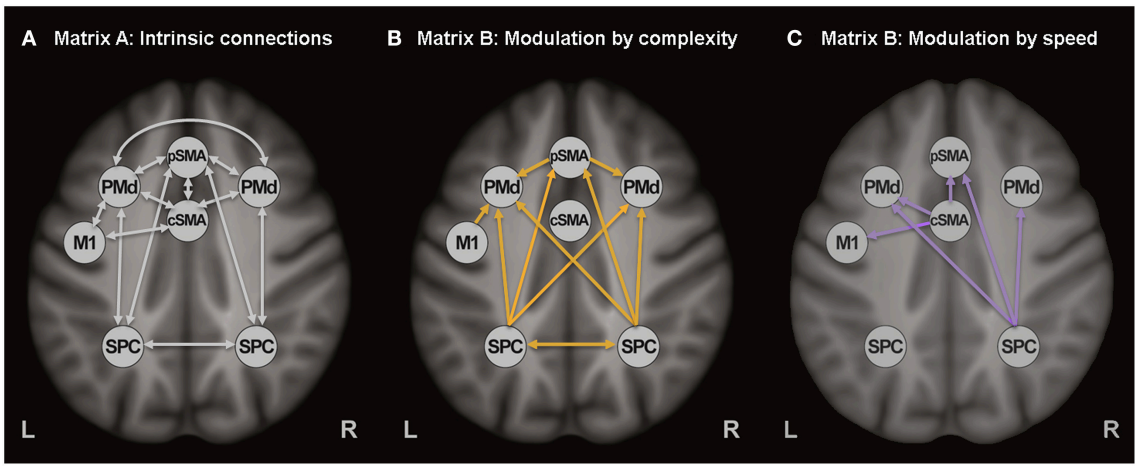

FIGURE 3 | Winning DCM model after *post-hoc* Bayesian model selection. (A) Task-independent, intrinsic connections, **(B)** Modulatory connections (complexity), and **(C)** Modulatory connections (speed).

putamen: $r = -0.186$, $p = 0.163$, simple fast: $r = -0.021$, $p = 0.873$, and complex fast: $r = -0.167$, $p = 0.211$).

Cluster Analysis Results

Three potentially meaningful clusters were identified, which were used to classify the HD mutation gene carriers accordingly (a scree plot of the agglomeration schedule is provided in the **Figure S2**). The group distribution was as follows: 23 participants were included in the first cluster, 46 in the second one, and 9 participants in the third cluster. The corresponding demographic, clinical, and motor performance information is provided in the **Table S4**. Sub-groups differed neither in their demographic (age, gender, and education) and clinical (DBS, CPO, and putamen volume) data, nor in their performance during scanning (i.e., means and SD of cue-response timing inaccuracies during the four movement conditions; **Table S4**).

Between-group differences were identified only for modulatory neural couplings (cSMA-pSMA modulated by speed: $F_{(2,\ 69)} = 3.70$, $p = 0.003$, and lSPC-lPMd modulated by complexity: $F_{(2,\ 69)} = 8.99$, $p < 0.001$), using ANCOVA analyses after adjusting for effects of age, gender, site, and education. Connectivity profiles for all modulatory connections are shown in **Figure 5**. Bonferroni *post-hoc* analyses revealed that group differences were present only between sub-group 3 ($N = 9$) and the other two sub-groups (**Figure 6A**). Specifically, there was a stronger excitatory coupling from cSMA toward pSMA modulated by speed and stronger inhibitory coupling from lSPC toward lPMd modulated by complexity in sub-group 3, relative to the other two sub-groups (all effects significant at $p < 0.001$). Interestingly, stronger excitatory coupling from cSMA toward pSMA was associated with decreased putamen volume ($r = -0.633$, $n = 9$, $p = 0.007$), as indicated by partial correlation analysis, adjusting for age, gender, education, and site (**Figure 6B**). With regard to the lSPC-lPMd connection, higher excitatory coupling in sub-groups 1 ($r = -0.496$, $n = 23$, $p = 0.043$) and 2 ($r = -0.483$, $n = 46$, $p = 0.002$), but not in sub-group 3 ($r = 0.283$, $n = 9$, $p = 0.645$), was associated with decreased putamen volume.

DISCUSSION

In this study, we sought to gain further insights into the neural circuitry of the motor network in Huntington's disease. For this purpose, a sequential finger-tapping fMRI task and DCM were used to assess the causal interactions among regions involved in both executive (movement speed) and cognitive (movement complexity) aspects of motor control. In the fMRI analysis, the same task-specific motor network was found as identified in our previous study (Klöppel et al., 2009). This included activations in pSMA, bilateral PMd, and bilateral SPC during complex tapping conditions, while the cSMA and lM1 were more strongly activated during fast finger tapping. Furthermore, it was shown here that, although preHD and earlyHD did not differ from each other in their behavioral performance, lower accuracy during tapping across all gene mutation carriers was associated with disease progression (i.e., cumulative probability of clinical onset). In the DCM analysis, on the other hand, the main focus was on the characterization of abnormal connectivity in the identified network of regions, which was common for both HD mutation gene carriers and healthy controls.

Effective Connectivity in HD

Our first aim was to extend on previously published DCM data in preclinical HD, which suggested the crucial role of premotor (i.e., PMd) and parietal areas (i.e., SPC), as part of fronto-parietal circuits, for the maintenance of motor functioning (Scheller et al., 2013). Our findings did not provide any evidence for the previously proposed compensatory role of premotor areas in preHD, characterized by an increased neural coupling from dorsal premotor cortex toward superior parietal cortex, which was regarded as indicative of neural reserve mechanisms that occurred during complex movements (i.e., high cognitive

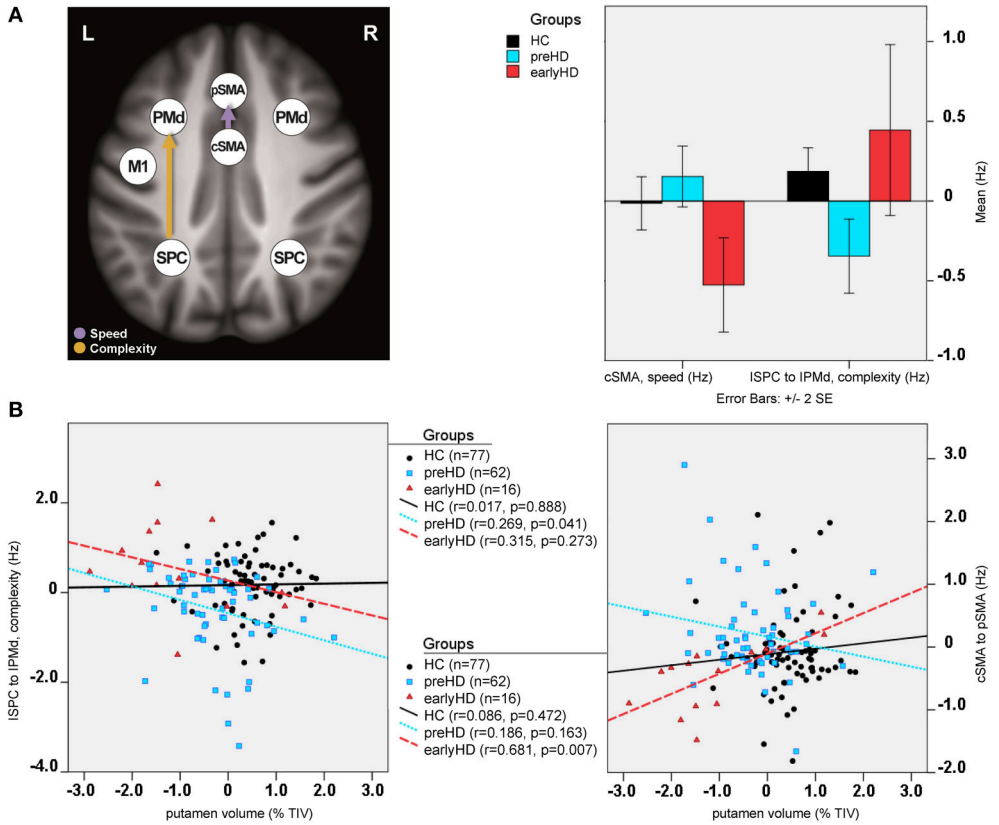

FIGURE 4 | DCM results: between-group differences. (A) Differential modulatory effects driven by complexity and speed. **(B)** Correlation analysis.

demand) in preHD individuals closer to clinical onset. However, it should be emphasized that the cognitive aspect in our experiment was less complex and might have been insufficiently demanding (i.e., participants in our study had to learn a complex sequence of 4 digits as compared to the 10-item sequence used in the previous study). Of note, a stronger inhibitory modulatory coupling was found from lSPC toward lPMd in preHD, relative to HC, which is in line with our previous findings (Scheller et al., 2013), but, interestingly, the reversed excitatory effect was also present in earlyHD. Furthermore, stronger excitatory effects from lSPC toward lPMd were associated with lower putamen volume in all gene carriers, which is only partly explained by group membership, as indicated by the substantially overlapping values for putamen volume between preHD and earlyHD (**Figure 3B**). Putamen volume was used as a disease marker, since striatal atrophy is a well-attested clinical hallmark of HD. Also, previous DTI data have confirmed that the putamen is interconnected with our regions of interest, including (but not limited to) the primary motor and premotor cortices and the supplementary motor area (Leh et al., 2007).

The present analysis also revealed that task-induced changes during speed conditions resulted in a stronger inhibitory coupling from cSMA to pSMA in those earlyHD patients who had lower putamen volume and performed worse at the fast motor conditions. However, this effect should be considered with caution because it reached only trend significance after correction for multiple comparisons. Also, the earlyHD group was overall slightly smaller in size than the healthy controls and the preHD, which might have introduced an additional bias. Nevertheless, we believe that the current study provides results that are complementary to our previous findings and suggests that the choice of experimental manipulation is critical for assessing and understanding the complex functional connectivity pattern between core regions maintaining motor function. It also points to the heterogeneity inherent across the HD gene mutation carriers and further supports the notion that identifying sub-groups of patients that are not merely defined according to clinical onset would be beneficial for future interventions.

Cluster Analysis for HD Sub-Group Classification

The second aim of our study was to explore the application of a hierarchical cluster analysis based on the DCM intrinsic and task-specific parameters in an attempt to identify clinically meaningful sub-groups within the HD gene carrier group. Cluster analysis approaches based on structural imaging data have already proven useful for stratification of patient populations and predictions of clinical outcomes in the context of aging and Alzheimer's disease (Nettiksimmons et al., 2010; Damian et al., 2013; Peter et al., 2014;

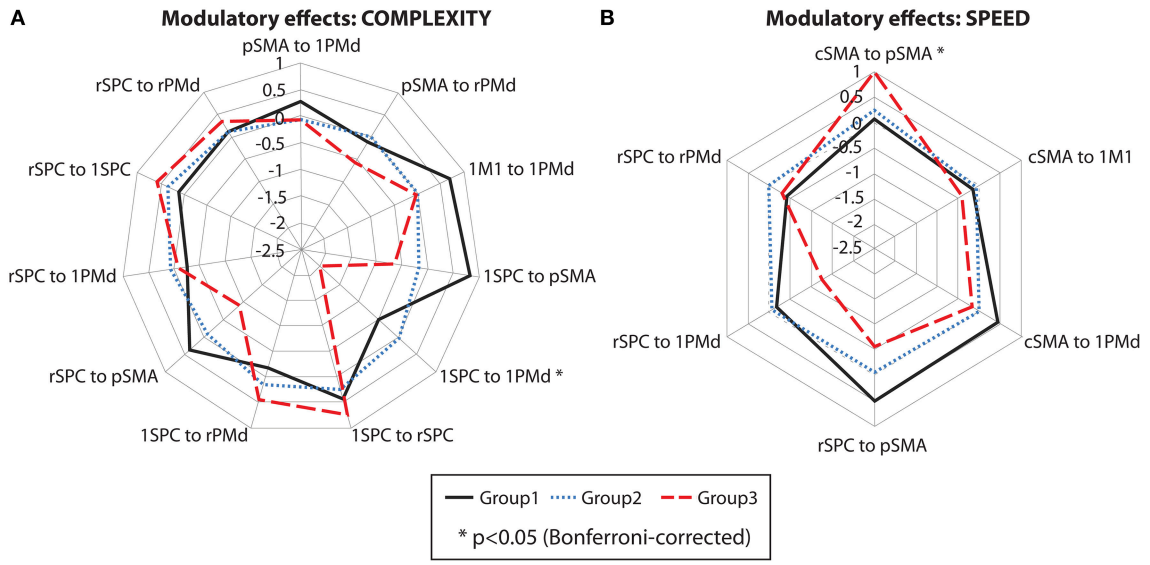

FIGURE 5 | Cluster analysis: connectivity profiles. Modulatory effects of **(A)** complexity and **(B)** speed on neural coupling strengths in all cluster sub-groups. Significant effects are marked with an asterisk ($p < 0.05$, Bonferroni-corrected).

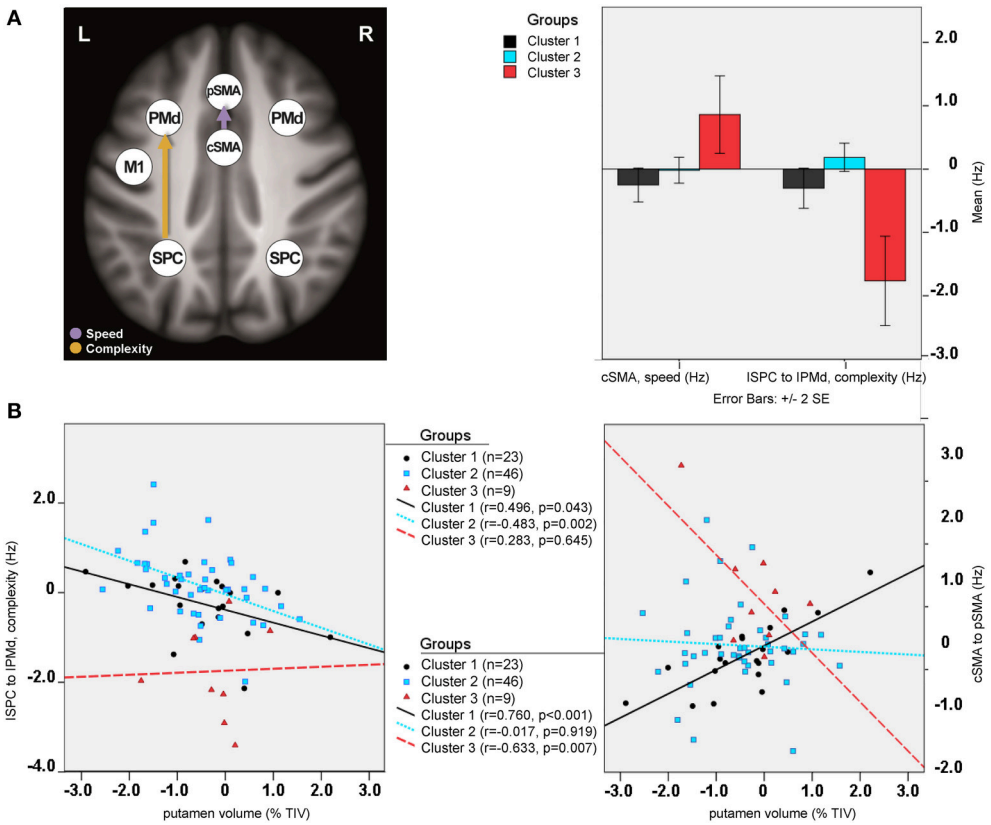

FIGURE 6 | Cluster analysis: sub-group differences. (A) Differential modulatory effects driven by complexity and speed. **(B)** Correlation analysis.

Quaranta et al., 2014). However, to our knowledge, this is the first study using task-based DCM neural couplings for classification of clinical sub-groups.

Hierarchical clustering is an unsupervised clustering approach, which may render the selection of optimal number of clusters arbitrary, as it is highly dependent on the similarity

measures used. Here, the HD gene carriers were divided into three different clusters after the visual inspection of the dendrogram and considering the change in agglomeration coefficients as the number of clusters increased. This is also consistent with previous divisions of pre-symptomatic HD into preHD-A (further from predicted diagnosis) and preHD-B (nearer) and of manifest HD into stage 1 (HD1) and stage 2 (HD2), depending on their total functioning capacity scores (Tabrizi et al., 2009). Of note, only early stage HD individuals were included in the current analysis, who were initially recruited as preHD but have converted during the course of the TrackOn-HD study. After close inspection of the clusters, it is of note that DCM-based cluster membership was not merely explained by disease burden and did not overlap with the differentiation between preHD and earlyHD.

The differences in DCM parameters among the three sub-groups reflected the same variation in modulatory neural coupling as observed in the DCM-based ANCOVA analysis, using the initially defined membership (i.e., HC, preHD, and earlyHD). It should be noted that the cluster consisting of 9 individuals (7 preHD-B and 2 preHD-A) differed significantly from the other two clusters ($N = 23$ and $N = 46$), but at the same time showed the opposite effects than those observed in earlyHD. Specifically, neural coupling strengths from left parietal regions toward premotor areas, modulated by complex tapping movements, was excitatory in nature in earlyHD and inhibitory in cluster sub-group 3. On the other hand, fast tapping movements differentially modulated the neural coupling from cSMA to pSMA in such a way that it was inhibitory in earlyHD, relative to preHD and HC, and excitatory in sub-group 3, relative to the other two clusters.

Clearly, this provides further support for the heterogeneity in neural circuits across the HD disease spectrum but, due to the lack of clear correlations with behavioral measures of speed and complexity, does not provide firm evidence for compensatory mechanisms. Nevertheless, the excitatory neural coupling from lSPC to lPMd, which increased with lower putamen volume, together with the association of CPO with lower behavioral performance, may possibly point to an attempted (as opposed to successful) compensatory mechanism (for an in-depth discussion of successful vs. attempted compensation please refer to Scheller et al., 2014). Of note, some regions involved in motor control, such as the cSMA and rSPC (Klöppel et al., 2009), as well as the bilateral PMd (Scheller et al., 2013), seem to be essential for maintaining motor functioning, and increased cortical recruitment has also been observed in anterior cingulate-frontal-motor-parietal cortex in HD during a working memory task (Georgiou-Karistianis et al., 2007). In a resting-state fMRI study in HD (Werner et al., 2014), however, increased functional connectivity in motor and parietal cortices was associated with motor impairments, pointing that cortical over-recruitment may not necessarily reflect compensation but could also be indicative of a dysfunction due to HD disease-related deficits. Thus, compensation could also be characterized by down-regulation or disengagement of brain regions (Cox et al., 2015). Alternatively, increased cortical activations may be beneficial in some individuals but become insufficient for retaining high level of functioning in others, as disease progresses.

Limitations and Future Directions

Altogether, the present study showed that DCM could successfully be applied to assess aberrant effective connectivity in Huntington's disease. Based on directed neural coupling strengths and their change caused by experimental perturbations, a potentially useful classification of HD mutation gene carriers was identified. However, certain limitations need to be mentioned in this regard. Clusters were defined in an exploratory manner and while an interesting pattern of DCM-based classification was observed, the clinical value of our findings still needs to be evaluated. It is still to be investigated whether cluster membership remains stable over time and whether it is predictive of future clinical outcomes (e.g., conversion to HD, disease progression, and domain-specific changes reflected by behavioral markers). Future studies focusing on longitudinal data should address these issues and should also aim at providing more mechanistic, biologically-relevant insights into the neural circuitry in HD, differentiating between maladaptive vs. compensatory mechanisms, which will be of great importance for future targeted interventions.

ACKNOWLEDGMENTS

The authors thank the TrackOn-HD study participants and the CHDI/ High Q Foundation, a not-for-profit organization dedicated to finding treatments for HD, as well as all TrackOn-HD investigators. This work was funded by CHDI/High Q Foundation Inc. The article processing charge was funded by the German Research Foundation (DFG) and the Albert-Ludwigs University Freiburg in the Open Access Publishing Funding Program.

TrackOn-HD INVESTIGATORS

A. Coleman, **J. Decolongon**, **M. Fan**, **T. Koren** (University of British Columbia, Vancouver); **C. Jauffret, D. Justo, S. Lehericy, K. Nigaud, R. Valabrègue** (ICM and APHP, Pitié-Salpêtrière University Hospital, Paris); **A. Schoonderbeek, E. P. 't Hart** (Leiden University Medical Centre, Leiden); **H. Crawford, S. Gregory, D. Hensman Moss, E. Johnson, J. Read, G. Owen, M. Papoutsi, C. Berna, A. Razi, G. Rees, R. I. Scahill** (University College London, London); **D. Craufurd** (Manchester University, Manchester); **R. Reilmann, N. Weber** (George Huntington Institute, Munster); **J. Stout, I. Labuschagne** (Monash University, Melbourne); **M. Orth, G. B. Landwehrmeyer** (Ulm University, Ulm); **D. Langbehn, H. Johnson, J. Long, J. Mills** (University of Iowa, Iowa).

SUPPLEMENTARY MATERIAL

The Supplementary Material for this article can be found online at: http://journal.frontiersin.org/article/10.3389/fnhum.2015.00634

Figure S1 | Experimental design: sequential motor finger-tapping task.

Figure S2 | Scree plot: change in agglomeration coefficients (y-axis) as the number of clusters increase (x-axis).

Table S1 | Exclusion criteria.

Table S2 | Descriptive information about motor performance.

Table S3 | Descriptive statistics of DCM connection strengths.

Table S4 | Cluster analysis: demographic, clinical, and motor performance information (HD gene mutation carriers only).

REFERENCES

Ashburner, J. (2007). A fast diffeomorphic image registration algorithm. *Neuroimage* 38, 95–113. doi: 10.1016/j.neuroimage.2007.07.007

Bartenstein, P., Weindl, A., Spiegel, S., Boecker, H., Wenzel, R., Ceballos-Baumann, A. O., et al. (1997). Central motor processing in Huntington's disease. A PET study. *Brain* 120, 1553–1567. doi: 10.1093/brain/120.9.1553

Biglan, K. M., Ross, C. A., Langbehn, D. R., Aylward, E. H., Stout, J. C., Queller, S., et al. (2009). Motor abnormalities in premanifest persons with Huntington's disease: the PREDICT-HD study. *Mov. Disord.* 24, 1763–1772. doi: 10.1002/mds.22601

Biglan, K. M., Zhang, Y., Long, J. D., Geschwind, M., Kang, G. A., Killoran, A., et al. (2013). Refining the diagnosis of Huntington disease: the PREDICT-HD study. *Front. Aging Neurosci* 5:12. doi: 10.3389/fnagi.2013.00012

Burns, R. P. (2009). "Chapter 23: Cluster analysis," in *Business Research Methods and Statistics Using SPSS*, ed R. P. Burns (London: Sage Publications), 552–567.

Buxton, R. B., Wong, E. C., and Frank, L. R. (1998). Dynamics of blood flow and oxygenation changes during brain activation: the balloon model. *Magn. Reson. Med.* 39, 885–864. doi: 10.1002/mrm.1910390602

Cox, S. R., Bastin, M. E., Ferguson, K. J., Allerhand, M., Royle, N. A., Maniega, S. M., et al. (2015). Compensation or inhibitory failure? Testing hypotheses of age-related right frontal lobe involvement in verbal memory ability using structural and diffusion MRI. *Cortex* 63, 4–15. doi: 10.1016/j.cortex.2014.08.001

Damian, M., Hausner, L., Jekel, K., Richter, M., Froelich, L., Almkvist, O., et al. (2013). Single-domain amnestic mild cognitive impairment identified by cluster analysis predicts Alzheimer's disease in the European prospective DESCRIPA study. *Dement. Geriatr. Cogn. Disord.* 36, 1–19. doi: 10.1159/000348354

Daunizeau, J., David, O., and Stephan, K. (2011). Dynamic causal modelling: a critical review of the biophysical and statistical foundations. *Neuroimage* 58, 312–322. doi: 10.1016/j.neuroimage.2009.11.062

Dickey, J. (1971). The weighted likelihood ratio, linear hypotheses on normal location parameters. *Ann. Mathemat. Statist.* 42, 204–223. doi: 10.1214/aoms/1177693507

Farrow, M., Chua, P., Churchyard, A., Bradshaw, J. L., Chiu, E., and Georgiou-Karistianis, N. (2006). Proximity to clinical onset influences motor and cognitive performance in presymptomatic Huntington disease gene carriers. *Cogn. Behav. Neurol.* 19, 208–216. doi: 10.1097/01.wnn.0000213914.64772.b6

Feigin, A., Ghilardi, M. F., Huang, C., Ma, Y., Carbon, M., Guttman, M., et al. (2006). Preclinical Huntington's disease: compensatory brain responses during learning. *Ann. Neurol.* 59, 53–59. doi: 10.1002/ana.20684

Friston, K. (2009). Causal modelling and brain connectivity in functional magnetic resonance imaging. *PLoS Biol.* 7:e33. doi: 10.1371/journal.pbio.1000033

Friston, K. J., Harrison, L., and Penny, W. (2003). Dynamic causal modelling. *Neuroimage* 19, 1273–1302. doi: 10.1016/S1053-8119(03)00202-7

Friston, K. J., Holmes, A. P., Worsley, K. J., Poline, J.-P., Frith, C. D., and Frackowiak, R. S. J. (1994). Statistical parametric maps in functional imaging: a general linear approach. *Hum. Brain Mapp.* 2, 189–210. doi: 10.1002/hbm.460020402

Friston, K., and Penny, W. (2011). Post hoc Bayesian model selection. *Neuroimage* 56, 2089–2099. doi: 10.1016/j.neuroimage.2011.03.062

Gavazzi, C., Nave, R. D., Petralli, R., Rocca, M. A., Guerrini, L., Tessa, C., et al. (2007). Combining functional and structural brain magnetic resonance imaging in Huntington disease. *J. Comput. Assist. Tomogr.* 31, 574–580. doi: 10.1097/01.rct.0000284390.53202.2e

Georgiou-Karistianis, N., Long, J. D., Lourens, S. G., Stout, J. C., Mills, J. A., and Paulsen, J. S. (2014). Movement sequencing in Huntington disease. *World J. Biol. Psychiatry* 15, 459–471. doi: 10.3109/15622975.2014.895042

Georgiou-Karistianis, N., Sritharan, A., Farrow, M., Cunnington, R., Stout, J., Bradshaw, J., et al. (2007). Increased cortical recruitment in Huntington's disease using a Simon task. *Neuropsychologia* 45, 1791–1800. doi: 10.1016/j.neuropsychologia.2006.12.023

Glover, G. H., Mueller, B. A., Turner, J. A., van Erp, T. G., Liu, T. T., Greve, D. N., et al. (2012). Function biomedical informatics research network recommendations for prospective multicenter functional MRI studies. *J. Magn. Reson. Imaging* 36, 39–54. doi: 10.1002/jmri.23572

Gountouna, V.-E., Job, D. E., McIntosh, A. M., Moorhead, T. W. J., Lymer, G. K. L., Whalley, H. C., et al. (2010). Functional Magnetic Resonance Imaging (fMRI) reproducibility and variance components across visits and scanning sites with a finger tapping task. *Neuroimage* 49, 552–560. doi: 10.1016/j.neuroimage.2009.07.026

Greve, D. N., Mueller, B. A., Liu, T., Turner, J. A., Voyvodic, J., Yetter, E., et al. (2011). A novel method for quantifying scanner instability in fMRI. *Magn. Reson. Med.* 65, 1053–1061. doi: 10.1002/mrm.22691

Hinton, S. C., Paulsen, J. S., Hoffmann, R. G., Reynolds, N. C., Zimbelman, J. L., and Rao, S. M. (2007). Motor timing variability increases in preclinical Huntington's disease patients as estimated onset of motor symptoms approaches. *J. Int. Neuropsychol. Soc.* 13, 539–543. doi: 10.1017/s1355617707070671

Hobbs, N. Z., Cole, J. H., Farmer, R. E., Rees, E. M., Crawford, H. E., Malone, I. B., et al. (2013). Evaluation of multi-modal, multi-site neuroimaging measures in Huntington's disease: baseline results from the PADDINGTON study. *Neuroimage Clin.* 2, 204–211. doi: 10.1016/j.nicl.2012.12.001

IBM Corp. (2011). *IBM SPSS Statistics for Windows, Version 20.0.* Armonk, NY: IBM Corp.

Kahan, J., and Foltynie, T. (2013). Understanding DCM: ten simple rules for the clinician. *Neuroimage* 83, 543–549. doi: 10.1016/j.neuroimage.2013.07.008

Klöppel, S., Draganski, B., Golding, C. V., Chu, C., Nagy, Z., Cook, P. A., et al. (2008). White matter connections reflect changes in voluntary-guided saccades in pre-symptomatic Huntington's disease. *Brain* 131(Pt 1), 196–204. doi: 10.1093/brain/awm275

Klöppel, S., Draganski, B., Siebner, H. R., Tabrizi, S. J., Weiller, C., and Frackowiak, R. S. J. (2009). Functional compensation of motor function in pre-symptomatic Huntington's disease. *Brain* 132, 1624–1632. doi: 10.1093/brain/awp081

Klöppel, S., Gregory, S., Scheller, E., Minkova, L., Razi, A., Durr, A., et al. (2015). Compensation in preclinical Huntington's disease. Evidence from the track-on hd study. *EBioMedicine* 2, 1420–1429. doi: 10.1016/j.ebiom.2015.08.002

Klöppel, S., Stonnington, C. M., Petrovic, P., Mobbs, D., Tüscher, O., Craufurd, D., et al. (2010). Irritability in pre-clinical Huntington's disease. *Neuropsychologia* 48, 549–557. doi: 10.1016/j.neuropsychologia.2009.10.016

Langbehn, D. R., Brinkman, R. R., Falush, D., Paulsen, J. S., and Hayden, M. R. (2004). A new model for prediction of the age of onset and penetrance for Huntington's disease based on CAG length. *Clin. Genet.* 65, 267–277. doi: 10.1111/j.1399-0004.2004.00241.x

Lawrence, A. (1998). Evidence for specific cognitive deficits in preclinical Huntington's disease. *Brain* 121, 1329–1341. doi: 10.1093/brain/121.7.1329

Leh, S. E., Ptito, A., Chakravarty, M. M., and Strafella, A. P. (2007). Fronto-striatal connections in the human brain: a probabilistic diffusion tractography study. *Neurosci. Lett.* 419, 113–118. doi: 10.1016/j.neulet.2007.04.049

Nana, A. L., Kim, E. H., Thu, D. C. V., Oorschot, D. E., Tippett, L. J., Hogg, V. M., et al. (2014). Widespread heterogeneous neuronal loss across the cerebral cortex in Huntington's Disease. *J. Huntingtons. Dis.* 3, 45–64. doi: 10.3233/JHD-140092

Nettiksimmons, J., Harvey, D., Brewer, J., Carmichael, O., DeCarli, C., Jack, C., et al. (2010). Subtypes based on cerebrospinal fluid and magnetic resonance imaging markers in normal elderly predict cognitive decline. *Neurobiol. Aging* 31, 1419–1428. doi: 10.1016/j.neurobiolaging.2010.04.025

Novak, M. J. U., Seunarine, K. K., Gibbard, C. R., Hobbs, N. Z., Scahill, R. I., Clark, C. A., et al. (2014). White matter integrity in premanifest and early Huntington's disease is related to caudate loss and disease progression. *Cortex* 52, 98–112. doi: 10.1016/j.cortex.2013.11.009

Parker Jones, O., Seghier, M. L., Kawabata Duncan, K. J., Leff, A. P., Green, D. W., and Price, C. J. (2013). Auditory-motor interactions for the production of native and non-native speech. *J. Neurosci.* 33, 2376–2387. doi: 10.1523/JNEUROSCI.3289-12.2013

Penney, J. B. Jr., Vonsattel, J. P., MacDonald, M. E., Gusella, J. F., and Myers, R. H. (1997). CAG repeat number governs the development rate of pathology in Huntington's disease. *Ann. Neurol.* 41, 689–692. doi: 10.1002/ana.410410521

Penny, W., Stephan, K., Mechelli, A., and Friston, K. (2004). Modelling functional integration: a comparison of structural equation and dynamic causal models. *Neuroimage* 23, S264–S274. doi: 10.1016/j.neuroimage.2004.07.041

Peter, J., Abdulkadir, A., Kaller, C., Kümmerer, D., Hüll, M., Vach, W., et al. (2014). Subgroups of Alzheimer's disease: stability of empirical clusters over time. *J. Alzheimers. Dis.* 42, 651–661. doi: 10.3233/JAD-140261

Poudel, G. R., Stout, J. C., Domínguez, D. J. F., Churchyard, A., Chua, P., Egan, G. F., et al. (2014). Longitudinal change in white matter microstructure in Huntington's disease: the IMAGE-HD study. *Neurobiol. Dis.* 74, 406–412. doi: 10.1016/j.nbd.2014.12.009

Power, J. D., Barnes, K. A., Snyder, A. Z., Schlaggar, B. L., and Petersen, S. E. (2012). Spurious but systematic correlations in functional connectivity MRI networks arise from subject motion. *Neuroimage* 59, 2142–2154. doi: 10.1016/j.neuroimage.2011.10.018

Quaranta, D., Vita, M. G., Spinelli, P., Scaricamazza, E., Castelli, D., Lacidogna, G., et al. (2014). Does semantic memory impairment in amnestic MCI with hippocampal atrophy conform to a distinctive pattern of progression? *Curr. Alzheimer Res.* 11, 399–407. doi: 10.2174/1567205011666140317104051

Rosa, M. J., Friston, K., and Penny, W. (2012). Post-hoc selection of dynamic causal models. *J. Neurosci. Methods* 208, 66–78. doi: 10.1016/j.jneumeth.2012.04.013

Rosas, H. D., Koroshetz, W. J., Chen, Y. I., Skeuse, C., Vangel, M., Cudkowicz, M. E., et al. (2003). Evidence for more widespread cerebral pathology in early HD: an MRI-based morphometric analysis. *Neurology* 60, 1615–1620. doi: 10.1212/01.wnl.0000065888.88988.6e

Rosas, H. D., Salat, D. H., Lee, S. Y., Zaleta, A. K., Pappu, V., Fischl, B., et al. (2008). Cerebral cortex and the clinical expression of Huntington's disease: complexity and heterogeneity. *Brain* 131(Pt 4), 1057–1068. doi: 10.1093/brain/awn025

Scheller, E., Abdulkadir, A., Peter, J., Tabrizi, S. J., Frackowiak, R. S. J., and Klöppel, S. (2013). Interregional compensatory mechanisms of motor functioning in progressing preclinical neurodegeneration. *Neuroimage* 75, 146–154. doi: 10.1016/j.neuroimage.2013.02.058

Scheller, E., Minkova, L., Leitner, M., and Klöppel, S. (2014). Attempted and successful compensation in preclinical and early manifest neurodegeneration: a review of task fMRI studies. *Front. Psychiatry* 5:132. doi: 10.3389/fpsyt.2014.00132

Seghier, M. L., and Friston, K. J. (2013). Network discovery with large DCMs. *Neuroimage* 68, 181–191. doi: 10.1016/j.neuroimage.2012.12.005

Seghier, M. L., Zeidman, P., Neufeld, N. H., Leff, A. P., and Price, C. J. (2010). Identifying abnormal connectivity in patients using dynamic causal modeling of FMRI responses. *Front. Syst. Neurosci.* 4:142. doi: 10.3389/fnsys.2010.00142

Shoulson, I., and Fahn, S. (1979). Huntington disease: clinical care and evaluation. *Neurology* 29, 1–3. doi: 10.1212/wnl.29.1.1

Stephan, K., Penny, W., Moran, R., den Ouden, H., Daunizeau, J., and Friston, K. (2010). Ten simple rules for dynamic causal modeling. *Neuroimage* 49, 3099–3109. doi: 10.1016/j.neuroimage.2009.11.015

Tabrizi, S. J., Langbehn, D. R., Leavitt, B. R., Roos, R. A., Durr, A., Craufurd, D., et al. (2009). Biological and clinical manifestations of Huntington's disease in the longitudinal TRACK-HD study: cross-sectional analysis of baseline data. *Lancet Neurol.* 8, 791–801. doi: 10.1016/S1474-4422(09)70170-X

Ward, J. H. (1963). Hierarchical grouping to optimize an objective function. *J. Am. Statist. Assoc.* 58, 236–244. doi: 10.1080/01621459.1963.10500845

Werner, C. J., Dogan, I., Saß, C., Mirzazade, S., Schiefer, J., Shah, N. J., et al. (2014). Altered resting-state connectivity in Huntington's disease. *Hum. Brain Mapp.* 35, 2582–2593. doi: 10.1002/hbm.22351

Witt, S. T., Laird, A. R., and Meyerand, M. E. (2008). Functional neuroimaging correlates of finger-tapping task variations: an ALE meta-analysis. *NeuroImage* 42, 343–356. doi: 10.1016/j.neuroimage.2008.04.025

Wolf, R. C., Grön, G., Sambataro, F., Vasic, N., Wolf, N. D., Thomann, P. A., et al. (2011). Magnetic resonance perfusion imaging of resting-state cerebral blood flow in preclinical Huntington's disease. *J. Cereb. Blood Flow Metab.* 31, 1908–1918. doi: 10.1038/jcbfm.2011.60

Wolf, R. C., Sambataro, F., Vasic, N., Schönfeldt-Lecuona, C., Ecker, D., and Landwehrmeyer, B. (2008). Aberrant connectivity of lateral prefrontal networks in presymptomatic Huntington's disease. *Exp. Neurol.* 213, 402–411. doi: 10.1016/j.expneurol.2008.05.017

Wolf, R. C., Sambataro, F., Vasic, N., Wolf, N. D., Thomann, P. A., Saft, C., et al. (2012). Default-mode network changes in preclinical Huntington's disease. *Exp. Neurol.* 237, 191–198. doi: 10.1016/j.expneurol.2012.06.014

World Medical Association (2013). World medical association declaration of helsinki. *JAMA* 310, 2191–2194. doi: 10.1001/jama.2013.281053

Conflict of Interest Statement: The authors declare that the research was conducted in the absence of any commercial or financial relationships that could be construed as a potential conflict of interest.

frontiers in Human Neuroscience

ORIGINAL RESEARCH
published: 03 November 2015
doi: 10.3389/fnhum.2015.00589

Anterior cingulate cortex-related connectivity in first-episode schizophrenia: a spectral dynamic causal modeling study with functional magnetic resonance imaging

Long-Biao Cui[1†], Jian Liu[2†], Liu-Xian Wang[1†], Chen Li[1], Yi-Bin Xi[1], Fan Guo[1], Hua-Ning Wang[3], Lin-Chuan Zhang[4], Wen-Ming Liu[3], Hong He[3], Ping Tian[1], Hong Yin[1] and Hongbing Lu[4*]*

[1] Department of Radiology, Xijing Hospital, The Fourth Military Medical University, Xi'an, China, [2] Network Center, The Fourth Military Medical University, Xi'an, China, [3] Department of Psychiatry, Xijing Hospital, The Fourth Military Medical University, Xi'an, China, [4] School of Biomedical Engineering, The Fourth Military Medical University, Xi'an, China

OPEN ACCESS

Edited by:
Adeel Razi,
University College London, UK

Reviewed by:
Karsten Specht,
University of Bergen, Norway
António J. Bastos-Leite,
University of Porto, Portugal
Benedetta Vai,
Scientifico Istitute Ospedale San Raffaele, Italy

***Correspondence:**
Hong Yin
yinhong@fmmu.edu.cn;
Hongbing Lu
luhb@fmmu.edu.cn

[†] These authors have contributed equally to this work.

Received: 08 June 2015
Accepted: 12 October 2015
Published: 03 November 2015

Citation:
Cui L-B, Liu J, Wang L-X, Li C, Xi Y-B, Guo F, Wang H-N, Zhang L-C, Liu W-M, He H, Tian P, Yin H and Lu H (2015) Anterior cingulate cortex-related connectivity in first-episode schizophrenia: a spectral dynamic causal modeling study with functional magnetic resonance imaging. Front. Hum. Neurosci. 9:589. doi: 10.3389/fnhum.2015.00589

Understanding the neural basis of schizophrenia (SZ) is important for shedding light on the neurobiological mechanisms underlying this mental disorder. Structural and functional alterations in the anterior cingulate cortex (ACC), dorsolateral prefrontal cortex (DLPFC), hippocampus, and medial prefrontal cortex (MPFC) have been implicated in the neurobiology of SZ. However, the effective connectivity among them in SZ remains unclear. The current study investigated how neuronal pathways involving these regions were affected in first-episode SZ using functional magnetic resonance imaging (fMRI). Forty-nine patients with a first-episode of psychosis and diagnosis of SZ—according to the Diagnostic and Statistical Manual of Mental Disorders, Fourth Edition, Text Revision—were studied. Fifty healthy controls (HCs) were included for comparison. All subjects underwent resting state fMRI. We used spectral dynamic causal modeling (DCM) to estimate directed connections among the bilateral ACC, DLPFC, hippocampus, and MPFC. We characterized the differences using Bayesian parameter averaging (BPA) in addition to classical inference (*t*-test). In addition to common effective connectivity in these two groups, HCs displayed widespread significant connections predominantly involved in ACC not detected in SZ patients, but SZ showed few connections. Based on BPA results, SZ patients exhibited anterior cingulate cortico-prefrontal-hippocampal hyperconnectivity, as well as ACC-related and hippocampal-dorsolateral prefrontal-medial prefrontal hypoconnectivity. In summary, spectral DCM revealed the pattern of effective connectivity involving ACC in patients with first-episode SZ. This study provides a potential link between SZ and dysfunction of ACC, creating an ideal situation to associate mechanisms behind SZ with aberrant connectivity among these cognition and emotion-related regions.

Keywords: schizophrenia, anterior cingulate cortex, functional magnetic resonance imaging, effective connectivity, spectral dynamic causal modeling

INTRODUCTION

Schizophrenia (SZ) affects approximately 1% of the population and is one of the leading causes of health burden all over the world (APA, 2013; Whiteford et al., 2013). It still remains unclear, however, regarding the pathogenesis of SZ, which has seriously hampered the efficacy of prevention and treatment for SZ. Understanding the neural basis of SZ is pivotal for shedding light on the neurobiological mechanisms behind this mental disease. The disconnection hypothesis suggests that the diverse symptoms of SZ are associated with abnormal neuronal connectivity between distinct regions (Friston and Frith, 1995; Friston, 1998; Stephan et al., 2009; Pettersson-Yeo et al., 2011). SZ, as a debilitating neuropsychiatric illness, involves both regional brain deficits and disruptions of communication among distinct brain regions (Friston and Frith, 1995; Stephan et al., 2009), including abnormal inter-hemispheric connectivity (Whitford et al., 2010; Chang et al., 2015). In the most recent years, increasing evidence has arisen supporting the notion that the structural and functional dysconnectivity within different brain regions is thought to account for the mechanism underlying SZ and its significant clinical and neuropathological heterogeneity on the basis of functional magnetic resonance imaging (fMRI) studies (Kubota et al., 2013; Voineskos et al., 2013; Liu et al., 2014a; Bastos-Leite et al., 2015; Genzel et al., 2015; Guo et al., 2015).

Structurally, on the one hand, SZ patients showed significant reduction of gray matter volume in the bilateral anterior cingulate cortex (ACC) as the largest effect size among all the areas investigated, as well as the bilateral posterior superior temporal gyri, bilateral inferior frontal gyri, left posterior amygdala-hippocampal complex (mostly hippocampus), and left insula (Yamasue et al., 2004). Concerning structural connectivity, major diffusion tensor imaging (DTI) findings highlighted a decreased fractional anisotropy (FA) value in the cingulate bundle, corpus callosum, and frontal and temporal white matter in chronic SZ (White et al., 2008; Pomarol-Clotet et al., 2010), whereas patients at the first-episode psychosis showed a decreased FA value in the inferior longitudinal fasciculus (Friedman et al., 2008) and a decreased mean diffusivity (MD) value in the left parahippocampal gyrus, left insula, and right ACC (Moriya et al., 2010). A previous meta-analysis of 15 DTI studies in SZ highlighted a significant FA reductions in two regions: the left frontal and temporal deep white matter (Ellison-Wright and Bullmore, 2009). Recently, Kubota et al. found SZ patients exhibited thalamo-orbitofrontal disconnection (Kubota et al., 2013). Specifically, reduced FA value in the right thalamo-orbitofrontal pathway and significantly positive correlation between FA value for this pathway and the right frontal polar and lateral orbitofrontal cortices were observed in this study. For patients with deficit SZ, they displayed disruption of white matter tracts at the right inferior longitudinal fasciculus, right arcuate fasciculus, and left uncinate fasciculus as compared with patients with nondeficit SZ (Voineskos et al., 2013). Furthermore, diffusion tensor tractography (DTT) analysis revealed a significant difference of connectivity between the bilateral medial prefrontal cortex (MPFC) and genu of the corpus callosum in SZ patients (Pomarol-Clotet et al., 2010).

Functionally, on the other hand, SZ is frequently characterized as not only a disorder of a large-scale brain connectivity but also a selective disruption of connectivity among central hub regions of the brain, but identifying its imaging-based connectomics is still challenging (Fornito et al., 2012; van den Heuvel et al., 2013). Resting state fMRI studies indicate widespread disconnectivity in the brain involved in the pathophysiology of SZ (Khadka et al., 2013; Mamah et al., 2013; Argyelan et al., 2014). For first-episode SZ patients, Bastos-Leite et al have reported reduced effective connectivity within the default mode network (DMN) using stochastic dynamic causal modeling (DCM), reflecting a reduced postsynaptic efficacy of prefrontal afferents (Bastos-Leite et al., 2015); Guo et al have demonstrated that patients revealed abnormal prefrontal-thalamic-cerebellar circuit using Granger causality analysis (GCA) (Guo et al., 2015). They found SZ may be associated with increased connectivity from the left MPFC or the right ACC to the sensorimotor regions and disrupted bilateral connections among sensorimotor regions, partly reflecting the effects of structural aberrancies in first-episode SZ on the prefrontal-thalamic-cerebellar circuit (Guo et al., 2015). Besides aberrant structural connectivity, the bilateral MPFC has been shown a marked failure of deactivation in SZ patients (Pomarol-Clotet et al., 2010). In addition, dorsolateral prefrontal cortex (DLPFC) is one of the most important cortical regions involved in the pathogenesis of SZ, and DLPFC-hippocampal formation dysconnectivity has been reported in SZ patients and links with the risk of developing SZ (Liu et al., 2014a). SZ patients also showed deficit in overnight memory consolidation associated with hippocampal-prefrontal connectivity (Genzel et al., 2015) and exhibited overactivation of DLPFC during social judgment (Mukherjee et al., 2014). In SZ, the connectivity between PFC and limbic regions (amygdala) was reduced during the resting state (Fan et al., 2013; Liu et al., 2014b), and absent and reversed or decreased during the processing of emotional stimuli (Das et al., 2007; Leitman et al., 2008). A reduced PFC-amygdala coupling was also associated with psychosis proneness in the general population (Modinos et al., 2010). Taken together, interactions among ACC, PFC (DLPFC and MPFC), and hippocampus have been crucially implicated in the neurobiology of SZ, and may represent a particular form of dysconnection in SZ. However, changes in connectivity patterns among these brain areas are largely unknown in SZ patients.

Effective connectivity is characterized by the causal (directed and weighted) influence of one brain region over another or itself. DCM, a technique used for measuring effective connectivity among different brain regions, is based on functional neuroimaging. Both functional and effective connectivity analyses are common methods used in resting state fMRI studies. However, DCM not only enables us to quantify the strength of connectivity among brain regions, but also allows the investigation of directed information flow from one region to another. An animal study has begun using spectral DCM to identify the pathophysiological theories of SZ recently (Moran et al., 2015). Here we used spectral DCM (Friston et al.,

2014; Razi et al., 2015) to identify abnormal effective connectivity underlying SZ.

In the present study, we used spectral DCM to elucidate the effective connectivity among previously reported regions (bilateral ACC, DLPFC, hippocampi, and MPFC) associated with SZ, thereby providing a better understanding of the pathophysiological correlates of SZ. We hypothesized that directed connectivity involving these brain regions may be disturbed in SZ patients, predisposing to impairment of perceptual and cognitive functions and emotional behavior.

METHODS

Subjects

The study sample consisted of 52 first-episode SZ patients from early intervention services within the outpatient clinic and inpatient department at Xijing Hospital, and 53 healthy controls (HCs) recruited by advertisement from the local community. Exclusion criteria comprised: pregnancy, major medical and neurological disorders, history of significant head trauma; illicit drug or alcohol abuse or dependence. Additional exclusion criteria for HCs included a current or past history of psychiatric illness and the presence of psychosis in first-degree relatives. The absence of any psychotic syndromes in HCs was confirmed using the Prodomal Questionnaire (Loewy et al., 2005). Two senior clinical psychiatrists performed the clinical-psychometric assessments—according to the Diagnostic and Statistical Manual of Mental Disorders, Fourth Edition, Text Revision (DSM-IV-TR)—with an interrater reliability >0.9. Patients were assessed with the Positive And Negative Syndrome Scale (PANSS) (Kay et al., 1987) on the day of scanning, as well as detailed information regarding past symptomatology acquired through patient interview and examination of patient's medical records. All participants gave written informed consent approved by the local Research Ethics Committee (Xijing Hospital, Fourth Military Medical University) after a complete description of this study.

Magnetic Resonance Imaging Acquisition

The fMRI images were acquired on a 3.0-T Siemens Magnetom Trio Tim scanner. During data acquisition, participants were asked to stay still in the scanner, keeping their eyes closed but not to fall asleep. The participants wore a custom-built MRI-compatible head coil fitted with foam pads and earplugs to minimize head motion and dampen scanner noise. Resting state functional scans were acquired with an echo planar imaging (EPI) sequence using the following parameters: repetition time = 2000 ms, echo time = 30 ms, filed of view = 220 mm × 220 mm, matrix = 64 × 64, flip angle = 90°, number of slices = 33, slice thickness = 4 mm, section gap = 0.6 mm. The whole scanning process lasted for 8 min and 240 scans were acquired for each subject.

Data Preprocessing

Images were preprocessed using SPM8 (http://www.fil.ion.ucl.ac.uk/spm/software/spm8/). For each subject, fMRI scans were first realigned to correct for head motion. Interscan motion was assessed with translation/rotation, and an exclusion criterion (>2.5 mm translation and/or >2.5° rotation in each direction) was set. Three SZ patients and three HCs met the criteria and were excluded from further analyses, resulting in that eventual 49 SZ patients and 50 HCs were included. Realigned images were then spatially normalized to the Montreal Neurological Institute space and finally smoothed using an 8 mm full width at half-maximum Gaussian kernel.

General Linear Model and Region of Interest

At the first (within subject) level, a general linear model (GLM) was constructed for each participant. Fluctuations in neuronal activity will models with cosine basis functions. In addition, the six motion parameters from the realignment procedure and, one constant regressor modeling the baseline, and cosine basis functions were included in the GLM. See the resulting constant images used for constraining the ROI extraction step in the spectral DCM (**Supplementary Figure 1**).

For each participant, symmetric eight regions of interest (ROIs) including bilateral ACC, DLPFC, hippocampi, and MPFC were selected. For each region, a mask was created using the WFU PickAtlas Tool and the automated anatomical labeling atlas template (Version 3.0.4, http://www.nitrc.org/projects/wfu_pickatlas/) (Tzourio-Mazoyer et al., 2002; Maldjian et al., 2003, 2004). For each ROI, subject-specific time series were extracted from a region defined by a thresholded SPM testing for the baseline and masked using the corresponding ROI from the WFU PickAtlas Tool (**Figure 1**). We used masks from the atlas for extraction of time series from the ROIs. All the voxels within the masks were used and first principle component was used as the extracted signal.

Spectral Dynamic Causal Modeling

Effective connectivity among the bilateral ACC, DLPFC, hippocampi, and MPFC was investigated using spectral DCM as described elsewhere (Friston et al., 2014). In the absence of a particular hypothesis or model space we used the fully connected model for an exploratory analysis of all possible reduced models, without one or more connections: after the full DCM for each participant was inverted, we employed a network discovery procedure using Bayesian model reduction (BMR) (Friston and Penny, 2011) to find the best model that explains the data. This procedure tests every possible model nested within the fully connected model. The model with the highest posterior probability is chosen as the winning model during this procedure. This BMR procedure is an efficient way to score a large model space without having to invert every reduced model. A fully connected model was constructed for each subject. This model was then inverted using generalized filtering (Friston et al., 2010). The model selection procedure was used to identify the model best explaining how the data are generated. Thus, we used a network discovery scheme in order to identify the optimal model pooling over all subjects

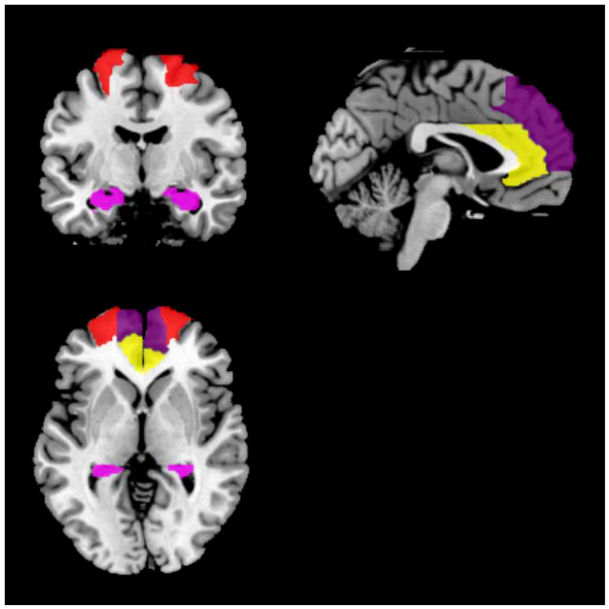

FIGURE 1 | Locations of the masks. Red indicates DLPFC; yellow indicates ACC; dark purple indicates MPFC; violet indicates the hippocampus.

(Friston et al., 2011). Model evidence of a fully connected model was used to approximate the model evidence of all the possible models and search for the model with the largest evidence. This network discovery-based model selection method can find the best model in the whole model space only by estimating parameters of a fully connected model (Li et al., 2012).

On the basis of spectral DCM analysis, the connection strength described the strength of a coupling according to the rate at which neuronal responses were induced in the target region (in other words connection strengths are effectively rate constants in 1/s, Hz). The resulting (maximum *a posteriori*) estimates of connectivity were then treated as summary statistics for classical random effects inference at the second (between subject) level using appropriate *t*-tests. We reported (Bonferroni corrected) *P*-values for all other connections to demonstrate the specificity of the differences. To see whether these differences could be estimated and detected reliably, we characterized the differences using Bayesian parameter averaging (BPA) in addition to classical inference (*t*-test) (Friston et al., 2014; Razi et al., 2015). Then, we used BPA for each group separately after network discovery procedure. See the flowchart of our each step (**Supplementary Figure 2**).

Correlation Analyses

To examine the correlations between effective connectivity and patients' symptomology scores, Pearson correlation coefficients were tentatively computed to test the relationship between connection strengths and PANSS positive, negative, general, and total scores in SZ patients.

TABLE 1 | Demographic and clinical characteristics of first-episode SZ patients ($n = 49$) and HCs ($n = 50$).

Characteristics	SZ Patients	HCs	Statistics	*P*
Age	26 ± 6	27 ± 4	$t = 1.57$	0.12
Sex (male/female)	29/20	31/19	$\chi^2 = 0.08$	0.77
Ethnicity	Han (Chinese)	Han (Chinese)		
Handedness (right/left)	49/0	50/0		
Duration of illness (months)	10 ± 14	–		
PANSS total score	162 ± 27	–		
PANSS positive score	24 ± 8	–		
PANSS negative score	24 ± 7	–		
PANSS general psychopathology	49 ± 9	–		

PANSS, Positive and Negative Syndrome Scale.

RESULTS

Clinical Data

The demographic and clinical data are shown in **Table 1**. No significant difference was present between SZ patients and HCs on any demographic variables.

Network Discovery-based Model Selection Findings

Having inverted a fully connected model with full extrinsic connectivity, the log model evidence for all reduced models (models with one or more missing connections) was then assessed. **Figure 2** shows the network discovery procedure compared the evidence of all reduced models for each group and the results of *post-hoc* optimization. The left panel is for SZ patients and right panel refers to HCs. The fully connected model was the full model with the highest evidence. The procedure selected the fully connected model as the best model with a posterior probability of almost 1. The fully connected model had 49 parameters describing the extrinsic connections between nodes and the intrinsic (self-connections) within nodes. This suggested that the fully connected model was the best explanation for these data, indicating eligible and rational ROI selection.

Effective Connectivity

Significant connections at the group level (one-sample *t*-test at *P*-value of 0.05, Bonferroni corrected for multiple comparisons) are shown in **Figure 3** and **Table 2** (in terms of simple main effects within group). See the *t*- and *P*-values for strength of connections at the group level (Supplementary Table 1). However, two-sample *t*-test did not show significant difference between SZ patients and HCs ($P > 0.05$, Bonferroni corrected for multiple comparisons, i.e., 0.05/56).

The BPA results of the effective connectivity are shown in **Figure 4**. We set the threshold to 0.6 Hz. SZ patients exerted increased connections from the left ACC to left DLPFC, and from the left DLPFC to right ACC and left hippocampus, but decreased connections from the right ACC to left ACC, left DLPFC, and right hippocampus, from the left hippocampus to left DLPFC, and from the left DLPFC to right MPFC.

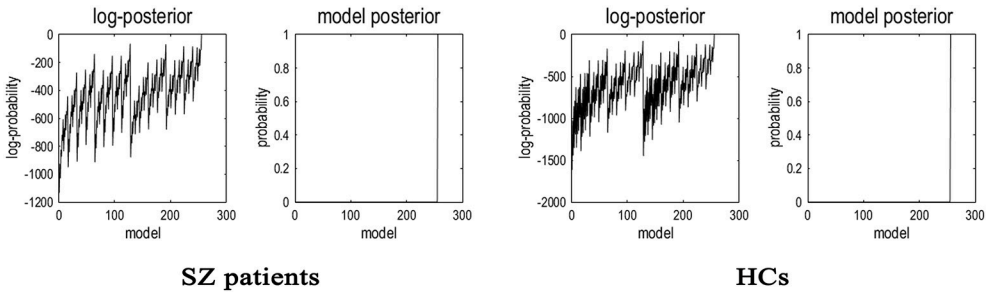

FIGURE 2 | Results of the *post-hoc* optimization or network findings. The corresponding conditional parameter estimates were shown over the 49 (intrinsic and extrinsic) connections. The profiles of model evidences are shown with the posterior probability for each model. In both groups, the full model had a probability of almost 1 and a log-probability of almost 0. As shown in the figure, the model with the highest evidence was the fully connected model based on the results of *post-hoc* optimization or network findings.

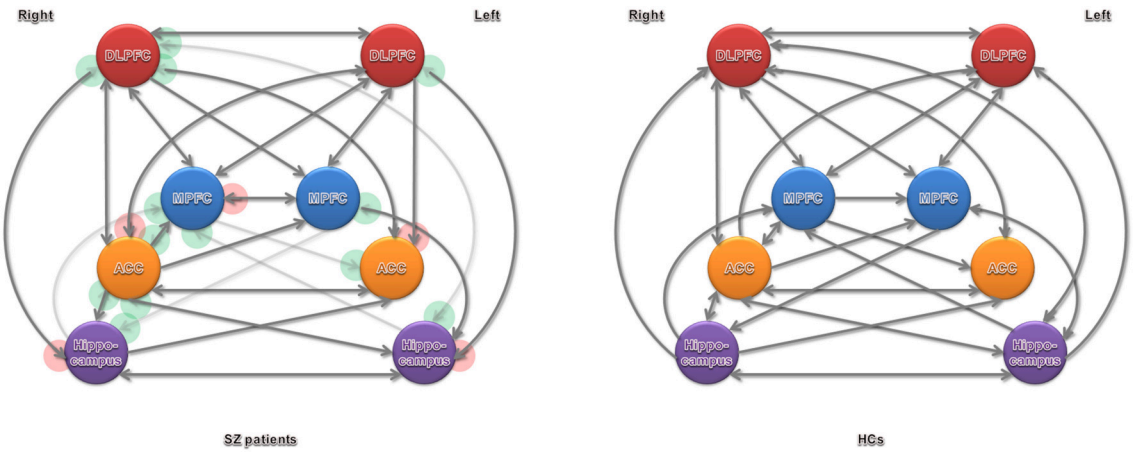

FIGURE 3 | Significant effective connectivity (at the group level) among ROIs in the SZ patients and HCs. Arrowheads in the red circles refers to significant connections detected in SZ patients but not in HCs, and green in HCs but not in SZ patients.

Correlation Analyses

Finally, we calculated the correlation between patients' symptomology scores and the strength of all the connections in SZ patients. But there was no significant correlation between PANSS score and strength of connections with differences in SZ patients relative to HCs ($P > 0.05$). On the basis of the current findings, these results do not provide a symptom-based validation of the quantitative effective connectivity estimates involving ACC, PFC, and hippocampus; in that they do not demonstrate the effective connectivity estimates among brain regions investigated in our present study have predictive validity in relation to clinical phenotype.

DISCUSSION

To our knowledge, this is the first study to demonstrate the effective connectivity among ACC, PFC, and hippocampus in patients with first-episode SZ using spectral DCM. In SZ patients, excessive effective connectivity is seen from the left ACC to left DLPFC, and from the left DLPFC to left hippocampus and right ACC; deficit effective connectivity is detected from the right ACC to left ACC, left DLPFC, and right hippocampus, as well as from the left hippocampus to left DLPFC and from the left DLPFC to right MPFC. Our results indicate abnormal effective connectivity involving ACC in first-episode SZ patients.

In the past decade, many studies have ever focused on structural and functional alterations of ACC, PFC, and hippocampus in SZ, and abnormalities of these regions in patients with SZ have been repeatedly reported. Compared with HCs, SZ patients showed significant gray matter volume reduction in ACC and hippocampus (Yamasue et al., 2004; Benedetti et al., 2011). A study combining fMRI and DTI demonstrated altered prefrontal structure-function relationships in SZ (Schlösser et al., 2007). It highlights a potential relationship between anatomical changes in a frontal-temporal anatomical circuit and functional alterations in the PFC. Brain fMRI neural responses to a face-matching paradigm and regional gray matter volumes were studied in the amygdala, hippocampus, ACC, and PFC (Benedetti et al., 2011). As compared with HCs, patients with chronic undifferentiated SZ reported higher adverse childhood

TABLE 2 | Strength of connections in first-episode SZ patients and HCs.

Connections	First-episode SZ patients	HCs	$t^{\#}$	$P^{\#}$
Left ACC-right ACC	0.1145 ± 0.2783*	0.1005 ± 0.2236*	0.28	0.78
Left ACC-left DLPFC	−0.0162 ± 0.1936	−0.0179 ± 0.2197	0.04	0.97
Left ACC-right DLPFC	−0.0453 ± 0.2523	−0.0861 ± 0.2426*	0.82	0.41
Left ACC-left MPFC	−0.0261 ± 0.2156	0.0395 ± 0.2169	−1.51	0.13
Left ACC-right MPFC	−0.0346 ± 0.2004	−0.0494 ± 0.2745	0.31	0.76
Left ACC-left hippocampus	−0.0367 ± 0.2116	−0.0223 ± 0.2075	−0.34	0.73
Left ACC-right hippocampus	0.0047 ± 0.3136	−0.0253 ± 0.2053	0.56	0.57
Right ACC-left ACC	0.4739 ± 0.2108*	0.4824 ± 0.1969*	−0.21	0.84
Right ACC-left DLPFC	0.1541 ± 0.1620*	0.1581 ± 0.1650*	−1.12	0.90
Right ACC-right DLPFC	0.1977 ± 0.1815*	0.1597 ± 0.1472*	1.15	0.25
Right ACC-left MPFC	0.1866 ± 0.1749*	0.1981 ± 0.1754*	−0.33	0.74
Right ACC-right MPFC	0.2116 ± 0.1485*	0.2222 ± 0.1694*	−0.33	0.74
Right ACC-left hippocampus	0.0862 ± 0.1655*	0.0494 ± 0.1520*	1.15	0.25
Right ACC-right hippocampus	0.1189 ± 0.2312*	0.0509 ± 0.1349*	1.79	0.08
Left DLPFC-left ACC	0.0929 ± 0.1856*	0.0577 ± 0.2022	0.90	0.37
Left DLPFC-right ACC	0.0943 ± 0.2102*	0.0482 ± 0.2590	0.97	0.33
Left DLPFC-right DLPFC	0.1042 ± 0.1694*	0.1560 ± 0.1749*	−1.50	0.14
Left DLPFC-left MPFC	0.2195 ± 0.1778*	0.2554 ± 0.1708*	−1.02	0.31
Left DLPFC-right MPFC	0.1365 ± 0.1693*	0.1572 ± 0.1682*	−0.61	0.54
Left DLPFC-left hippocampus	0.0759 ± 0.1713*	0.0028 ± 0.1299	2.40	0.02
Left DLPFC-right hippocampus	0.0449 ± 0.1617	0.0206 ± 0.1304	0.82	0.41
Right DLPFC-left ACC	0.0724 ± 0.2217*	0.1254 ± 0.2171*	−1.20	0.23
Right DLPFC-right ACC	0.0946 ± 0.2593*	0.1569 ± 0.3082*	−1.09	0.28
Right DLPFC-left DLPFC	0.1538 ± 0.2354*	0.1953 ± 0.2196*	−0.91	0.37
Right DLPFC-left MPFC	0.1323 ± 0.2054*	0.1564 ± 0.2132*	−0.57	0.57
Right DLPFC-right MPFC	0.2201 ± 0.2080*	0.2981 ± 0.2186*	−1.82	0.07
Right DLPFC-left hippocampus	0.0531 ± 0.1870	0.0545 ± 0.1743*	−0.04	0.97
Right DLPFC-right hippocampus	0.0535 ± 0.1575*	0.0332 ± 0.1783	0.60	0.55
Left MPFC-left ACC	0.0455 ± 0.2294	−0.0221 ± 0.2118	1.52	0.13
Left MPFC-right ACC	0.0257 ± 0.2497	−0.0511 ± 0.2471	1.54	0.13
Left MPFC-left DLPFC	0.1033 ± 0.1810*	0.1012 ± 0.1987*	0.05	0.96
Left MPFC-right DLPFC	−0.0040 ± 0.1963	−0.0318 ± 0.2056	0.69	0.49
Left MPFC-right MPFC	0.0687 ± 0.2102*	0.0385 ± 0.2139	0.71	0.48
Left MPFC-left hippocampus	0.0611 ± 0.1920*	−0.0598 ± 0.1663*	3.35	0.00
Left MPFC-right hippocampus	−0.0301 ± 0.2014	−0.0514 ± 0.1499*	0.60	0.55
Right MPFC-left ACC	0.0130 ± 0.2290	0.0861 ± 0.2633*	−1.47	0.14
Right MPFC-right ACC	0.0613 ± 0.2475	0.1037 ± 0.2857*	−0.79	0.43
Right MPFC-left DLPFC	0.1146 ± 0.1663*	0.1136 ± 0.1946*	0.03	0.98
Right MPFC-right DLPFC	0.1751 ± 0.1557*	0.1965 ± 0.1744*	−0.64	0.52
Right MPFC-left MPFC	0.1503 ± 0.1764*	0.1969 ± 0.2051*	−1.21	0.23
Right MPFC-left hippocampus	0.0425 ± 0.1591	−0.0099 ± 0.1367	1.76	0.08
Right MPFC-right hippocampus	0.0217 ± 0.1825	−0.0071 ± 0.1460	0.87	0.39
Left hippocampus-left ACC	0.0553 ± 0.2922	0.0695 ± 0.2859	−0.24	0.81
Left hippocampus-right ACC	0.0986 ± 0.3714	0.1038 ± 0.3491*	−0.07	0.94
Left hippocampus-left DLPFC	0.0305 ± 0.2759	0.1099 ± 0.3088*	−1.35	0.18
Left hippocampus-right DLPFC	0.0393 ± 0.2713	0.1012 ± 0.3161*	−1.05	0.30
Left hippocampus-left MPFC	0.0620 ± 0.2660	0.0825 ± 0.2795*	−0.37	0.71
Left hippocampus-right MPFC	0.0300 ± 0.2834	0.0961 ± 0.3044*	−1.12	0.27
Left hippocampus-right hippocampus	0.1672 ± 0.3269*	0.2188 ± 0.3074*	−0.81	0.42

(Continued)

TABLE 2 | Continued

Connections	First-episode SZ patients	HCs	$t^{\#}$	$P^{\#}$
Right hippocampus-left ACC	0.0934 ± 0.3193*	0.0823 ± 0.2694*	0.19	0.85
Right hippocampus-right ACC	0.0923 ± 0.3510	0.1485 ± 0.3468*	−0.80	0.43
Right hippocampus-left DLPFC	0.0461 ± 0.3041	0.0844 ± 0.3066	−0.62	0.53
Right hippocampus-right DLPFC	0.0693 ± 0.2612	0.1085 ± 0.3097*	−0.68	0.50
Right hippocampus-left MPFC	0.0735 ± 0.2661	0.0675 ± 0.2667	0.11	0.91
Right hippocampus-right MPFC	0.0457 ± 0.2851	0.0951 ± 0.2867*	−0.86	0.39
Right hippocampus-left hippocampus	0.2198 ± 0.2791*	0.2513 ± 0.2341*	−0.61	0.54

**Significant effective connectivity at the group level ($P < 0.05$, Bonferroni corrected). $^{\#}$Between the group level. ACC, anterior cingulate cortex; DLPFC, dorsolateral prefrontal cortex; MPFC, medial prefrontal cortex.*

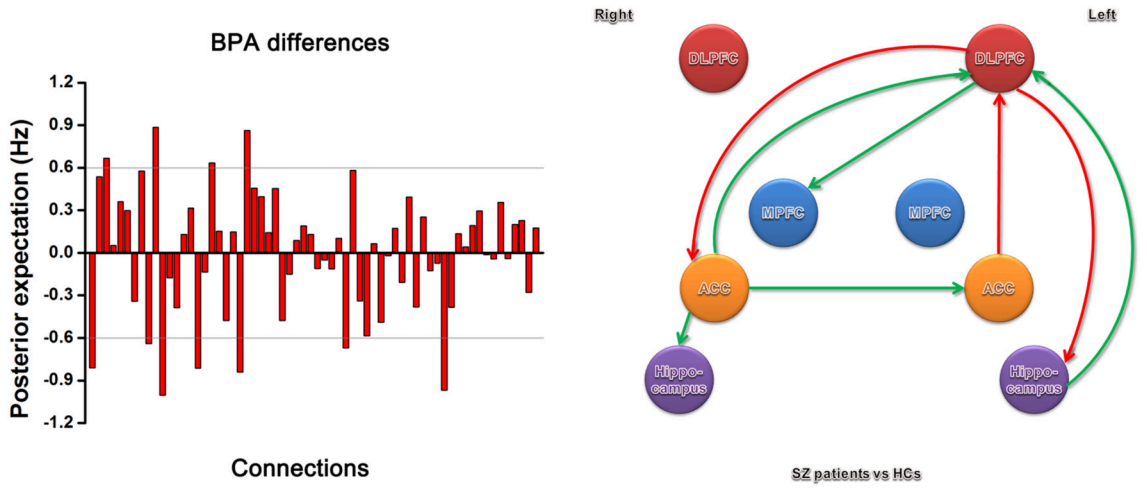

FIGURE 4 | Significant effective connectivity (between the group level) among ROIs in the SZ patients and HCs. The left panel shows the BPA of the differences for spectral DCM. The right panel shows only those edges on the graph that survive the threshold of 0.6 Hz in the left panel, i.e., the increased (red) and decreased (green) connections in SZ patients relative to HCs.

experiences, proportionally leading to decreasing responses in the amygdala and hippocampus, and increasing responses in PFC and ACC. Lui et al found a decreased amplitude of low-frequency fluctuation in ACC and reduced functional connectivity between the left ACC and right middle temporal gyrus using resting state fMRI (Lui et al., 2015). Altered functional connections associated with ACC, MPFC, hippocampus, thalamus, and cerebellum were also observed in SZ patients (Yu et al., 2013). Both at resting state and during emotional stimuli, abnormalities can be observed in PFC-amygdala connection (Das et al., 2007; Leitman et al., 2008; Fan et al., 2013; Liu et al., 2014b). PFC can be subdivided into MPFC and DLPFC. SZ patients revealed abnormal activation in the bilateral MPFC (Pomarol-Clotet et al., 2010). With the exception of MPFC, SZ patients also exhibited overactivation of DLPFC during social judgment (Mukherjee et al., 2014). During face-matching paradigms, aberrancies were detected in DLPFC-amygdala connection using DCM (Diwadkar et al., 2012; Vai et al., 2015). These findings indicate the importance of ACC, PFC, and hippocampal abnormalities in the pathophysiology of SZ.

From the perspective of neurochemical abnormalities of neurotransmitters or their receptors, regions mentioned above are in line with studies determining *in vivo* glutamate and glutamine concentrations in SZ patients' brains. Glutamatergic dysfunction has been implicated in the pathophysiology of SZ. Chun et al. identified that an SZ-associated microdeletion disrupted glutamatergic synaptic transmission at thalamocortical projections to the auditory cortex in SZ mouse models (Chun et al., 2014). Likewise, a previous study reported increased levels of glutamate in prefrontal and hippocampal areas in patients with SZ using magnetic resonance spectroscopy (van Elst et al., 2005). Magnetic resonance spectroscopy and tissue protein concentrations sampling SZ patients *in vivo* and postmortem brain tissue *in vitro*, respectively, together suggest lower glutamate level in dentate gyrus, implicating the excitatory system within hippocampus in the pathophysiology of SZ (Stan et al., 2015). With the exception of altered concentration of glutamate, in DLPFC, decoupling of the sum of glutamate and glutamine and N-acetylaspartate was observed in SZ patients (Coughlin et al., 2015). These findings provide strong evidence

supporting the hypothesis of glutamatergic dysfunction within PFC and hippocampus in SZ.

From functional aspect, SZ is a mental illness involved in abnormality of emotional responses and difficulty with social interactions. Both resting-state functional connectivity analysis by Mamah et al. (2013) and effective connectivity analyses during face-matching paradigms by Diwadkar et al. (2012) and Vai et al. (2015) indicate dysfunction in the connections between networks involved in cognitive and emotional processing in the pathophysiology SZ. ACC might interact with other cortical and subcortical structures as a part of the circuits involved in the regulation of mental and emotional activity. Hoptman et al. investigate the construct of urgency in association with aggression in individuals with SZ or schizoaffective disorder and its underlying neural circuitry. Their findings revealed that greater urgency was related to lower cortical thickness and functional connectivity within the medial/lateral orbitofrontal and inferior frontal regions, and rostral ACC (Hoptman et al., 2014). Clinically, patients with chronic SZ often show lack of motivation and difficulty with decision-making. At the neural level, the orbitofrontal cortex and ACC are thought to interact, together, to form a network involved in emotional processing and mediating emotion and social behavior (Ohtani et al., 2014). Reductions in FA were observed in connections between the left anterior medial orbitofrontal cortex and rostral ACC, and between bilateral posterior medial orbitofrontal cortex and rostral ACC in SZ patients relative to HCs. In addition, reduced FA was correlated with more severe anhedonia-asociality and avolition-apathy using the Scale for the Assessment of Negative Symptoms, which suggests that ACC may be pivotal in understanding aberrant emotional responses and social behavior in SZ patients. Finally, cognitive deficits are a defining feature of SZ, affecting quality of life and functional outcomes in work, relationships, and independent living. While viewing faces, SZ patients showed significantly weaker deactivation of MPFC, including ACC, and decreased activation in the left cerebellum, compared to controls (Mothersill et al., 2014). Considering the role of ACC in processing negative emotion, weaker deactivation of this region in SZ patients while viewing faces may lead to an elevated perception of social threat. Future studies examining the neurobiology of cognitive function in SZ using fMRI may aid in establishing strategy of targeted treatment.

Additionally, previous studies consistently demonstrated the key role of the dorsal ACC and DLPFC in cognitive control (Carter and van Veen, 2007). For these regions aberrant activation patterns in association with deficient behavioral performance were observed in SZ (Minzenberg et al., 2009). Our effective connectivity study showed decreased bilateral connectivity between ACC and DLPFC in first-episode SZ patients. Through effective connectivity and white matter connectivity analysis, combined utilization of DCM and diffusion tensor imaging provides some support for that weaker connectivity involved in ACC may be the neural basis of specific cognitive impairments in SZ (Wagner et al., 2015). Cognitive deficits are considered as a core feature of SZ (Elvevåg and Goldberg, 2000). Converging evidence from fMRI studies may shed light on that ACC and DLPFC play a crucial role in cognitive function in SZ, albeit the neural underpinnings of impaired cognition in SZ remain uncertain.

In addition, as stated previously, spectal DCM has started to be used in a recent animal studies to disclose the pathophysiology of SZ. Administration of ketamine disrupted desynchronized electrical activity between MPFC and hippocampus (Moran et al., 2015). Our current study also demonstrated hippocampal-prefrontal hypoconnectivity *in vivo* in first-episode SZ. Strictly speaking, SZ patients showed decreased hippocampal-dorsolateral prefrontal-medial prefrontal connectivity. To some extent, connections associated with PFC and hippocampus that we have found, show promise as an intermediate link in this neural pathway for SZ.

In this study, we found no significant correlation between these connections with differences and PANSS scores. The lack of significant correlation may relate to our modest sample size of SZ patients.

The strengthen of our study is that there may be no potential confounds related to medications and state of illness due to first-episode SZ patients. The inclusion criterion minimized the influences of medication, cohort effects and illness-related environmental factors. Nevertheless, we acknowledge that there were several limitations. First, significance in one group and not in the other group does not imply that there are differences between these two groups. Group difference was not significant in our study, which was the major limitation. Second, we enrolled a large sample size of participants in our study, thus doubling or tripling the numbers investigated in most previous fMRI studies. But larger sample and multi-center studies, like some recent investigations (Ivleva et al., 2013; Skudlarski et al., 2013; Meda et al., 2014; Bois et al., 2015), are desirable to confirm our present findings. We hope to extend this research to a larger patient population, which will increase statistical efficiency and sensitivity to more subtle changes. Third, effective connectivity was only measured during the resting state without giving any tasks. A comparison study at resting state and active state might highlight the specificity of functional brain changes. Fourth, the current findings were only based on the changes of BOLD signal in SZ patients. In addition to BOLD-fMRI, a combination of multimodalities, including diffusion tensor imaging, magnetic resonance spectroscopy, electroencephalography, and positron emission tomography, might further strengthen the conclusion.

The present study characterized the abnormal ACC-related connectivity *in vivo* in first-episode SZ by means of spectral DCM, revealing anterior cingulate cortico-prefrontal-hippocampal hyperconnectivity, as well as ACC-related and hippocampal-dorsolateral prefrontal-medial prefrontal hypoconnectivity. Spectral DCM revealed abnormal effective connectivity involving ACC in patients with first-episode SZ. This suggests the SZ subjects fail to recruit these neural pathways. This study further provides a link between SZ and dysconnection hypothesis, creating an ideal situation to associate mechanisms behind SZ with aberrant connectivity among these cognition and emotion-related regions.

ACKNOWLEDGMENTS

This work was supported by the National Key Basic Research and Development Program (973) (Grant No. 2011CB707805). We would like to thank Baojuan Li and Liang Li from School of Biomedical Engineering, The Fourth Military Medical University for their technique support and assistance. We are indebted to our editor and three reviewers for guidance in clarifying and elaborating this report.

SUPPLEMENTARY MATERIAL

The Supplementary Material for this article can be found online at: http://journal.frontiersin.org/article/10.3389/fnhum.2015.00589

Supplementary Figure 1 | Presentative images of fMRI first-level results. The left is for one healthy control and the right is for one SZ patient.

Supplementary Figure 2 | Steps for data analysis.

REFERENCES

APA (2013). *Diagnostic and Statistical Manual of Mental Disorders, 5th Edn*. Washington, DC: American Psychiatric Association.

Argyelan, M., Ikuta, T., DeRosse, P., Braga, R. J., Burdick, K. E., John, M., et al. (2014). Resting-state fMRI connectivity impairment in schizophrenia and bipolar disorder. *Schizophr. Bull.* 40, 100–110. doi: 10.1093/schbul/sbt092

Bastos-Leite, A. J., Ridgway, G. R., Silveira, C., Norton, A., Reis, S., and Friston, K. J. (2015). Dysconnectivity within the default mode in first-episode schizophrenia: a stochastic dynamic causal modeling study with functional magnetic resonance imaging. *Schizophr. Bull.* 41, 144–153. doi: 10.1093/schbul/sbu080

Benedetti, F., Radaelli, D., Poletti, S., Falini, A., Cavallaro, R., Dallaspezia, S., et al. (2011). Emotional reactivity in chronic schizophrenia: structural and functional brain correlates and the influence of adverse childhood experiences. *Psychol. Med.* 41, 509–519. doi: 10.1017/S0033291710001108

Bois, C., Ronan, L., Levita, L., Whalley, H. C., Giles, S., Mcintosh, A. M., et al. (2015). Cortical surface area differentiates familial high risk individuals who go on to develop schizophrenia. *Biol. Psychiatry* 78, 413–420. doi: 10.1016/j.biopsych.2014.12.030

Carter, C. S., and van Veen, V. (2007). Anterior cingulate cortex and conflict detection: an update of theory and data. *Cogn. Affect. Behav. Neurosci.* 7, 367–379. doi: 10.3758/CABN.7.4.367

Chang, X., Xi, Y. B., Cui, L. B., Wang, H. N., Sun, J. B., Zhu, Y. Q., et al. (2015). Distinct inter-hemispheric dysconnectivity in schizophrenia patients with and without auditory verbal hallucinations. *Sci. Rep.* 5:11218. doi: 10.1038/srep11218

Chun, S., Westmoreland, J. J., Bayazitov, I. T., Eddins, D., Pani, A. K., Smeyne, R. J., et al. (2014). Specific disruption of thalamic inputs to the auditory cortex in schizophrenia models. *Science* 344, 1178–1182. doi: 10.1126/science.1253895

Coughlin, J. M., Tanaka, T., Marsman, A., Wang, H., Bonekamp, S., Kim, P. K., et al. (2015). Decoupling of N-acetyl-aspartate and Glutamate within the Dorsolateral prefrontal cortex in Schizophrenia. *Curr. Mol. Med.* 15, 176–183. doi: 10.2174/1566524015666150303104811

Das, P., Kemp, A. H., Flynn, G., Harris, A. W., Liddell, B. J., Whitford, T. J., et al. (2007). Functional disconnections in the direct and indirect amygdala pathways for fear processing in schizophrenia. *Schizophr. Res.* 90, 284–294. doi: 10.1016/j.schres.2006.11.023

Diwadkar, V. A., Wadehra, S., Pruitt, P., Keshavan, M. S., Rajan, U., Zajac-Benitez, C., et al. (2012). Disordered corticolimbic interactions during affective processing in children and adolescents at risk for schizophrenia revealed by functional magnetic resonance imaging and dynamic causal modeling. *Arch. Gen. Psychiatry* 69, 231–242. doi: 10.1001/archgenpsychiatry.2011.1349

Ellison-Wright, I., and Bullmore, E. (2009). Meta-analysis of diffusion tensor imaging studies in schizophrenia. *Schizophr. Res.* 108, 3–10. doi: 10.1016/j.schres.2008.11.021

Elvevåg, B., and Goldberg, T. E. (2000). Cognitive impairment in schizophrenia is the core of the disorder. *Crit. Rev. Neurobiol.* 14, 1–21. doi: 10.1615/critrevneurobiol.v14.i1.10

Fan, F. M., Tan, S. P., Yang, F. D., Tan, Y. L., Zhao, Y. L., Chen, N., et al. (2013). Ventral medial prefrontal functional connectivity and emotion regulation in chronic schizophrenia: a pilot study. *Neurosci. Bull.* 29, 59–74. doi: 10.1007/s12264-013-1300-8

Fornito, A., Zalesky, A., Pantelis, C., and Bullmore, E. T. (2012). Schizophrenia, neuroimaging and connectomics. *Neuroimage* 62, 2296–2314. doi: 10.1016/j.neuroimage.2011.12.090

Friedman, J. I., Tang, C., Carpenter, D., Buchsbaum, M., Schmeidler, J., Flanagan, L., et al. (2008). Diffusion tensor imaging findings in first-episode and chronic schizophrenia patients. *Am. J. Psychiatry* 165, 1024–1032. doi: 10.1176/appi.ajp.2008.07101640

Friston, K., and Penny, W. (2011). *Post hoc* Bayesian model selection. *Neuroimage* 56, 2089–2099. doi: 10.1016/j.neuroimage.2011.03.062

Friston, K. J. (1998). The disconnection hypothesis. *Schizophr. Res.* 30, 115–125. doi: 10.1016/S0920-9964(97)00140-0

Friston, K. J., and Frith, C. D. (1995). Schizophrenia: a disconnection syndrome? *Clin. Neurosci.* 3, 89–97.

Friston, K. J., Kahan, J., Biswal, B., and Razi, A. (2014). A DCM for resting state fMRI. *Neuroimage* 94, 396–407. doi: 10.1016/j.neuroimage.2013.12.009

Friston, K. J., Li, B., Daunizeau, J., and Stephan, K. E. (2011). Network discovery with DCM. *Neuroimage* 56, 1202–1221. doi: 10.1016/j.neuroimage.2010.12.039

Friston, K. J., Stephan, K., Li, B. J., and Daunizeau, J. (2010). Generalised filtering. *Math. Probl. Eng.* 2010:621670. doi: 10.1155/2010/621670

Genzel, L., Dresler, M., Cornu, M., Jäger, E., Konrad, B., Adamczyk, M., et al. (2015). Medial prefrontal-hippocampal connectivity and motor memory consolidation in depression and schizophrenia. *Biol. Psychiatry* 77, 177–186. doi: 10.1016/j.biopsych.2014.06.004

Guo, W., Liu, F., Liu, J., Yu, L., Zhang, J., Zhang, Z., et al. (2015). Abnormal causal connectivity by structural deficits in first-episode, drug-naive schizophrenia at rest. *Schizophr. Bull.* 41, 57–65. doi: 10.1093/schbul/sbu126

Hoptman, M. J., Antonius, D., Mauro, C. J., Parker, E. M., and Javitt, D. C. (2014). Cortical thinning, functional connectivity, and mood-related impulsivity in schizophrenia: relationship to aggressive attitudes and behavior. *Am. J. Psychiatry* 171, 939–948. doi: 10.1176/appi.ajp.2014.13111553

Ivleva, E. I., Bidesi, A. S., Keshavan, M. S., Pearlson, G. D., Meda, S. A., Dodig, D., et al. (2013). Gray matter volume as an intermediate phenotype for psychosis: bipolar-schizophrenia network on intermediate phenotypes (B-SNIP). *Am. J. Psychiatry* 170, 1285–1296. doi: 10.1176/appi.ajp.2013.13010126

Kay, S. R., Fiszbein, A., and Opler, L. A. (1987). The positive and negative syndrome scale (PANSS) for schizophrenia. *Schizophr. Bull.* 13, 261–276. doi: 10.1093/schbul/13.2.261

Khadka, S., Meda, S. A., Stevens, M. C., Glahn, D. C., Calhoun, V. D., Sweeney, J. A., et al. (2013). Is aberrant functional connectivity a psychosis endophenotype? A resting state functional magnetic resonance imaging study. *Biol. Psychiatry* 74, 458–466. doi: 10.1016/j.biopsych.2013.04.024

Kubota, M., Miyata, J., Sasamoto, A., Sugihara, G., Yoshida, H., Kawada, R., et al. (2013). Thalamocortical disconnection in the orbitofrontal region associated with cortical thinning in schizophrenia. *JAMA Psychiatry* 70, 12–21. doi: 10.1001/archgenpsychiatry.2012.1023

Leitman, D. I., Loughead, J., Wolf, D. H., Ruparel, K., Kohler, C. G., Elliott, M. A., et al. (2008). Abnormal superior temporal connectivity during fear perception in schizophrenia. *Schizophr. Bull.* 34, 673–678. doi: 10.1093/schbul/sbn052

Li, B., Wang, X., Yao, S., Hu, D., and Friston, K. (2012). Task-dependent modulation of effective connectivity within the default mode network. *Front. Psychol.* 3:206. doi: 10.3389/fpsyg.2012.00206

Liu, B., Zhang, X., Hou, B., Li, J., Qiu, C., Qin, W., et al. (2014a). The impact of MIR137 on dorsolateral prefrontal-hippocampal functional connectivity in healthy subjects. *Neuropsychopharmacology* 39, 2153–2160. doi: 10.1038/npp.2014.63

Liu, H., Tang, Y., Womer, F., Fan, G., Lu, T., Driesen, N., et al. (2014b). Differentiating patterns of amygdala-frontal functional connectivity in

schizophrenia and bipolar disorder. *Schizophr. Bull.* 40, 469–477. doi: 10.1093/schbul/sbt044

Loewy, R. L., Bearden, C. E., Johnson, J. K., Raine, A., and Cannon, T. D. (2005). The prodromal questionnaire (PQ): preliminary validation of a self-report screening measure for prodromal and psychotic syndromes. *Schizophr. Res.* 79, 117–125. doi: 10.1016/j.schres.2005.03.007

Lui, S., Yao, L., Xiao, Y., Keedy, S. K., Reilly, J. L., Keefe, R. S., et al. (2015). Resting-state brain function in schizophrenia and psychotic bipolar probands and their first-degree relatives. *Psychol. Med.* 45, 97–108. doi: 10.1017/S003329171400110X

Maldjian, J. A., Laurienti, P. J., and Burdette, J. H. (2004). Precentral gyrus discrepancy in electronic versions of the Talairach atlas. *Neuroimage* 21, 450–455. doi: 10.1016/j.neuroimage.2003.09.032

Maldjian, J. A., Laurienti, P. J., Kraft, R. A., and Burdette, J. H. (2003). An automated method for neuroanatomic and cytoarchitectonic atlas-based interrogation of fMRI data sets. *Neuroimage* 19, 1233–1239. doi: 10.1016/S1053-8119(03)00169-1

Mamah, D., Barch, D. M., and Repovš, G. (2013). Resting state functional connectivity of five neural networks in bipolar disorder and schizophrenia. *J. Affect. Disord.* 150, 601–609. doi: 10.1016/j.jad.2013.01.051

Meda, S. A., Ruaño, G., Windemuth, A., O'Neil, K., Berwise, C., Dunn, S. M., et al. (2014). Multivariate analysis reveals genetic associations of the resting default mode network in psychotic bipolar disorder and schizophrenia. *Proc. Natl. Acad. Sci. U.S.A* 111, E2066–E2075. doi: 10.1073/pnas.1313093111

Minzenberg, M. J., Laird, A. R., Thelen, S., Carter, C. S., and Glahn, D. C. (2009). Meta-analysis of 41 functional neuroimaging studies of executive function in schizophrenia. *Arch. Gen. Psychiatry* 66, 811–822. doi: 10.1001/archgenpsychiatry.2009.91

Modinos, G., Ormel, J., and Aleman, A. (2010). Altered activation and functional connectivity of neural systems supporting cognitive control of emotion in psychosis proneness. *Schizophr. Res.* 118, 88–97. doi: 10.1016/j.schres.2010.01.030

Moran, R. J., Jones, M. W., Blockeel, A. J., Adams, R. A., Stephan, K. E., and Friston, K. J. (2015). Losing control under ketamine: suppressed cortico-hippocampal drive following acute ketamine in rats. *Neuropsychopharmacology* 40, 268–277. doi: 10.1038/npp.2014.184

Moriya, J., Kakeda, S., Abe, O., Goto, N., Yoshimura, R., Hori, H., et al. (2010). Gray and white matter volumetric and diffusion tensor imaging (DTI) analyses in the early stage of first-episode schizophrenia. *Schizophr. Res.* 116, 196–203. doi: 10.1016/j.schres.2009.10.002

Mothersill, O., Morris, D. W., Kelly, S., Rose, E. J., Bokde, A., Reilly, R., et al. (2014). Altered medial prefrontal activity during dynamic face processing in schizophrenia spectrum patients. *Schizophr. Res.* 157, 225–230. doi: 10.1016/j.schres.2014.05.023

Mukherjee, P., Whalley, H. C., McKirdy, J. W., Sprengelmeyer, R., Young, A. W., McIntosh, A. M., et al. (2014). Altered amygdala connectivity within the social brain in schizophrenia. *Schizophr. Bull.* 40, 152–160. doi: 10.1093/schbul/sbt086

Ohtani, T., Bouix, S., Hosokawa, T., Saito, Y., Eckbo, R., Ballinger, T., et al. (2014). Abnormalities in white matter connections between orbitofrontal cortex and anterior cingulate cortex and their associations with negative symptoms in schizophrenia: a DTI study. *Schizophr. Res.* 157, 190–197. doi: 10.1016/j.schres.2014.05.016

Pettersson-Yeo, W., Allen, P., Benetti, S., McGuire, P., and Mechelli, A. (2011). Dysconnectivity in schizophrenia: where are we now? *Neurosci. Biobehav. Rev.* 35, 1110–1124. doi: 10.1016/j.neubiorev.2010.11.004

Pomarol-Clotet, E., Canales-Rodríguez, E. J., Salvador, R., Sarró, S., Gomar, J. J., Vila, F., et al. (2010). Medial prefrontal cortex pathology in schizophrenia as revealed by convergent findings from multimodal imaging. *Mol. Psychiatry* 15, 823–830. doi: 10.1038/mp.2009.146

Razi, A., Kahan, J., Rees, G., and Friston, K. J. (2015). Construct validation of a DCM for resting state fMRI. *Neuroimage* 106, 1–14. doi: 10.1016/j.neuroimage.2014.11.027

Schlösser, R. G. M., Nenadic, I., Wagner, G., Güllmar, D., von Consbruch, K., Köhler, S., et al. (2007). White matter abnormalities and brain activation in schizophrenia: a combined DTI and fMRI study. *Schizophr. Res.* 89, 1–11. doi: 10.1016/j.schres.2006.09.007

Skudlarski, P., Schretlen, D. J., Thaker, G. K., Stevens, M. C., Keshavan, M. S., Sweeney, J. A., et al. (2013). Diffusion tensor imaging white matter endophenotypes in patients with schizophrenia or psychotic bipolar disorder and their relatives. *Am. J. Psychiatry* 170, 886–898. doi: 10.1176/appi.ajp.2013.12111448

Stan, A. D., Ghose, S., Zhao, C., Hulsey, K., Mihalakos, P., Yanagi, M., et al. (2015). Magnetic resonance spectroscopy and tissue protein concentrations together suggest lower glutamate signaling in dentate gyrus in schizophrenia. *Mol. Psychiatry* 20, 433–439. doi: 10.1038/mp.2014.54

Stephan, K. E., Friston, K. J., and Frith, C. D. (2009). Dysconnection in schizophrenia: from abnormal synaptic plasticity to failures of self-monitoring. *Schizophr. Bull.* 35, 509–527. doi: 10.1093/schbul/sbn176

Tzourio-Mazoyer, N., Landeau, B., Papathanassiou, D., Crivello, F., Etard, O., Delcroix, N., et al. (2002). Automated anatomical labeling of activations in SPM using a macroscopic anatomical parcellation of the MNI MRI single-subject brain. *Neuroimage* 15, 273–289. doi: 10.1006/nimg.2001.0978

Vai, B., Sferrazza Papa, G., Poletti, S., Radaelli, D., Donnici, E., Bollettini, I., et al. (2015). Abnormal cortico-limbic connectivity during emotional processing correlates with symptom severity in schizophrenia. *Eur. Psychiatry* 30, 590–597. doi: 10.1016/j.eurpsy.2015.01.002

van den Heuvel, M. P., Sporns, O., Collin, G., Scheewe, T., Mandl, R. C., Cahn, W., et al. (2013). Abnormal rich club organization and functional brain dynamics in schizophrenia. *JAMA Psychiatry* 70, 783–792. doi: 10.1001/jamapsychiatry.2013.1328

van Elst, L. T., Valerius, G., Büchert, M., Thiel, T., Rüsch, N., Bubl, E., et al. (2005). Increased prefrontal and hippocampal glutamate concentration in schizophrenia: evidence from a magnetic resonance spectroscopy study. *Biol. Psychiatry* 58, 724–730. doi: 10.1016/j.biopsych.2005.04.041

Voineskos, A. N., Foussias, G., Lerch, J., Felsky, D., Remington, G., Rajji, T. K., et al. (2013). Neuroimaging evidence for the deficit subtype of schizophrenia. *JAMA Psychiatry* 70, 472–480. doi: 10.1001/jamapsychiatry.2013.786

Wagner, G., De la Cruz, F., Schachtzabel, C., Güllmar, D., Schultz, C. C., Schlösser, R. G., et al. (2015). Structural and functional dysconnectivity of the fronto-thalamic system in schizophrenia: a DCM-DTI study. *Cortex* 66, 35–45. doi: 10.1016/j.cortex.2015.02.004

White, T., Nelson, M., and Lim, K. O. (2008). Diffusion tensor imaging in psychiatric disorders. *Top. Magn. Reson. Imaging* 19, 97–109. doi: 10.1097/RMR.0b013e3181809f1e

Whiteford, H. A., Degenhardt, L., Rehm, J., Baxter, A. J., Ferrari, A. J., Erskine, H. E., et al. (2013). Global burden of disease attributable to mental and substance use disorders: findings from the Global Burden of Disease Study 2010. *Lancet* 382, 1575–1586. doi: 10.1016/S0140-6736(13)61611-6

Whitford, T. J., Kubicki, M., Schneiderman, J. S., O'Donnell, L. J., King, R., Alvarado, J. L., et al. (2010). Corpus callosum abnormalities and their association with psychotic symptoms in patients with schizophrenia. *Biol. Psychiatry* 68, 70–77. doi: 10.1016/j.biopsych.2010.03.025

Yamasue, H., Iwanami, A., Hirayasu, Y., Yamada, H., Abe, O., Kuroki, N., et al. (2004). Localized volume reduction in prefrontal, temporolimbic, and paralimbic regions in schizophrenia: an MRI parcellation study. *Psychiatry Res.* 131, 195–207. doi: 10.1016/j.pscychresns.2004.05.004

Yu, Y., Shen, H., Zeng, L. L., Ma, Q., and Hu, D. (2013). Convergent and divergent functional connectivity patterns in schizophrenia and depression. *PLoS ONE* 8:e68250. doi: 10.1371/journal.pone.0068250

Conflict of Interest Statement: The authors declare that the research was conducted in the absence of any commercial or financial relationships that could be construed as a potential conflict of interest.

frontiers in Human Neuroscience

ORIGINAL RESEARCH
published: 30 September 2015
doi: 10.3389/fnhum.2015.00516

Dysfunctional putamen modulation during bimanual finger-to-thumb movement in patients with Parkinson's disease

Li-rong Yan[1], Yi-bo Wu[2], Xiao-hua Zeng[3] and Li-chen Gao[3]*

[1] Department of Information, Wuhan General Hospital of Guangzhou Command, Wuhan, China, [2] Department of Unmanned Aerial Vehicle, Wuhan Mechanical Technology College, Wuhan, China, [3] Department of Radiology, Wuhan General Hospital of Guangzhou Command, Wuhan, China

Parkinson's disease (PD) is a neurodegenerative disorder affecting middle-aged and elderly people. PD can be viewed as "circuit disorder," indicating that large scale cortico-subcortical pathways were involved in its pathophysiology. The brain network in an experimental context is emerging as an important biomarker in disease diagnosis and prognosis prediction. This context-dependent network for PD and the underling functional mechanism remains unclear. In this paper, the brain network profiles in 11 PD patients without dementia were studied and compared with 12 healthy controls. The functional magnetic resonance imaging (fMRI) data were acquired when the subjects were performing a pseudorandomized unimanual or bimanual finger-to-thumb movement task. The activation was detected and the network profiles were analyzed by psychophysiological interaction (PPI) toolbox. For the controls and PD patients, the motor areas including the primary motor and premotor areas, supplementary motor area, the cerebellum and parts of the frontal, temporal and parietal gyrus were activated. The right putamen exhibited significant control > PD activation and weaker activity during the bimanual movement relative to the unimanual movement in the control group. The decreased putamen modulation on some nucleus in basal ganglia, such as putamen, thalamus and caudate, and some cortical areas, such as cingulate, parietal, angular, frontal, temporal and occipital gyrus was detected in the bimanual movement condition relative to the unimanual movement condition. Between-group PPI difference was detected in cingulate gyrus, angular gyrus and precuneus (control > PD) and inferior frontal gyrus (PD > control). The deficient putamen activation and its enhanced connectivity with the frontal gyrus could be a correlate of impaired basal ganglia inhibition and frontal gyrus compensation to maintain the task performance during the motor programs of PD patients.

Keywords: Parkinson's disease, putamen, movement, network, functional magnetic resonance imaging

OPEN ACCESS

Edited by:
Baojuan Li,
Fourth Military Medical University, China

Reviewed by:
Jinhui Wang,
Hangzhou Normal University, China
Feng Liu,
Tianjin Medical University, China

****Correspondence:***
Yi-bo Wu,
Department of Unmanned Aerial Vehicle, Wuhan Mechanical Technology College, Luoyudong Road 1038, Wuhan 430075, China
wybbok@hotmail.com

Received: *09 June 2015*
Accepted: *04 September 2015*
Published: *30 September 2015*

Citation:
Yan L, Wu Y, Zeng X and Gao L (2015) Dysfunctional putamen modulation during bimanual finger-to-thumb movement in patients with Parkinson's disease. Front. Hum. Neurosci. 9:516. doi: 10.3389/fnhum.2015.00516

Introduction

Parkinson's disease (PD) is a common neurodegenerative disorder affecting middle-aged and elderly people. PD is related with aging, heredity, cell dysfunction and environment (Lang and Lozano, 1998a,b; Samii et al., 2004), but its pathology remains unclear. The National Institute of Mental Health suggested that, exploring the brain network profiles and dysfunction may enhance the understanding of specific bio-behavioral impairments which underpin the psychiatric disorders with complex behavioral phenotypes (Insel et al., 2010). Network dysfunction is emerging as a characteristic of the neural substrates of multiple psychiatric conditions (Friston, 1998; Schmidt et al., 2013). Studies over the past decades have demonstrated that PD can be viewed as "circuit disorder" or "network dysfunction," indicating that multiple, large scale networks were involved in its pathophysiology (Eckert et al., 2007; Eidelberg, 2009; Göttlich et al., 2013; Zhang et al., 2015). A combined magnetoencephalographic and subthalamic local field potential recording research indicated two spatially and spectrally separated networks, i.e., a temporoparietal-brainstem network coherent with subthalamic nucleus (STN) in the alpha (7–13 Hz) band, and a predominantly frontal network coherent in the beta (15–35 Hz) band (Litvak et al., 2011). Resting-state fMRI research indicated that, PD patients at off state had significantly decreased functional connectivity in the supplementary motor area, left dorsal lateral prefrontal cortex and left putamen, and had increased functional connectivity in the left cerebellum, left primary motor cortex and left parietal cortex (Wu et al., 2009). It's believed that the dysfunction of cortico-striatal-thalamic-cortical loops leads to the motor symptoms of PD including tremor, akinesia and rigor (Lang and Lozano, 1998b; Jankovic, 2008) and the cognitive dysfunction including mild cognitive impairment (MCI; Huang et al., 2007; Lin et al., 2008; Kwak et al., 2010).

As the initial and most obvious symptoms are movement-related in the PD course, the motor function and the underlying cerebral mechanisms have become the focus of PD pathology research. The changes of the structure and functional network of basal ganglia, the abnormal oscillations of the neurons in the basal ganglia and motor-related cerebral cortex (Timmermann et al., 2003; de Solages et al., 2010), and the abnormal projection from basal ganglia to cerebral cortex (Lang and Lozano, 1998b) may relate with the motor dysfunction of PD patients. Besides basal ganglia, many literatures demonstrated that there exists abnormality in the large scale cerebral motor functional network (including cerebellum, motor cortex, frontal gyrus, etc.) of PD patients. Elevated putamen-external globus pallidus (GP) and STN-internal GP inputs), internal GPi-thalamus, caudate-putamen, and internal GPi-pedunculopontine nucleus (PPN) inputs (Asanuma et al., 2006; Eidelberg, 2009; Mure et al., 2011), and decreased metabolism in premotor cortex (PMC), supplementary motor area (SMA), and posterior parietal cortex (PPC; Asanuma et al., 2006; Ma, 2007; Eidelberg, 2009) were reported.

In recent years much attention has been devoted to characterizing the neural networks under multiple conditions (Friston et al., 1997; Friston, 1998; Yan et al., 2008) and psychophysiological interaction (PPI) analysis has become more commonly used in identifying the task-dependent functional connectivity changes (Deco et al., 2011; O'Reilly et al., 2012). PPI analysis was originally proposed by Friston et al. (1997), and promotes the understanding of the brain in terms of networks and interactions between brain regions (Bullmore and Sporns, 2009; Friston, 2011). PPI aims to identify regions whose activity is dependent on an interaction between psychological factors (the task) and physiological factors (the activity of a region of interest). Researchers have found interesting results using PPI in cognition such as conflict adaptation (Wang et al., 2015) and emotion recognition (Pulkkinen et al., 2015), and disease such as small-fiber neuropathy (Hsieh et al., 2015) and Social Anxiety Disorder (Cremers et al., 2015). PPI as the brain network in an experimental context, is emerging as an important biomarker of interest in disease diagnosis and prognosis prediction. For PD patients, this context-dependent brain network and the underling functional mechanism remains unclear.

We speculated that the dysfunctional motor network of PD patients might exhibit different profiles under different movement conditions. And considering the importance of the nuclei in the basal ganglia in PD pathology, they might play crucial roles in the context-dependent network. To test these hypotheses, a randomized unimanual or bimanual finger-to-thumb movement paradigm was designed to evaluate the impact of movement conditions on the neural networks. The motor network profiles in PD patients without dementia were investigated and compared with healthy controls using PPI analysis with the specific focus on the function of the basal ganglia. We found reduced putamen-modulation to the precuneus, cingulate gyrus, and the angular gyrus in PD patients, which implies the dysfunctional interactions and impaired basal ganglia inhibition in movements and hyperactivation/connectivity of the frontal gyrus which might be the compensation to maintain the task performance during the motor programs.

Materials and Methods

Subjects

Fifteen PD patients were studied. Four patients were excluded because they did not follow the instruction correctly during the experiments. The remaining 11 patients ranged in age from 51 to 81 (61.5 ± 7.1) years, and included eight males and three females. The diagnosis of Parkinson's disease was based on medical history, physical and neurological examinations, response to levodopa or dopaminergic drugs, and laboratory tests and MRI scans to exclude other diseases. Patients were assessed with the Unified Parkinson's Disease Rating Scale (UPDRS; Lang and Fahn, 1989) and Mini-Mental State Examination (MMSE) while off their medications. None patient had cognitive impairments (MMSE score were $\geq$ 21 for the subjects with eighth grade education, $\geq$ 23 for the subjects with high school education and $\geq$ 24 for the subjects with college education). Twelve health subjects (eight males and four females) with no history

of neruological, psychiatric, or medical disorders, aged from 52 to 81 (65.5 ± 10.1) years served as the control group. All the subjects were right-handed. The clinical and demographic data are shown in **Table 1**. Both groups were matched regarding age (t-test, $t = 1.0889$, $P = 0.1443$), gender (Fisher's exact test, $P = 0.556$) and MMSE score (t-test, $t = 1.2194$, $P = 0.1181$). All participants gave written informed consent and the study protocol was approved by the Ethics Committee of Wuhan General Hospital.

Experimental Design and Image Acquisition

The subjects participated in an auditory-cueing bimanual or unimanual finger-to-thumb movement task. Three kinds of movements were elicited by an auditory instruction (move left hand, move right hand, move both hands) in a pseudo-random and balanced sequence and stopped by "stop" instruction. Each movement lasted for 8 s followed by 12 s of rest. The whole experiment lasted for 360 s. During the experiments the subjects were instructed to close their eyes and focus their attention as much as possible. Patients were scanned after their medication had been withdrawn for 4 h.

Data were acquired in a GE Signa System operating at 1.5 T with a gradient echo EPI sequence (TR = 2000 ms, TE = 40 ms, FOV = 24 cm, matrix = 64 × 64 × 24, slice thickness = 5 mm, gap = 1 mm). The 3D structural images were also acquired for each subject with the parameters TR = 12.1 ms, TE = 4.2 ms, FOV = 24 cm, matrix = 256 × 256 × 172, slice thickness = 1.8 mm and gap = 0 mm.

Data Processing

The dataset was analyzed by SPM8 software package (www.fil.ion.ucl.ac.uk/spm, Wellcome Department of Cognitive Neurology). The processing steps for the activation and PPI analysis were shown in **Figure 1**. The following steps were included: (i) spatial preprocessing, to make the data adequate for the analysis; (ii) activation detection, to find out the activated areas during the finger-to-thumb movement task; (iii) region of interest (ROI) definition and PPI variables extraction, to determine the specific location of the ROI and create the interaction and the main effects terms; (iv) PPI analysis, to detect the interaction between the source ROI and experimental context. In the following, the analysis procedure was elaborated.

Spatial transformation (realignment, normalization) was performed on the functional images to correct for motion and normalize to the Montreal Neurological Institute (MNI) template brain. It is noted that the magnitude (minimum to maximum) of the six realignment parameters (i.e., x, y, and z translations, pitch, roll and yaw angles) of the normal control group were (0.4216 ± 0.3240), (0.3777 ± 0.2182), (0.9240 ± 0.6210) mm, (0.6875 ± 0.4125), (0.4354 ± 0.3839), (0.5844 ± 0.4469), degrees respectively, and of the PD group were (0.3317 ± 0.2256), (0.2971 ± 0.1174), (0.9141 ± 0.5368) mm, (0.6704 ± 0.4641), (0.3380 ± 0.1547), (0.3782 ± 0.2464) degrees, respectively, which were not significantly different between two groups ($t = 0.7652$, 1.0879, 0.0407, 0.0936, 0.7839, 1.3519, $P = 0.2263$, 0.1445, 0.4840, 0.4632, 0.2209, 0.0954, respectively). The 3D structural images were utilized to determine the normalization parameters.

Three task-related regressors for left or/and right hand movement conditions were modeled as the boxcar vectors convolved with a canonical hemodynamic reference waveform. Low frequency components were removed using a high-pass filter

TABLE 1 | Clinical details and demographics of patients with Parkinson's disease and the normal control subjects.

Measure	Normal control subjects ($n = 12$)	Subjects with Parkinson's disease ($n = 11$)
Age (years)	65.5 ± 10.1	61.5 ± 7.1
Gender, male:female	8:4	8:3
Duration of disease (years)	N/A	4.9 ± 3.9
UPDRS III score (off medication)	N/A	20.1 ± 6.3
MMSE score	27.5 ± 1.6	26.5 ± 2.3

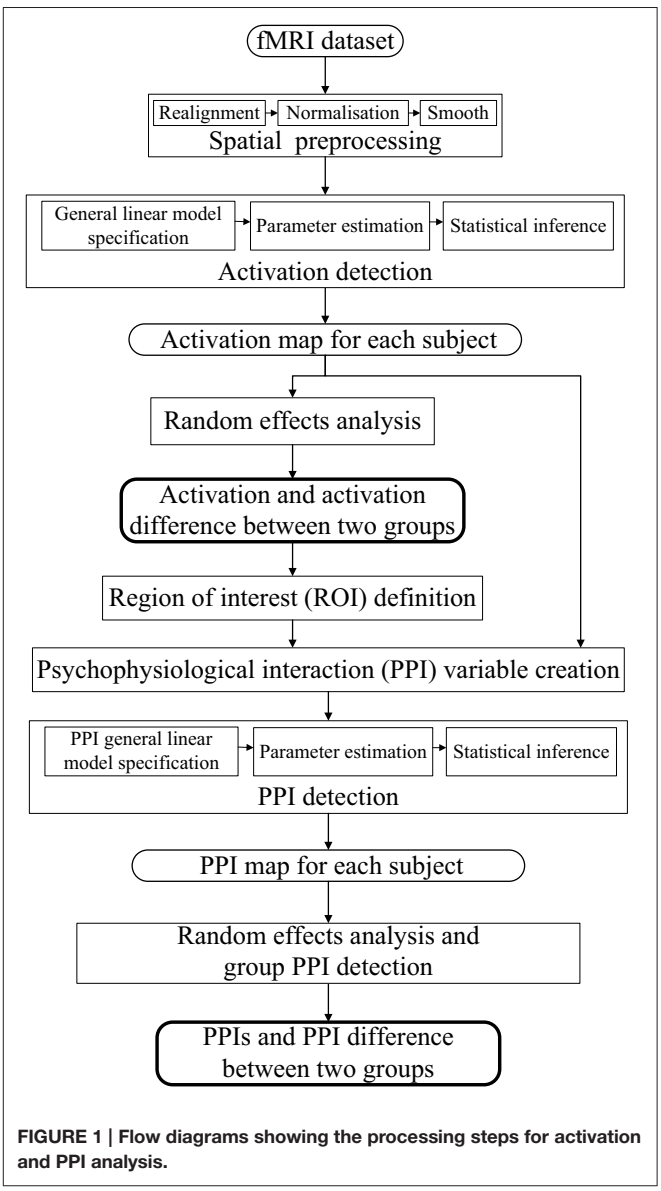

FIGURE 1 | Flow diagrams showing the processing steps for activation and PPI analysis.

(128 s) and the data were smoothed spatially with a Gaussian filter (full-width half-maximum (FWHM) = 8 mm). An autoregressive AR(1) model was included to account for serial correlation. The activation corresponding to each condition of each subject was detected and submitted to a second-level random effects analyses using the model of analysis of variance (ANOVA). Ages and sexes of the subjects were included as covariates. The activation of each group under three conditions were detected, and the activation difference between conditions (left + right vs. both) or groups (PD vs. control) was tested by applying appropriate linear contrasts to the ANOVA parameter estimates (t-test, $P < 0.05$, family-wise error (FWE) correction, extent threshold $k > 10$).

The regions with activation difference between unimanual movement and bimanual finger-to-thumb movement were defined as the ROIs. Time series from the effects of interest contrast were extracted from the ROIs, which provides an estimate of the continuous physiological response of the specific ROI (one main effect in the PPI model). The extracted time series was subsequently convolved with the contrasts of interest reflecting effects of differential movement loads, specifically, left hand movement + right hand movement > both hand movement or vice versa (the other main effect in the PPI model). The resultant interaction term was positively weighted to assess the facilitating influence of the ROI on other areas. The first level PPI maps from each subject were submitted to a second-level random effects analyses (ANOVA). The group PPIs and the PPI difference between groups were detected using t-test with a slightly more liberal threshold of $P < 0.001$ (uncorrected, extent threshold $k > 10$). Individual voxel peaks in significant clusters are reported in terms of MNI coordinates. The anatomical structures and the BA number were obtained using MRIcron (Rorden et al., 2007).

Results

Activation of Two Groups under Three Conditions

The group and condition specific activations are shown in **Figure 2** and the details are listed in **Table 2**. For the controls, in the left or right hand movement conditions, the contralateral sensorimotor (BA 1, 2, 3), primary motor (M1, BA 4) and premotor (BA 6) areas, SMA (BA 6), and the ipsilateral cerebellum were activated. In addition, parts of the frontal (BA 44), temporal (BA 21, 22) and parietal gyrus and basal ganglia (putamen) were activated. In the bimanual movement condition, the bilateral motor cortical areas and cerebellum, the frontal, temporal and parietal gyrus and putamen were activated.

For the PD patients, in the left or right hand movement conditions, the contralateral primary motor (M1, BA 4) and premotor (BA 6) areas, SMA, the ipsilateral cerebellum, parts of the frontal, temporal, parietal and cingulate gyrus were activated. In the bimanual movement condition, the left premotor area and bilateral cerebellum, the frontal, temporal, parietal and occipital gyrus were activated.

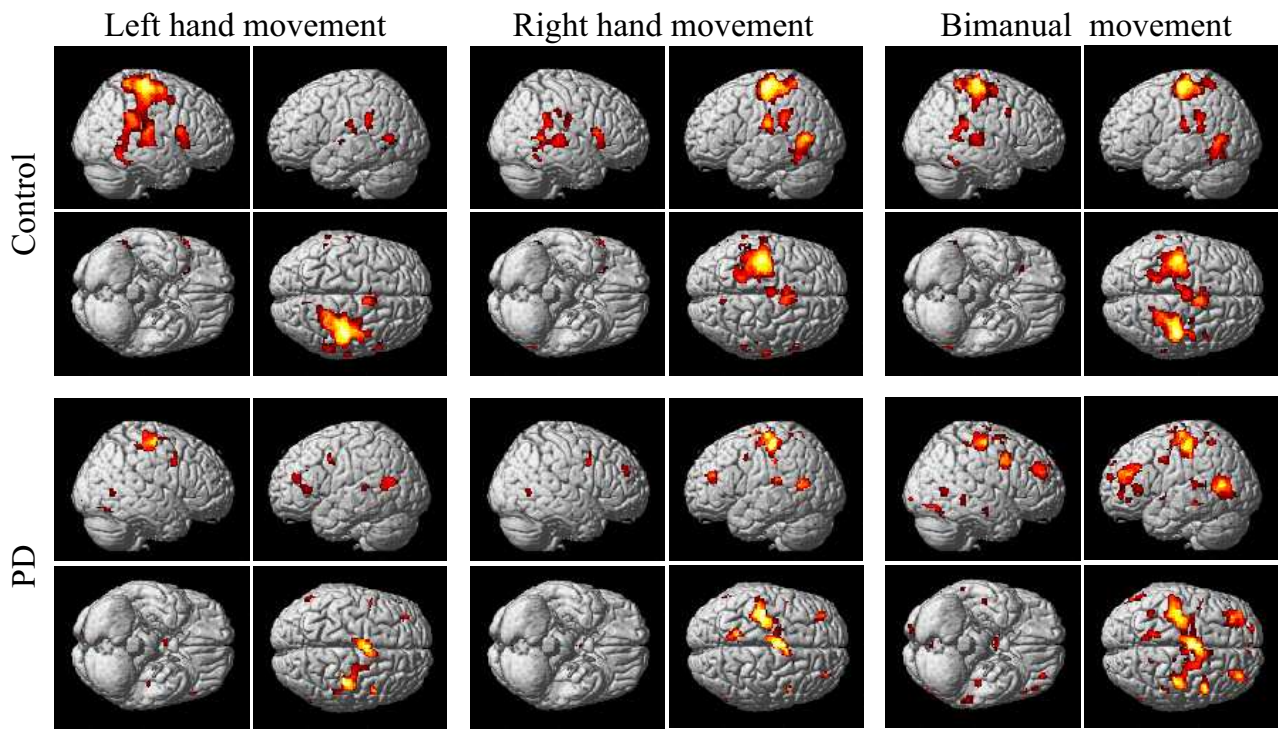

FIGURE 2 | Activation of the control and PD groups in the unimanual or bimanual finger-to-thumb movement experiments (SPM8, t-test, $P < 0.05$, FWE-corrected, extent threshold $k > 10$). The names of the movement trials are shown in the upside. The subject groups are shown in the left side. PD, Parkinson's disease.

TABLE 2 | Anatomical structure, stereotaxic coordinates, and *Z* score of the activated areas in the control or patient groups.

Anatomical structure	Left hand movement					Right hand movement					Both hand movement				
	Peak location			*Z* score	Cluster size (voxels)	Peak location			*Z* score	Cluster size (voxels)	Peak location			*Z* score	Cluster size (voxels)
	x	*y*	*z*			*x*	*y*	*z*			*x*	*y*	*z*		
CONTROL															
Premotor/SMA	8	4	62	6.18	470	−26	−16	62	6.39	–	40	−26	64	7.15	1914
Primary motor/	40	−26	64	7.83	5250	−38	−22	62	7.52	2517	−38	−22	62	7.08	2642
Sensorimotor	−62	−22	20	4.96	80	−58	−22	22	5.99	380	26	−30	70	5.68	–
	–	–	–	–	–	66	−20	20	4.95	71	–	–	–	–	–
Cerebellum	−18	−54	−26	6.83	1075	14	−50	−14	6.71	872	−20	−52	−30	6.80	2102
	–	–	–	–	–	−20	−62	−24	4.86	52	14	−48	−18	6.46	–
Frontal	56	16	10	5.58	339	6	4	62	6.12	551	38	8	32	5.54	125
	46	−4	58	5.93		−2	−10	62	5.15	139	–	–	–	–	–
Temporal	−46	−64	6	5.76	124	−46	−64	6	6.79	756	−64	−40	16	5.76	267
	−48	−38	24	5.26	171	64	−30	0	5.68	728	60	−36	20	5.40	333
Parietal	–	–	–	–	–	−46	−36	26	5.75	328	−64	−24	18	5.19	116
Putamen	28	−10	8	6.65	1592	−24	4	8	6.54	721	−22	4	12	5.71	239
	−22	2	14	5.69	315	30	8	10	6.19	1000	26	12	8	5.71	758
PD															
Premotor/SMA	38	−26	66	5.78	717	−26	−16	60	6.11	1116	−26	−18	56	7.57	–
M1	32	−22	50	4.99	–	−36	−28	60	5.83	–	–	–	–	–	–
Cerebellum	−14	−50	−26	5.84	422	−38	−70	−22	4.51	10	22	−54	−28	5.14	253
	–	–	–	–	–	22	−60	−16	4.66	25	−18	−52	−30	5.96	–
Frontal	6	4	60	5.85	708	−6	−8	62	5.95	739	−30	38	18	6.49	1003
	−30	38	18	5.44	121	30	50	24	4.65	43	46	6	38	6.01	435
Temporal	−62	−36	8	4.68	26	−54	−56	12	5.45	179	−52	−58	8	5.97	628
	−56	−60	18	5.45	196	−52	−30	18	4.87	74	60	−60	4	5.45	47
Parietal	–	–	–	–	–	−10	−58	66	5.14	367	−10	−58	66	5.13	316
	–	–	–	–	–	–	–	–	–	–	−36	−52	56	4.84	44
Cingulate	−8	2	50	5.20	–	−8	0	50	5.36	180	−4	−42	12	6.07	2252
	−4	−42	12	5.22	203	−4	−42	12	5.52	377	–	–	–	–	–
Occipital	–	–	–	–	–	–	–	–	–	–	48	−74	−14	5.71	109
	–	–	–	–	–	–	–	–	–	–	14	−92	−8	4.85	51
Thalamus	4	−16	10	5.08	169	–	–	–	–	–	–	–	–	–	–

For each anatomical structure, the representative regions in the left and right hemispheres are listed. The height and extent thresholds were set at $P < 0.05$, FWE-corrected, $k > 10$. The location is in MNI coordinates. PD, Parkinson's disease; SMA, supplementary motor area; M1, primary motor area.

Activation Difference within and between Two Groups

The within-group activation difference (left + right > both) was found in putamen (with peak voxel at [26, 18, −4] and [32, 8, 10]) in the control group (**Figure 3**) and was not found in the PD group. Activation difference between two groups under left or right handmovement conditions are shown in **Figure 4**. The control > PD activation mainly located in putamen in the basal ganglia. The PD > control activation mainly located in the superior frontal and temporal gyrus. There was no activation difference between two groups under the bimanual movement condition. The details of the activation difference are listed in **Table 3**.

PPIs Corresponding to Putamen in the Two Groups

From **Figures 3**, **4** and **Table 3**, it can be seen that putamen might play an important role in the movement coordination of the both hands. The subject-specific PPIs corresponding to putamen (with peak voxel at [26, 18, −4] and [32, 8, 10]) were detected and then submitted to a second-level random effects analyses of variance ($P < 0.001$, uncorrected). The group-specific PPIs are shown in **Figure 5** and the details are listed in **Table 4**. For the controls, decreased modulation of putamen on cingulate, parietal, frontal, occipital, angular and temporal gyrus, putamen and thalamus were detected in the bimanual movement condition relative to the unimanual movement condition. While for PD patients, the decreased modulation of putamen were detected in frontal

and occipital gyrus, extra-nuclear, thalamus, putamen and caudate.

PPI Difference between Two Groups

Figure 6 and **Table 5** depict the difference of PPIs corresponding to putamen between control and PD groups ($P < 0.001$, uncorrected), which included cingulate gyrus, angular gyrus, superior occipital gyrus and precuneus (control > PD) and inferior frontal gyrus (PD > control).

Discussion

General Characteristics of the Activation and Network Profiles of Control and PD Groups

For the controls and PD patients, the motor areas including the primary motor and premotor areas, SMA, and the cerebellum were activated in the movement conditions. These motor areas play the important roles in processing sensory information, and planning or executing hand movement (Moritz et al., 2000; Umests et al., 2002). Besides these areas, parts of the frontal, temporal and parietal gyrus were activated in both groups. As for the activation difference between two groups, generally the sizes of the activated areas, especially the motor cortex, were larger in the control group than those in the PD group, which was in accordance with the former results (Wu et al., 2010). The putamen was strongly and bimanually activated in control group, but not activated in the PD group in the movement conditions (**Figure 2**, **Table 2**). The right putamen exhibited significant control > PD activation difference (**Figure 4**, **Table 3**). In addition, the right putamen seemed to have weaker activity during the bimanual movement relative to the unimanual movement in the control group (**Figure 3**, **Table 3**). All these results implicated the importance of putamen, especially the right putamen, in hand movement and the coordination of two hands and its dysfunction in PD. The activation of the left frontal and temporal gyrus was stronger apparently in PD group than that in control group (**Figure 4**, **Table 3**).

The control of the hands involves a distributed network in which interactive processes task place between many neural assemblies to ensure efferent organization and sensory integration (Wu et al., 2010). Hence exploration on the interaction among brain regions may be more important than simply detecting the activation areas in understanding the coordination of the two hands. In consideration of the important finding of putamen with significant within-group and between-group activation difference and our hypothesis on the crucial role of the basal ganglia in the context-dependent network, the PPIs corresponding to putamen were explored. For the controls, decreased modulation of putamen on cingulate, parietal, frontal, occipital, angular and temporal gyrus, precuneus, putamen, and thalamus were detected in the bimanual movement condition relative to the unimanual movement condition. While for PD patients, the decreased modulation of putamen were detected

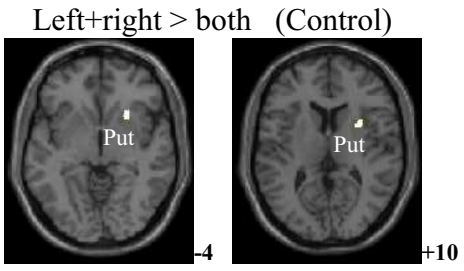

FIGURE 3 | Activation difference in the control group (left + right > both hand movement, SPM8, ANOVA, $P < 0.05$, FWE-corrected, extent threshold $k > 10$) with the peak Z score at [26, 18, −4] and [32, 8, 10]. The images were superimposed on a standard statistical parametric mapping anatomical template brain in neurological convention with z coordinate in MNI space for each slice shown in the right side. Put, Putamen.

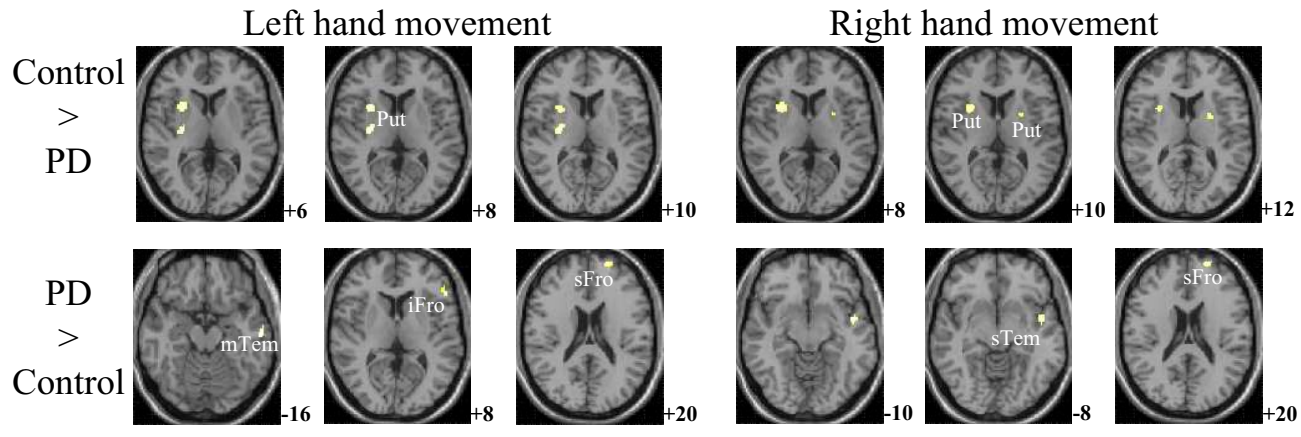

FIGURE 4 | Activation difference between control and PD groups in the left hand and/or right hand movement conditions (SPM8, ANOVA, $P < 0.05$, FWE-corrected, extent threshold $k > 10$). The images were superimposed on a standard statistical parametric mapping anatomical template brain in neurological convention with z coordinate in MNI space for each slice shown in the right side. PD, Parkinson's disease; Put, putamen; mTem, medial temporal gyrus; iFro, inferior frontal gyrus; sFro, superior frontal gyrus; mFro, medial frontal gyrus; sTem, superior temporal gyrus.

TABLE 3 | Anatomical structure, stereotaxic coordinates, and *Z* score of the different peak areas between the activated area in the control or patient groups.

Anatomical structure		BA	Peak location			*Z* score	Cluster size (voxels)
			x	*y*	*z*		
LEFT HAND MOVEMENT							
Control > PD	Putamen	–	30	−12	10	3.77	81
	Putamen	–	30	12	6	3.67	116
PD > Control	Superior frontal	10	−20	62	20	4.88	61
	Inferior frontal	45	−52	30	8	4.60	48
	Middle temporal gyrus	20	−58	−14	−16	3.70	31
RIGHT HAND MOVEMENT							
Control > PD	Putamen	–	30	12	8	4.04	123
	Putamen	–	−24	2	12	3.38	20
PD > Control	Superior frontal	10	−20	62	20	4.34	39
	Superior temporal gyrus	48	−46	2	−10	3.73	55
CONTROL							
left +right > both hand movement	Putamen	–	26	18	−4	4.84	30
	Putamen	–	32	8	10	4.73	41

The height and extent thresholds were set at P < 0.05, FWE-corrected, k > 10. The location is in MNI coordinates. PD, Parkinson's disease; BA, Brodmann's area.

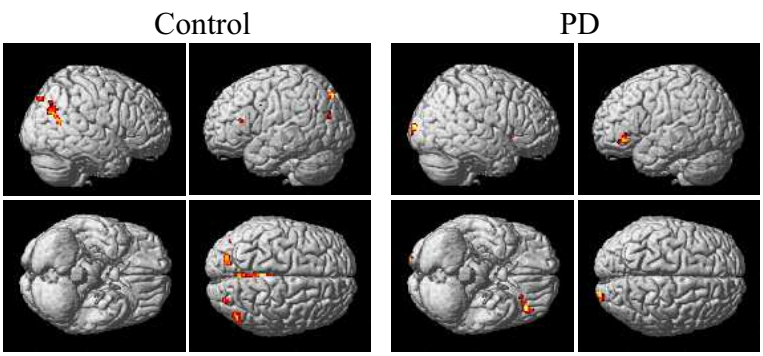

FIGURE 5 | PPIs corresponding to putamen in control and PD groups (SPM8, ANOVA, *P* < 0.001, uncorrected, extent threshold *k* > 10). PD, Parkinson's disease.

in frontal and occipital gyrus, thalamus, putamen, and caudate (**Figure 5**, **Table 4**). For both groups, the PPIs corresponding to putamen included not only some nucleus in basal ganglia, such as putamen, thalamus and caudate, but also some cortical areas, such as frontal and occipital gyrus. Between group PPI difference was detected in cingulate gyrus, angular gyrus, and precuneus (control > PD) and inferior frontal gyrus (PD > control). See **Figure 6**, **Table 5**. Generally the PPI scope in the control group was much larger. Several studies reported the relatively reduced functional connectivity in PD patients (van Eimeren et al., 2009; Skidmore et al., 2011; Hacker et al., 2012). Specifically in accordance with our results, the functional connectivity corresponding to putamen seemed weaker in PD patients (Hacker et al., 2012). Lower striatal correlations with thalamus, midbrain, pons and cerebellum in PD patients (Hacker et al., 2012), decreased activity in the putamen and increased cortical activity in the frontal lobe (Disbrow et al., 2013) have been reported. In our study, the PPI map of the control group was generally symmetric except in the putamen and thalamus, while the PPI map of the PD group was obviously asymmetric, which was similar with former observation in the functional connectivity of PD patients (Barnes et al., 2010; Hacker et al., 2012).

Key Regions in the Activation and Network Profiles of Control and PD Groups

In the activation and network profiles of the control and PD groups, two regions, i.e., the putamen and frontal regions seemed to play the specific roles. The putamen exhibited the control > PD activation and left + right > both hand movement activation within the control group. The frontal gyrus exhibited PD > control activation and connectivity with the putamen. These two

TABLE 4 | Anatomical structure, stereotaxic coordinates, and *Z* score of the peak areas in the PPI profiles in the control or patient groups.

Anatomical structure	BA	Peak location			*Z* score	Cluster size (voxels)
		x	*y*	*z*		
CONTROL						
Cingulate	23	10	−32	34	4.55	1447
Precuneus	7	−4	−62	36	4.10	–
Superior parietal	19	−22	−84	48	4.04	84
Precentral	44	−40	2	28	3.77	52
Putamen	–	22	14	2	3.67	42
Inferior frontal	45	−46	28	16	3.55	12
Superior occipital	19	28	−84	42	3.51	31
Angular	39	−36	−62	30	3.47	23
Angular	39	44	−64	30	3.40	179
Middle temporal	37	54	−60	16	3.32	–
Thalamus	–	−14	−14	4	3.29	11
PD						
Putamen	–	26	18	−4	4.45	21
Caudate	–	−12	14	4	3.97	73
Inferior frontal	47	−40	36	−8	3.80	98
Superior occipital	17	24	−98	10	3.79	63
Caudate	–	18	10	8	3.75	148
Putamen	–	28	2	6	3.71	33
Thalamus	–	−12	−18	8	3.30	10

The height and extent thresholds were set at $P < 0.001$, uncorrected, $k > 10$. The location is in MNI coordinates. PD, Parkinson's disease; BA, Brodmann's area.

regions are specifically crucial in the cortico-subcortical network and frontal network of the PD patients (Litvak et al., 2011).

The human brain network of motor function is composed of basal ganglia, cerebral motor cortex and cerebellum, among which the basal ganglia connect dorsal thalamus, ventromedial nucleus, premotor area and prefrontal cortex, and play the critical role in the complex cortical-subcortical circuits, i.e., the basal ganglia-thalamus-cortex circuits (Alexander and Moeller, 1994). Many researchers have emphasized the pathophysiology of PD as degeneration of dopaminergic nigrostriatal neurons with consequent dysfunction of these circuits (Lang and Lozano, 1998b; Jankovic, 2008; Hacker et al., 2012). The basal ganglia serve motor control functions such as scaling or focusing of movements (Alexander and Crutcher, 1990), and sustain the balance between facilitation and suppression of movements (Mink, 1996). Previous finding on functional connectivity indicated that the dorsal striatum (caudate and putamen) preferentially receives inputs from motor, sensory and premotor cortices, the ventral striatum (the nucleus accumbens and the olfactory tubercle) receives afferent inputs from cingulate cortex (Graybiel et al., 1994; Brooks, 1995). Specifically the putamen is the projection site of the cortical inputs into the basal ganglia and its activity is mainly movement related instead of cognition related (Kraft et al., 2007). Histologically, afferent fibers from the dorsal part of the putamen project somatotopically to the lateral parts of the substantia nigra (SN), which relates to the motor circuit system, and fibers from the caudate project to the rostral nigra, which relates to cingulate and association cortical system (Parent and Hazrati, 1994). In accordance with these results, we observed the putamen modulation on the thalamus, cingulate gyrus and the association area in control group (**Table 4**). The putamen activity and its modulation to cingulate gyrus and the association area seemed larger in control group than in PD group (**Tables 3**, **5**).

The functional role of the basal ganglia in bimanual coordination isn't quite clear till now. Putaminal activity was the greatest during the period of motor task initiation and was critical in the neural control of bimanual coordination (Kraft et al., 2007). An animal experiment found that the majority of the 58 recorded neurons in the basal ganglia exhibited a significant modulation of activity in unimanualtrials irrespective of the movement hand and one-third of the neurons exhibited activity reflecting a bimanual synergy, suggesting a possible role for basal ganglia in bimanual co-ordination (Wannier et al., 2002). In PD patients, the disturbed effective connectivity between prefrontal cortex, premotor areas, and putamen were reported (Ceballos-Baumann et al., 1994; Rowe et al., 2002; Wu et al., 2010). As the important node in the direct and indirect efferent pathways in the basal ganglia, the striatum can influence the basal ganglia output and exert either excitatory or inhibitory effect on the movement behavior including action selection as well as execution (Disbrow et al., 2013; Freeze et al., 2013). In PD, the abnormal interconnection among putamen, SN and GP causes excessive inhibition of the thalamus, and results tremors and difficulty in voluntary movements of the patients (DeLong and Wichmann, 2007). Because the putamen had stronger activation in the unimanual movement than bimanual movement in the control group, we speculated that the putamen mainly had the inhibitory effect and its function should be weakened to include more areas in bimanual movement. The control > PD putamen activation is reasonable considering that the weakened putamen inhibition would result in more involuntary movement in PD patients.

The activation of the left superior frontal gyrus and the connectivity between the left inferior frontal gyrus and putamen was stronger in PD group than that in the control group. These results implied the abnormal function of the left frontal gyrus in PD patients. The activity of the frontal area is related with the shift of the attention and the executive control, which are the crucial pre-movement processes (Wu et al., 2010; Disbrow et al., 2013). There is evidence indicating the hemodynamic responses in the mesiofrontal and sensorimotor cortex, putamen/pallidum, thalamus, and cerebellum and the participation of frontal area in the network for motor preparation (Riecker et al., 2005), movement initiation (Toxopeus et al., 2012), amplitude adjustment (Fabbri et al., 2012; Davare et al., 2015), and speed adjustment (Michely et al., 2015). It is noted that the executive functions of the PD patients may be affected even at early stages of the disease which would result in impaired motor planning, response preparation, and inhibition (Obeso et al., 2011; Toxopeus et al., 2012; Michely et al., 2015). While we noted that in our research, the patients reported no obvious difficulty in performing the unimanual or bimanual finger-to-thumb movements and the preserved movement performance

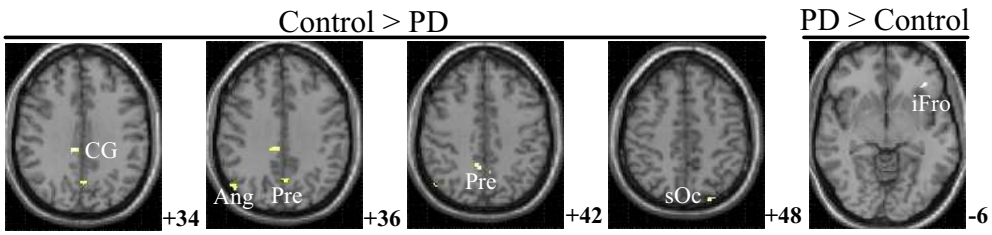

FIGURE 6 | PPI difference between control and PD groups (SPM8, ANOVA, $P < 0.001$, uncorrected, extent threshold $k > 10$). The images were superimposed on a standard statistical parametric mapping anatomical template brain in neurological convention with *z* coordinate in MNI space for each slice shown in the right side. PD, Parkinson's disease; CG, Cingulate gyrus; Ang, Angular gyrus; Pre, Precuneus; sOc, superior occipital gyrus; iFro, inferior frontal gyrus.

TABLE 5 | Anatomical structure, stereotaxic coordinates, and *Z* score of the different peak areas between the PPI profiles in the control or patient groups.

Anatomical structure		BA	Peak location			*Z* score	Cluster size (voxels)
			x	*y*	*z*		
Control > PD	Angular	39	52	−70	38	3.84	26
	Superior occipital	7	−24	−84	48	3.82	10
	Cingulate	23	10	−32	34	3.71	27
	Precuneus	7	8	−50	42	3.50	20
	Precuneus	7	0	−64	36	3.18	19
PD > Control	Inferior frontal	47	−38	32	−6	3.45	22

The height and extent thresholds were set at P < 0.001, uncorrected, k > 10. The location is in MNI coordinates. PD, Parkinson's disease; BA, Brodmann's area.

was observed. The hyperactivation/connectivity of the prefrontal cortex was suggested to constitute a compensatory mechanism in the patients' hypodopaminergic state to maintain the task performance at normal levels (Rowe et al., 2002; Wu et al., 2010; Michely et al., 2015). We spectulated that the stronger activation and connectivity with putamen of the left frontal gyrus may express the compensatory neuroplasticity during the motor programs.

Limitations and Conclusion

The present study is limited principally by the relatively small size of the subject samples. This limitation is partially because of the rigorous quality assurance standards applied to the fMRI data. However, our results need to be replicated in much larger size of samples. Furthermore, because of the small sample size, the patient group can't be subdivided according to their motor symptoms and phenotypes, which have been demonstrated to functionally relate with the brain activities (Rajput et al., 2008; Bunzeck et al., 2013). Further studies might help in establishing which pathological features are common and different between motor phenotypes.

In contrast to cortical and cerebellar activity, the activity of the basal ganglia is more inconsistently reported in fMRI motor studies (Lehéricy et al., 2006), which may be caused by small signal change in the subareas (for example about 0.5% in the putamen; Lehéricy et al., 2006), the movement paradigm (externally or internally generated), the imaging resolution inefficiency to discriminate the substructures (GP vs. putamen) of basal ganglia (Scholz et al., 2000). It's possible that SN degeneration is common to all the PD patients, but the factors in other parts of the basal ganglia distinguish between phenotypes (Rajput et al., 2008; Bunzeck et al., 2013). Several studies have indicated that there existed different grades of connectivity depending on the striatal subdivision, such as posterior putamen > anterior putamen connectivity with the brainstem (Hacker et al., 2012). In our research, the dysfunction of the putamen was observed, but the further exploration within this region was not performed. In addition, when detecting PPI and PPI difference, we applied the uncorrected hypothesis test. These limitations are subject to the current research condition that only the 1.5T MRI scanner with the relatively low signal-to-noise ratio (SNR) is available in our hospital, which has the inefficient spatial resolution and can only generate the signal with small changes in these substructures of the basal ganglia. MRI scanner with higher magnetic field strength or the multi-modal neuroimaging is promising to solve these issues.

There exists the formal possibility that the drug discontinuance time (4 h) might be not long enough to eliminate the medication effects. We didn't request the subjects to withdraw the drug for 1 day or to take their usual medication like other research (Hacker et al., 2012) based on the consideration to fulfill a tradeoff between the impact of head motion on imaging and the impact of medication on data analysis. This warrants the further research to include both the medicated and unmedicated states. The fMRI studies of the unmedicated (drug-naive) patients are challenging and some powerful regression techniques might help to reduce the motion-related artifacts (Helmich et al., 2010). Further studies might examine how PPI differences change depending on medication status and types.

In this paper, the brain network profiles in 11 PD patients without dementia were studied and compared with 12 healthy controls. The right putamen exhibited significant control > PD activation difference and weaker activity during the bimanual movement relative to the unimanual movement in control groups. The PPIs corresponding to the putamen (with peak voxel at [26, 18, −4] and [32, 8, 10]) were explored. Between group PPI difference was detected in cingulate gyrus, angular gyrus and precuneus (control > PD) and inferior frontal gyrus (PD > control). PD patients exhibited reduced putamen activation as well as modulation to the cingulate gyrus, angular gyrus, and precuneus during the finger-to-thumb movement, which implies the impaired basal ganglia inhibition in movements. The hyperactivation/connectivity of the frontal gyrus is the compensation to maintain the task performance during the motor programs.

Acknowledgments

This work was supported by the Natural Science Foundation of China (Grant 30800253, 31200777).

References

Alexander, G. E., and Crutcher, M. D. (1990). Functional architecture of basal ganglia circuits: neural substrates of parallel processing. *Trends Neurosci.* 13, 266–271. doi: 10.1016/0166-2236(90)90107-L

Alexander, G. E., and Moeller. J. R. (1994). Application of the scaled subprofile model to functional imaging in neuropsychiatric disorders: a principal component approach to modeling brain function in disease. *Hum. Brain Mapp.* 2, 79–94. doi: 10.1002/hbm.460020108

Asanuma, K., Tang, C., Ma, Y., Dhawan, V., Mattis, P., Edwards, C., et al. (2006). Network modulation in the treatment of Parkinson's disease. *Brain* 129(Pt 10), 2667–2678. doi: 10.1093/brain/awl162

Barnes, K. A., Cohen, A. L., Power, J. D., Nelson, S. M., Dosenbach, Y. B., Miezin, F. M., et al. (2010). Identifying Basal Ganglia divisions in individuals using resting-state functional connectivity MRI. *Front. Syst. Neurosci.* 4:18. doi: 10.3389/fnsys.2010.00018

Brooks, D. J. (1995). The role of the basal ganglia in motor control: contributions from PET. *J. Neurol. Sci.* 128, 1–13. doi: 10.1016/0022-510X(94)00206-4

Bullmore, E., and Sporns, O. (2009). Complex brain networks: graph theoretical analysis of structural and functional systems. *Nat. Rev. Neurosci.* 10, 186–198. doi: 10.1038/nrn2575

Bunzeck, N., Singh-Curry, V., Eckart, C., Weiskopf, N., Perry, R. J., Bain, P. G., et al. (2013). Motor phenotype and magnetic resonance measures of basal ganglia iron levels in Parkinson's disease. *Parkinsonism Relat. Disord.* 19, 1136–1142. doi: 10.1016/j.parkreldis.2013.08.011

Ceballos-Baumann, A. O., Obeso, J. A., Vitek, J. L., Delong, M. R., Bakay, R., Linazasoro, G., et al. (1994). Restoration of thalamocortical activity after posteroventral pallidotomy in Parkinson's disease. *Lancet* 344, 814. doi: 10.1016/S0140-6736(94)92369-8

Cremers, H. R., Veer, I. M., Spinhoven, P., Rombouts, S. A., and Roelofs, K. (2015). Neural sensitivity to social reward and punishment anticipation in social anxiety disorder. *Front. Behav. Neurosci.* 8:439. doi: 10.3389/fnbeh.2014.00439

Davare, M., Zénon, A., Desmurget, M., and Olivier, E. (2015). Dissociable contribution of the parietal and frontal cortex to coding movement direction and amplitude. *Front. Hum. Neurosci.* 9:241. doi: 10.3389/fnhum.2015.00241

Deco, G., Jirsa, V. K., and McIntosh, A. R. (2011). Emerging concepts for the dynamical organization of resting-state activity in the brain. *Nat. Rev. Neurosci.* 12, 43–56. doi: 10.1038/nrn2961

DeLong, M. R., and Wichmann, T. (2007). Circuits and circuit disorders of the basal ganglia. *Arch. Neurol.* 64, 20–24. doi: 10.1001/archneur.64.1.20

de Solages, C., Hill, B. C., Koop, M. M., Henderson, J. M., and Bronte-Stewart, H. (2010). Bilateral symmetry and coherence of subthalamic nuclei beta band activity in Parkinson's disease. *Exp. Neurol.* 221, 260–266. doi: 10.1016/j.expneurol.2009.11.012

Disbrow, E. A., Sigvardt, K. A., Franz, E. A., Turner, R. S., Russo, K. A., Hinkley, L. B., et al. (2013). Movement activation and inhibition in Parkinson's disease: a functional imaging study. *J. Parkinsons. Dis.* 3, 181–192. doi: 10.3233/JPD-130181

Eckert, T., Van Laere, K., Tang, C., Lewis, D. E., Edwards, C., Santens, P., et al. (2007). Quantification of Parkinson's disease-related network expression with ECD SPECT. *Eur. J. Nucl. Med. Mol. Imaging* 34, 496–501. doi: 10.1007/s00259-006-0261-9

Eidelberg, D. (2009). Metabolic brain networks in neurodegenerative disorders: a functional imaging approach. *Trends Neurosci.* 32, 548–557. doi: 10.1016/j.tins.2009.06.003

Fabbri, S., Caramazza, A., and Lingnau, A. (2012). Distributed sensitivity for movement amplitude in directionally tuned neuronal populations. *J. Neurophysiol.* 107, 1845–1856. doi: 10.1152/jn.00435.2011

Freeze, B. S., Kravitz, A. V., Hammack, N., Berke, J. D., and Kreitzer, A. C. (2013). Control of basal ganglia output by direct and indirect pathway projection neurons. *J. Neurosci.* 33, 18531–18539. doi: 10.1523/JNEUROSCI.1278-13.2013

Friston, K. J. (2011). Functional and effective connectivity: a review. *Brain Connect.* 1, 13–36. doi: 10.1089/brain.2011.0008

Friston, K. J., Buechel, C., Fink, G. R., Morris, J., Rolls, E., and Dolan, R. J. (1997). Psychophysiological and modulatory interactions in neuroimaging. *Neuroimage* 6, 218–229. doi: 10.1006/nimg.1997.0291

Friston, K. J. (1998). The disconnection hypothesis. *Schizophr. Res.* 30, 115–125. doi: 10.1016/S0920-9964(97)00140-0

Göttlich, M., Münte, T. F., Heldmann, M., Kasten, M., Hagenah, J., and Krämer, U. M. (2013). Altered resting state brain networks in Parkinson's disease. *PLoS ONE* 8:e77336. doi: 10.1371/journal.pone.0077336

Graybiel, A. M., Aosaki, T., Flaherty, A. W., and Kimura, M. (1994). The basal ganglia and adaptive motor control. *Science* 265, 1826–1831. doi: 10.1126/science.8091209

Hacker, C. D., Perlmutter, J. S., Criswell, S. R., Ances, B. M., and Snyder, A. Z. (2012). Resting state functional connectivity of the striatum in Parkinson's disease. *Brain* 135(Pt 12), 3699–3711. doi: 10.1093/brain/aws281

Helmich, R. C., Derikx, L. C., Bakker, M., Scheeringa, R., Bloem, B. R., and Toni, I. (2010). Spatial remapping of cortico-striatal connectivity in Parkinson's disease. *Cereb. Cortex* 20, 1175–1186. doi: 10.1093/cercor/bhp178

Hsieh, P. C., Tseng, M. T., Chao, C. C., Lin, Y. H., Tseng, W. Y., Liu, K. H., et al. (2015). Imaging signatures of altered brain responses in small-fiber neuropathy: reduced functional connectivity of the limbic system after peripheral nerve degeneration. *Pain* 156, 904–916. doi: 10.1097/j.pain.0000000000000128

Huang, C., Tang, C., Feigin, A., Lesser, M., Ma, Y., Pourfar, M., et al. (2007). Changes in network activity with the progression of Parkinson's disease. *Brain* 130, 1834–1846. doi: 10.1093/brain/awm086

Insel, T., Cuthbert, B., Garvey, M., Heinssen, R., Pine, D. S., Quinn, K., et al. (2010). Research domain criteria (RDoC): toward a new classification framework for research on mental disorders. *Am. J. Psychiatry* 167, 748–751. doi: 10.1176/appi.ajp.2010.09091379

Jankovic, J. (2008). Parkinson's disease: clinical features and diagnosis. *J. Neurol. Neurosurg. Psychiatry* 79, 368–376. doi: 10.1136/jnnp.2007.131045

Kraft, E., Chen, A. W., Flaherty, A. W., Blood, A. J., Kwong, K. K., and Jenkins, B. G. (2007). The role of the basal ganglia in bimanual coordination. *Brain Res.* 1151, 62–73. doi: 10.1016/j.brainres.2007.01.142

Kwak, Y., Peltier, S., Bohnen, N. I., Müller, M. L., Dayalu, P., and Seidler, R. D. (2010). Altered resting state cortico-striatal connectivity in mild to moderate stage Parkinson's disease. *Front. Syst. Neurosci.* 4:143. doi: 10.3389/fnsys.2010.00143

Lang, A. E., and Fahn, S. (1989). "Assessment of Parkinson's disease," in *Quantification of Neurological Deficit*, ed T. L. Munsat (Boston: Butterworths), 285–309.

Lang, A. E., and Lozano, A. M. (1998a). Parkinson's disease. Part I. *New Engl. J. Med.* 339, 1044–1053. doi: 10.1056/NEJM199810083391506

Lang, A. E., and Lozano, A. M. (1998b). Parkinson's disease. Part II. *New Engl. J. Med.* 339, 1130–1143. doi: 10.1056/NEJM199810153391607

Lehéricy, S., Bardinet, E., Tremblay, L., Van de Moortele, P. F., Pochon, J. B., Dormont, D., et al. (2006). Motor control in basal ganglia circuits using fMRI and brain atlas approaches. *Cereb. Cortex* 16, 149–161. doi: 10.1093/cercor/bhi089

Lin, T. P., Carbon, M., Tang, C., Mogilner, A. Y., Sterio, D., Beric, A., et al. (2008). Metabolic correlates of subthalamic nucleus activity in Parkinson's disease. *Brain* 131, 1373–1380. doi: 10.1093/brain/awn031

Litvak, V., Jha, A., Eusebio, A., Oostenveld, R., Foltynie, T., Limousin, P., et al. (2011). Resting oscillatory cortico-subthalamic connectivity in patients with Parkinson's disease. *Brain* 134(Pt 2), 359–374. doi: 10.1093/brain/awq332

Ma, Y. (2007). Abnormal metabolic network activity in Parkinson's disease: test-retest reproducibility. *J. Cereb. Blood Flow Metab.* 27, 597–605. doi: 10.1038/sj.jcbfm.9600358

Michely, J., Volz, L. J., Barbe, M. T., Hoffstaedter, F., Viswanathan, S., Timmermann, L., et al. (2015). Dopaminergic modulation of motor network dynamics in Parkinson's disease. *Brain* 138(Pt 3), 664–678. doi: 10.1093/brain/awu381

Mink, J. W. (1996). The basal ganglia: focused selection and inhibition of competing motor programs. *Prog. Neurobiol.* 50, 381–425. doi: 10.1016/S0301-0082(96)00042-1

Moritz, C. H., Haughton, V. M., Cordes, D., Quigley, M., and Meyerand, M. E. (2000). Whole-brain functional MR imaging activation from a finger-tapping task examined with independent component analysis. *AJNR Am. J. Neuroradiol.* 21, 1629–1635.

Mure, H., Hirano, S., Tang, C. C., Isaias, I. U., Antonini, A., Ma, Y., et al. (2011). Parkinson's disease tremor-related metabolic network: characterization, progression, and treatment effects. *Neuroimage* 54, 1244–1253. doi: 10.1016/j.neuroimage.2010.09.028

Obeso, I., Wilkinson, L., Casabona, E., Bringas, M. L., Alvarez, M., Alvarez, L., et al. (2011). Deficits in inhibitory control and conflict resolution on cognitive and motor tasks in Parkinson's disease. *Exp. Brain Res.* 212, 371–384. doi: 10.1007/s00221-011-2736-6

O'Reilly, J. X., Woolrich, M. W., Behrens, T. E., Smith, S. M., and Johansen-Berg, H. (2012). Tools of the trade: psychophysiological interactions and functional connectivity. *Soc. Cogn. Affect. Neurosci.* 7, 604–609. doi: 10.1093/scan/nss055

Parent, A., and Hazrati, L. N. (1994). Multiple striatal representation in primate substantia nigra. *J. Comp. Neurol.* 344, 305–320. doi: 10.1002/cne.903440211

Pulkkinen, J., Nikkinen, J., Kiviniemi, V., Mäki, P., Miettunen, J., Koivukangas, J., et al. (2015). Functional mapping of dynamic happy and fearful facial expressions in young adults with familial risk for psychosis - oulu brain and mind study. *Schizophr. Res.* 164, 242–249. doi: 10.1016/j.schres.2015.01.039

Rajput, A. H., Sitte, H. H., Rajput, A., Fenton, M. E., Pifl, C., and Hornykiewicz, O. (2008). Globus pallidus dopamine and Parkinson motor subtypes: clinical and brain biochemical correlation. *Neurology* 70(16 Pt 2), 1403–1410. doi: 10.1212/01.wnl.0000285082.18969.3a

Riecker, A., Mathiak, K., Wildgruber, D., Erb, M., Hertrich, I., Grodd, W., et al. (2005). fMRI reveals two distinct cerebral networks subserving speech motor control. *Neurology* 64, 700–706. doi: 10.1212/01.WNL.0000152156.90779.89

Rorden, C., Karnath, H. O., and Bonilha, L. (2007). Improving lesion-symptom mapping. *J. Cogn. Neurosci.* 19, 1081–1088. doi: 10.1162/jocn.2007.19.7.1081

Rowe, J., Stephan, K. E., Friston, K., Frackowiak, R., Lees, A., and Passingham, R. (2002). Attention to action in Parkinson's disease: impaired effective connectivity among frontal cortical regions. *Brain* 125(Pt 2), 276–289. doi: 10.1093/brain/awf036

Samii, A., Nutt, J. G., and Ransom, B. R. (2004). Parkinson's disease. *Lancet* 363, 1783–1793. doi: 10.1016/S0140-6736(04)16305-8

Schmidt, A., Smieskova, R., Aston, J., Simon, A., Allen, P., Fusar-Poli, P., et al. (2013). Brain connectivity abnormalities predating the onset of psychosis: correlation with the effect of medication. *JAMA Psychiatry* 70, 903–912. doi: 10.1001/jamapsychiatry.2013.117

Scholz, V. H., Flaherty, A. W., Kraft, E., Keltner, J. R., Kwong, K. K., Chen, Y. I., et al. (2000). Laterality, somatotopy and reproducibility of the basal ganglia and motor cortex during motor tasks. *Brain Res.* 879, 204–215. doi: 10.1016/S0006-8993(00)02749-9

Skidmore, F., Korenkevych, D., Liu, Y., He, G., Bullmore, E., and Pardalos, P. M. (2011). Connectivity brain networks based on wavelet correlation analysis in Parkinson fMRI data. *Neurosci. Lett.* 499, 47–51. doi: 10.1016/j.neulet.2011.05.030

Timmermann, L., Gross, J., Dirks, M., Volkmann, J., Freund, H. J., and Schnitzler, A. (2003). The cerebral oscillatory network of parkinsonian resting tremor. *Brain* 126(Pt 1), 199–212. doi: 10.1093/brain/awg022

Toxopeus, C. M., Maurits, N. M., Valsan, G., Conway, B. A., Leenders, K. L., and de Jong, B. M. (2012). Cerebral activations related to ballistic, stepwise interrupted and gradually modulated movements in Parkinson patients. *PLoS ONE* 7:e41042. doi: 10.1371/journal.pone.0041042

Umests, A., Okuda, J., Fujii, T., Tsukiura, T., Nagasaka, T., Yanagawa, I., et al. (2002). Brain activation during the fist-edge-palm test: a functional MRI study. *Neuroimage* 17, 385–392. doi: 10.1006/nimg.2002.1218

van Eimeren, T., Monchi, O., Ballanger, B., and Strafella, A. P. (2009). Dysfunction of the default mode network in Parkinson disease: a functional magnetic resonance imaging study. *Arch. Neurol.* 66, 877–883. doi: 10.1001/archneurol.2009.97

Wang, X., Wang, T., Chen, Z., Hitchman, G., Liu, Y., and Chen, A. (2015). Functional connectivity Patterns reflect individual differences in conflict adaptation. *Neuropsychologia* 70, 177–184. doi: 10.1016/j.neuropsychologia.2015.02.031

Wannier, T., Liu, J., Morel, A., Jouffrais, C., and Rouiller, E. M. (2002). Neuronal activity in primate striatum and pallidum related to bimanual motor actions. *Neuroreport* 13, 143–147. doi: 10.1097/00001756-200201210-00033

Wu, T., Wang, L., Chen, Y., Zhao, C., Li, K., and Chan, P. (2009). Changes of functional connectivity of the motor network in the resting state in Parkinson's disease. *Neurosci. Lett.* 460, 6–10. doi: 10.1016/j.neulet.2009.05.046

Wu, T., Wang, L., Hallett, M., Li, K., and Chan, P. (2010). Neural correlates of bimanual anti-phase and in-phase movements in Parkinson's disease. *Brain* 133(Pt 8), 2394–2409. doi: 10.1093/brain/awq151

Yan, L., Wu, Y., Wu, D., Qin, S., and Xu, G. (2008). Pattern analysis of motor functional connectivity. *Funct. Neurol.* 23, 141–147.

Zhang, J., Wei, L., Hu, X., Xie, B., Zhang, Y., Wu, G. R., et al. (2015). Akinetic-rigid and tremor-dominant Parkinson's disease patients show different patterns of intrinsic brain activity. *Parkinsonism Relat. Disord.* 21, 23–30. doi: 10.1016/j.parkreldis.2014.10.017

Conflict of Interest Statement: The authors declare that the research was conducted in the absence of any commercial or financial relationships that could be construed as a potential conflict of interest.

frontiers in
HUMAN NEUROSCIENCE

ORIGINAL RESEARCH ARTICLE
published: 17 March 2015
doi: 10.3389/fnhum.2015.00149

Dysfunctional activation and brain network profiles in youth with obsessive-compulsive disorder: a focus on the dorsal anterior cingulate during working memory

Vaibhav A. Diwadkar[1]*, Ashley Burgess[1], Ella Hong[1], Carrie Rix[1], Paul D. Arnold[2], Gregory L. Hanna[3] and David R. Rosenberg[1]

[1] *Department of Psychiatry and Behavioral Neurosciences, Brain Imaging Research Division, Wayne State University School of Medicine, Detroit, MI, USA*
[2] *Department of Psychiatry, Hospital for Sick Children, University of Toronto, Toronto, ON, Canada*
[3] *Department of Psychiatry, University of Michigan, Ann Arbor, MI, USA*

Edited by:
Baojuan Li, Fourth Military Medical University, China

Reviewed by:
Dewen Hu, National University of Defense Technology, China
Lirong Yan, Wuhan General Hospital, China

****Correspondence:***
Vaibhav A. Diwadkar, Department of Psychiatry and Behavioral Neurosciences, Brain Imaging Research Division, Wayne State University School of Medicine, Suite 5B, 3901 Chrysler Drive, Detroit, MI 48201, USA
e-mail: vdiwadka@med.wayne.edu

Brain network dysfunction is emerging as a central biomarker of interest in psychiatry, in large part, because psychiatric conditions are increasingly seen as disconnection syndromes. Understanding dysfunctional brain network profiles in task-active states provides important information on network engagement in an experimental context. This in turn may be predictive of many of the cognitive and behavioral deficits associated with complex behavioral phenotypes. Here we investigated brain network profiles in youth with obsessive-compulsive disorder (OCD), contrasting them with a group of age-comparable controls. Network interactions were assessed during simple working memory: in particular, we focused on the modulation by the dorsal anterior cingulate cortex (dACC) of cortical, striatal, and thalamic regions. The focus on the dACC was motivated by its hypothesized role in the pathophysiology of OCD. However, its task-active network signatures have not been investigated before. Network interactions were modeled using psychophysiological interaction, a simple directional model of seed to target brain interactions. Our results indicate that OCD is characterized by significantly increased dACC modulation of cortical, striatal, and thalamic targets during working memory, and that this aberrant increase in OCD patients is maintained regardless of working memory demand. The results constitute compelling evidence of dysfunctional brain network interactions in OCD and suggest that these interactions may be related to a combination of network inefficiencies and dACC hyper-activity that has been associated with the phenotype.

Keywords: dorsal anterior cingulate cortex, obsessive-compulsive disorder, network analysis, working memory, fMRI

INTRODUCTION

Obsessive-compulsive disorder (OCD) is a commonly occurring childhood and adolescent-onset neuropsychiatric disorder. It is characterized by obsessions (recurrent and persistent thoughts that typically induce marked distress) and compulsions (repetitive behaviors aimed at alleviating distress). OCD represents the upper extreme of an underlying continuous trait distribution encompassing obsessive-compulsive behaviors common in the general population that are heritable and cross traditional diagnostic boundaries. Thus, OCD represents a clinical "end-point" for a commonly observed trait (~45% of adolescents report OCD symptoms) (Berg et al., 1988; Apter et al., 1996). The 1-year incidence of OCD and sub-clinical OCD in adolescents is ~0.7 and 8.4%, respectively (Valleni-Basile et al., 1996). These relatively high rates of incidence and the association with a trait evident in the general population emphasize the importance of characterizing biological mechanisms underlying OCD. In this report, we aim to characterize these biological mechanisms by investigating brain network interactions in OCD and their differences from typical healthy controls.

Understanding brain network profiles and brain network dysfunction is a central theme of interest in clinical neuroscience. As suggested by the National Institute of Mental Health (Insel et al., 2010), such a focus may lead to an enhanced understanding of specific bio-behavioral impairments that underpin the emergence of complex behavioral phenotypes which are classified as psychiatric disorders. Indeed, understanding network dysfunction, in particular, is emerging as a leading framework for characterizing the neural substrates of multiple psychiatric conditions (Friston, 1998; Stephan et al., 2006; Almeida et al., 2009; Shaw et al., 2009; Diwadkar, 2012; Schmidt et al., 2013).

Obsessive-compulsive disorder, like most neuropsychiatric conditions, often has its origins in childhood and adolescence when brain network function is still maturing (Paus et al., 2008). Ensuing disordered neurodevelopmental trajectories (in the absence of adaptive responses) may in turn mediate the continued expression of symptoms through adolescence and into early adulthood (Tottenham and Sheridan, 2009). Furthermore,

Abbreviations: dACC, dorsal anterior cingulate cortex; FSTC, frontal striatal thalamic circuits; OCD, obsessive-compulsive disorder; PPI, psychophysiological interaction.

the complex patterns of OCD symptoms are linked to the inability to disengage behaviors from intrusive thoughts, implying aberrantly increased inhibitory control (Bari and Robbins, 2013). These patterns are highly suggestive of dysfunctions in control mechanisms within relevant brain networks (Piras et al., 2013). In this context, the role of the dorsal anterior cingulate cortex (dACC) assumes significance.

The dACC is positioned as a principal control region in the brain (Paus, 2001) that by itself, or through its mediation of cortical-striatal networks, exercises aspects of cognitive and motor control (Bakshi et al., 2011). The region has been of particular interest in OCD: glutamate dysregulation in the anterior cingulate and striatum has been implicated in pediatric OCD patients (Rosenberg et al., 2000, 2004). Altered glutamate concentrations may be linked to dysfunctional fMRI responses during tasks of behavioral engagement and disengagement. For instance, during conflict processing and action monitoring, OCD subjects evince higher activation in regions including the anterior cingulate cortex and the striatum (Fitzgerald et al., 2005; Maltby et al., 2005; Marsh et al., 2014) that may provide functional expressions of dACC dysfunction in the illness. A question of interest is whether these hyper-activations in the dACC are associated with dysfunctional network profiles.

Network models of fMRI have been applied in OCD. However, a principle focus of network-analyses of *in vivo* imaging data has been on the classification of resting state *functional connectivity* within (and across) cortical, limbic, striatal, and cerebellar networks (Harrison et al., 2009; Peng et al., 2014). These analyses have been notable as they have revealed categorical and developmental distinctions in resting state functional connectivity (rsFC) between OCD and typical controls in frontal, striatal and thalamic (FSTC) circuits (Fitzgerald et al., 2011). rsFC results are not directly informative about dysfunctional dACC-related profiles in a task-active state. For instance, the relationship between resting state functional connectivity (rsFC) and *task-dependent* functional interactions between regions remains uncertain (Stephan, 2004) and experimental analyses of within subject data have been equivocal (Rehme et al., 2013). Thus rsFC and the low-frequency bold signals it correlates between provide a complimentary snapshot of pathology; task-active analyses of functional network interactions are important for assessing a measure of network dynamics. Moreover, a separate question of interest is whether dysfunctional activation and brain network profiles in OCD are observed in tasks *not involving conflict monitoring*. Such evidence will provide strong support for general network based dysfunction in the disorder extending beyond highly circumscribed behavioral domains.

We had two principal aims in this study (summarized in **Figure 1**): (a) to investigate network profiles originating in the dACC in the task-active state using psychophysiological

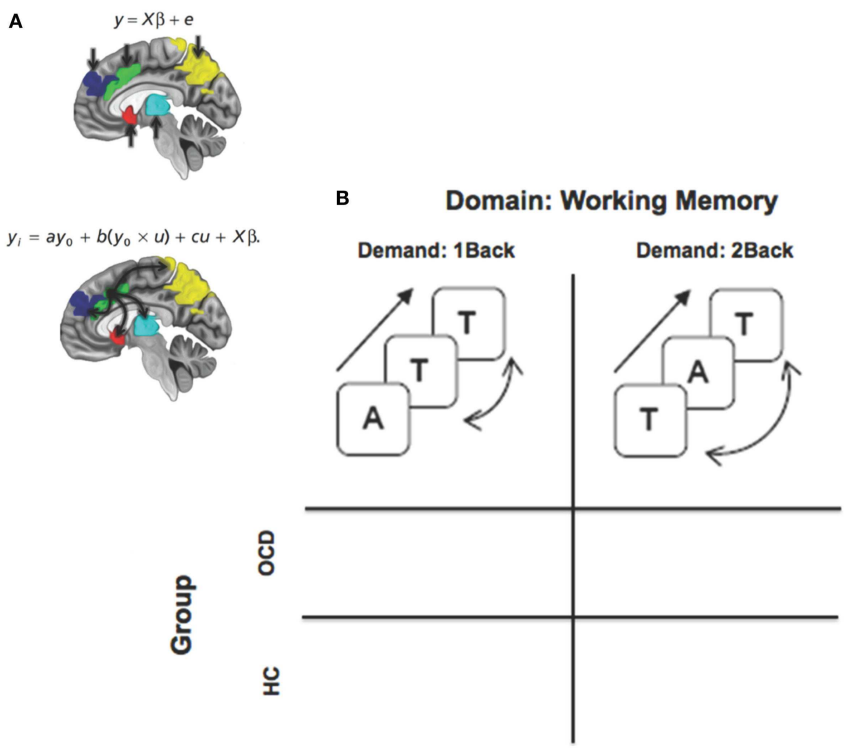

FIGURE 1 | A framework for assessing dysfunctional activation and dACC-related network profiles of cortical, striatal, and thalamic networks in OCD. **(A)** The two panels depictive activation-based and seed-based approaches to identifying function and dysfunction. The equations represent basic linear model formalisms for each class of models. Note the convolution term ($y_0 \times u$) in the PPI based model that accounts for seed (y_0 = dACC) modulation of targets in the task-oriented (u = working memory > rest) context. The regions of interest are schematically depicted on the mid-sagittal surface. The second figure schematically depicts the modulatory effects of the dACC assessed using psychophysiological interaction. **(B)** The factorial design space used for the study that assessed the effects of task-demand (1Back vs. 2Back) crossed with group.

Table 1 | The table depicts the demographics for healthy control (HC) and OCD participants.

	M/F	Mean age	Range	Height (inches)	Weight (lbs)	Handedness (R/L/M)	CY-BOCS (*T*)	CY-BOCS (*O*)	CY-BOCS (*C*)
Typical controls ($n = 27$)	18/9	17.4 (3.14)	12–21	67.3 (4.8)	147.8 (52.9)	24/2/1			
OCD ($n = 18$)	11/7	17.2 (3.33)	11–21	65.6 (4.3)	146.3 (60)	17/1/0	31/16 (4.5/9.4)	15/8 (2.7/4.8)	16/8 (2.7/4.9)

Groups did not differ in terms of age ($t = 0.32$, $p = 0.75$), height ($t = 1.22$, $p = 0.23$), or weight ($t = 0.08$, $p = 0.94$). Also comparable were gender ($\chi^2 = 0.15$, $p = 0.70$) and handedness frequencies ($\chi^2 = 0.76$, $p = 0.68$). Values in parenthesis represent SD. For lifetime CY-BOCS (lifetime/current): T = Total symptoms, O = Obsessive Symptoms, C = Compulsive symptoms.

interaction (PPI) (Friston et al., 1997; O'Reilly et al., 2012), PPI is a simple framework within the general linear model for investigating contextual modulation of targets (e.g., regions within FSTC) by a seed (e.g., dACC) in a task-active context; (b) to investigate these profiles during parametrically manipulated verbal working memory, (Casey et al., 1995; Diwadkar et al., 2011, 2013), a domain that provides a rich window for investigating normal and dysfunctional activation and network profiles in the FSTC.

MATERIALS AND METHODS

PARTICIPANTS

Eighteen participants with a diagnosis of OCD and 27 controls participated in the fMRI studies (see **Table 1**). All participants and their parents were interviewed with the Schedule for Schizophrenia and Affective Disorders for School-Aged Children-Present and Lifetime Version and Schedule for Obsessive-Compulsive and Other Behavioral Syndromes (Wolff and Wolff, 1991; Kaufman et al., 1997). The lifetime (maximum) and current severity of OCD were assessed in the patients with a modified version of the Children's Yale-Brown Obsessive Compulsive Disorder Scale (Goodman et al., 1989; Scahill et al., 1997). Lifetime and current axis I diagnoses were made independently by two clinicians (David R. Rosenberg, Gregory L. Hanna) using all sources of information according to DSM-IV criteria. All patients with OCD had a total lifetime CY-BOCS score of at least 20. Exclusion criteria for patients and controls included lifetime history of psychosis, bipolar disorder, substance abuse or dependence, anorexia or bulimia nervosa, epilepsy, head injury with sustained loss of consciousness, Huntington's disease, dyskinesia, chronically disabling medical illness, autism, mental retardation, or a score >15 on the lifetime version of the Social Communication Questionnaire. Controls were free of all psychiatric illness. Legal guardians provided written informed consent prior and children gave written assent prior to participating in the study. The Human Subjects Investigative committee at Wayne State University and the University of Michigan approved the protocol and all methods therein.

fMRI

Gradient echo EPI fMRI data acquisition was conducted at Vaitkevicius Magnetic Resonance Centre on a 3T Siemens Verio system using a 12-channel volume head coil (TR: 2.6 s, TE: 29 ms, FOV: 256 mm × 256 mm, acquisition matrix: 128 × 128, 36 axial slices, voxel dimensions: 2 mm × 2 mm × 3 mm). In addition, a 3D T1-weighted anatomical MRI image was acquired (TR: 2200 ms, TI: 778 ms, TE: 3 ms, flip-angle = 13°, FOV: 256 mm × 256 mm,

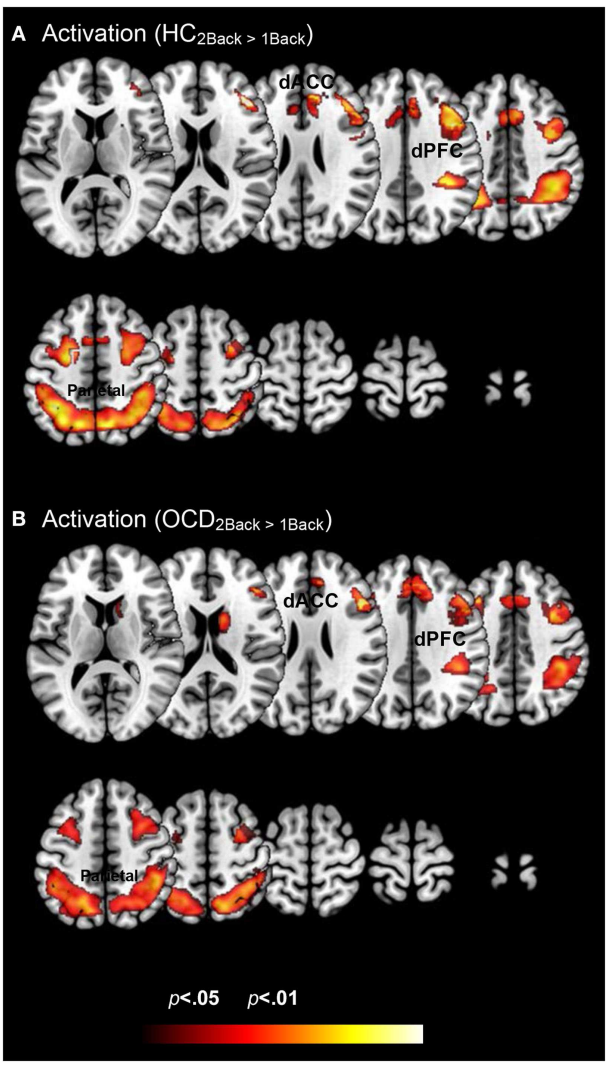

FIGURE 2 | Within group changes in activation profiles as a function of load are depicted on identical ascending mosaics of axial views. The significant clusters ($p < 0.05$, cluster level) show significant increases in activation with increases in working memory related load. As seen, these increases are evident within both **(A)** healthy control and **(B)** OCD groups. These activation profiles establish within group effects of memory load across previously implicated load sensitive working memory related regions. These include dorsolateral prefrontal cortex (dPFC), the dorsal anterior cingulate (dACC), and the parietal cortex.

256 axial slices of thickness = 1.0 mm, matrix = 256 × 256). A neuroradiologist reviewed all scans to rule out clinically significant abnormalities.

During fMRI, subjects were positioned with adjustable padded restraints employed for head stabilization. Stimuli were rear-projected using an IFIS-SA presentation system (MRI Devices), and subjects responded with a button box unit. During fMRI, subjects participated in an established verbal *n*-back paradigm (Casey et al., 1995). Parametric working memory load was varied between maintaining 0, 1, or 2 items in memory (0-, 1-, or 2-Back; see **Figure 1** insets). Runs were blocked by condition. During each block (30 s), letters were projected in sequence (presentation time: 500 ms; ISI: 2500 ms; 10 letters per block) on a screen; subjects signaled with a two-choice optical response box if the presented letter was a target or not. The paradigm cycled between rest (20 s), 0-, 1-, and 2-Back epochs (three blocks each). The experiment was controlled using presentation (Neurobehavioral Systems Inc.).

fMRI PROCESSING

fMRI data were processed in SPM8 using typical methods. All images were manually oriented to the AC-PC line, realigned to correct for head movement, spatially normalized to the MNI (Montreal Neurological Institute) template brain and resliced (2 mm × 2 mm × 2 mm). Low frequency components were removed using a low-pass filter (128 s) and images were spatially smoothed using a Gaussian filter (8 mm full-width half maximum; FWHM). An autoregressive AR(1) model was used to account for serial correlation, and regressors modeled as a 30 s box-car vectors (for each of the task-related conditions) were convolved with a canonical hemodynamic reference waveform.

Subjects' head motion was within accepted limits (<4 mm). Furthermore, in all first level models, the effects of motion were modeled by including the six motion parameters as covariates of no interest. First-level contrasts (1Back > 0Back; 2Back > 0Back) were used to assess the effects of memory load on activation.

PPI (implemented in SPM8) was employed to model dACC modulation of FSTC targets during working memory (Friston et al., 1997; Honey et al., 2005). For *each subject*, time series from the effects of interest contrast ($p < 0.05$) were extracted from the dACC peak (including Brodmann areas 32 and the supra-genual aspects of BA24) (Palomero-Gallagher et al., 2008). The extracted time series (the wave form of which provides an estimate of the continuous physiological response of the dACC) was subsequently convolved with the two contrasts of interest reflecting effects of differential memorial load, specifically, 1-Back > 0-Back (low load) and 2-Back > 0-Back (high load). The resultant interaction term was positively weighted to assess the facilitating influence of the dACC on FSTC targets (with the slope of the effect parametrically encoded in the convolution term and reflecting the degree of modulation).

For all activation or network analyses, first level maps (activation or PPI) from each subject were submitted to a second-level random effects analyses of variance with group modeled as an independent factor and memory load as non-independent factor. The factorial design permitted assessment of intra-group load-related effects, as well as between-group differences at varying levels of memory load.

All second level analyses were spatially thresholded in the FSTC regions of interest using deterministic anatomical masks defined in stereotactic space (Maldjian et al., 2003). These maps constitute anatomical representations in stereotactic space representing each of the regions of interest and are widely employed to spatially localize activations in neuroimaging research. Images were corrected using cluster level correction (cluster extent thresholds, $p_c < 0.05$) derived from 10^4 Monte Carlo simulations from voxels across the individual regions of interest (Ward, 2000). Individual voxel peaks in significant clusters are reported in terms of Montreal Neurological Institute coordinates.

RESULTS

Results are organized to sequentially present evidence of (1) dysfunctional activation profiles and (2) dysfunctional brain network profiles in OCD and HC:

(1a) We first show load-related effects on *activation profiles* within both HC and OCD. These results provide evidence

Table 2 | The table provides information on clusters of significance and peaks within where each of the groups showed increased *activation* to variations in memory load (Figure 2).

Region	Brodmann area	MNI coordinates (*x, y, z*)			*Z* score	Cluster extent	*p* (peak)
Table 2: activation							
$HC_{2Back > 1Back}$							
Parietal lobe	40	−36	−51	49	5.23	734	0.000
Mid frontal gyrus	8	27	15	45	1.93	135	0.027
Dorsal prefrontal cortex	46	−42	20	27	4.45	74	0.000
Basal ganglia	–	28	18	6	3.37	32	0.000
dACC	24	−18	−1	51	4.42	177	0.000
$OCD_{2Back > 1Back}$							
Parietal lobe	40	46	−40	51	4.08	739	0.000
Mid frontal gyrus	6	32	8	52	3.17	175	0.001
Dorsal prefrontal cortex	9	−39	12	39	3.08	103	0.001
Basal ganglia	–	14	6	19	3.37	70	0.000
dACC	32	8	20	46	3.19	189	0.001

of *within-group* effects of parametric increases in working memory load on FSTC.

(1b) Next we present *between-group* results showing aberrantly increased *activation profiles* in FSTC in OCD patients compared to HC at both levels of memory load. These results demonstrate that OCD participants more extensively activate FSTC than HC at both levels of memory load.

(2) We show between group results assessing dysfunctional brain network profiles in OCD compared to HC. These results indicate aberrantly increased modulation of FSTC by the dACC in OCD, especially at the lower level of memory load.

LOAD-RELATED EFFECTS ON ACTIVATION PROFILES

Figure 2 depicts clusters ($p_c < 0.05$) in FSTC showing increased within-group activation in response to increases in memory load (cluster relevant information in **Table 2**). In both groups, increased memory load results in increased recruitment of frontal and parietal regions, and the dACC. These results are unsurprising for the HC group. They are highly consistent with previous assessments of activation profiles in this circuit in HC (Braver et al., 1997; Cohen et al., 1997; Diwadkar et al., 2000), showing increased recruitment in brain circuits committed to implementing working memory related functions. The results in OCD are notable as they demonstrate that the memory effect exerts within-group effects consistent with HC. This is important evidence that FSTC in OCD is sensitive to load-related variations in working memory and that the overall implementation of the task generates load-related effects on activation profiles. Notable is an absence of load-related activation effects in the striatum or the thalamus, regions not typically implicated in core memory-related processing. The basal ganglia contribute to cortical-striatal processing loops that sub-serve complex processing, by supplementing prefrontal function (Hazy et al., 2006; Calzavara et al., 2007; Voytek and Knight, 2010). The thalamus forms cortical-thalamic processing units that integrate information from cortical and striatal loops to modulate complex behavior, but has generally not been sensitive to load-related variations in working memory (Haber and Calzavara, 2009).

BETWEEN-GROUP RESULTS SHOWING ABERRANTLY INCREASED ACTIVATION PROFILES IN FSTC IN OCD PATIENTS

Figure 3 depicts clusters ($p_c < 0.05$) in FSTC showing increased activation in OCD (relative to HC) at each level of memory load (cluster relevant information in **Table 3**). Several effects are evident. Dysfunctional activation profiles are observed in the frontal and parietal cortices and in the dACC at both levels of load. Absent is evidence of dysfunctional activation profiles in the striatum or the thalamus. Moreover, dysfunction in activation profiles scales as a function of memory load: Increased memory demand leads to increased activation in cortical regions. These analyses are consistent with previous studies in FSTC in OCD participants in other behavioral domains such as conflict monitoring that are closely associated with behavioral phenotypes in the illness (Huyser et al., 2011). As one of our study aims was to assess whether hyper-activation in FSTC constitutes a domain-general property of brain regions in OCD, these analyses extend the findings beyond the domain of conflict processing and suggest that multiple tasks engaging FSTC are sensitive for detecting activation-related dysfunction.

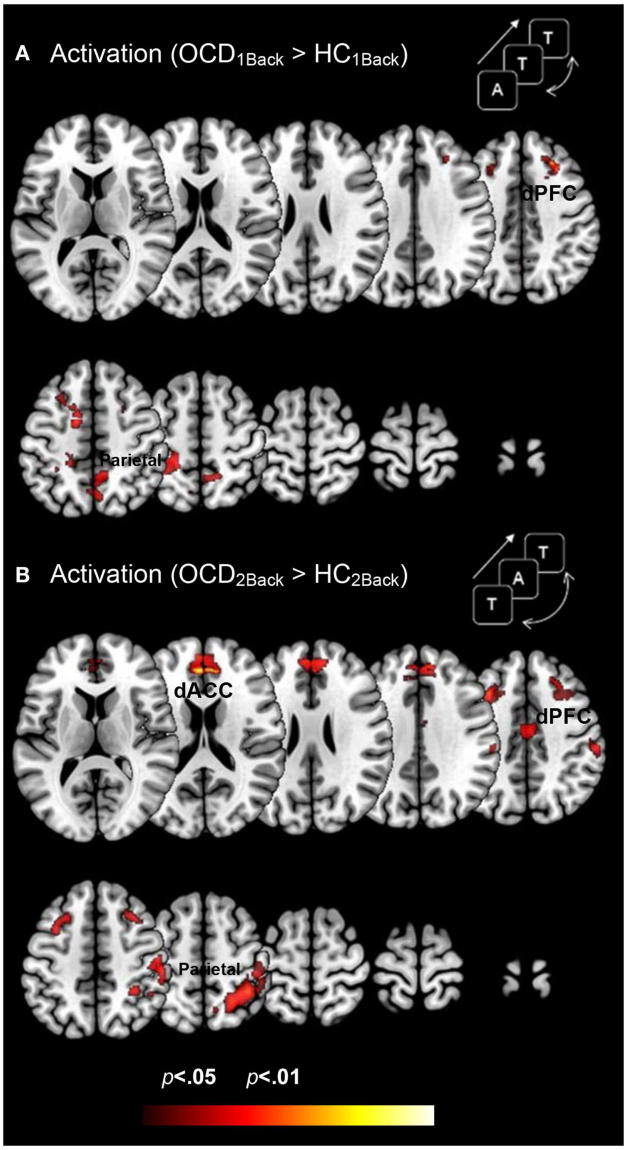

FIGURE 3 | Dysfunctional activation profiles in OCD (relative to controls) are depicted for both (A) the 1Back level of memory and (B) the 2Back level of memory load. Increased activation in OCD ($p < 0.05$, cluster level) is depicted on identical ascending mosaics of axial views. These activation profiles indicate increased activation in dorsolateral prefrontal cortex (dPFC), the dorsal anterior cingulate (dACC), and the parietal cortex in OCD. Notably the degree of dysfunctional activation in OCD scales as a function of memory load. We speculate that the parametric demands as expressed in dysfunctional activation profiles load disproportionately in OCD participants. As will be seen, brain network profiles in OCD do not strictly follow activation patterns, evidence that signatures of network interactions may complement psychopathology revealed in activation models.

BETWEEN GROUP RESULTS ASSESSING DYSFUNCTIONAL BRAIN NETWORK PROFILES IN OCD

Figure 4 depicts clusters ($p_c < 0.05$) in FSTC showing *increased modulation by the dACC in OCD* (relative to HC) at each level of memory load (cluster relevant information in **Table 4**). We

Table 3 | The table provides information regarding clusters of significant and significant peaks showing *dysfunctional activation profiles* in OCD (compared to HC) at each level of memory load (Figure 3).

Region	Brodmann area	MNI coordinates (*x, y, z*)			*Z* score	Cluster extent	*p* (peak)
Table 3: activation							
$OCD_{1Back} > HC_{1Back}$							
Parietal lobe	5	−18	−40	61	3.05	385	0.001
Mid frontal gyrus	8	27	27	42	2.45	83	0.007
Dorsal prefrontal cortex	9	24	38	36	2.8	58	0.003
dACC	24	−15	−1	49	2.87	117	0.002
$OCD_{2Back} > HC_{2Back}$							
Parietal lobe	3	50	−22	56	3.18	392	0.001
Mid frontal gyrus	6	38	21	45	3.03	124	0.001
Dorsal prefrontal cortex	9	9	47	33	3.07	97	0.001
dACC	32	−3	42	18	2.78	197	0.003

highlight several notable effects. First, dysfunctional network profiles in OCD form a pattern that is distinct and complimentary to that observed in activation profiles. OCD is characterized by increased dACC related modulation at the 1Back level of load but not the 2Back level, suggesting that the degree of dACC modulation (and the mechanisms that can be inferred from it) do not scale with load. We speculate (see Discussion) that this effect may be related to aberrantly increased dACC modulation at the 1Back level itself. The hyper-modulation may reflect inefficiencies in control-related network function or hyper-activity of the dACC, or both. Second, dysfunctional modulation of the striatum is evident, with significantly increased dACC modulation of the caudate and putamen observed at the 1Back level (**Figure 4A**). This effect also constitutes a complementary pattern of dysfunction from activation in OCD where profiles in the striatum appeared normal (**Figure 3**).

DISCUSSION

We conducted a simple investigation of brain activation and network profiles in a group of OCD youth and age-comparable controls. Participants were assessed with fMRI using a simple working memory paradigm with variable demands (**Figure 1**). Three principle results are highlighted across both classes of analyses: *Activation Profiles*: (1a) Activation profiles were highly sensitive to increases in memory load within each group (**Figure 2**). (1b) Youth with OCD were characterized by aberrantly increased recruitment of frontal and parietal regions (but not striatal or thalamic regions) during both levels of working memory. The degree of hyper-activation scaled as a function of working memory demand (**Figure 3**). *Network Profiles*: (2) Compared to HC, youth with OCD were characterized by increased dACC modulation of frontal, parietal, and striatal regions, particular at lower levels of working memory load (**Figure 4**).

Taken together, these results establish that OCD is characterized by dysfunction in core FSTC regions, detectable using both activation- and network-based analyses of fMRI signals. We suggest that the network-based analyses are notable for being the first to demonstrate dysfunctional network signatures of the dACC, a region closely associated with OCD related pathophysiology. Moreover, these profiles observed using a basic working memory paradigm, suggest that FSTC deficits are a basic pathophysiologic mechanism underlying OCD, are detectable with a multiplicity of tasks, and affect frontal, striatal, and thalamic circuits. In the remainder of the paper, we discuss the putative mechanisms that may underpin these observations and the implications for OCD related pathology and function.

CINGULATE, FRONTAL, STRIATAL, AND THALAMIC REGIONS: A CRITICAL CIRCUIT SUB-SERVING COMPLEX FUNCTION

The regions targeted in this investigation collectively form core sub-circuits that implement function in a multiplicity of higher-order domains including working memory (Owen et al., 2005; Diwadkar et al., 2011), sustained attention (Fan et al., 2005; Langner and Eickhoff, 2013; Diwadkar et al., 2014), and cognitive control (Carter et al., 1999; Anderson et al., 2008). These functional sub-circuits are also underpinned by dense patterns of anatomical connectivity. The dorsal-prefrontal cortex and the basal ganglia share topographically mapped monosynaptic connections (Calzavara et al., 2007) that may explain co-activation patterns frequently observed in fMRI studies. Descending connections from cortical regions including the prefrontal cortex and sensory, motor, and frontal regions synapse on multiple thalamic nuclei including the ventral and posteromedial complexes (Ray and Price, 1993; Klein et al., 2010; Li et al., 2013) leading to the notion of "cortical-thalamic processing units" (Briggs and Usrey, 2008). The dACC is uniquely positioned from an anatomical standpoint, with connections to frontal and motor regions, to play a mediating influence in control related mechanisms (Paus, 2001). Each of these regions appears to be relatively specialized for highly sophisticated functions.

The dorsal-prefrontal cortex sub-serves working memory in multiple ways. Phasic activity in prefrontal neurons is strongly correlated with the temporary maintenance of memoranda in working memory (Vijayraghavan et al., 2007), suggestive of a direct link between neuronal responses and overt behavior. Moreover, the prefrontal cortex sub-serves goal-directed behavior in multiple domains (including working memory) through direct "command" signals to multiple cortical and sub-cortical targets (Crowe et al., 2013; Funahashi and Andreau, 2013). The anatomical positions of the basal ganglia allow the structure to receive

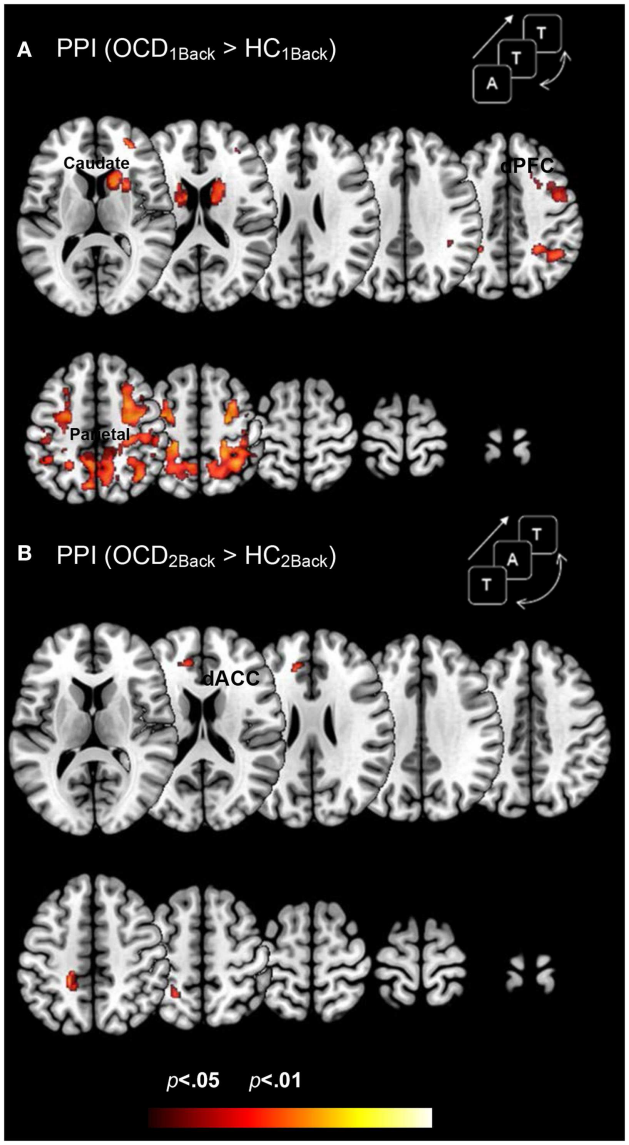

FIGURE 4 | Dysfunctional brain network profiles in OCD (relative to controls) are depicted for both (A) the 1Back level of memory and (B) the 2Back level of memory load. The clusters depict significantly increased dACC-modulation of cortical and striatal targets in OCD compared to typical controls ($p < 0.05$, cluster level) depicted on identical ascending mosaics of axial views. These brain network profiles complement dysfunctional activation profiles (**Figure 3**). Note the implication of the caudate, not implicated in dysfunctional activation. The increased modulation by the dACC may reflect increased control-related inputs demanded in OCD to sub-serve network function associated with this fundamental domain. The lack of a parametric effect may reflect the fact that dACC related network engagement is already aberrantly increased at the 1Back level. Indeed, OCD participants did not show an increase in dACC modulation going from the 1Back to the 2Back level of demand (whereas HC participants did).

inputs from multiple uni- and heteromodal regions (Ragsdale and Graybiel, 1990). Thus the structure serves as a critical node in multiple network pathways, playing executive and supporting roles in several behavioral domains. Along with the prefrontal cortex, the basal ganglia appear to exert attention-related modulation of working memory related function (Herrero et al., 2002; McNab and Klingberg, 2008). The thalamus is considered a principle gateway to the cortex (McAlonan et al., 2008), engaged in filtering of massive sensory inputs, particularly in the visual domain, and sending extensive outputs to cortical and sub-cortical regions (Haber and Calzavara, 2009). The structure also plays essential computational roles by integrating network activity essential for modulating behaviors. Many of the psychological domains that are underpinned by regional function are implicated in OCD. Thus pediatric OCD patients in particular show deficits in sustained attention (Lucke et al., 2014), executive function and working memory (Melloni et al., 2012), and cognitive control and metacognition (Koch and Exner, 2015). It is therefore not surprising that frontal, striatal, and thalamic circuits have been identified as central to potential interventions in OCD (Burguiere et al., 2015).

HYPER-*ACTIVATION* IN OCD DURING WORKING MEMORY: POSSIBLE MECHANISMS AND RELATIONSHIP WITH OTHER DISORDERS

Though working memory deficits are generally seen as secondary to the core pathology of OCD (Harkin and Kessler, 2011), our activation results provide good convergence with recent reports. Memory load-related hyper-activation in frontal-parietal regions has been proposed as an intermediate phenotype for OCD, where the hyper-activation has been labeled as compensatory (Nakao et al., 2009; Koch et al., 2012; de Vries et al., 2013). Effects on dACC activation have, however, been equivocal; previous studies have shown a reverse effect of complexity on dACC activation in OCD, with disengagement of the structure following load related effects. Nevertheless, our results provide good conceptual overlap with studies in pathology that have linked hyper-activation under conditions of task compliance with regional efficiency. This concept of inefficiency finds pronounced expression in the schizophrenia spectrum, where disease-related effects (that have been associated with dopamine dysfunction) are presumed to affect the "duty cycle" of task-relevant brain regions including the prefrontal cortex and the striatum (Callicott et al., 2003; Manoach, 2003; Jansma et al., 2004; Meisenzahl et al., 2007; Diwadkar et al., 2012). These inefficiencies might imply that neuronal pools (that form one electrophysiological origin of the fMRI signal) (Logothetis and Wandell, 2004) engage in excess excitatory firing responses when demand is exerted on FSTC. Moreover, inefficiencies provide a window into the "scalability" of brain regions in response to demand. In other words, the functioning limits of FSTC in OCD may be compromised such that excessive cognitive demand may stretch FSTC ability to sub-serve function. In this view, FSTC hyper-activation during working memory far, from being a peripheral correlate of OCD, is a central mechanism underlying the illness, and a primary intermediate phenotype as previously proposed (de Vries et al., 2013).

A parallel explanation for hyper-activity is that it reflects glutamate-related dysfunction that affects how relevant regions are recruited for a task (Wu et al., 2012, 2013; Stewart et al., 2013; Pauls et al., 2014). As a principle excitatory neurotransmitter,

Table 4 | The table provides information regarding clusters of significant and significant peaks showing *dysfunctional network profiles* in OCD (compared to HC) at each level of memory load (Figure 4).

Region	Brodmann area	MNI coordinates (*x, y, z*)			*Z* score	Cluster extent	*p* (peak]
Table 4: PPI							
$OCD_{1Back} > HC_{1Back}$							
Parietal lobe	7	20	−57	60	3.36	529	0.000
Mid frontal gyrus	6	−32	−6	54	3.13	144	0.001
Basal ganglia	–	20	9	15	3	61	0.001
$OCD_{2Back} > HC_{2Back}$							
Parietal lobe	7	−18	−36	48	2.72	223	0.003
Dorsal prefrontal cortex	9	−12	36	22	2.76	89	0.003

glutamate exerts substantial effects on brain function, particularly in the excitatory model. Glutamate dysfunction in OCD can alter the neurochemical-electrophysiological relationship that sub-serves BOLD-based activation. A more complete assessment of the Glutamate-fMRI relationship will require assessment of both classes of signals acquired within subjects. This is an ongoing endeavor in our studies that involves multi-modal acquisition of fMRI and MRS data within subjects.

HYPER-MODULATION OF FSTC BY THE dACC: NOVEL EVIDENCE OF DYSFUNCTIONAL NETWORK PROFILES

Relatively few studies have assessed connectivity in the task-active state in OCD. Psychophysiological interactions provide a straightforward model of directional effects of seed regions on their targets in a task-related context, providing a window into network interactions. This window is considered intermediate between functional and effective connectivity (Friston, 2011). The interpretations of PPI are constrained by the choice of seeds and the hypothesized role(s) ascribed to the seed. Toward that end, our choice of the dACC was motivated by its role in cognitive control of brain networks (Carter et al., 1999; Paus, 2001; Bakshi et al., 2011).

The dACC plays an integral role in tasks of explicit cognitive control including response conflict and response monitoring (Braver et al., 2001; van Veen et al., 2001), and choice selection (Eshel et al., 2007). The dACC may serve to amplify task-relevant signals to heteromodal association regions of the cortex (Egner and Hirsch, 2005; Sohn et al., 2007). Thus, control processes from the dACC may influence the activity of core working memory systems, and the degree of this modulation may reflect the efficiency of interaction between control and working memory systems. Increased control-related modulation in part reflects decreased efficiency. This hyper-modulation by the dACC may strongly suggest inefficient control-related network profiles in OCD. These effects are again consistent with observed evidence in other disorders, for example, in the schizophrenia spectrum where increased dACC related modulation is strongly associated with the illness and risk for the illness (Bakshi et al., 2011). The absence of a parametric effect on dACC modulation appears related to highly increased aberrant dACC modulation at the lower level of demand in OCD: no intra-group increases in dACC modulation were observed in OCD as memory load increases. As such, the network effects constitute complementary signatures of FSTC dysfunction in OCD.

LIMITATIONS AND CONCLUSION

Brain network profiles will constitute an important frontier in the search for mechanisms and endophenotypes, and their evidence is an important expression of the goals advocated by Research Domain Criteria (RDoC: Insel et al., 2010). While our sample size (though small) is comparable to several other published studies, it nevertheless precludes us from assessing the role of co-morbid diagnoses and medication effects within OCD youth. These are important clinical questions, and an expansion of this sample is ongoing, and may permit more detailed assessment of our observed effects.

The specific neurochemical and molecular bases of these effects are obscured by the interpretational limits of both the fMRI signal (Logothetis, 2008) that cannot distinguish between a multiplicity of neuronal contributions to the hemodynamic response, and by the relatively limited class of inferences that can be drawn from the application of PPI analyses (Stephan, 2004). Moreover, these technical challenges are compounded by the fundamental limitation in understanding the correlates of brain structure and function: the fact that functional characteristics of brain networks exist in a regressive relationship with their structural substrates (Park and Friston, 2013). Thus, the same underlying structural networks can give rise to a multiplicity of functions and dysfunctions. Nevertheless, our results (and other studies we have cited) promise to reveal mechanisms of disease-related dysfunction as expressed in brain profiles. An understanding of putative mechanisms is a necessary precursor of treatment and cure. Therefore we propose that studies such as ours (and future extensions) will provide better elucidation of disease mechanisms than currently exist.

ACKNOWLEDGMENTS

This work was supported by the National Institute of Mental Health (MH059299), the Children's Hospital of Michigan Foundation, the Prechter World Bipolar Foundation, the Lyckaki-Young Fund from the State of Michigan, the Miriam Hamburger Endowed Chair of Child Psychiatry, the Paul and Anita Strauss Endowment, the Donald and Mary Kosch Foundation, Detroit Wayne County Authority, and Gateway Community Health. The funding agencies played no role in the analyses or reporting of the data.

REFERENCES

Almeida, J. R., Versace, A., Mechelli, A., Hassel, S., Quevedo, K., Kupfer, D. J., et al. (2009). Abnormal amygdala-prefrontal effective connectivity to happy faces differentiates bipolar from major depression. *Biol. Psychiatry* 66, 451–459. doi:10.1016/j.biopsych.2009.03.024

Anderson, J. R., Fincham, J. M., Qin, Y., and Stocco, A. (2008). A central circuit of the mind. *Trends Cogn. Sci.* 12, 136–143. doi:10.1016/j.tics.2008.01.006

Apter, A., Fallon, T. J. Jr., King, R. A., Ratzoni, G., Zohar, A. H., Binder, M., et al. (1996). Obsessive-compulsive characteristics: from symptoms to syndrome. *J. Am. Acad. Child Adolesc. Psychiatry* 35, 907–912. doi:10.1097/00004583-199607000-00016

Bakshi, N., Pruitt, P., Radwan, J., Keshavan, M. S., Rajan, U., Zajac-Benitez, C., et al. (2011). Inefficiently increased anterior cingulate modulation of cortical systems during working memory in young offspring of schizophrenia patients. *J. Psychiatr. Res.* 45, 1067–1076. doi:10.1016/j.jpsychires.2011.01.002

Bari, A., and Robbins, T. W. (2013). Inhibition and impulsivity: behavioral and neural basis of response control. *Prog. Neurobiol.* 108, 44–79. doi:10.1016/j.pneurobio.2013.06.005

Berg, C. Z., Whitaker, A., Davies, M., Flament, M. F., and Rapoport, J. L. (1988). The survey form of the Leyton obsessional inventory-child version: norms from an epidemiological study. *J. Am. Acad. Child Adolesc. Psychiatry* 27, 759–763. doi:10.1097/00004583-198811000-00017

Braver, T. S., Barch, D. M., Gray, J. R., Molfese, D. L., and Snyder, A. (2001). Anterior cingulate cortex and response conflict: effects of frequency, inhibition and errors. *Cereb. Cortex* 11, 825–836. doi:10.1093/cercor/11.9.825

Braver, T. S., Cohen, J. D., Nystrom, L. E., Jonides, J., Smith, E. E., and Noll, D. C. (1997). A parametric study of prefrontal cortex involvement in human working memory. *Neuroimage* 5, 49–62. doi:10.1006/nimg.1996.0247

Briggs, F., and Usrey, W. M. (2008). Emerging views of corticothalamic function. *Curr. Opin. Neurobiol.* 18, 403–407. doi:10.1016/j.conb.2008.09.002

Burguiere, E., Monteiro, P., Mallet, L., Feng, G., and Graybiel, A. M. (2015). Striatal circuits, habits, and implications for obsessive-compulsive disorder. *Curr. Opin. Neurobiol.* 30C, 59–65. doi:10.1016/j.conb.2014.08.008

Callicott, J. H., Egan, M. F., Mattay, V. S., Bertolino, A., Bone, A. D., Verchinksi, B., et al. (2003). Abnormal fMRI response of the dorsolateral prefrontal cortex in cognitively intact siblings of patients with schizophrenia. *Am. J. Psychiatry* 160, 709–719. doi:10.1176/appi.ajp.160.4.709

Calzavara, R., Mailly, P., and Haber, S. N. (2007). Relationship between the corticostriatal terminals from areas 9 and 46, and those from area 8A, dorsal and rostral premotor cortex and area 24c: an anatomical substrate for cognition to action. *Eur. J. Neurosci.* 26, 2005–2024. doi:10.1111/j.1460-9568.2007.05825.x

Carter, C. S., Botvinick, M. M., and Cohen, J. D. (1999). The contribution of the anterior cingulate cortex to executive processes in cognition. *Rev. Neurosci.* 10, 49–57. doi:10.1515/REVNEURO.1999.10.1.49

Casey, B. J., Cohen, J. D., Jezzard, P., Turner, R., Noll, D. C., Trainor, R. J., et al. (1995). Activation of prefrontal cortex in children during a nonspatial working memory task with functional MRI. *Neuroimage* 2, 221–229. doi:10.1006/nimg.1995.1029

Cohen, J. D., Perlstein, W. M., Braver, T. S., Nystrom, L. E., Noll, D. C., Jonides, J., et al. (1997). Temporal dynamics of brain activation during a working memory task. *Nature* 386, 604–608. doi:10.1038/386604a0

Crowe, D. A., Goodwin, S. J., Blackman, R. K., Sakellaridi, S., Sponheim, S. R., Macdonald, A. W. III, et al. (2013). Prefrontal neurons transmit signals to parietal neurons that reflect executive control of cognition. *Nat. Neurosci.* 16, 1484–1491. doi:10.1038/nn.3509

de Vries, F. E., De Wit, S. J., Cath, D. C., Van Der Werf, Y. D., Van Der Borden, V., Van Rossum, T. B., et al. (2013). Compensatory frontoparietal activity during working memory: an endophenotype of obsessive-compulsive disorder. *Biol. Psychiatry* 76, 878–887. doi:10.1016/j.biopsych.2013.11.021

Diwadkar, V. A. (2012). Adolescent risk pathways toward schizophrenia: sustained attention and the brain. *Curr. Top. Med. Chem.* 12, 2339–2347. doi:10.2174/156802612805289962

Diwadkar, V. A., Bakshi, N., Gupta, G., Pruitt, P., White, R., and Eickhoff, S. B. (2014). Dysfunction and dysconnection in cortical-striatal networks during sustained attention: genetic risk for schizophrenia or bipolar disorder and its impact on brain network function. *Front. Psychiatry* 5:50. doi:10.3389/fpsyt.2014.00050

Diwadkar, V. A., Carpenter, P. A., and Just, M. A. (2000). Collaborative activity between parietal and dorso-lateral prefrontal cortex in dynamic spatial working memory revealed by fMRI. *Neuroimage* 12, 85–99. doi:10.1006/nimg.2000.0586

Diwadkar, V. A., Meintjes, E. M., Goradia, D., Dodge, N. C., Warton, C., Molteno, C. D., et al. (2013). Differences in cortico-striatal-cerebellar activation during working memory in syndromal and nonsyndromal children with prenatal alcohol exposure. *Hum. Brain Mapp.* 34, 1931–1945. doi:10.1002/hbm.22042

Diwadkar, V. A., Pruitt, P., Goradia, D., Murphy, E., Bakshi, N., Keshavan, M. S., et al. (2011). Fronto-parietal hypo-activation during working memory independent of structural abnormalities: conjoint fMRI and sMRI analyses in adolescent offspring of schizophrenia patients. *Neuroimage* 58, 234–241. doi:10.1016/j.neuroimage.2011.06.033

Diwadkar, V. A., Pruitt, P., Zhang, A., Radwan, J., Keshavan, M. S., Murphy, E., et al. (2012). The neural correlates of performance in adolescents at risk for schizophrenia: inefficiently increased cortico-striatal responses measured with fMRI. *J. Psychiatr. Res.* 46, 12–21. doi:10.1016/j.jpsychires.2011.09.016

Egner, T., and Hirsch, J. (2005). Cognitive control mechanisms resolve conflict through cortical amplification of task-relevant information. *Nat. Neurosci.* 8, 1784–1790. doi:10.1038/nn1594

Eshel, N., Nelson, E. E., Blair, R. J., Pine, D. S., and Ernst, M. (2007). Neural substrates of choice selection in adults and adolescents: development of the ventrolateral prefrontal and anterior cingulate cortices. *Neuropsychologia* 45, 1270–1279. doi:10.1016/j.neuropsychologia.2006.10.004

Fan, J., Mccandliss, B. D., Fossella, J., Flombaum, J. I., and Posner, M. I. (2005). The activation of attentional networks. *Neuroimage* 26, 471–479. doi:10.1016/j.neuroimage.2005.02.004

Fitzgerald, K. D., Welsh, R. C., Gehring, W. J., Abelson, J. L., Himle, J. A., Liberzon, I., et al. (2005). Error-related hyperactivity of the anterior cingulate cortex in obsessive-compulsive disorder. *Biol. Psychiatry* 57, 287–294. doi:10.1016/j.biopsych.2004.10.038

Fitzgerald, K. D., Welsh, R. C., Stern, E. R., Angstadt, M., Hanna, G. L., Abelson, J. L., et al. (2011). Developmental alterations of frontal-striatal-thalamic connectivity in obsessive-compulsive disorder. *J. Am. Acad. Child Adolesc. Psychiatry* 50, e933. doi:10.1016/j.jaac.2011.06.011

Friston, K. J. (1998). The disconnection hypothesis. *Schizophr. Res.* 30, 115–125. doi:10.1016/S0920-9964(97)00140-0

Friston, K. J. (2011). Functional and effective connectivity: a review. *Brain Connect.* 1, 13–36. doi:10.1089/brain.2011.0008

Friston, K. J., Buechel, C., Fink, G. R., Morris, J., Rolls, E., and Dolan, R. J. (1997). Psychophysiological and modulatory interactions in neuroimaging. *Neuroimage* 6, 218–229. doi:10.1006/nimg.1997.0291

Funahashi, S., and Andreau, J. M. (2013). Prefrontal cortex and neural mechanisms of executive function. *J. Physiol. Paris* 107, 471–482. doi:10.1016/j.jphysparis.2013.05.001

Goodman, W. K., Price, L. H., Rasmussen, S. A., Mazure, C., Delgado, P., Heninger, G. R., et al. (1989). The Yale-Brown obsessive compulsive scale. II. Validity. *Arch. Gen. Psychiatry* 46, 1012–1016. doi:10.1001/archpsyc.1989.01810110048007

Haber, S. N., and Calzavara, R. (2009). The cortico-basal ganglia integrative network: the role of the thalamus. *Brain Res. Bull.* 78, 69–74. doi:10.1016/j.brainresbull.2008.09.013

Harkin, B., and Kessler, K. (2011). The role of working memory in compulsive checking and OCD: a systematic classification of 58 experimental findings. *Clin. Psychol. Rev.* 31, 1004–1021. doi:10.1016/j.cpr.2011.06.004

Harrison, B. J., Soriano-Mas, C., Pujol, J., Ortiz, H., Lopez-Sola, M., Hernandez-Ribas, R., et al. (2009). Altered corticostriatal functional connectivity in obsessive-compulsive disorder. *Arch. Gen. Psychiatry* 66, 1189–1200. doi:10.1001/archgenpsychiatry.2009.152

Hazy, T. E., Frank, M. J., and O'reilly, R. C. (2006). Banishing the homunculus: making working memory work. *Neuroscience* 139, 105–118. doi:10.1016/j.neuroscience.2005.04.067

Herrero, M. T., Barcia, C., and Navarro, J. M. (2002). Functional anatomy of thalamus and basal ganglia. *Childs Nerv. Syst.* 18, 386–404. doi:10.1007/s00381-002-0604-1

Honey, G. D., Pomarol-Clotet, E., Corlett, P. R., Honey, R. A., Mckenna, P. J., Bullmore, E. T., et al. (2005). Functional dysconnectivity in schizophrenia associated with attentional modulation of motor function. *Brain* 128, 2597–2611. doi:10.1093/brain/awh632

Huyser, C., Veltman, D. J., Wolters, L. H., De Haan, E., and Boer, F. (2011). Developmental aspects of error and high-conflict-related brain activity in pediatric

obsessive-compulsive disorder: a fMRI study with a Flanker task before and after CBT. *J. Child Psychol. Psychiatry* 52, 1251–1260. doi:10.1111/j.1469-7610.2011.02439.x

Insel, T., Cuthbert, B., Garvey, M., Heinssen, R., Pine, D. S., Quinn, K., et al. (2010). Research domain criteria (RDoC): toward a new classification framework for research on mental disorders. *Am. J. Psychiatry* 167, 748–751. doi:10.1176/appi.ajp.2010.09091379

Jansma, J. M., Ramsey, N. F., Van Der Wee, N. J., and Kahn, R. S. (2004). Working memory capacity in schizophrenia: a parametric fMRI study. *Schizophr. Res.* 68, 159–171. doi:10.1016/S0920-9964(03)00127-0

Kaufman, J., Birmaher, B., Brent, D., Rao, U., Flynn, C., Moreci, P., et al. (1997). Schedule for affective disorders and schizophrenia for school-age children-present and lifetime version (K-SADS-PL): initial reliability and validity data. *J. Am. Acad. Child Adolesc. Psychiatry* 36, 980–988. doi:10.1097/00004583-199707000-00021

Klein, J. C., Rushworth, M. F., Behrens, T. E., Mackay, C. E., De Crespigny, A. J., D'arceuil, H., et al. (2010). Topography of connections between human prefrontal cortex and mediodorsal thalamus studied with diffusion tractography. *Neuroimage* 51, 555–564. doi:10.1016/j.neuroimage.2010.02.062

Koch, J., and Exner, C. (2015). Selective attention deficits in obsessive-compulsive disorder: the role of metacognitive processes. *Psychiatry Res.* 225, 550–555. doi:10.1016/j.psychres.2014.11.049

Koch, K., Wagner, G., Schachtzabel, C., Peikert, G., Schultz, C. C., Sauer, H., et al. (2012). Aberrant anterior cingulate activation in obsessive-compulsive disorder is related to task complexity. *Neuropsychologia* 50, 958–964. doi:10.1016/j.neuropsychologia.2012.02.002

Langner, R., and Eickhoff, S. B. (2013). Sustaining attention to simple tasks: a meta-analytic review of the neural mechanisms of vigilant attention. *Psychol. Bull.* 139, 870–900. doi:10.1037/a0030694

Li, W., Qin, W., Liu, H., Fan, L., Wang, J., Jiang, T., et al. (2013). Subregions of the human superior frontal gyrus and their connections. *Neuroimage* 78, 46–58. doi:10.1016/j.neuroimage.2013.04.011

Logothetis, N. K. (2008). What we can do and what we cannot do with fMRI. *Nature* 453, 869–878. doi:10.1038/nature06976

Logothetis, N. K., and Wandell, B. A. (2004). Interpreting the BOLD signal. *Annu. Rev. Physiol.* 66, 735–769. doi:10.1146/annurev.physiol.66.082602.092845

Lucke, I. M., Lin, C., Conteh, F., Federline, A., Sung, H., Specht, M., et al. (2014). Continuous performance test in pediatric obsessive-compulsive disorder and tic disorders: the role of sustained attention. *CNS Spectr.* 1–11. doi:10.1017/S1092852914000467

Maldjian, J. A., Laurienti, P. J., Kraft, R. A., and Burdette, J. H. (2003). An automated method for neuroanatomic and cytoarchitectonic atlas-based interrogation of fMRI data sets. *Neuroimage* 19, 1233–1239. doi:10.1016/S1053-8119(03)00169-1

Maltby, N., Tolin, D. F., Worhunsky, P., O'keefe, T. M., and Kiehl, K. A. (2005). Dysfunctional action monitoring hyperactivates frontal-striatal circuits in obsessive-compulsive disorder: an event-related fMRI study. *Neuroimage* 24, 495–503. doi:10.1016/j.neuroimage.2004.08.041

Manoach, D. S. (2003). Prefrontal cortex dysfunction during working memory performance in schizophrenia: reconciling discrepant findings. *Schizophr. Res.* 60, 285–298. doi:10.1016/S0920-9964(02)00294-3

Marsh, R., Horga, G., Parashar, N., Wang, Z., Peterson, B. S., and Simpson, H. B. (2014). Altered activation in fronto-striatal circuits during sequential processing of conflict in unmedicated adults with obsessive-compulsive disorder. *Biol. Psychiatry* 75, 615–622. doi:10.1016/j.biopsych.2013.02.004

McAlonan, K., Cavanaugh, J., and Wurtz, R. H. (2008). Guarding the gateway to cortex with attention in visual thalamus. *Nature* 456, 391–394. doi:10.1038/nature07382

McNab, F., and Klingberg, T. (2008). Prefrontal cortex and basal ganglia control access to working memory. *Nat. Neurosci.* 11, 103–107. doi:10.1038/nn2024

Meisenzahl, E. M., Schmitt, G. J., Scheuerecker, J., and Moller, H. J. (2007). The role of dopamine for the pathophysiology of schizophrenia. *Int. Rev. Psychiatry* 19, 337–345. doi:10.1080/09540260701502468

Melloni, M., Urbistondo, C., Sedeno, L., Gelormini, C., Kichic, R., and Ibanez, A. (2012). The extended fronto-striatal model of obsessive compulsive disorder: convergence from event-related potentials, neuropsychology and neuroimaging. *Front. Hum. Neurosci.* 6:259. doi:10.3389/fnhum.2012.00259

Nakao, T., Nakagawa, A., Nakatani, E., Nabeyama, M., Sanematsu, H., Yoshiura, T., et al. (2009). Working memory dysfunction in obsessive-compulsive disorder: a neuropsychological and functional MRI study. *J. Psychiatr. Res.* 43, 784–791. doi:10.1016/j.jpsychires.2008.10.013

O'Reilly, J. X., Woolrich, M. W., Behrens, T. E., Smith, S. M., and Johansen-Berg, H. (2012). Tools of the trade: psychophysiological interactions and functional connectivity. *Soc. Cogn. Affect. Neurosci.* 7, 604–609. doi:10.1093/scan/nss055

Owen, A. M., Mcmillan, K. M., Laird, A. R., and Bullmore, E. (2005). N-back working memory paradigm: a meta-analysis of normative functional neuroimaging studies. *Hum. Brain Mapp.* 25, 46–59. doi:10.1002/hbm.20131

Palomero-Gallagher, N., Mohlberg, H., Zilles, K., and Vogt, B. (2008). Cytology and receptor architecture of human anterior cingulate cortex. *J. Comp. Neurol.* 508, 906–926. doi:10.1002/cne.21684

Park, H. J., and Friston, K. (2013). Structural and functional brain networks: from connections to cognition. *Science* 342, 1238411. doi:10.1126/science.1238411

Pauls, D. L., Abramovitch, A., Rauch, S. L., and Geller, D. A. (2014). Obsessive-compulsive disorder: an integrative genetic and neurobiological perspective. *Nat. Rev. Neurosci.* 15, 410–424. doi:10.1038/nrn3746

Paus, T. (2001). Primate anterior cingulate cortex: where motor control, drive and cognition interface. *Nat. Rev. Neurosci.* 2, 417–424. doi:10.1038/35077500

Paus, T., Keshavan, M., and Giedd, J. N. (2008). Why do many psychiatric disorders emerge during adolescence? *Nat. Rev. Neurosci.* 9, 947–957. doi:10.1038/nrn2513

Peng, Z., Shi, F., Shi, C., Yang, Q., Chan, R. C., and Shen, D. (2014). Disrupted cortical network as a vulnerability marker for obsessive-compulsive disorder. *Brain Struct. Funct.* 219, 1801–1812. doi:10.1007/s00429-013-0602-y

Piras, F., Piras, F., Caltagirone, C., and Spalletta, G. (2013). Brain circuitries of obsessive compulsive disorder: a systematic review and meta-analysis of diffusion tensor imaging studies. *Neurosci. Biobehav. Rev.* 37, 2856–2877. doi:10.1016/j.neubiorev.2013.10.008

Ragsdale, C. W. Jr., and Graybiel, A. M. (1990). A simple ordering of neocortical areas established by the compartmental organization of their striatal projections. *Proc. Natl. Acad. Sci. U.S.A.* 87, 6196–6199. doi:10.1073/pnas.87.16.6196

Ray, J. P., and Price, J. L. (1993). The organization of projections from the mediodorsal nucleus of the thalamus to orbital and medial prefrontal cortex in macaque monkeys. *J. Comp. Neurol.* 337, 1–31. doi:10.1002/cne.903370102

Rehme, A. K., Eickhoff, S. B., and Grefkes, C. (2013). State-dependent differences between functional and effective connectivity of the human cortical motor system. *Neuroimage* 67, 237–246. doi:10.1016/j.neuroimage.2012.11.027

Rosenberg, D. R., Macmaster, F. P., Keshavan, M. S., Fitzgerald, K. D., Stewart, C. M., and Moore, G. J. (2000). Decrease in caudate glutamatergic concentrations in pediatric obsessive - compulsive disorder patients taking paroxetine. *J. Am. Acad. Child Adolesc. Psychiatry* 39, 1096–1103. doi:10.1097/00004583-200009000-00008

Rosenberg, D. R., Mirza, Y., Russell, A., Tang, J., Smith, J. M., Banerjee, S. P., et al. (2004). Reduced anterior cingulate glutamatergic concentrations in childhood OCD and major depression versus healthy controls. *J. Am. Acad. Child Adolesc. Psychiatry* 43, 1146–1153. doi:10.1097/01.chi.0000132812.44664.2d

Scahill, L., Riddle, M. A., Mcswiggin-Hardin, M., Ort, S. I., King, R. A., Goodman, W. K., et al. (1997). Children's Yale-Brown obsessive compulsive scale: reliability and validity. *J. Am. Acad. Child Adolesc. Psychiatry* 36, 844–852. doi:10.1097/00004583-199706000-00023

Schmidt, A., Smieskova, R., Aston, J., Simon, A., Allen, P., Fusar-Poli, P., et al. (2013). Brain connectivity abnormalities predating the onset of psychosis: correlation with the effect of medication. *JAMA Psychiatry* 70, 903–912. doi:10.1001/jamapsychiatry.2013.117

Shaw, M. E., Moores, K. A., Clark, R. C., Mcfarlane, A. C., Strother, S. C., Bryant, R. A., et al. (2009). Functional connectivity reveals inefficient working memory systems in post-traumatic stress disorder. *Psychiatry Res.* 172, 235–241. doi:10.1016/j.pscychresns.2008.07.014

Sohn, M. H., Albert, M. V., Jung, K., Carter, C. S., and Anderson, J. R. (2007). Anticipation of conflict monitoring in the anterior cingulate cortex and the prefrontal cortex. *Proc. Natl. Acad. Sci. U.S.A.* 104, 10330–10334. doi:10.1073/pnas.0703225104

Stephan, K. E. (2004). On the role of general system theory for functional neuroimaging. *J. Anat.* 205, 443–470. doi:10.1111/j.0021-8782.2004.00359.x

Stephan, K. E., Baldeweg, T., and Friston, K. J. (2006). Synaptic plasticity and dysconnection in schizophrenia. *Biol. Psychiatry* 59, 929–939. doi:10.1016/j.biopsych.2005.10.005

Stewart, S. E., Mayerfeld, C., Arnold, P. D., Crane, J. R., O'dushlaine, C., Fagerness, J. A., et al. (2013). Meta-analysis of association between obsessive-compulsive disorder and the 3' region of neuronal glutamate transporter gene SLC1A1. *Am. J. Med. Genet. B Neuropsychiatr. Genet.* 162b, 367–379. doi:10.1002/ajmg.b.32137

Tottenham, N., and Sheridan, M. A. (2009). A review of adversity, the amygdala and the hippocampus: a consideration of developmental timing. *Front. Hum. Neurosci.* 3:68. doi:10.3389/neuro.09.068.2009

Valleni-Basile, L. A., Garrison, C. Z., Waller, J. L., Addy, C. L., Mckeown, R. E., Jackson, K. L., et al. (1996). Incidence of obsessive-compulsive disorder in a community sample of young adolescents. *J. Am. Acad. Child Adolesc. Psychiatry* 35, 898–906. doi:10.1097/00004583-199607000-00015

van Veen, V., Cohen, J. D., Botvinick, M. M., Stenger, V. A., and Carter, C. S. (2001). Anterior cingulate cortex, conflict monitoring, and levels of processing. *Neuroimage* 14, 1302–1308. doi:10.1006/nimg.2001.0923

Vijayraghavan, S., Wang, M., Birnbaum, S. G., Williams, G. V., and Arnsten, A. F. (2007). Inverted-U dopamine D1 receptor actions on prefrontal neurons engaged in working memory. *Nat. Neurosci.* 10, 376–384. doi:10.1038/nn1846

Voytek, B., and Knight, R. T. (2010). Prefrontal cortex and basal ganglia contributions to visual working memory. *Proc. Natl. Acad. Sci. U.S.A.* 107, 18167–18172. doi:10.1073/pnas.1007277107

Ward, B. D. (2000). *Simultaneous Inference for fMRI Data.* Milwaukee, WI: Medical College of Wisconsin.

Wolff, R. P., and Wolff, L. S. (1991). Assessment and treatment of obsessive-compulsive disorder in children. *Behav. Modif.* 15, 372–393. doi:10.1177/01454455910153006

Wu, K., Hanna, G. L., Easter, P., Kennedy, J. L., Rosenberg, D. R., and Arnold, P. D. (2013). Glutamate system genes and brain volume alterations in pediatric obsessive-compulsive disorder: a preliminary study. *Psychiatry Res.* 211, 214–220. doi:10.1016/j.pscychresns.2012.07.003

Wu, K., Hanna, G. L., Rosenberg, D. R., and Arnold, P. D. (2012). The role of glutamate signaling in the pathogenesis and treatment of obsessive-compulsive disorder. *Pharmacol. Biochem. Behav.* 100, 726–735. doi:10.1016/j.pbb.2011.10.007

Conflict of Interest Statement: The authors declare that the research was conducted in the absence of any commercial or financial relationships that could be construed as a potential conflict of interest.

Received: 12 November 2014; accepted: 03 March 2015; published online: 17 March 2015.

Citation: Diwadkar VA, Burgess A, Hong E, Rix C, Arnold PD, Hanna GL and Rosenberg DR (2015) Dysfunctional activation and brain network profiles in youth with obsessive-compulsive disorder: a focus on the dorsal anterior cingulate during working memory. Front. Hum. Neurosci. ***9****:149. doi: 10.3389/fnhum.2015.00149*

This article was submitted to the journal Frontiers in Human Neuroscience.

frontiers in Human Neuroscience

ORIGINAL RESEARCH
published: 07 September 2016
doi: 10.3389/fnhum.2016.00447

Altered Effective Connectivity among Core Neurocognitive Networks in Idiopathic Generalized Epilepsy: An fMRI Evidence

Huilin Wei[1], Jie An[2†], Hui Shen[1], Ling-Li Zeng[1], Shijun Qiu[2] and Dewen Hu[1*]*

[1] Department of Automatic Control, College of Mechatronics and Automation, National University of Defense Technology, Changsha, China, [2] Department of Medical Imaging, The First Affiliated Hospital of Guangzhou University of Chinese Medicine, Guangzhou, China

Idiopathic generalized epilepsy (IGE) patients with generalized tonic-clonic seizures (GTCS) suffer long-term cognitive impairments, and present a higher incidence of psychosocial and psychiatric disturbances than healthy people. It is possible that the cognitive dysfunctions and higher psychopathological risk in IGE-GTCS derive from disturbed causal relationship among core neurocognitive brain networks. To test this hypothesis, we examined the effective connectivity across the salience network (SN), default mode network (DMN), and central executive network (CEN) using resting-state functional magnetic resonance imaging (fMRI) data collected from 27 IGE-GTCS patients and 29 healthy controls. In the study, a combination framework of time domain and frequency domain multivariate Granger causality analysis was firstly proposed, and proved to be valid and accurate by simulation experiments. Using this method, we then observed significant differences in the effective connectivity graphs between the patient and control groups. Specifically, between-group statistical analysis revealed that relative to the healthy controls, the patients established significantly enhanced Granger causal influence from the dorsolateral prefrontal cortex to the dorsal anterior cingulate cortex, which is coherent both in the time and frequency domains analyses. Meanwhile, time domain analysis also revealed decreased Granger causal influence from the right fronto-insular cortex to the posterior cingulate cortex in the patients. These findings may provide new evidence for functional brain organization disruption underlying cognitive dysfunctions and psychopathological risk in IGE-GTCS.

Keywords: idiopathic generalized epilepsy, resting-state fMRI, effective connectivity, multivariate Granger causality, core neurocognitive networks

OPEN ACCESS

Edited by:
Adeel Razi,
Wellcome Trust Centre for Neuroimaging, UK

Reviewed by:
Hao He,
Mind Research Network, USA
Yuhui Du,
Mind Research Network, USA

***Correspondence:**
Shijun Qiu
qiu-sj@163.com
Dewen Hu
dwhu@nudt.edu.cn

† Co-first author.

***Received:** 29 April 2016*
***Accepted:** 22 August 2016*
***Published:** 07 September 2016*

Citation:
Wei H, An J, Shen H, Zeng L-L, Qiu S and Hu D (2016) Altered Effective Connectivity among Core Neurocognitive Networks in Idiopathic Generalized Epilepsy: An fMRI Evidence. Front. Hum. Neurosci. 10:447. doi: 10.3389/fnhum.2016.00447

INTRODUCTION

Previous studies have revealed that patients with epilepsy suffer a higher incidence of psychosocial and psychiatric disturbances than healthy people (Mignone et al., 1970; Baker et al., 1996; Cutting et al., 2001; Gelisse et al., 2007). Idiopathic generalized epilepsy (IGE) is the most common type of epilepsy, which can be characterized by electroencephalography (EEG) recordings with generalized spike-and-waves or polyspike-waves (Engel, 2001; Hamandi et al., 2006). As one of the IGE subtypes, IGE patients with generalized tonic-clonic seizures

(IGE-GTCS) suffer various neuropsychological impairments such as deficits in working memory, sustained attention, language, as well as executive functions (Hommet et al., 2006; Chowdhury et al., 2014). Prior studies have suggested that disruptions to these higher-order control processes may constitute a key aspect of psychopathology (Sridharan et al., 2008; Menon and Uddin, 2010). Therefore, distinguishing dysfunctional brain architecture may provide greater insight into the psychopathology in IGE-GTCS.

In recent years, identifying disturbed dynamic interactions of large-scale brain networks associated with cognitive and affective dysfunctions has shed new lights on the study of psychopathology. Of the many spatially distinct and functionally specialized stable brain networks, three have tended to be particularly crucial for understanding higher-order cognitive and perceptive processes thus described as core neurocognitive networks, they are: (1) the salience network (SN), involved in conflict monitoring, attention, as well as interoceptive and affective processes; (2) the default mode network (DMN), related to self-referential and social cognitive processes; and (3) the central executive network (CEN), associated with working memory, cognitive control implementation, and decision making in goal-directed behavior (Menon, 2011). Moreover, each of the three core neurocognitive networks are anchored in some key nodes that show strong intrinsic functional coupling as well as co-activation across different cognitively demanding tasks (Sridharan et al., 2008; Menon and Uddin, 2010). These key nodes are: (1) the right fronto-insular cortex (rFIC) and the dorsal anterior cingulate cortex (dACC) of the SN; (2) the ventromedial pre-frontal cortex (VMPFC) and the posterior cingulate cortex (PCC) of the DMN; as well as (3) the dorsolateral pre-frontal cortex (DLPFC) and the posterior parietal cortex (PPC) of the CEN. Particularly, the two key nodes of the SN have been highlighted in numerous researches, suggesting that the rFIC is crucial for initiating network switching between the CEN and the DMN (Sridharan et al., 2008; Menon and Uddin, 2010; Uddin et al., 2011), and the dACC most closely associated with conflict monitoring to mediate higher-order cognitive processes (Botvinick et al., 2004; Menon, 2011). Investigating disruptions to functional dynamics among these key nodes is beginning to identify an important aspect of dysfunctions in psychopathology, thus the three core neurocognitive networks represented by the associated key nodes have been concluded as a "triple network" model (Menon, 2011). Aberrant interconnectivity and intrinsic organization of the triple network is characteristic of various neurological and psychiatric disorders, such as schizophrenia, depression, anxiety disorders and autism (Paulus and Stein, 2006; Walter et al., 2009; White et al., 2010; Uddin et al., 2015), and is likely to provide better understanding of fundamental brain mechanisms underlying cognitive dysfunctions and psychopathology in IGE-GTCS.

Measurement of causal influence that a system exerts over one other is called effective connectivity (Friston et al., 1993). Applying effective connectivity to brain network analysis can obtain full understanding of the network interaction structure including the strength and direction of information flow between brain regions. Granger causality analysis, as an important analytical technique of effective connectivity, has been widely applied in cognitive neuroscience studies since it can measure directional dependence between time courses without any prior model specifications. In Granger causality definition, time course X_2 causes time course X_1 if combined past value of both X_1 and X_2 can significantly improve the prediction accuracy of current value of X_1, rather than using the past value of X_1 alone (Granger, 1969; Seth, 2010). Granger causality is often estimated with multivariate autoregressive (MVAR) modeling of the time courses, and has various time domain as well as frequency domain formulations, including conditional Granger causality (Geweke, 1984), partial Granger causality (Guo et al., 2008), directed transfer function (DTF) (Kaminski et al., 2001), and partial directed coherence (PDC) (Baccalá and Sameshima, 2001), etc. The mentioned time domain Granger causality measures are the straightforward generalization of the notion of Granger causality thus easy to comprehend, the introduced frequency domain Granger causality measures could describe the dynamics of causal relationships between time courses by evaluating Granger causality over different frequency portions (Sato et al., 2009). Based on these, the combined performance of Granger causality analysis in two domains is expected to provide more accurate and informative analysis results.

Little is known about the alteration of effective connectivity among core neurocognitive networks underlying cognitive impairments and psychopathology in IGE-GTCS. Additionally, to our knowledge, no IGE study has conducted multivariate Granger causality analysis in both time and frequency domains and presented the combined analysis results. In the current study, we examined IGE-related changes in effective connectivity across core neurocognitive brain networks using resting-state functional magnetic resonance imaging (fMRI), combining time domain and frequency domain multivariate Granger causality analysis. We hypothesized that the altered causal interactions likely occur among the key nodes of the SN, DMN, and CEN in IGE-GTCS, which may underline cognitive dysfunctions, improving our understanding of the psychopathological mechanism of IGE-GTCS.

MATERIALS AND METHODS

Subjects

Twenty-seven right-handed IGE-GTCS patients (age 24.93 $\pm$ 5.95 years; education 10.59 $\pm$ 2.58 years; eight female; epilepsy duration 7.76 $\pm$ 5.62 years; age of onset 17.13 $\pm$ 6.11 years) were recruited in the study. The diagnosis was determined by a comprehensive evaluation including detailed history, video-EEG telemetry, and neuroimaging. All patients had IGE with GTCS only according to the International League against Epilepsy (ILAE) classification, and met the following inclusion criteria: (i) presence of typical clinical symptoms of GTCS, including myoclonus, loss of consciousness, and no partial seizures; (ii) presence of generalized spike-and-wave or polyspike-wave discharges in their scalp EEG; (iii) no focal abnormality in routine structural MRI examinations; and (iv) no obvious history of etiology. All patients were treated with antiepileptic drugs (AEDs), but received no medication for

at least 48 h prior to the MRI scanning. All patients had been seizure-free for at least 1 month prior to the MRI scanning.

Twenty-nine right-handed healthy subjects (age 26.93 ± 7.54 years; education 11.45 ± 2.40 years; 12 female) were recruited, with gender, age, and education level demographically matched. All participants had no mass lesion (including tumor, vascular malformation or malformations of cortical development), traumatic brain injury or history of neurological or psychiatric disorder. This study was approved by the Ethics Committee of Guangdong 999 Brain hospital, and all participants provided written informed consent.

MRI Data Acquisition and Pre-processing

For the resting-state fMRI scan acquired at a 1.5-T Philips Intera MR scanner, all subjects were instructed to stay awake, keep their eyes open, and minimize head movement; no other task instruction was provided. For the patients, scans were conducted during interictal without combined EEG confirmation. All fMRI images were collected using a gradient-echo echo-planar pulse sequence sensitive to blood-oxygenation-level-dependent (BOLD) contrast with the following parameters: TR/TE = 3000/30 ms, thickness/gap = 4.5/0 mm, field of view (FOV) = 230 × 230 mm, flip angle (FA) = 90°, matrix = 128 × 128, and slices = 31. Each resting-state fMRI run lasted 8 min, obtaining 160 volumes.

For each subject, the first five volumes of the scanned data were discarded to allow for T1-equilibration effects, and then the fMRI data were pre-processed with SPM8 package (Welcome Department of Cognitive Neurology, Institute of Neurology, London, UK, http://www.fil.ion.ucl.ac.uk/spm), included the following steps (Zeng et al., 2012): (1) slice timing correction; (2) rigid body correction for head motion; (3) atlas registration with an EPI template in the Montreal Neurological Institute (MNI) atlas space, resampling to 3-mm isotropic voxels; (4) spatially smoothing using an 8-mm full-width half-maximum (FWHM) Gaussian kernel; and (5) regressing out nine nuisance signals including signals averaged from white matter, cerebrospinal fluid, and the whole brain, and six parameters obtained by head motion correction. Temporal filtering was not conducted as with some prior studies (Hamandi et al., 2006; Wu et al., 2013), so that the whole effective frequency band of the fMRI data could be included in the frequency domain Granger causality analysis (see Section Effective connectivity: time and frequency domains multivariate Granger causality measures below). After calculation, no subjects were removed due to excessive motion (translation > 2 mm and rotation >2°); there was no significant difference in mean motion between the two groups ($p = 0.32$, two-tailed two-sample t-test; Zeng et al., 2014), thus the effective connectivity would be less probably affected by the head motion (Van Dijk et al., 2012).

Region of Interest Definition and Time Course Extraction

Six functional regions of interest (ROIs) were selected, including the rFIC and the dACC of the SN, the VMPFC and the PCC of the DMN, as well as the rDLPFC and the rPPC of the CEN. The coordinates of the ROIs (**Table 1**) were set according to a published study delimiting these regions in an independent dataset (Uddin et al., 2011). In that study, MNI coordinates of peak voxels (voxels with the highest z-scores) of the six regions chosen from ICA maps were defined as the centers of the ROIs. In our study, the final ROIs were defined as 8 mm radius spheres centered on the coordinates, and the mean time course in each ROI was extracted by averaging the time courses of all voxels within the ROI. At last, each mean time course of the ROIs was detrended and its temporal mean was removed for further analysis. All the time courses were covariance stationarity (i.e., unchanging mean and variance) after time course pre-processing.

TABLE 1 | Coordinates of ROIs.

Region	BA	Peak MNI coordinates (mm)
SALIENCE NETWORK (SN)		
Right fronto-insular cortex (rFIC)	47	39, 23, −4
Dorsal anterior cingulate cortex (dACC)	24	6, 24, 32
DEFAULT MODE NETWORK (DMN)		
Ventromedial pre-frontal cortex (VMPFC)	11	−2, 38, −12
Posterior cingulate cortex (PCC)	23/30	−6, −44, 34
CENTRAL EXECUTIVE NETWORK (CEN)		
Right dorsolateral pre-frontal cortex (rDLPFC)	9	46, 20, 44
Right posterior parietal cortex (rPPC)	40	52, −52, 50

Effective Connectivity: Time and Frequency Domains Multivariate Granger Causality Measures

On the basis of MVAR modeling, we intended to calculate the effective connectivity strength in both time and frequency domains, thus the well-chosen Granger causality measures in two domains were introduced in the current study, they are: partial Granger causality (Guo et al., 2008) in time domain analysis, and PDC (Baccalá and Sameshima, 2001) in frequency domain analysis. The formalism for these Granger causality measures is given in Appendix.

To obtain the time domain and frequency domain Granger causality measures between each pair of the six ROIs for each subject, the following steps were conducted: (1) MVAR model estimation: six time courses were fit to obtain the unrestricted autoregressive model (see Appendix for details), the model order was set to 1 determined by Bayesian information criterion (BIC), and the regression coefficients were estimated using standard least squares optimization. (2) Calculation of time domain Granger causality measures: for each pair of the six time courses in both directions, the partial Granger causality and the DOI were calculated (see Equations A11 and A12 in Appendix); thus, 30 (6×5) individual partial Granger causality values of time domain Granger causal links and 30 DOI terms of time domain Granger causal links were obtained for each subject. (3) Calculation of frequency domain Granger causality measure: for each pair of the six time courses in both directions, the PDC was calculated (see Equation A13 in Appendix) every 0.001 Hz of the interesting frequency range [0, Fs/2], where Fs is the sampling rate of the

fMRI data (i.e., 1/TR); thus 30 × 168 individual PDC values of frequency domain Granger causal links were obtained for each subject.

Constructing Within-Group Effective Connectivity Graph

Having computed the Granger causality measures in both time and frequency domains, we proceeded to construct effective connectivity graph for each group, respectively. Since all the Granger causality measures used in the study lack known statistical distributions (Seth, 2010), the creation of empirical null distributions that hypothesize no causality between ROIs is of great importance. Meanwhile, we hypothesized that the combined performance of time domain and frequency domain analysis of multivariate Granger causality would present more accurate and informative analysis results. Therefore, based on the procedure conducted in Sato et al. (2009) and Havlicek et al. (2010), we proposed a combination framework of time domain and frequency domain multivariate Granger causality analysis to evaluate the direct causal interactions between time courses. An overview of this method (see **Figure 1**) is given below, and each step is described in detail as follows:

Step 1 Fit MVAR model for the time courses of each subject separately to obtain the model coefficients (including regression coefficients and residuals, see Appendix for details), then calculate the time and frequency domains Granger causality measures for each subject (see Equations A11–A13 in Appendix). Record the median values of each Granger causality measure across subjects.

Step 2 For each subject, resample the residuals (bootstrap resampling for N repetitions) and set the regression coefficients $A_{ij}(l),\ l = 1, \ldots, p$ to zero (see Appendix for details) when assessing the Granger causality from time courses j to i, the other coefficients remain as originally estimated in step 1. Then simulate a multivariate time courses based on the modified MVAR model coefficients to generate time courses under the null hypothesis of "no Granger causality" from time courses j to i. After that, calculate the Granger causality measures of the simulated time courses (see Equations A11–A13 in Appendix), then record the median values of the Granger causality measures across the simulated samples. Repeat this step until the desired number of repetition (N times) is achieved. When finished, the null distributions of the median Granger causality measures are obtained. Note, in general, the value of N = 200–5000 is sufficient (in the current study, we set $N = 1000$) (Efron and Tibshirani, 1994).

Step 3 Estimate the critical value (defined as the $(1 - \alpha)$ quantile, $\alpha = 0.05$, FDR corrected; Seth, 2010) of each null distribution, and take the critical value as significance threshold. For time domain analysis, a per-interaction significance threshold is obtained above which the median values of the Granger causality measures recorded in step 1 are assumed to be significant. For frequency domain analysis, we get a per-interaction-per-frequency significance threshold; the significant effective connectivity is thus defined as the connection which has non-null significant frequency interval. Finally, the consistent results of time domain and frequency domain analysis are determined as significant effective connectivity given by the proposed method.

The validity and improvement in resulting accuracy of the proposed method is proved by several toy models in the following subsection (see Section Simulations). For the IGE study, we used the median partial Granger causality and median PDC to determine the significant connectivity in time domain and frequency domain analysis, respectively. Finally, the significant effective connectivity was defined as the connection that was significant in both time domain and frequency domain analysis, and the within-group effective connectivity graph was thus composed of the significant effective connections of each group. In addition, the significant connections identified by DOI terms in time domain analysis were also recorded as a subset of the final results.

Evaluating between-Group Effective Connectivity Difference

Among the connections that exhibited significant Granger causality in at least one group (obtained in Section Constructing within-group effective connectivity graph), we further assessed the presence of significant group differences in both time domain and frequency domain Granger causality definition. In time domain analysis, Mann-Whitney U-tests ($p < 0.05$, FDR corrected) were applied across the 30 time domain Granger causal links to assess the presence of significant group differences (Sridharan et al., 2008). In frequency domain analysis, for each link, Mann-Whitney U-tests ($p < 0.05$, FDR corrected) were applied across the 168 frequency slices to determine the group-level significant frequency interval of that link. And finally the links with non-null significant frequency intervals were taken as the interesting results in frequency domain analysis.

RESULTS

Simulations

Two typical and widely used toy models (Baccalá and Sameshima, 2001; Seth, 2010) were presented here to demonstrate the validity and improvement in resulting accuracy of the proposed combination framework described in Section Constructing within-group effective connectivity graph. In the simulation experiments, the same methods of time course pre-processing (including detrend and removal of temporal mean), MVAR model estimation (using standard least squares optimization to calculate the regression coefficients and residuals, and setting the model order as the real model order of each toy model), time and frequency domains Granger causality calculation, and significance testing (1000 times repetition to get the significance thresholds) that described in Section Effective connectivity: time and frequency domains multivariate Granger causality measures

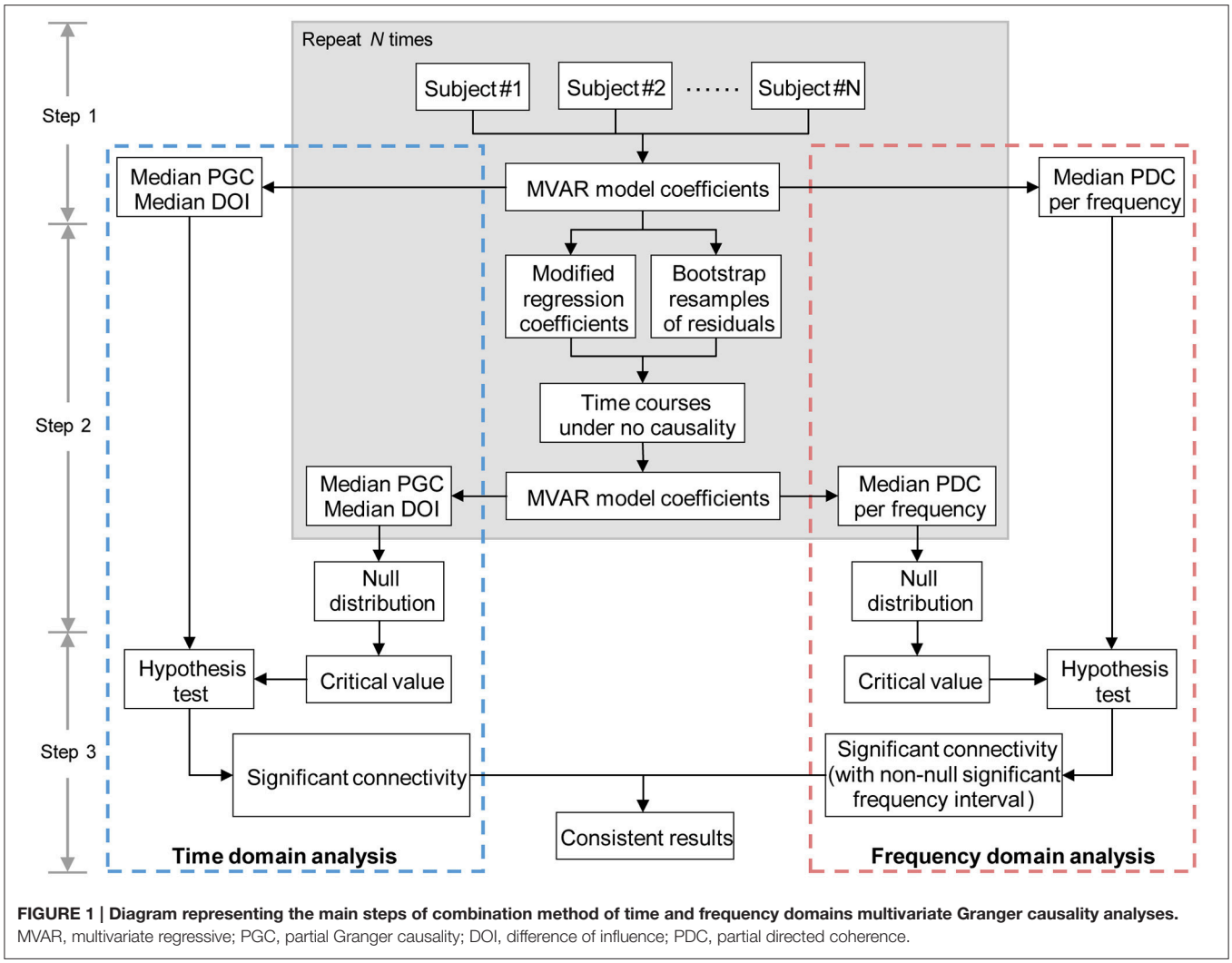

FIGURE 1 | Diagram representing the main steps of combination method of time and frequency domains multivariate Granger causality analyses. MVAR, multivariate regressive; PGC, partial Granger causality; DOI, difference of influence; PDC, partial directed coherence.

and Constructing within-group effective connectivity graph were conducted to the toy models.

Model 1. Suppose that four simultaneously observed time courses were generated by the equations:

$$\begin{aligned} x_1(n) &= 0.95\sqrt{2}x_1(n-1) - 0.9025x_1(n-2) + \omega_1(n) \\ x_2(n) &= 0.5x_1(n-2) + \omega_2(n) \\ x_3(n) &= -0.4x_4(n-3) + \omega_3(n) \\ x_4(n) &= 0.35x_4(n-2) + \omega_4(n) \end{aligned} \quad (1)$$

The model contains two direct Granger causal influences, i.e., connections from x_1 to x_2, and from x_4 to x_3. The model order is three, $\omega_1 \sim \omega_4$ are zero-mean uncorrelated white processes with identical variances. The signal to noise ratio (SNR) of the generated time courses is 0.01. **Figure 2** illustrates the simulation results. The Granger causal structure and the raw time courses of each variable are shown in **Figures 2A,B**. The time domain Granger causality analysis result is expressed as a colormap in **Figure 2C**. As expected, the partial Granger causality values of the connections from x_1 to x_2, and from x_4 to x_3 were significantly larger and exceeded the corresponding thresholds. **Figure 2D** shows the PDC values (black solid line) and significance thresholds (black dotted line) of each connection. The significant frequency intervals were highlighted in red. Using the PDC representation we could observe the dynamics of causal relationships between time courses. It can be seen that, except for two correct causal influences, the connection from x_1 to x_3 was misjudged in frequency domain analysis. Obviously, when we conducted the proposed combination method, only the corrected causal interactions would be identified.

Model 2. A more complicated system that contains indirect causal influence was generated by the equations:

$$\begin{aligned} x_1(n) &= 0.95\sqrt{2}x_1(n-1) - 0.9025x_1(n-2) + \omega_1(n) \\ x_2(n) &= 0.5x_1(n-2) + \omega_2(n) \\ x_3(n) &= -0.4x_1(n-3) + \omega_3(n) \\ x_4(n) &= -0.5x_1(n-2) + 0.25\sqrt{2}x_4(n-1) \\ &\quad + 0.25\sqrt{2}x_5(n-1) + \omega_4(n) \\ x_5(n) &= -0.25\sqrt{2}x_4(n-1) + 0.25\sqrt{2}x_5(n-1) + \omega_5(n) \end{aligned} \quad (2)$$

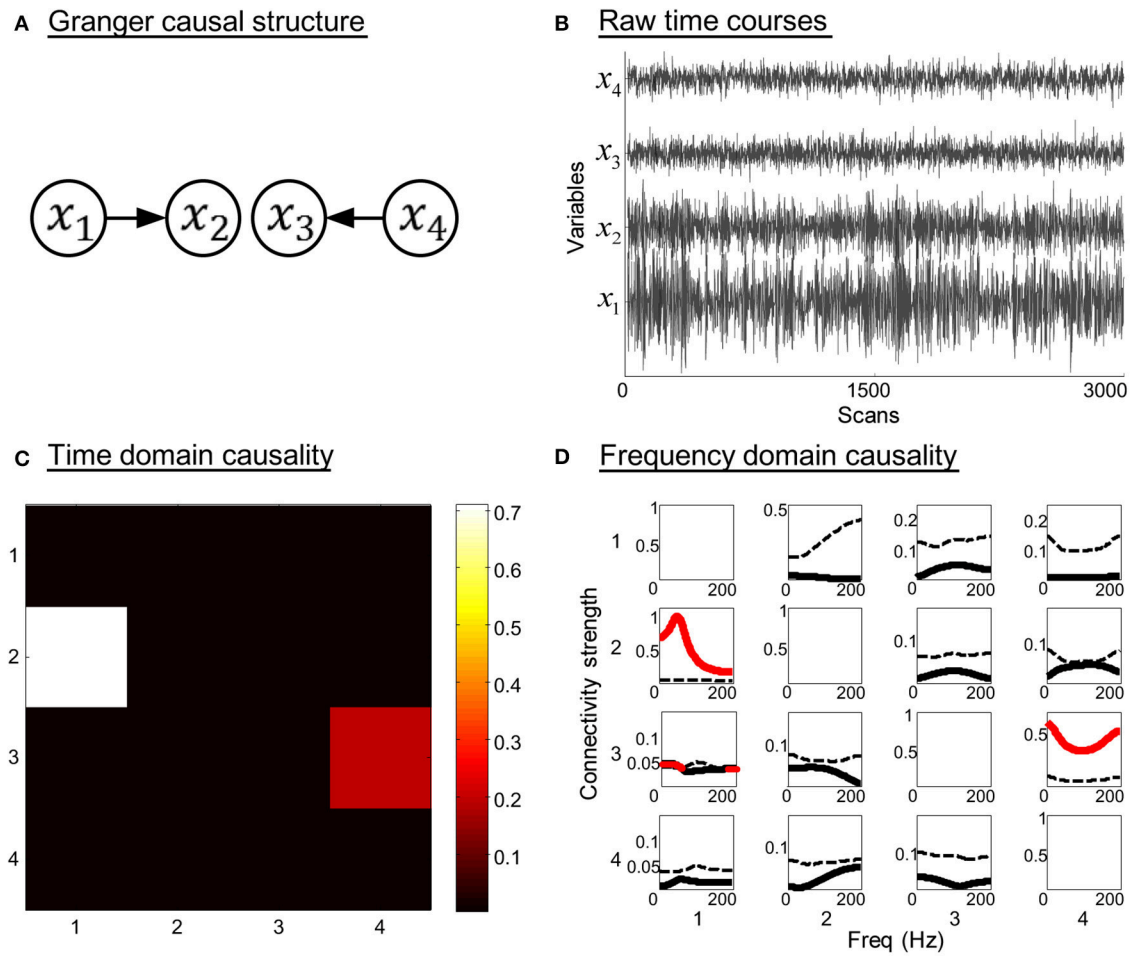

FIGURE 2 | Simulation results of toy model 1. (A) Granger causal structure of the variables. **(B)** Raw time courses of the variables. **(C)** The colormap of partial Granger causality values in time domain analysis. **(D)** The spectrum of significance thresholds (black dotted line) and partial directed coherence (PDC) values (black solid line, values greater than the thresholds are highlighted in red) in frequency domain analysis. Note: in **(C,D)** the direction of causality is from column to row.

In this three order system, x_1 is a direct source to x_2, x_3, and x_4, bidirectional connectivity exists between x_4 and x_5. There is no direct coupling from x_1 to x_5. The SNR of the generated time courses is 0.01. The simulation results are shown in **Figure 3**. **Figures 3C,D** illustrate the time domain and frequency domain analysis results, respectively. In addition, the results given by DTF (Kaminski et al., 2001) are presented in **Figure 3B** as a reference (see Equation A14 in Appendix). It is obvious that both the time domain partial Granger causality and frequency domain PDC could correctly detect all the direct causal influences, while the DTF mistakenly identified the indirect causal influence from x_1 to x_5. These results indicate that the Granger causality measures we used in the study could avoid the influence of indirect causal relationship.

Based on the above analysis, we can conclude that the analytical methods and Granger causality measures adopted in the study can efficiently detect the direct causal relationships between time courses, and the combined approach takes the consistent results of the two domains' analyses, which can be seen as a double verification process to present more accurate and confident results. The simulation results were stable under different noise condition. Therefore, using the proposed method in Section Constructing within-group effective connectivity graph is considered to present a convincing result for fMRI data analysis.

Within-Group Effective Connectivity Graph

The causal connectivity graphs of healthy controls and IGE-GTCS patients are presented in **Figures 4A,B**. The connecting arrows are weighted according to the strengths of the time domain causal influences (partial Granger causality values normalized by the maximum partial Granger causality value). Meanwhile, each significant connection is respectively marked with the frequency interval where the PDC values are higher than the significance thresholds. And finally a subset of the significant connections that showed a dominant direction of influence (significant DOI term) are highlighted in red in the same figure. It was observed that comparing to the healthy

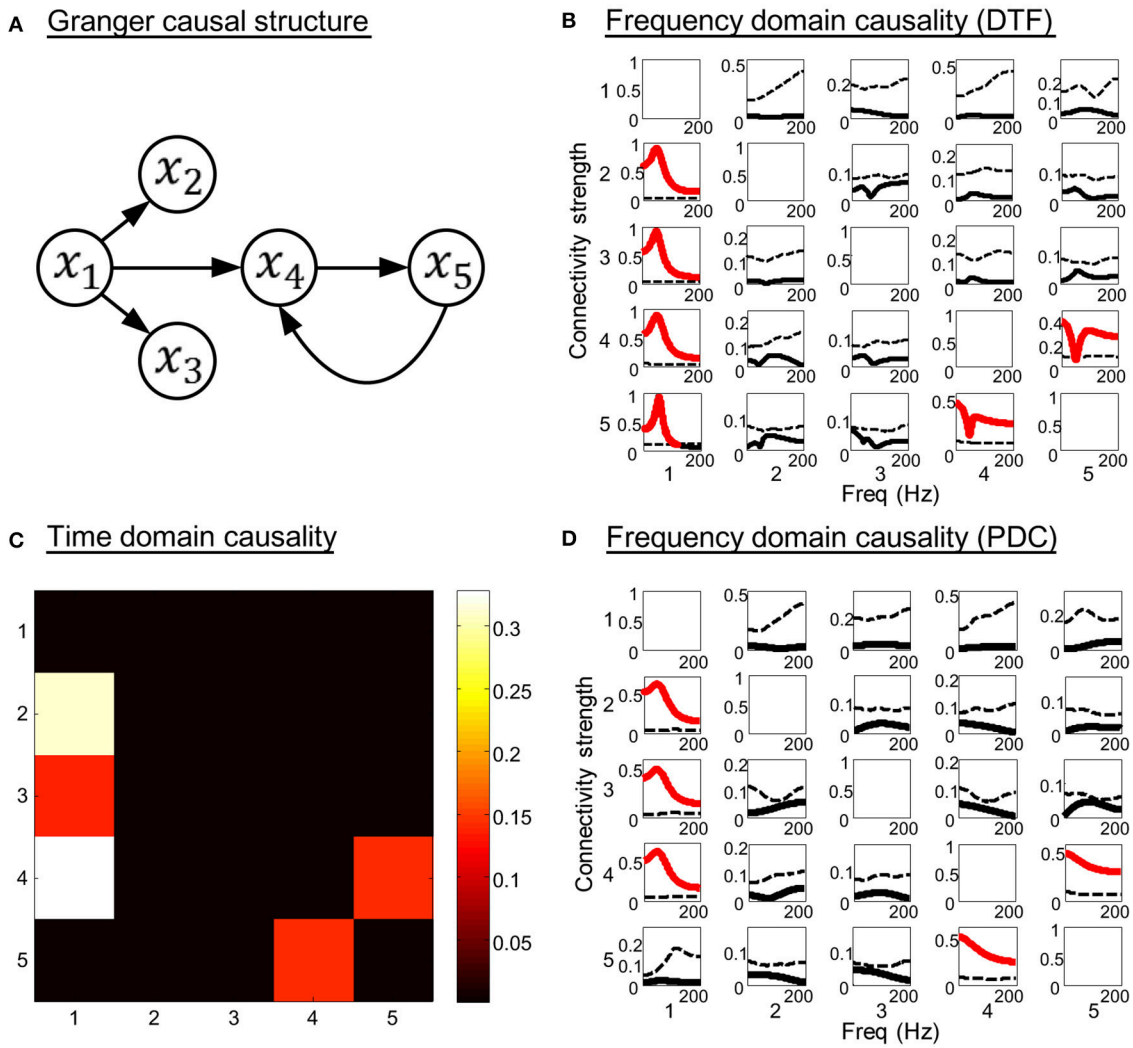

FIGURE 3 | Simulation results of toy model 2. (A) Granger causal structure of the variables. **(B)** The spectrum of significance thresholds (black dotted line) and directed transfer function (DTF) values (black solid line, values greater than the thresholds are highlighted in red). **(C)** The colormap of partial Granger causality values in time domain analysis. **(D)** The spectrum of significance thresholds (black dotted line) and partial directed coherence (PDC) values (black solid line, values greater than the thresholds are highlighted in red) in frequency domain analysis. Note: in **(B–D)** the direction of causality is from column to row.

controls (21 influences), the IGE-GTCS patients (16 influences) established less causal connections among the six ROIs.

Between-Group Effective Connectivity Differences

The group differences of effective connectivity are illustrated in **Figure 5**. In time domain analysis, two connections exhibited significance, i.e., the increased causal influence from the rDLPFC to the dACC ($p < 0.05$, FDR corrected), and the decreased causal influence from the rFIC to the PCC ($p < 0.05$, uncorrected) in the IGE-GTCS patients relative to healthy controls. The connections' means and standard errors of partial Granger causality values across subjects within each group were illustrated in the blue box in **Figure 5**. Meanwhile, frequency domain analysis also found the enhanced causal influence from the rDLPFC to the dACC ($p < 0.05$, FDR corrected) in patients than healthy controls. The mean PDC values across subjects within each group, as well as the p-value spectrum of this significant connection were shown in the pink box. It can be seen that the group difference of this causal influence was significant in a band of frequencies, [0 0.167] Hz, and the minimum p-value ($p = 0.028$) was obtained at 0.034 Hz.

DISCUSSION

Human high-level attention and cognitive control processes rely on the well-balanced dynamic interactions between large-scale brain networks, and three core neurocognitive networks including the SN, DMN, and CEN have been highlighted in the study of psychopathology. Our prior work used static as well as dynamic measures of functional connectivity, however,

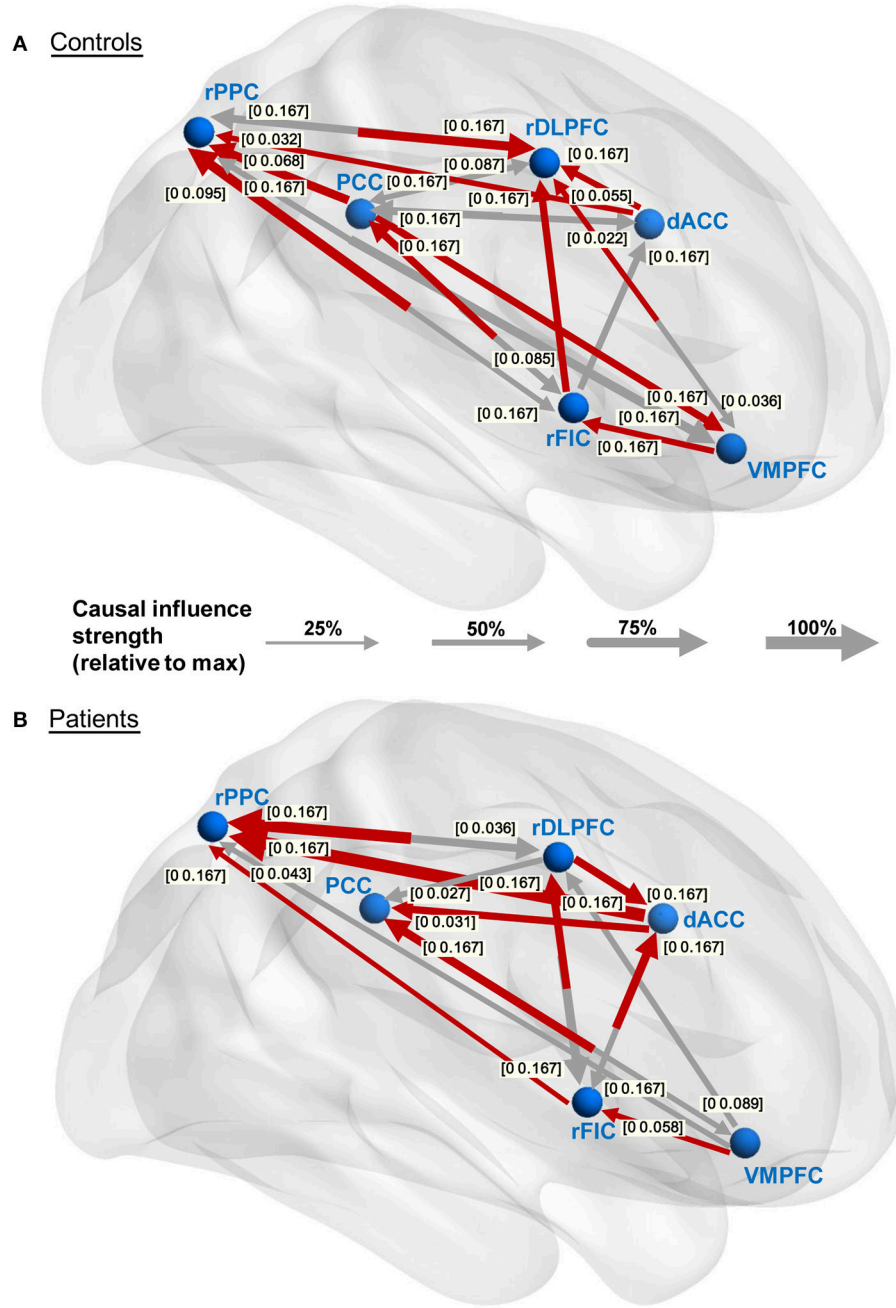

FIGURE 4 | Within-group effective connectivity graphs. (A,B) Effective connectivity graphs of the healthy controls and IGE-GTCS patients, respectively. The connecting lines are weighted according to the normalized partial Granger causality values. The numbers next to the arrowheads indicate the significant frequency intervals of the corresponding connections. The significant connections showing a dominant direction of influence (significant DOI term) are highlighted in red.

did not evaluate effective connectivity among brain networks for cognitive dysfunctions and psychopathological risk in IGE-GTCS (Wei et al., 2015). In this study, we have proposed a combination framework of time domain and frequency domain multivariate Granger causality analysis, to reveal alterations in direct causal relationship across key nodes of the SN, DMN, and CEN in the IGE-GTCS patients relative to the healthy controls. The key findings of the study include: (1) the establishment of less causal interactions among the key nodes in the patients compared with healthy controls; (2) two SN-involved effective connectivity that exhibited significant group difference, they are: enhanced causal influence from the rDLPFC to the dACC ($p < 0.05$, FDR corrected) throughout the whole evaluated frequency range ([0 0.167] Hz) in patients than healthy controls revealed by both the time and frequency domains analyses, and decreased causal influence from the rFIC to the PCC ($p < 0.05$, uncorrected) in

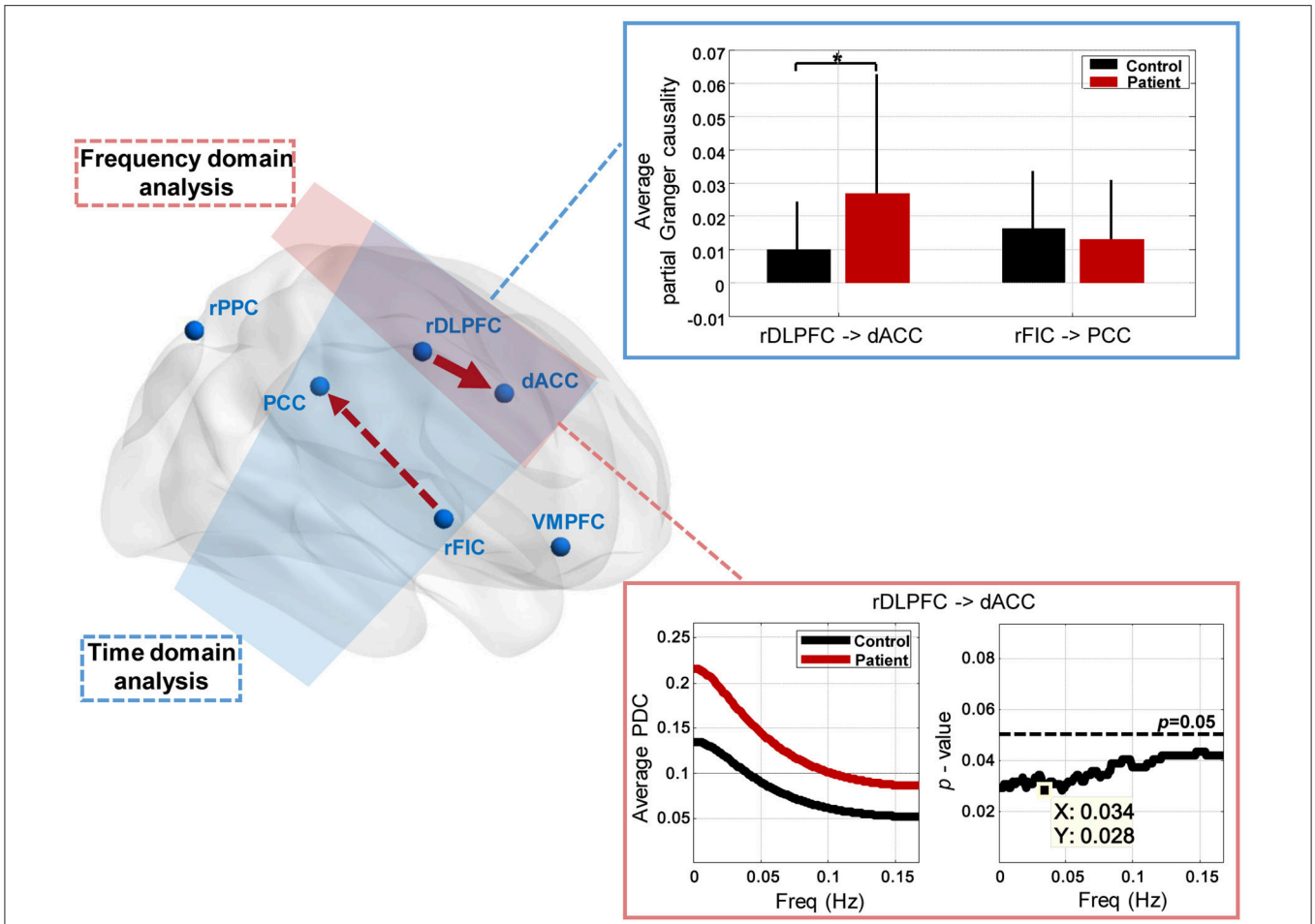

FIGURE 5 | Between-group effective connectivity differences. Two connections exhibit significant between-group difference revealed by Mann-Whitney *U*-tests in time domain analysis, including the increased connection from the rDLPFC to the dACC (*$p < 0.05$, FDR corrected), and the decreased connection from the rFIC to the PCC ($p < 0.05$, uncorrected) in patients than healthy controls. The connections' means and standard errors of partial Granger causality values across subjects within each group are illustrated in the blue box. Frequency domain analysis also reveals the enhanced connection from the rDLPFC to the dACC ($p < 0.05$, FDR corrected) in patients. The mean partial directed coherence (PDC) values across subjects within each group, and the *p*-value spectrum are shown in the pink box.

patients than healthy controls given by the time domain analysis. These findings provide new insights into the brain functional architecture of IGE-GTCS.

Methodological Considerations

Several methodological considerations in the present study need to be addressed aforehand. First, the basis of multivariate Granger causality and well-chosen time and frequency domains Granger causality measures ensure the indirect causality between ROIs to be eliminated, and this could be certified by the simulation results of the toy model 2 in Section Simulations. Second, the MVAR model order was set to 1 for all subjects according to the BIC criterion, thus we evaluated the Granger causal relationship between ROIs with a maximum time delay of 3 s (since TR is 3 s). The low model order is common and recommended in several Granger causality studies using resting-state fMRI data considering the low time resolution of fMRI data itself (Sato et al., 2010; Hamilton et al., 2011). Third, to our knowledge, no previous study has evaluated the Granger causal connectivity in IGE-GTCS combined the time domain and frequency domain analysis. In the current study, we have revealed aberrant causal interactions among the core neurocognitive networks in IGE-GTCS confirmed by analyses in two domains. Besides, a combination framework of time domain and frequency domain multivariate Granger causality analysis was proposed, and the improvement of accuracy using this method was verified by the simulation experiments. This general combination framework can also be used in other multisubject studies when effective connectivity measured by multivariate Granger causality is needed.

The Causal Relationship between the rFIC and the PCC

In the current study, the controls group established bidirectional effective connectivity between the rFIC and the PCC (the influence from the rFIC to the PCC also exhibited significant

DOI value), while none of these two connections was significant in the patients group (see **Figure 4**). Further, the between-group analysis based on time domain partial Granger causality revealed that the effective connectivity from the rFIC to the PCC exhibited significance ($p < 0.05$, uncorrected, Mann-Whitney U-test), with decreased connectivity strength in the patients relative to the healthy controls (see **Figure 5**). It is well known that the function of the SN is to identify internal and extra-personal stimuli to guide flexible behavior (Corbetta and Shulman, 2002; Seeley et al., 2007), and the DMN is associated with spontaneous activities and internally oriented cognition (Raichle et al., 2001). Previous task-based as well as resting-state fMRI studies using Granger causality analysis have confirmed that there exists effective connectivity between the SN and the DMN (Sridharan et al., 2008; Uddin et al., 2011). Among these researches, one commonly approved conclusion is that the rFIC acts as a critical causal outflow hub in initiating control signals to activate the CEN and deactivate the DMN, thus provides an interpretation of the directionality of signaling from the rFIC to the PCC. Moreover, a relevant neurodevelopmental study reported that the Granger causal influence from the rFIC to the PCC was significant in the adults group while vanished in the children, suggesting the maturation of rFIC-related causal connectivity is crucial for the sophisticated cognitive abilities (Uddin et al., 2011). For the causal influence from the PCC to the rFIC, Uddin et al. (2009) using Granger causality analysis provided evidence that the PCC may negatively regulate activity in the SN. Such an information inflow may be interpreted as a feedback circuit establishment that suppresses the activity of the DMN in a primed state to make better preparation for the rFIC to release cognitive control processes when salient stimuli occur.

For the frequency-domain interpretation of the causal interactions between the rFIC and the PCC, the significant frequency intervals of the two connections in the control group showed that the PCC conducted causal influence on the rFIC for the lower frequencies ([0 0.085] Hz). This is reasonable given the fact that the PCC as a key node of the DMN, is responsible for information integration in the spontaneous low-frequency range (Leech and Sharp, 2014). Meanwhile, the drive from the rFIC to the PCC was significant throughout the evaluated frequency interval, [0 0.167] Hz, probably indicating that the brain responses for cognitive control processes in switching between exogenous and endogenous stimuli are needed for the whole spectrum of signal changing frequencies (see **Figure 4A**).

Based on the above, we inferred that the bidirectional effective connectivity between the rFIC and the PCC may be associated with well-balanced performance in cognitive flexibility, with which one can flexibly switch between mental processes to appropriately react to salient events in the environment (Scott, 1962). Additionally, prior study has suggested that the active dynamic interactions among brain networks are indispensable for adaptive and flexible cognition and behavior (Cole et al., 2013), while the IGE-GTCS patients (16 influences) established less causal connections among the SN, DMN, and CEN relative to the healthy controls (21 influences, see **Figure 4**). For all the aforementioned proofs, we inferred that the hypoconnectivity of the patients group, especially the decreased causal influence from the rFIC to the PCC, may be associated with impaired cognitive abilities as well as mental inflexibility in IGE-GTCS (Hommet et al., 2006; Chowdhury et al., 2014).

The Causal Relationship between the dACC and the rDLPFC

Both the time domain and frequency domain analysis in our study consistently revealed the significantly enhanced effective connectivity ($p < 0.05$, FDR corrected, Mann-Whitney U-test) from the rDLPFC to the dACC in the patients relative to the healthy controls (see **Figure 5**). Interestingly, the within-group connectivity graphs indicated that the direction of the Granger causality between the rDLPFC and the dACC is opposite in the two groups, i.e., the dACC drives the rDLPFC (also with significant DOI value) in the controls while the rDLPFC drives the dACC (also with significant DOI value) in the IGE patients (see **Figure 4**). Since both the ACC and the DLPFC are co-activated in cognitive control processing and tests of sustained attention (Adler et al., 2001; Miller and Cohen, 2001), the dissociation and functional interactions of the two areas have arouse the interests of the researchers (Kondo et al., 2004; Dosenbach et al., 2007; Seeley et al., 2007). In an event-related fMRI study, Macdonald et al. (2000) conducted a task-switching vision of the Stroop task and suggested that the DLPFC (Brodmann's area (BA) 9) supports implementation of control, while the ACC (BA 24 and BA 32) is responsible for performance monitoring. Furthermore, based on the conflict hypothesis of the ACC, Kerns et al. (2004) explored whether ACC activity associated with conflict and error trial predicted pre-frontal cortex activity under Stroop task, and concluded that once the ACC detects conflicts, it modulates the strength of the rDLPFC (BA 9 and BA 8) representations, which then executes appropriate cognitive control and products corresponding behavioral adjustments. Our study revealed the effective connectivity from the dACC (BA 24) to the rDLPFC (BA 9) in the healthy controls, which may underline the existence of neural circuitry in terms of resting-state Granger causality supporting the above cognitive control processes. By contrast, the establishment of the significantly enhanced causal influence from rDLPFC to dACC in the patients may thus indicate a disruption to the well-organized cognitive control processes, and probably associated with cognitive dysfunctions in IGE-GTCS, such as deficits in working memory, sustained attention, as well as executive dysfunction (Mirsky et al., 2002). This altered causal influence as well as the aberrant connection from the rFIC to the PCC demonstrate that the IGE-GTCS patients exhibit inappropriate mapping with the SN. The findings together with various prior studies highlight the critical role of SN in connecting with DMN and CEN (Sridharan et al., 2008; Menon, 2011; Uddin et al., 2011), which provide informative evidence for the understanding of the cognitive dysfunctions and psychopathological mechanism of IGE-GTCS.

In addition, prior study using Granger causality analysis on EEG/fMRI data of IGE patients found the frontal lobe had the maximum net causal strength, suggesting that frontal and

parietal areas were the initiation of absence seizures (Szaflarski et al., 2010). Similarly, our study using both time domain and frequency domain multivariate Granger causal analysis revealed the significantly enhanced causal influence directed from the rDLPFC to the dACC throughout the whole evaluated frequency range ([0 0.167] Hz) in the IGE-GTCS patients, which may as well indicate that the pre-frontal cortex is probably the initiation of GTCS.

Evaluating hemodynamic response function (HRF) effects in the Granger causality analysis of BOLD-fMRI data is a controversial topic (Barnett and Seth, 2014). Noticing that BOLD-fMRI is an indirect transformation of underlying neural activity and Granger causality is a purely data-driven method without biological modeling, in the current study, we have carefully considered the effects of HRF on Granger causality analysis on BOLD-fMRI data. The use of DOI terms in the within-group effective connectivity analysis, the main concern of identifying different effective connectivity patterns between the patients and controls rather than revealing canonical causal structure, as well as the group-level strategy for multisubject Granger causality analysis in the current study, have been suggested by recent analyses that are theoretically useful to relieve the HRF effects (Schippers et al., 2011; Barnett and Seth, 2014). Furthermore, considering that the HRF has been reported to be different in epilepsy subjects (David et al., 2008), we adopted the blind-deconvolution technique proposed by Wu et al. (2013) to deconvolve the mean time courses of the six ROIs (obtained in Section Region of interest definition and time course extraction) for each subject separately, and on the basis of the deconvolved BOLD time courses, we repeated the Granger causality analysis described in Section Evaluating between-group effective connectivity difference. In this case, both the time domain partial Granger causality and the frequency domain PDC have revealed only one effective connectivity that showed significant group difference (Mann-Whitney U-tests, $p < 0.05$, FDR corrected), i.e., the increased causal influence from the rDLPFC to the dACC in the IGE-GTCS patients than controls, which is consistent with our prior result based on the BOLD time courses without deconvolution. We thus infer that, the altered effective connectivity from the rDLPFC to the dACC, which is consistently revealed by the two domains' multivariate Granger causality analyses on both the BOLD and deconvolved BOLD time courses, is probably a key factor associated with cognitive dysfunctions in IGE-GTCS.

Limitations and Future Directions

Several limitations in this study should be mentioned. First, due to the absence of neuropsychological tests for both the patients and the controls, we cannot precisely relate the significant Granger causal connectivity to the specific cognitive functions and neuropsychological parameters, the interpretations of the results are simply inferences derived from earlier researches. Second, it is reported that AED toxicity is related to psychopathology and abnormal neuronal function in epilepsy (Schmitz, 1999). In the current study, all patients were treated with AEDs, including 24 patients with monotherapy and 3 patients with polytherapy; the AEDs included sodium valproate (VBA), phenytoin (PHT), carbamazepine (CBZ), lamotrigine (LTG), phenobarbital (PB), and topiramate (TPM). However, we have carefully considered the potential confounding effects of AEDs on ICNs in the study. We ensured that all patients received no medication for at least 48 h prior to the MRI scanning to avoid direct effects of AEDs on the effective connectivity analysis. Nonetheless, the long-term effects of AEDs could not be excluded. Third, a relatively small number of ROIs were used in the current study to investigate the interconnectivity between networks. An extension to a larger set of nodes across different brain networks would be considered in the future. In addition to the above mentioned aspects, future works could also focus on EEG-fMRI multimodal integration for resting-state as well as task-based time-frequency multivariate Granger causality analysis, and evaluate causal relationship between ROIs using dynamic causal modeling (Friston et al., 2003).

CONCLUSIONS

In this study, we conducted combined time and frequency domains multivariate Granger causality analyses to investigate effective connectivity among the key nodes of the three core neurocognitive networks in IGE-GTCS patients and matched healthy controls. The results revealed two SN-involved effective connectivity that exhibited significant group difference. One is the decreased Granger causal influence from the rFIC to the PCC in the patients relative to the healthy controls given by time domain analysis, which may underline impaired cognitive abilities as well as mental inflexibility in IGE-GTCS. Another is the significantly increased Granger causal influence from the rDLPFC to the dACC in patients than controls revealed by both the time and frequency domains analyses. This altered effective connectivity may indicate a disruption to the well-organized cognitive control processes thus probably leading to disorders in working memory, sustained attention, as well as executive dysfunction in IGE-GTCS. The current work proposes a combination framework of time and frequency domains multivariate Granger causality analyses that is suitable for multisubject studies, and demonstrates for the first time that patients with IGE-GTCS exhibited altered Granger causal interactions across the SN, DMN, and CEN, shedding new lights on the psychopathological mechanism of IGE-GTCS.

AUTHOR CONTRIBUTIONS

DH, SQ designed research; HW, JA, HS, and LZ performed research; HW analyzed the data; and HW, JA, HS, and LZ wrote the paper.

ACKNOWLEDGMENTS

We thank the editor and reviewers for their kindly help and constructive suggestions to improve the work. This work is supported by the National Natural Science Foundation of China (61420106001, 61375111, 61503397, 81271389, and 81471251).

REFERENCES

Adler, C. M., Sax, K. W., Holland, S. K., Schmithorst, V., Rosenberg, L., and Strakowski, S. M. (2001). Changes in neuronal activation with increasing attention demand in healthy volunteers: an fMRI study. *Synapse* 42, 266–272. doi: 10.1002/syn.1112

Baccalá, L. A., and Sameshima, K. (2001). Partial directed coherence: a new concept in neural structure determination. *Biol. Cybern.* 84, 463–474. doi: 10.1007/PL00007990

Baker, G. A., Jacoby, A., and Chadwick, D. W. (1996). The associations of psychopathology in epilepsy: a community study. *Epilepsy Res.* 25, 29–39. doi: 10.1016/0920-1211(96)00017-4

Barnett, L., and Seth, A. K. (2014). The MVGC multivariate Granger causality toolbox: a new approach to Granger-causal inference. *J. Neurosci. Methods* 223, 50–68. doi: 10.1016/j.jneumeth.2013.10.018

Botvinick, M. M., Cohen, J. D., and Carter, C. S. (2004). Conflict monitoring and anterior cingulate cortex: an update. *Trends Cogn. Sci.* 8, 539–546. doi: 10.1016/j.tics.2004.10.003

Chowdhury, F. A., Elwes, R. D., Koutroumanidis, M., Morris, R. G., Nashef, L., and Richardson, M. P. (2014). Impaired cognitive function in idiopathic generalized epilepsy and unaffected family members: an epilepsy endophenotype. *Epilepsia* 55, 835–840. doi: 10.1111/epi.12604

Cole, M. W., Reynolds, J. R., Power, J. D., Repovs, G., Anticevic, A., and Braver, T. S. (2013). Multi-task connectivity reveals flexible hubs for adaptive task control. *Nat. Neurosci.* 16, 1348–1355. doi: 10.1038/nn.3470

Corbetta, M., and Shulman, G. L. (2002). Control of goal-directed and stimulus-driven attention in the brain. *Nat. Rev. Neurosci.* 3, 201–215. doi: 10.1038/nrn755

Cutting, S., Lauchheimer, A., Barr, W., and Devinsky, O. (2001). Adult-onset idiopathic generalized epilepsy: clinical and behavioral features. *Epilepsia* 42, 1395–1398. doi: 10.1046/j.1528-1157.2001.14901.x

David, O., Guillemain, I., Saillet, S., Reyt, S., Deransart, C., Segebarth, C., et al. (2008). Identifying neurl drivers with functional MRI: an electrophysiological validation. *PLoS Biol.* 6, 2683–2697. doi: 10.1371/journal.pbio.0060315

Dosenbach, N. U., Fair, D. A., Miezin, F. M., Cohen, A. L., Wenger, K. K., Dosenbach, R. A., et al. (2007). Distinct brain networks for adaptive and stable task control in humans. *Proc. Natl. Acad. Sci. U.S.A.* 104, 11073–11078. doi: 10.1073/pnas.0704320104

Efron, B., and Tibshirani, R. (1994). *An Introduction to the Bootstrap*. New York, NY: Chapman and Hall.

Engel, J. Jr. (2001). A proposed diagnostic scheme for people with epileptic seizures and with epilepsy: report of the ILAE Task Force on Classification and Terminology. *Epilepsia* 42, 796–803. doi: 10.1046/j.1528-1157.2001.10401.x

Friston, K. J., Frith, C. D., Liddle, P. F., and Frackowiak, R. S. (1993). Functional connectivity: the principal-component analysis of large (PET) data sets. *J. Cereb. Blood Flow Metab.* 13, 5–14. doi: 10.1038/jcbfm.1993.4

Friston, K. J., Harrison, L., and Penny, W. (2003). Dynamic causal modelling. *Neuroimage* 19, 1273–1302. doi: 10.1016/S1053-8119(03)00202-7

Gelisse, P., Thomas, P., Samuelian, J. C., and Gentin, P. (2007). Psychiatric disorders in juvenile myoclonic epilepsy. *Epilepsia* 48, 1032–1033. doi: 10.1111/j.1528-1167.2007.01009_4.x

Geweke, J. F. (1984). Measures of conditional linear dependence and feedback between time series. *J. Am. Stat. Assoc.* 79, 907–915. doi: 10.1080/01621459.1984.10477110

Granger, C. W. (1969). Investigating causal relations by econometric models and cross-spectral methods. *Econometrica* 37, 424–438. doi: 10.2307/1912791

Guo, S., Seth, A. K., Kendrick, K. M., Zhou, C., and Feng, J. (2008). Partial Granger causality–eliminating exogenous inputs and latent variables. *J. Neurosci. Methods* 172, 79–93. doi: 10.1016/j.jneumeth.2008.04.011

Hamandi, K., Salek-Haddadi, A., Laufs, H., Liston, A., Friston, K., Fish, D. R., et al. (2006). EEG-fMRI of idiopathic and secondarily generalized epilepsies. *Neuroimage* 31, 1700–1710. doi: 10.1016/j.neuroimage.2006.02.016

Hamilton, J. P., Chen, G., Thomason, M. E., Schwartz, M. E., and Gotlib, I. H. (2011). Investigating neural primacy in Major Depressive Disorder: multivariate Granger causality analysis of resting-state fMRI time-series data. *Mol. Psychiatry* 16, 763–772. doi: 10.1038/mp.2010.46

Havlicek, M., Jan, J., Brazdil, M., and Calhoun, V. D. (2010). Dynamic Granger causality based on Kalman filter for evaluation of functional network connectivity in fMRI data. *Neuroimage* 53, 65–77. doi: 10.1016/j.neuroimage.2010.05.063

Hommet, C., Sauerwein, H. C., De Toffol, B., and Lassonde, M. (2006). Idiopathic epileptic syndromes and cognition. *Neurosci. Biobehav. Rev.* 30, 85–96. doi: 10.1016/j.neubiorev.2005.06.004

Kaminski, M., Ding, M., Truccolo, W. A., and Bressler, S. L. (2001). Evaluating causal relations in neural systems: granger causality, directed transfer function and statistical assessment of significance. *Biol. Cybern.* 85, 145–157. doi: 10.1007/s004220000235

Kerns, J. G., Cohen, J. D., Macdonald, A. W. III, Cho, R. Y., Stenger, V. A., and Carter, C. S. (2004). Anterior cingulate conflict monitoring and adjustments in control. *Science* 303, 1023–1026. doi: 10.1126/science.1089910

Kondo, H., Osaka, N., and Osaka, M. (2004). Cooperation of the anterior cingulate cortex and dorsolateral prefrontal cortex for attention shifting. *Neuroimage* 23, 670–679. doi: 10.1016/j.neuroimage.2004.06.014

Leech, R., and Sharp, D. J. (2014). The role of the posterior cingulate cortex in cognition and disease. *Brain* 137, 12–32. doi: 10.1093/brain/awt162

Macdonald, A. W. III, Cohen, J. D., Stenger, V. A., and Carter, C. S. (2000). Dissociating the role of the dorsolateral prefrontal and anterior cingulate cortex in cognitive control. *Science* 288, 1835–1838. doi: 10.1126/science.288.5472.1835

Menon, V. (2011). Large-scale brain networks and psychopathology: a unifying triple network model. *Trends Cogn. Sci.* 15, 483–506. doi: 10.1016/j.tics.2011.08.003

Menon, V., and Uddin, L. Q. (2010). Saliency, switching, attention and control: a network model of insula function. *Brain Struct. Funct.* 214, 655–667. doi: 10.1007/s00429-010-0262-0

Mignone, R. J., Donnelly, E. F., and Sadowsky, D. (1970). Psychological and neurological comparisons of psychomotor and non-psychomotor epileptic patients. *Epilepsia* 11, 345–359. doi: 10.1111/j.1528-1157.1970.tb03902.x

Miller, E. K., and Cohen, J. D. (2001). An integrative theory of prefrontal cortex function. *Annu. Rev. Neurosci.* 24, 167–202. doi: 10.1146/annurev.neuro.24.1.167

Mirsky, A. F., Duncan, C. C., and Levav, M. (2002). "Neuropsychological studies in idiopathic generalized epilepsy," in *Neuropsychology of Childhood Epilepsy*, eds I. Jambaqué, M. Lassonde and O. Dulac (Springer), 141–150. Available online at: http://link.springer.com/chapter/10.1007/0-306-47612-6_15?no-access=true; http://link.springer.com/book/10.1007/b111137?no-access=true

Paulus, M. P., and Stein, M. B. (2006). An insular view of anxiety. *Biol. Psychiatry* 60, 383–387. doi: 10.1016/j.biopsych.2006.03.042

Raichle, M. E., Macleod, A. M., Snyder, A. Z., Powers, W. J., Gusnard, D. A., and Shulman, G. L. (2001). A default mode of brain function. *Proc. Natl. Acad. Sci. U.S.A.* 98, 676–682. doi: 10.1073/pnas.98.2.676

Roebroeck, A., Formisano, E., and Goebel, R. (2005). Mapping directed influence over the brain using Granger causality and fMRI. *Neuroimage* 25, 230–242. doi: 10.1016/j.neuroimage.2004.11.017

Sato, J. R., Fujita, A., Cardoso, E. F., Thomaz, C. E., Brammer, M. J., and Amaro, E. Jr. (2010). Analyzing the connectivity between regions of interest: an approach based on cluster Granger causality for fMRI data analysis. *Neuroimage* 52, 1444–1455. doi: 10.1016/j.neuroimage.2010.05.022

Sato, J. R., Takahashi, D. Y., Arcuri, S. M., Sameshima, K., Morettin, P. A., and Baccala, L. A. (2009). Frequency domain connectivity identification: an application of partial directed coherence in fMRI. *Hum. Brain Mapp.* 30, 452–461. doi: 10.1002/hbm.20513

Schippers, M. B., Renken, R., and Keysers, C. (2011). The effect of intra- and inter-subject variability of hemodynamic responses on group level Granger causality analyses. *Neuroimage* 57, 22–36. doi: 10.1016/j.neuroimage.2011.02.008

Schmitz, B. (1999). Psychiatric syndromes related to antiepileptic drugs. *Epilepsia* 40, s65–s70. doi: 10.1111/j.1528-1157.1999.tb00887.x

Scott, W. A. (1962). Cognitive complexity and cognitive flexibility. *Sociometry* 25, 405–414. doi: 10.2307/2785779

Seeley, W. W., Menon, V., Schatzberg, A. F., Keller, J., Glover, G. H., Kenna, H., et al. (2007). Dissociable intrinsic connectivity networks for salience processing and executive control. *J. Neurosci.* 27, 2349–2356. doi: 10.1523/JNEUROSCI.5587-06.2007

Seth, A. K. (2010). A MATLAB toolbox for Granger causal connectivity analysis. *J. Neurosci. Methods* 186, 262–273. doi: 10.1016/j.jneumeth.2009.11.020

Sridharan, D., Levitin, D. J., and Menon, V. (2008). A critical role for the right fronto-insular cortex in switching between central-executive and default-mode networks. *Proc. Natl. Acad. Sci. U.S.A.* 105, 12569–12574. doi: 10.1073/pnas.0800005105

Szaflarski, J. P., Difrancesco, M., Hirschauer, T., Banks, C., Privitera, M. D., Gotman, J., et al. (2010). Cortical and subcortical contributions to absence seizure onset examined with EEG/fMRI. *Epilepsy Behav.* 18, 404–413. doi: 10.1016/j.yebeh.2010.05.009

Uddin, L. Q., Kelly, A. M., Biswal, B. B., Castellanos, F. X., and Milham, M. P. (2009). Functional connectivity of default mode network components: correlation, anticorrelation, and causality. *Hum. Brain Mapp.* 30, 625–637. doi: 10.1002/hbm.20531

Uddin, L. Q., Supekar, K., Lynch, C. J., Cheng, K. M., Odriozola, P., Barth, M. E., et al. (2015). Brain state differentiation and behavioral inflexibility in Autism. *Cereb. Cortex* 25, 4740–4747. doi: 10.1093/cercor/bhu161

Uddin, L. Q., Supekar, K. S., Ryali, S., and Menon, V. (2011). Dynamic reconfiguration of structural and functional connectivity across core neurocognitive brain networks with development. *J. Neurosci.* 31, 18578–18589. doi: 10.1523/JNEUROSCI.4465-11.2011

Van Dijk, K. R., Sabuncu, M. R., and Buckner, R. L. (2012). The influence of head motion on intrinsic functional connectivity MRI. *Neuroimage* 59, 431–438. doi: 10.1016/j.neuroimage.2011.07.044

Walter, M., Henning, A., Grimm, S., Schulte, R. F., Beck, J., Dydak, U., et al. (2009). The relationship between aberrant neuronal activation in the pregenual anterior cingulate, altered glutamatergic metabolism, and anhedonia in major depression. *Arch. Gen. Psychiatry* 66, 478–486. doi: 10.1001/archgenpsychiatry.2009.39

Wei, H. L., An, J., Zeng, L. L., Shen, H., Qiu, S. J., and Hu, D. W. (2015). Altered functional connectivity among default, attention, and control networks in idiopathic generalized epilepsy. *Epilepsy Behav.* 46, 118–125. doi: 10.1016/j.yebeh.2015.03.031

White, T. P., Joseph, V., Francis, S. T., and Liddle, P. F. (2010). Aberrant salience network (bilateral insula and anterior cingulate cortex) connectivity during information processing in schizophrenia. *Schizophr. Res.* 123, 105–115. doi: 10.1016/j.schres.2010.07.020

Wu, G. R., Liao, W., Stramaglia, S., Ding, J. R., Chen, H., and Marinazzo, D. (2013). A blind deconvolution approach to recover effective connectivity brain networks from resting state fMRI data. *Med. Image Anal.* 17, 365–374. doi: 10.1016/j.media.2013.01.003

Zeng, L. L., Shen, H., Liu, L., Wang, L., Li, B., Fang, P., et al. (2012). Identifying major depression using whole-brain functional connectivity: a multivariate pattern analysis. *Brain* 135, 1498–1507. doi: 10.1093/brain/aws059

Zeng, L. L., Wang, D., Fox, M. D., Sabuncu, M., Hu, D., Ge, M., et al. (2014). Neurobiological basis of head motion in brain imaging. *Proc. Natl. Acad. Sci. U.S.A.* 111, 6058–6062. doi: 10.1073/pnas.1317424111

Conflict of Interest Statement: The authors declare that the research was conducted in the absence of any commercial or financial relationships that could be construed as a potential conflict of interest.

APPENDIX

COMPUTATION OF GRANGER CAUSALITY MEASURES

For better understanding of the calculation process and the definition of each Granger causality measures, we took a general system of N $(N \geq 3)$ variables $X_i(t)$, $i = 1, 2, \ldots N$ as an example. The unrestricted MVAR model of the system can be written as:

$$\begin{bmatrix} X_1(t) \\ X_2(t) \\ \vdots \\ X_N(t) \end{bmatrix} = \sum_{j=1}^{p} \begin{bmatrix} A_{11}(j) & A_{12}(j) & \ldots & A_{1N}(j) \\ A_{21}(j) & A_{22}(j) & \ldots & A_{2N}(j) \\ \vdots & \vdots & \ddots & \vdots \\ A_{N1}(j) & A_{N2}(j) & \ldots & A_{NN}(j) \end{bmatrix} \cdot \begin{bmatrix} X_1(t-j) \\ X_2(t-j) \\ \vdots \\ X_N(t-j) \end{bmatrix} + \begin{bmatrix} E_1(t) \\ E_2(t) \\ \vdots \\ E_N(t) \end{bmatrix} \tag{A3}$$

where p is the model order, E_i, $i = 1, 2, \ldots N$ are the model residuals (prediction errors), the elements of $\mathbf{A}(j)$ are called regression coefficients. The noise covariance matrix of the unrestricted model can be represented as:

$$\Sigma = \begin{bmatrix} \mathrm{var}(E_1) & \mathrm{cov}(E_1, E_2) & \cdots & \mathrm{cov}(E_1, E_N) \\ \mathrm{cov}(E_2, E_1) & \mathrm{var}(E_2) & \cdots & \mathrm{cov}(E_2, E_N) \\ \vdots & \vdots & \ddots & \vdots \\ \mathrm{cov}(E_N, E_1) & \mathrm{cov}(E_N, E_2) & \cdots & \mathrm{var}(E_N) \end{bmatrix} \tag{A4}$$

To measure the Granger causality from $X_2(t)$ to $X_1(t)$, we delete the row 2 and column 2 of the noise covariance matrix of the unrestricted model, then partition the matrix into blocks:

$$\Sigma = \left[\begin{array}{c|ccc} \mathrm{var}(E_1) & \mathrm{cov}(E_1, E_3) & \cdots & \mathrm{cov}(E_1, E_N) \\ \hline \mathrm{cov}(E_3, E_1) & \mathrm{var}(E_3) & \cdots & \mathrm{cov}(E_3, E_N) \\ \vdots & \vdots & \ddots & \vdots \\ \mathrm{cov}(E_N, E_1) & \mathrm{cov}(E_N, E_3) & \cdots & \mathrm{var}(E_N) \end{array}\right] = \left[\begin{array}{c|c} \sum_{11} & \sum_{12} \\ \hline \sum_{21} & \sum_{22} \end{array}\right] \tag{A5}$$

and omit the time course $X_2(t)$ to obtain a restricted MVAR model as:

$$\begin{bmatrix} X_1(t) \\ X_3(t) \\ \vdots \\ X_N(t) \end{bmatrix} = \sum_{j=1}^{p} \begin{bmatrix} A'_{11}(j) & A'_{13}(j) & \ldots & A'_{1N}(j) \\ A'_{31}(j) & A'_{33}(j) & \ldots & A'_{3N}(j) \\ \vdots & \vdots & \ddots & \vdots \\ A'_{N1}(j) & A'_{N3}(j) & \ldots & A'_{NN}(j) \end{bmatrix} \cdot \begin{bmatrix} X_1(t-j) \\ X_3(t-j) \\ \vdots \\ X_N(t-j) \end{bmatrix} + \begin{bmatrix} E'_1(t) \\ E'_3(t) \\ \vdots \\ E'_N(t) \end{bmatrix} \tag{A6}$$

and the noise covariance matrix of the restricted model is:

$$\boldsymbol{\rho} = \left[\begin{array}{c|ccc} \mathrm{var}(E'_1) & \mathrm{cov}(E'_1, E'_3) & \cdots & \mathrm{cov}(E'_1, E'_N) \\ \hline \mathrm{cov}(E'_3, E'_1) & \mathrm{var}(E'_3) & \cdots & \mathrm{cov}(E'_3, E'_N) \\ \vdots & \vdots & \ddots & \vdots \\ \mathrm{cov}(E'_N, E'_1) & \mathrm{cov}(E'_N, E'_3) & \cdots & \mathrm{var}(E'_N) \end{array}\right] = \left[\begin{array}{c|c} \rho_{11} & \rho_{12} \\ \hline \rho_{21} & \rho_{22} \end{array}\right] \tag{A7}$$

Next, we explore the frequency domain representation of MVAR model. The Fourier transform of (A3) gives:

$$\begin{bmatrix} A_{11}(f) & A_{12}(f) & \ldots & A_{1N}(f) \\ A_{21}(f) & A_{22}(f) & \ldots & A_{2N}(f) \\ \vdots & \vdots & \ddots & \vdots \\ A_{N1}(f) & A_{N2}(f) & \ldots & A_{NN}(f) \end{bmatrix} \begin{bmatrix} X_1(f) \\ X_2(f) \\ \vdots \\ X_N(f) \end{bmatrix} = \begin{bmatrix} E_1(f) \\ E_2(f) \\ \vdots \\ E_N(f) \end{bmatrix} \tag{A8}$$

where the components of the $\mathbf{A}(f)$ matrix are:

$$A_{lm}(f) = \delta_{lm} - \sum_{j=1}^{p} A_{lm}(j) e^{-i2\pi fj} \tag{A9}$$

$$\delta_{lm} = \begin{cases} 1, & l = m \\ 0, & l \neq m \end{cases}$$

and we rewrite the $\mathbf{A}(f)$ to the following form:

$$\mathbf{A}(f) = \begin{bmatrix} A_{11}(f) & A_{12}(f) & \ldots & A_{1N}(f) \\ A_{21}(f) & A_{22}(f) & \ldots & A_{2N}(f) \\ \vdots & \vdots & \ddots & \vdots \\ A_{N1}(f) & A_{N2}(f) & \ldots & A_{NN}(f) \end{bmatrix} = \begin{bmatrix} \mathbf{a}_1(f) & \mathbf{a}_2(f) & \ldots & \mathbf{a}_N(f) \end{bmatrix} \tag{A10}$$

then the Granger causality measures in two domains can be formalized as follows:

TIME DOMAIN PARTIAL GRANGER CAUSALITY

Referring to (A5) and (A7), the partial Granger causality from $X_2(t)$ to $X_1(t)$, conditioned on all the remaining variables besides $X_1(t)$ and $X_2(t)$, is given by:

$$F^{p}_{2\to 1|\mathrm{others}} = \ln \frac{\left|\rho_{11} - \rho_{12}\rho_{22}^{-1}\rho_{21}\right|}{\left|\sum_{11} - \sum_{12}\sum_{22}^{-1}\sum_{21}\right|} \tag{A11}$$

which can avoid influence of exogenous inputs and latent variables, and describe the direct causal relationships between time courses (Guo et al., 2008). When there is no direct influence from $X_2(t)$ to $X_1(t)$, the $A_{12}(j)$, $j = 1 \ldots p$ in (A3) are uniformly

equal to zero, leading to $F^P_{2\to 1|\text{others}} = 0$. On the contrary, when a direct influence from $X_2(t)$ to $X_1(t)$ exists, we will get $F^P_{2\to 1|\text{others}} > 0$.

In addition, a difference of influence (DOI) term is introduced to describe the dominant direction of causal influence that measured as the difference (Roebroeck et al., 2005):

$$D^P_{2\to 1|\text{others}} = F^P_{2\to 1|\text{others}} - F^P_{1\to 2|\text{others}} \tag{A12}$$

which can further limits potentially spurious links caused by hemodynamic blurring (Seth, 2010).

FREQUENCY DOMAIN PARTIAL DIRECTED COHERENCE

To measure the Granger causality from $X_2(t)$ to $X_1(t)$ in frequency domain, the PDC is defined as (Baccalá and Sameshima, 2001):

$$\pi_{12}(f) = \frac{A_{12}(f)}{\sqrt{\mathbf{a}_2^H(f)\mathbf{a}_2(f)}} \tag{A13}$$

It can be seen that the evaluation of Granger causality from $X_2(t)$ to $X_1(t)$ is discretized into a set of frequency slices. Therefore, by selecting the interested frequency range, we can use PDC to evaluate direct Granger causality between time courses at each discrete frequency.

Additionally, the non-normalized DTF from $X_2(t)$ to $X_1(t)$ is given by Kaminski et al. (2001):

$$\theta^2_{12}(f) = \frac{|\mathbf{M_{21}}|^2}{|\mathbf{A(f)}|^2} \tag{A14}$$

where $|\mathbf{M_{21}}|$ is a minor of $\mathbf{A(f)}$ with row 2 and column 1 removed. The DTF in the multivariate condition could not avoid the detection of indirect causal relationship between time courses (Kaminski et al., 2001).

frontiers in Human Neuroscience

ORIGINAL RESEARCH
published: 04 November 2016
doi: 10.3389/fnhum.2016.00549

Aberrant Functional Connectivity between the Amygdala and the Temporal Pole in Drug-Free Generalized Anxiety Disorder

Wei Li[1], Huiru Cui[1], Zhipei Zhu[1], Li Kong[2], Qian Guo[1], Yikang Zhu[1], Qiang Hu[3], Lanlan Zhang[4], Hui Li[1], Qingwei Li[5], Jiangling Jiang[1], Jordan Meyers[6], Jianqi Li[7], Jijun Wang[1, 8, 9], Zhi Yang[10]* and Chunbo Li[1, 8, 9]**

[1] Shanghai Key Laboratory of Psychotic Disorders, Shanghai Mental Health Center, Shanghai Jiao Tong University School of Medicine, Shanghai, China, [2] College of Education, Shanghai Normal University, Shanghai, China, [3] Department of Psychology, Qiqihar Mental Health Center, Qiqihar, China, [4] Guangji Hospital of Suzhou, Suzhou, China, [5] Department of Psychiatry, Tongji Hospital of Tongji University, Shanghai, China, [6] Nathan S. Kline Institute for Psychiatric Research, New York, NY, USA, [7] Shanghai Key Laboratory of Magnetic Resonance, Department of Physics, East China Normal University, Shanghai, China, [8] Key Laboratory for the Genetics of Developmental and Neuropsychiatric Disorders, Bio-X Institutes, Ministry of Education, Shanghai Jiao Tong University, Shanghai, China, [9] Brain Science and Technology Research Center, Shanghai Jiao Tong University, Shanghai, China, [10] CAS Key Laboratory of Behavioral Science and MRI Research Center, Institute of Psychology, Chinese Academy of Sciences, Beijing, China

OPEN ACCESS

Edited by:
Baojuan Li,
Massachusetts General Hospital, USA

Reviewed by:
Xin Di,
New Jersey Institute of Technology, USA
Dawei Li,
Duke University, USA

***Correspondence:**
Jijun Wang
jijunwang27@163.com
Zhi Yang
yangz@psych.ac.cn
Chunbo Li
chunbo_li@163.com

Received: *01 June 2016*
Accepted: *14 October 2016*
Published: *04 November 2016*

Citation:
Li W, Cui H, Zhu Z, Kong L, Guo Q, Zhu Y, Hu Q, Zhang L, Li H, Li Q, Jiang J, Meyers J, Li J, Wang J, Yang Z and Li C (2016) Aberrant Functional Connectivity between the Amygdala and the Temporal Pole in Drug-Free Generalized Anxiety Disorder. Front. Hum. Neurosci. 10:549. doi: 10.3389/fnhum.2016.00549

The amygdala and the dorsolateral prefrontal cortex (DLPFC) play important roles in "emotion dysregulation," which has a profound impact on etiologic research of generalized anxiety disorder (GAD). The present study analyzed both eyes-open and eyes-closed resting state functional MRI (rs-fMRI) of 43 subjects (21 GAD patients with medicine free and 22 matched healthy controls). The amygdala and the DLPFC were defined as regions of interest (ROI) to analyze functional connectivity (FC) in GAD patients compared with healthy controls. The main findings revealed GAD patients had increased FC between the amygdala and the temporal pole compared to healthy controls, which was found in both eyes-open and eyes-closed rs-fMRI. And altered FC between the ROIs and brain regions that mainly belonged to the default mode network (DMN) were found. These findings suggest that the abnormal FC between the amygdala and the temporal pole may contribute to the pathophysiology of GAD, and provide insights into the current understanding of the emotion dysregulation of anxiety disorders.

Keywords: amygdala, DLPFC, temporal pole, DMN, functional connectivity, generalized anxiety disorder

INTRODUCTION

Anxiety disorders are the most common of all mental disorders with 30% prevalence in the population, and they significantly contribute to the economic burden of disease (Andlin-Sobocki and Wittchen, 2005; Kessler et al., 2005; Bereza et al., 2009). Among anxiety disorders, generalized anxiety disorder (GAD) is the most common type (Roy-Byrne and Wagner, 2004; Lieb et al., 2005; Kroenke et al., 2007). GAD is characterized by excessive and continuous worry, anxiety, and apprehension. It may also produce distress and/or functional impairments.

Previous studies have argued that "emotional dysregulation," the inability to control or regulate emotional responses, may be responsible for the development of GAD. This hypothesis is grounded in the observation that individuals with GAD concentrate their attention on threatening thoughts. This cognitive model has been widely adopted for understanding GAD (Mathews and MacLeod, 1985; Bar-Haim et al., 2007; Amir et al., 2009; Behar et al., 2009).

The dorsolateral prefrontal cortex (DLPFC), an important region for performing cognitive operations during the regulation of emotional responses, has been shown to play a key role in the pathophysiology of GAD (MacDonald et al., 2000; Miller and Cohen, 2001; Blasi et al., 2007; Meyer et al., 2011; Moon et al., 2015). Altered activation of the DLPFC in patients with GAD has been associated with emotional dysregulation and attention deficit. Functional MRI studies have reported increased activity of the DLPFC under affective stroop and emotion reappraisal tasks in patients with GAD (Ball et al., 2012; Blair et al., 2012). Additionally, functional abnormalities of the amygdala, known as the most prominent "fear-circuit" structure in the brain that plays a central role in automatic affective processing, have been found in most anxiety disorders (LeDoux, 2000; Anderson et al., 2003; Ohman, 2005; Etkin and Wager, 2007; Adolphs, 2008; Shin and Liberzon, 2010; Linares et al., 2012). The amygdala has also demonstrated responsibility for facilitating perceptual processing and bottom-up emotional control in individuals with GAD (LeDoux, 2000; Davis and Whalen, 2001; Phelps, 2006). Models of emotional regulation have therefore focused primarily on the DLPFC and the amygdala. Accordingly, we assume that individuals with GAD display aberrant FC seeded from the amygdala and the DLPFC compared to healthy controls.

Studies have shed less light on the relationship between the temporal cortex, especially the temporal pole, and GAD. Although the function of the temporal pole is not well understood, a damaged temporal pole can impair ability to use experiential knowledge and therefore may cause affective symptoms (Funnell, 2001). The temporal cortex binds complex, highly processed perceptual inputs to visceral emotional responses (Olson et al., 2007). The temporal pole is located at the end of the ventral visual stream and is strongly interconnected with the amygdala (Nakamura and Kubota, 1996; Stefanacci and Amaral, 2002). It integrates conceptual knowledge and meaning with semantic, visual and auditory information (Carlson et al., 2014), and influences emotions via top-down modulations (Pehrs et al., 2015). Studies have reported altered functional connectivity (FC) between the temporal pole and the amygdala in anxiety disorders (Aghajani et al., 2014; Modi et al., 2015). This finding has prompted us to explore the FC between the temporal pole and the amygdala in GAD patients. Therefore, one of our hypotheses is that altered FC between these two areas is attributed to the etiology of GAD.

Accordingly, the amygdala and the DLPFC will be defined as regions of interest (ROIs) to explore in GAD patients. Because the number of volumes in the eyes-open resting state fMRI (rs-fMRI) we collected was too small, we also analyzed the eyes-closed rs-fMRI using the same protocol to improve the reliability of our results.

MATERIALS AND METHODS

Participants

All participants received the Mini-International Neuropsychiatric Interview (MINI), Chinese version (Si et al., 2009). Twenty two GAD patients who met the criteria for DSM-IV (Association, 2000) and who were not found to have lifetime psychosis, substance dependence or severe somatic diseases were recruited from the psychological outpatient clinic at the Shanghai Mental Health Center. We excluded patients who had comorbid moods or other anxiety disorders. Twenty one healthy controls were recruited from local communities and Shanghai Jiao Tong University. Controls were matched for gender, age, education level, and did not meet DSM-IV criteria for lifetime mood, anxiety, psychotic, or substance dependence disorders. Forty three participants were enrolled in total for this study and according to the Edinburgh Inventory (Oldfield, 1971), all of them are right-handed adults free of psychotropic medications for at least 2 weeks before enrollment. The study was conducted between August 2011 and November 2012.

This study was approved by the Research Ethics Committee of Shanghai Mental Health Center, China (SMHC-IRB 201217). Written informed consent was acquired from every participant.

All participants were informed of the safety and eligibility criteria for fMRI scanning: no neurological conditions and no implanted ferrous metal. The Hamilton Rating Scale for Anxiety (HAMA) (Hamilton, 1959) and Hamilton Rating Scale for Depression (HAMD) (Hamilton, 1967) were administered to all participants on the day of scanning. Demographic and clinical characteristics of the 43 participants are shown in **Table 1**.

Image Acquisition

Images were obtained using a Siemens Trio 3.0 Tesla MRI scanner (Siemens, Erlangen, Germany) with a standard 12-channel head coil. Restraining foam pads was used to reduce head motion and earplugs were used to reduce scanner noise. High-resolution T1-weighted anatomical images (repetition time (TR) = 1900 ms, echo time (TE) = 2.46 ms, flip angle = 9 degrees, 32 transverse slices, field of view (FOV) = 240 × 240 mm, matrix = 256 × 256, slice thickness = 1 mm) were acquired using a magnetization prepared rapid gradient-echo sequence. Resting-state functional MRI data were acquired using a single-shot, gradient-recalled echo planar imaging sequence (TR = 2000

TABLE 1 | Demographic and clinical data.

Parameter	GAD	HC	*p*-value
	n = 21	*n* = 22	
Age (years)	39.90 ± 12.24	38.05 ± 10.32	0.593
Gender (M/F)	13/7	14/8	0.927
Education (years)	11.19 ± 3.31	12.50 ± 2.59	0.142
HAMA	18.6 ± 9.01	0.76 ± 0.94	0.000
HAMD	9.23 ± 5.10	0.86 ± 1.20	0.000

HAMA, Hamilton Anxiety Scale; HAMD, Hamilton Depression Scale; GAD, generalized anxiety disorder; HC: healthy control.

ms, TE = 25 ms, flip angle = 90 degrees). 32 transverse slices (FOV = 240 × 240 mm, matrix = 64 × 64, slice thickness = 5 mm) resulting in a total of 80/157 volumes and a scan time of 164/314 s, respectively, in eyes-open and eyes-closed rs-fMRI. During the scan, participants were instructed to stay aware. After the scan, the technicians would check the quality of structural images. If any abnormalities were found in the images, participants were re-scanned.

Data Processing and Analysis

Demographic and Clinical Data Analysis

Using Statistical Product and Service Solutions software 17.0 (SPSS, Inc., Chicago, Illinois), we conducted analysis of age, gender, years of education, HAMA, and HAMD. Independent sample *t*-tests for continuous variables and chi-square tests for categorical variables were used.

Resting-State fMRI Analysis

The Data Processing Assistant for Resting-State fMRI 2.0 (DPARSFA2.0, http://restfmri.net/forum/) (Chao-Gan and Yu-Feng, 2010), which works with the Statistical Parametric Mapping Software (SPM8, http://www.fil.ion.ucl.ac.uk/spm) (Friston et al., 1994) was used to analyze the rs-fMRI data. Preprocessing was completed in 7 steps: (1) Convert DICOM data to NIFTI format and remove first 10 time points of the image; (2) Slice timing correction and realignment of image; (3) Parallel movements in any direction >2.5 mm, or rotary movements >2.5 degree were excluded and subjects using a threshold of frame-wise displacement >0.5 mm (Power et al., 2012) were also excluded; (4) Spatial normalization to the standard Montreal Neurological Institute (MNI) echo-planar imaging template and the resampled voxel size was 3 × 3 × 3 mm; (5) Conduct Friston 24-parameter correction (Yan et al., 2013) to minimize the effect of head motion; (6) Smoothing with a Gaussian kernel of 8-mm full-width at half-maximum (FWHM); (7) After linear detrending, the functional data was band-pass filtered (pass frequence band: 0.01–0.1 Hz) to reduce the effects of low-frequency drift as well as high-frequency respiratory and cardiac noise (Biswal et al., 1995).

According to previous studies (Cieslik et al., 2013; Comte et al., 2014; Cui et al., 2016), the bilateral amygdala (MNI: 32,−2,−26;−28, 4,−22) and the bilateral DLPFC (MNI: 30, 43, 23;−51, 27, 30) were defined as ROIs. The peak voxel of each ROI and a 6 mm-radius sphere were selected to proceed with the FC analysis. The Pearson correlation coefficients were calculated between the ROI and the other voxels of the whole brain. Fisher's r-to-z transformation was used to convert correlation coefficients into z-scores so that the correlation coefficient would improve the normality of the data (Hampson et al., 2002; Chao-Gan and Yu-Feng, 2010; Song et al., 2011), and generate FC maps. Voxel-wise two-sample *t*-tests were conducted to compare group differences between GAD patients and controls. Spearman correlation analysis was performed in GAD patients to investigate the correlation between FC and disease severity (HAMA score). Both *t*-tests and correlation analysis were conducted under the BrainMask_61*73*61. As correction for multiple comparisons, a corrected threshold of $p < 0.05$ (two-tailed) was derived from a combined threshold of $p < 0.005$ for individual voxel with a cluster size >53 voxels. These threshold were determined using the 3dFWHM and 3dClustSim program in AFNI software (https://afni.nimh.nih.gov/afni, parameters: single voxel $p < 0.005$, 2000 Monte Carlo iterations, estimated FWHM = 9.5 mm, the BrainMask_61*73*61 was used as mask in estimation of smoothness and correction). Additionally, age, years of education, HAMD score and intracranial volume (ICV) were modeled as covariates. The analyses above were conducted in both eyes-open and eyes-closed rs-fMRI.

In order to improve the reliability of these results, we calculated mean frame-wise displacement for each group and conducted *t*-tests between matched groups in SPSS.

RESULTS

Demographic and Clinical Characteristics

Compared with the healthy control group, the HAMA scores and HAMD scores were significantly different in GAD patients ($P < 0.05$). Except that, there is no significant difference between GAD patients and healthy controls.

Resting-State fMRI Results

Functional Connectivity

Compared with healthy controls, GAD patients showed increased FC between the left amygdala and the temporal pole both in eyes-open and eyes-closed rs-fMRI ($P < 0.005$ to define cluster, AlphaSim correction, cluster size >53 voxels, overall $p < 0.05$).

In eyes-open rs-fMRI, there was increased connectivity between the left amygdala and the inferior frontal gyrus in the GAD group compared with the control group ($P < 0.005$ to define cluster, AlphaSim correction, cluster size >53 voxels, overall $p < 0.05$). (**Figure 1**, **Table 2**) There was no significant abnormal FC between GAD subjects and controls seeded from the DLPFC.

In eyes-closed rs-fMRI, we found increased FC in the left amygdala with the middle temporal gyrus ($P < 0.005$ to define cluster, AlphaSim correction, cluster size >53 voxels, overall $p < 0.05$). Decreased FC between the left DLPFC and the precuneus, the lingual gyrus, the calcarine sulcus, and the cerebellar vermis was detected in GAD subjects compared with healthy controls ($P < 0.005$ to define cluster, AlphaSim correction, cluster size >53 voxels, overall $p < 0.05$). There was decreased connectivity between the right DLPFC and the medial prefrontal cortex (mPFC), the dorsal anterior cingulate cortex (dACC), the middle temporal gyrus, the angular gyrus, the precuneus, the calcarine sulcus, and the cerebellar vermis in GAD subjects compared with healthy controls ($P < 0.005$ to define cluster, AlphaSim correction, cluster size >53 voxels, overall $p < 0.05$). (**Figure 2**, **Table 2**).

Correlation Analysis of FC and Illness Severity

In eyes-open rs-fMRI, the HAMA score had a significant negative correlation with the FC between the left amygdala and the superior frontal gyrus in GAD subjects ($P < 0.005$ to define cluster, AlphaSim correction, cluster size >53 voxels, overall $p < 0.05$). The FC between the right amygdala and the

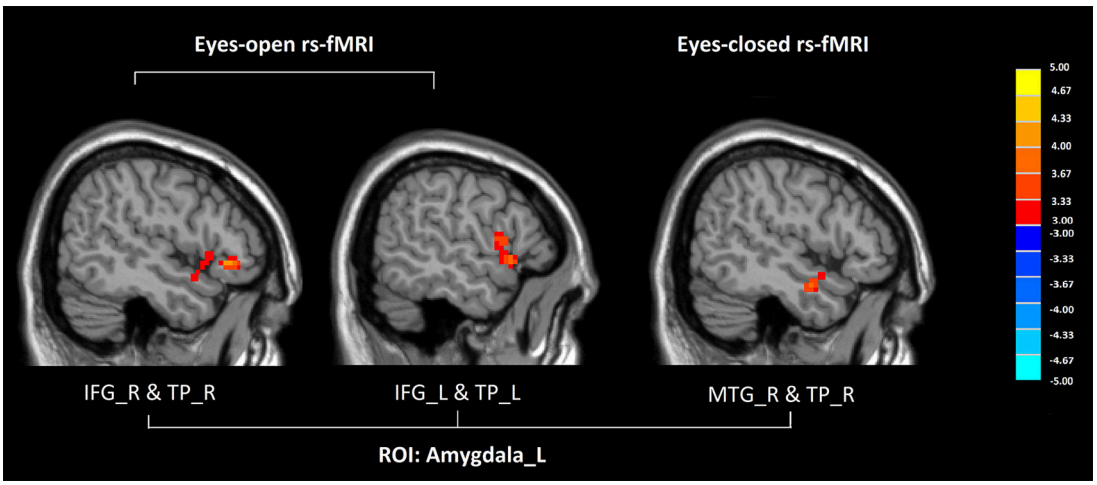

FIGURE 1 | Altered functional connectivity seeded from the left amygdala in GAD, compared with HC ($P < 0.005$ to define cluster, AlphaSim correction, cluster size >53 voxels, overall $p < 0.05$). Hot colors indicate increased functional connectivity in GAD compared with HC. (GAD, generalized anxiety disorder; HC, healthy control; rs-fMRI, resting state fMRI; IFG, inferior frontal gyrus; TP, temporal gyrus; MTG, middle temporal gyrus; L, left; R, right).

TABLE 2 | Alterations in FC seeded from the amygdala and DLPFC between GAD and HC.

Brain regions	BA	MNI coordinates			Voxel	Peak *t*-value
		X	*Y*	*Z*		
EYES-OPEN rs-fMRI						
ROI: AMYGDALA_L						
Inferior frontal gyrus_R	47, 22, 38	57	36	−6	76	4.40
Temporal pole_R						
Inferior frontal gyrus_L	22, 44, 47	−57	12	−3	58	3.93
Temporal pole_L						
EYES-CLOSED rs-fMRI						
ROI: AMYGDALA_L						
Middle temporal gyrus_R	21, 38	48	−6	−24	54	4.12
Temporal pole_R						
ROI: DLPFC_R						
Medial prefrontal cortex_L/R	11, 32, 25	6	36	−9	867	−6.16
Dorsal anterior cingulate cortex_L/R						
Middle temporal gyrus_R	21	60	3	−21	95	−4.84
Precuneus_L						
Calcarine sulcus_L	30, 29, 23	6	−51	0	412	−4.93
Cerebellar vermis						
Angular gyrus_R	39	42	−63	21	74	−4.37
ROI: DLPFC_L						
Precuneus_L	29, 30	−21	−48	0	258	−4.14
Lingual gyrus_L						
Calcarine sulcus_L						
Cerebellar vermis						

R, right; L, left; BA, Brodmann's area; MNI, Montreal Neurological Institute; GAD, generalized anxiety disorder; HC, healthy control; FC, functional connectivity; DLPFC, dorsolateral prefrontal cortex; ROI, region of interest.

fusiform gyrus, the superior/middle occipital gyrus, and the cerebellum was positively correlated to the HAMA score in GAD subjects ($P < 0.005$ to define cluster, AlphaSim correction, cluster size >53 voxels, overall $p < 0.05$). We found that the HAMA score was positively correlated with the FC between the DLPFC and the inferior frontal gyrus, the supplementary motor area (SMA), and the cerebellum in GAD subjects ($P < 0.005$ to define cluster, AlphaSim correction, cluster size >53 voxels, overall $p < 0.05$). (**Table 3**, Supplement Figure 1)

In eyes-closed rs-fMRI, the HAMA score had a significant positive correlation with the FC between the right DLPFC and the lingual gyrus, the cuneus, the fusiform gyrus, the inferior/middle occipital gyrus, and the cerebellum in GAD subjects ($P < 0.005$ to define cluster, AlphaSim correction, cluster size >53 voxels, overall $p < 0.05$). (**Table 3**, Supplement Figure 1).

Additionally, both in eyes-open and eyes-closed rs-fMRI, we did not find a significant difference in frame-wise displacement between GAD patients and healthy controls [$p = 0.926$ (eyes-open), 0.271 (eyes-closed)].

DISCUSSION

In this study, we conducted analysis to characterize alterations in FC that may show the pathological basis of GAD using both the eyes-open and the eyes-closed rs-fMRI. While exploring FC seeded from the amygdala and the DLPFC, we found: (1) Patients with GAD showed increased FC between the left amygdala and the temporal pole compared with health controls. (2) In both eyes-open and eyes-closed conditions, the brain regions showed altered FC with amygdala/DLPFC were primarily from the default mode network (DMN).

Increased FC between the amygdala and the temporal pole was detected by both eyes-open and eyes-closed rs-fMRI. This finding may illustrate that the altered FC may contribute to the etiology

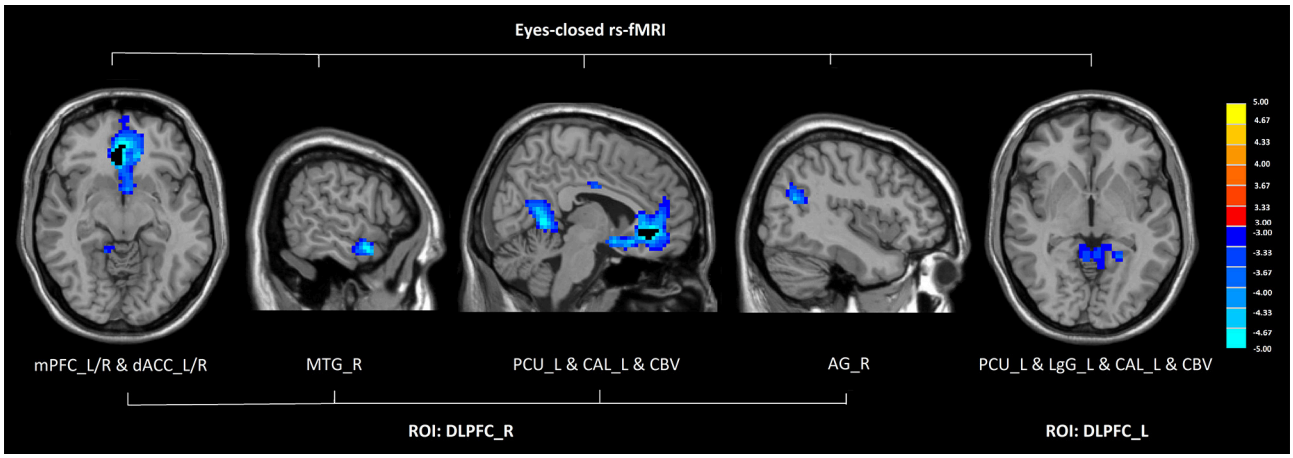

FIGURE 2 | Altered functional connectivity seeded from the bilateral DLPFC in GAD, compared with HC ($P < 0.005$ to define cluster, AlphaSim correction, cluster size >53 voxels, overall $p < 0.05$). Hot and cold colors indicate increased and decreased FC in GAD compared with HC. (DLPFC, dorsolateral prefrontal cortex; GAD, generalized anxiety disorder; HC, healthy control; rs-fMRI, resting state fMRI; mPFC, medial prefrontal cortex; dACC, dorsal anterior cingulate cortex; MTG, middle temporal gyrus; PCU, precuneus; CAL, calcarine sulcus; CBV, cerebellar vermis; AG, angular gyrus; LgG, lingual gyrus; L, left; R, right).

of GAD. Previous findings indicate that the temporal pole plays a role in both social and emotional processing, including specific recognition, theory of mind (Wong and Gallate, 2012), memory (Damasio et al., 1996), and encodes similarity relations among different concepts (Patterson et al., 2007). It is also thought to be involved in access to knowledge during "mentalizing," which refers to the attribution of intentions and other mental states (Frith and Frith, 2003). The amygdala is one of the most investigated structures of the brain, especially in the context of emotional processing. The amygdala is marked as the most prominent "fear-circuit" structure, and hyperactivation of the amygdala is found in most anxiety disorders (Etkin and Wager, 2007; Shin and Liberzon, 2010; Linares et al., 2012). And it has been studied extensively within the context of fear conditioning and extinction as key processes for the pathophysiology of anxiety disorders. The FC between the amygdala and the temporal pole may reflect integration of emotional regulation with knowledge during stimuli perception and mentalizing in healthy subjects. This neural process is presumably disrupted in GAD, which is consistent with observations of deficits in socio-emotional behaviors (Aghajani et al., 2014). The increased connectivity between the temporal pole and the amygdala in GAD patients may be responsible for why stimuli more easily evoke anxiety in GAD patients.

The default mode network (DMN) is defined as the set of regions in the brain that are consistently more activated during resting condition than other brain networks (Fox and Raichle, 2007). It is often described as a unitary, homogeneous system that is largely involved in the integration of autobiographical memories and in self-monitoring, in the retrieval and manipulation of past events in an effort to solve problems and develop future plans, and in emotion regulation (Greicius et al., 2003). When a task requires attention, however, the activation of such network is suppressed. Deficits in DMN suppression are reported in several mental illnesses, notably anxiety disorders (Anticevic et al., 2012). Our results showed altered FC between the amygdala and several regions of the brain including the temporal pole, the middle temporal gyrus, which belong to the DMN, in the GAD group compared with the control group. Altered FC was also found between the DLPFC and brain regions of the DMN, such as the mPFC, the angular gyrus, and the precuneus in the GAD group.

The middle temporal gyrus is regarded as an important brain structure in the integration of memory, audiovisual association, object-recognition and visual perception (Li et al., 2013; Shao et al., 2013). The middle temporal gyrus was found to have increased FC between the amygdala. This finding may reflect an increased predisposition for inaccurate interpretation of stimuli (Pannekoek et al., 2013). However, the FC between the DLPFC and the middle temporal gyrus, and the mPFC was decreased in GAD patients compared with healthy controls. The DLPFC is involved in the function of working memory, executive functions, emotion regulation, subjective feelings, and self-awareness (Craig, 2002; Critchley et al., 2004). The mPFC is widely known to be crucial for emotion regulation, especially for controlling negative emotional responses (Etkin et al., 2009). The angular gyrus, which is also a part of the DMN, has been implicated in affective regulation associated with empathic response, anxiety, and mood (Leung et al., 2013). The precuneus is implicated in episodic memory, visuospatial processing, self-reflection and aspects of consciousness (Fox et al., 2015; Hannawi et al., 2015; Kwok and Macaluso, 2015). The decreased FC between the DLPFC and the brain regions in the DMN may explain uncontrolled emotional regulation in GAD patients. This finding was consistent with our previous study and the models of "bottom-up" and "top-down" emotional processing (Phillips et al., 2003, 2008; Ochsner and Gross, 2005; Phan et al., 2005; Goldin et al., 2008; Cui et al., 2016).

TABLE 3 | Correlation between altered functional connectivity and HAMA scores for GAD patients.

Brain regions	BA	MNI coordinates			Voxel	Rho
		X	*Y*	*Z*		
EYES-OPEN rs-fMRI						
ROI: AMYGDALA_R						
Fusiform gyrus_L	37, 19	−24	−42	−18	66	0.77
Cerebellar vermis	NA	6	−48	−9	100	0.82
Cerebellum_L						
Superior occipital gyrus_R	19	24	−78	36	71	0.81
Middle occipital gyrus_R						
ROI: AMYGDALA_L						
Superior frontal gyrus_L	9	−3	36	33	67	−0.79
ROI: DLPFC_R						
Cerebellum_R	NA	12	−48	−60	76	0.81
Supplementary motor area_L	6	−15	3	75	72	0.85
ROI: DLPFC_L						
Cerebellum_R	NA	33	−48	−51	78	0.83
Inferior frontal gyrus_L	38, 47	−51	24	6	119	0.84
EYES-CLOSED rs-fMRI						
ROI: DLPFC_R						
Cerebellum_R	19	30	−51	−18	70	0.82
Fusiform gyrus_R						
Fusiform gyrus_L	37, 19	−24	−51	−12	80	0.82
Lingual gyrus_L						
Inferior occipital gyrus_L	19	−48	−72	−9	74	0.86
Middle occipital gyrus_R	19	42	−78	9	69	0.85
Cuneus_ R	19, 18	6	−81	39	125	0.81

R, right; L, left; BA, Brodmann's area; MNI, Montreal Neurological Institute; GAD, generalized anxiety disorder; HC, healthy control; DLPFC, dorsolateral prefrontal cortex; HAMA, Hamilton Anxiety Scale; ROI, region of interest.

The lingual gyrus, the cuneus, and the fusiform gyrus all belong to the visual network (VN). Functional abnormalities of these regions reflect excessive vigilance as a hallmark of anxiety disorders. The VN is associated with pathological memories and planning a response to potentially threatening stimuli (Bremner et al., 1999). The dACC, a part of the salience network (SN), plays a central role in detecting emotional salience and triggering cognitive control via FC with the DLPFC (Sridharan et al., 2008; Bressler and Menon, 2010). Both the DLPFC and the dorsal ACC are implicated in emotional regulation circuits (Bush et al., 2000; Brühl et al., 2014). Therefore, the decreased FC between the DLPFC and the VN/SN may be related to the loss of emotional regulation from the DLPFC in GAD patients. The cerebellum is linked with the cerebrum, brainstem, and spinal cord through efferent and afferent fibers, and the cerebellar vermis is connected to the amygdala anatomically in animals (De Bellis et al., 2002). Recently, more and more studies have reported the cerebellum is functionally related to expressing fear and processing fear memory (Supple et al., 1987; Sacchetti et al., 2005). Cerebellar cognitive affective syndrome was observed in patients with cerebellar damage (Stoodley, 2012). The DLPFC is involved in executive control (Habas et al., 2009; O'Reilly et al., 2010; Yeo et al., 2011), so the connectivity between the cerebellum and the DLPFC may mediate anxiety (Caulfield et al., 2016). And it supports our finding that the decreased FC between the DLPFC and the cerebellum in GAD patients compared with healthy controls.

Regarding the underlying mechanism, the temporal lobe, especially the temporal pole, may be the emphasis for future treatment of GAD. Although there some studies reported the effect of transcranial direct current stimulation (tDSC) and repetitive transcranial magnetic stimulation (rTMS) in curing GAD, the outcomes are various. According to our findings, we prefer the temporal pole as the stimulated target. By decreasing the related abnormal FC may remit anxiety in GAD patients.

CONCLUSION AND LIMITATIONS

In conclusion, our study found altered FC seeded from the amygdala and the DLPFC in GAD patients using eyes-open and eyes-closed rs-fMRI. We found that the increased FC between the amygdala and the temporal pole may be underlying the neural pathophysiology of GAD. We hope these findings will shed light on the current understanding of GAD and on advanced therapeutic interventions.

A limitation in this study is that we were only able to acquire 164 s in the eyes-open resting state fMRI data and the reliability of FC analysis under this condition is limited (Shehzad et al., 2009; Thomason et al., 2011; Braun et al., 2012; Li et al., 2012). Nonetheless, the consistency between eyes-open and eyes-closed conditions alleviates this concern and provides support for our conclusion. Additionally, as fMRI data was acquired using the parameters TR = 2s, slices = 30, band pass filtering in the range $0.01 < f < 0.1$ Hz, cardiac and respiratory fluctuations may still reduce the specificity of low frequency fluctuations to functional connected regions (Lowe et al., 1998). Future research will focus on MRI follow-up and will explore changes in neuroimaging of GAD.

AUTHOR CONTRIBUTIONS

WL: manuscript, data gathering and analysis. HC, ZZ, QH, LZ, JM, and HL: manuscript and data gathering. LK, JJ, QG, and YZ: manuscript and analysis. JL and QL: data gathering and quality control. JW and ZY: manuscript, administration, and editing. CL: research plan development, manuscript, administration, and editing.

FUNDING

Funding for this study was provided by the National Natural Science Foundation of China (81071098, 81270023, 81571756)(to CL and ZY), Shanghai Health System Leadership in Health Research Program (XBR2011005) (to CL), Shanghai Health Bureau Project (2013SY003) (to JW), the Science

and Technology Commission of Shanghai Municipality (13dz2260500, 15411950201, 14411961400, 20154Y0080) (to CL, ZZ, and JW), Shanghai Clinical Center for Mental Disorders (2014), National Key Clinical Disciplines at Shanghai Mental Health Center (Office of Medical Affairs, Ministry of Health, 2011-873; OMA-MH, 2011-873)(to HC), Beijing Nova Program for Science and Technology (XXJH2015B079)(to ZY), Pfizer Investigator Initiation Research Fund (WI173560)(to CL) and Chinese Government Scholarship (CSC NO.201606230115) (to WL).

ACKNOWLEDGMENTS

The authors wish to thank all the subjects for their participation in the study.

SUPPLEMENTARY MATERIAL

The Supplementary Material for this article can be found online at: http://journal.frontiersin.org/article/10.3389/fnhum.2016.00549/full#supplementary-material

REFERENCES

Adolphs, R. (2008). Fear, faces, and the human amygdala. *Curr. Opin. Neurobiol.* 18, 166–172. doi: 10.1016/j.conb.2008.06.006

Aghajani, M., Veer, I. M., van Tol, M. J., Aleman, A., van Buchem, M. A., Veltman, D. J., et al. (2014). Neuroticism and extraversion are associated with amygdala resting-state functional connectivity. *Cogn. Affect. Behav. Neurosci.* 14, 836–848. doi: 10.3758/s13415-013-0224-0

Amir, N., Beard, C., Burns, M., and Bomyea, J. (2009). Attention modification program in individuals with generalized anxiety disorder. *J. Abnorm. Psychol.* 118, 28–33. doi: 10.1037/a0012589

Anderson, A. K., Christoff, K., Panitz, D., De Rosa, E., and Gabrieli, J. D. (2003). Neural correlates of the automatic processing of threat facial signals. *J. Neurosci.* 23, 5627–5633.

Andlin-Sobocki, P., and Wittchen, H. U. (2005). Cost of anxiety disorders in Europe. *Eur. J. Neurol.* 12(Suppl. 1), 39–44. doi: 10.1111/j.1468-1331.2005.01196.x

Anticevic, A., Cole, M. W., Murray, J. D., Corlett, P. R., Wang, X.-J., and Krystal, J. H. (2012). The role of default network deactivation in cognition and disease. *Trends Cogn. Sci.* 16, 584–592. doi: 10.1016/j.tics.2012.10.008

Association, A. P. (2000). *Diagnostic and Statistical Manual of Mental Disorders. 4*. Washington, DC: American Psychiatric Association.

Ball, T. M., Sullivan, S., Flagan, T., Hitchcock, C. A., Simmons, A., Paulus, M. P., et al. (2012). Selective effects of social anxiety, anxiety sensitivity, and negative affectivity on the neural bases of emotional face processing. *Neuroimage* 59, 1879–1887. doi: 10.1016/j.neuroimage.2011.08.074

Bar-Haim, Y., Lamy, D., Pergamin, L., Bakermans-Kranenburg, M. J., and van IJzendoorn, M. H. (2007). Threat-related attentional bias in anxious and nonanxious individuals: a meta-analytic study. *Psychol. Bull.* 133, 1–24. doi: 10.1037/0033-2909.133.1.1

Behar, E., DiMarco, I. D., Hekler, E. B., Mohlman, J., and Staples, A. M. (2009). Current theoretical models of generalized anxiety disorder (GAD): conceptual review and treatment implications. *J. Anxiety Disord.* 23, 1011–1023. doi: 10.1016/j.janxdis.2009.07.006

Bereza, B. G., Machado, M., and Einarson, T. R. (2009). Systematic review and quality assessment of economic evaluations and quality-of-life studies related to generalized anxiety disorder. *Clin. Ther.* 31, 1279–1308. doi: 10.1016/j.clinthera.2009.06.004

Biswal, B., Zerrin Yetkin, F. Z., Haughton, V. M., and Hyde, J. S. (1995). Functional connectivity in the motor cortex of resting human brain using echo-planar mri. *Magn. Reson. Med.* 34, 537–541. doi: 10.1002/mrm.1910340409

Blair, K. S., Geraci, M., Smith, B. W., Hollon, N., DeVido, J., Otero, M., et al. (2012). Reduced dorsal anterior cingulate cortical activity during emotional regulation and top-down attentional control in generalized social phobia, generalized anxiety disorder, and comorbid generalized social phobia/generalized anxiety disorder. *Biol. Psychiatry* 72, 476–482. doi: 10.1016/j.biopsych.2012.04.013

Blasi, G., Goldberg, T. E., Elvevåg, B., Rasetti, R., Bertolino, A., Cohen, J., et al. (2007). Differentiating allocation of resources and conflict detection within attentional control processing. *Eur. J. Neurosci.* 25, 594–602. doi: 10.1111/j.1460-9568.2007.05283.x

Braun, U., Plichta, M. M., Esslinger, C., Sauer, C., Haddad, L., Grimm, O., et al. (2012). Test–retest reliability of resting-state connectivity network characteristics using fMRI and graph theoretical measures. *Neuroimage* 59, 1404–1412. doi: 10.1016/j.neuroimage.2011.08.044

Bremner, J. D., Narayan, M., Staib, L. H., Southwick, S. M., McGlashan, T., and Charney, D. S. (1999). Neural correlates of memories of childhood sexual abuse in women with and without posttraumatic stress disorder. *Am. J. Psychiatry* 156, 1787–1795.

Bressler, S. L., and Menon, V. (2010). Large-scale brain networks in cognition: emerging methods and principles. *Trends Cogn. Sci.* 14, 277–290. doi: 10.1016/j.tics.2010.04.004

Brühl, A. B., Hänggi, J., Baur, V., Rufer, M., Delsignore, A., Weidt, S., et al. (2014). Increased cortical thickness in a frontoparietal network in social anxiety disorder. *Hum. Brain Mapp.* 35, 2966–2977. doi: 10.1002/hbm.22378

Bush, G., Luu, P., and Posner, M. I. (2000). Cognitive and emotional influences in anterior cingulate cortex. *Trends Cogn. Sci.* 4, 215–222. doi: 10.1016/S1364-6613(00)01483-2

Carlson, T. A., Simmons, R. A., Kriegeskorte, N., and Slevc, L. R. (2014). The emergence of semantic meaning in the ventral temporal pathway. *J. Cogn. Neurosci.* 26, 120–131. doi: 10.1162/jocn_a_00458

Caulfield, M. D., Zhu, D. C., McAuley, J. D., and Servatius, R. J. (2016). Individual differences in resting-state functional connectivity with the executive network: support for a cerebellar role in anxiety vulnerability. *Brain Struct. Funct.* 221, 3081–3093. doi: 10.1007/s00429-015-1088-6

Chao-Gan, Y., and Yu-Feng, Z. (2010). DPARSF: a MATLAB toolbox for "pipeline" data analysis of resting-state fMRI. *Front. Syst. Neurosci.* 4:13. doi: 10.3389/fnsys.2010.00013

Cieslik, E. C., Zilles, K., Caspers, S., Roski, C., Kellermann, T. S., Jakobs, O., et al. (2013). Is there "one" DLPFC in cognitive action control? Evidence for heterogeneity from co-activation-based parcellation. *Cereb. Cortex* 23, 2677–2689. doi: 10.1093/cercor/bhs256

Comte, M., Schön, D., Coull, J. T., Reynaud, E., Khalfa, S., Belzeaux, R., et al. (2014). Dissociating bottom-up and top-down mechanisms in the cortico-limbic system during emotion processing. *Cereb. Cortex* 26, 144–155. doi: 10.1093/cercor/bhu185

Craig, A. D. (2002). How do you feel? Interoception: the sense of the physiological condition of the body. *Nat. Rev. Neurosci.* 3, 655–666. doi: 10.1038/nrn894

Critchley, H. D., Wiens, S., Rotshtein, P., and Öhman, A., Dolan, R. J. (2004). Neural systems supporting interoceptive awareness. *Nat. Neurosci.* 7, 189–195. doi: 10.1038/nn1176

Cui, H., Zhang, J., Liu, Y., Li, Q., Li, H., Zhang, L., et al. (2016). Differential alterations of resting-state functional connectivity in generalized anxiety disorder and panic disorder. *Hum. Brain Mapp.* 37, 1459–1473. doi: 10.1002/hbm.23113

Damasio, H., Grabowski, T. J., Tranel, D., Hichwa, R. D., and Damasio, A. R. (1996). A neural basis for lexical retrieval. *Nature* 380, 499–505. doi: 10.1038/380499a0

Davis, M., and Whalen, P. J. (2001). The amygdala: vigilance and emotion. *Mol. Psychiatry* 6, 13–34. doi: 10.1038/sj.mp.4000812

De Bellis, M. D., Keshavan, M. S., Shifflett, H., Iyengar, S., Dahl, R. E., Axelson, D. A., et al. (2002). Superior temporal gyrus volumes in pediatric generalized anxiety disorder. *Biol. Psychiatry* 51, 553–562. doi: 10.1016/S0006-3223(01)01375-0

Etkin, A., Prater, K. E., Schatzberg, A. F., Menon, V., and Greicius, M. D. (2009). Disrupted amygdalar subregion functional connectivity and evidence of a compensatory network in generalized anxiety disorder. *Arch. Gen. Psychiatry* 66, 1361–1372. doi: 10.1001/archgenpsychiatry.2009.104

Etkin, A., and Wager, T. D. (2007). Functional neuroimaging of anxiety: a meta-analysis of emotional processing in PTSD, social anxiety disorder, and specific phobia. *Am. J. Psychiatry* 164, 1476–1488. doi: 10.1176/appi.ajp.2007.07030504

Fox, K. C. R., Spreng, R. N., Ellamil, M., Andrews-Hanna, J. R., and Christoff, K. (2015). The wandering brain: meta-analysis of functional neuroimaging studies of mind-wandering and related spontaneous thought processes. *Neuroimage* 111, 611–621. doi: 10.1016/j.neuroimage.2015.02.039

Fox, M. D., and Raichle, M. E. (2007). Spontaneous fluctuations in brain activity observed with functional magnetic resonance imaging. *Nat. Rev. Neurosci.* 8, 700–711. doi: 10.1038/nrn2201

Friston, K. J., Holmes, A. P., Worsley, K. J., Poline, J. P., Frith, C. D., and Frackowiak, R. S. (1994). Statistical parametric maps in functional imaging: a general linear approach. *Hum. Brain Mapp.* 2, 189–210. doi: 10.1002/hbm.460020402

Frith, U., and Frith, C. D. (2003). Development and neurophysiology of mentalizing. *Philos. Trans. R. Soc. Lond. B Biol. Sci.* 358, 459–473. doi: 10.1098/rstb.2002.1218

Funnell, E. (2001). Evidence for scripts in semantic dementia: implications for theories of semantic memory. *Cogn. Neuropsychol.* 18, 323–341. doi: 10.1080/02643290042000134

Goldin, P. R., McRae, K., Ramel, W., and Gross, J. J. (2008). The neural bases of emotion regulation: reappraisal and suppression of negative emotion. *Biol. Psychiatry* 63, 577–586. doi: 10.1016/j.biopsych.2007.05.031

Greicius, M. D., Krasnow, B., Reiss, A. L., and Menon, V. (2003). Functional connectivity in the resting brain: a network analysis of the default mode hypothesis. *Proc. Natl. Acad. Sci. U.S.A.* 100, 253–258. doi: 10.1073/pnas.0135058100

Habas, C., Kamdar, N., Nguyen, D., Prater, K., Beckmann, C. F., Menon, V., et al. (2009). Distinct cerebellar contributions to intrinsic connectivity networks. *J. Neurosci.* 29, 8586–8594. doi: 10.1523/JNEUROSCI.1868-09.2009

Hamilton, M. (1959). The assessment of anxiety states by rating. *Br. J. Med. Psychol.* 32, 50–55. doi: 10.1111/j.2044-8341.1959.tb00467.x

Hamilton, M. (1967). Development of a rating scale for primary depressive illness. *Br. J. Soc. Clin. Psychol.* 6, 278–296. doi: 10.1111/j.2044-8260.1967.tb00530.x

Hampson, M., Peterson, B. S., Skudlarski, P., Gatenby, J. C., and Gore, J. C. (2002). Detection of functional connectivity using temporal correlations in MR images. *Hum. Brain Mapp.* 15, 247–262. doi: 10.1002/hbm.10022

Hannawi, Y., Lindquist, M. A., Caffo, B. S., Sair, H. I., and Stevens, R. D. (2015). Resting brain activity in disorders of consciousness A systematic review and meta-analysis. *Neurology* 84, 1272–1280. doi: 10.1212/WNL.0000000000001404

Kessler, R. C., Berglund, P., Demler, O., Jin, R., Merikangas, K. R., and Walters, E. E. (2005). Lifetime prevalence and age-of-onset distributions of DSM-IV disorders in the national comorbidity survey replication. *Arch. Gen. Psychiatry* 62, 593–602. doi: 10.1001/archpsyc.62.6.593

Kroenke, K., Spitzer, R. L., Williams, J. B., Monahan, P. O., and Lowe, B. (2007). Anxiety disorders in primary care: prevalence, impairment, comorbidity, and detection. *Ann. Intern. Med.* 146, 317–325. doi: 10.7326/0003-4819-146-5-200703060-00004

Kwok, S. C., and Macaluso, E. (2015). Immediate memory for "when, where and what:" short-delay retrieval using dynamic naturalistic material. *Hum. Brain Mapp.* 36, 2495–2513. doi: 10.1002/hbm.22787

LeDoux, J. E. (2000). Emotion circuits in the brain. *Annu. Rev. Neurosci.* 23, 155–184. doi: 10.1146/annurev.neuro.23.1.155

Leung, M.-K., Chan, C. C. H., Yin, J., Lee, C.-F., So, K.-F., and Lee, T. M. C. (2013). Increased gray matter volume in the right angular and posterior parahippocampal gyri in loving-kindness meditators. *Soc. Cogn. Affect. Neurosci.* 8, 34–39. doi: 10.1093/scan/nss076

Li, R., Wang, S., Zhu, L., Guo, J., Zeng, L., Gong, Q., et al. (2013). Aberrant functional connectivity of resting state networks in transient ischemic attack. *PLoS ONE* 8:e71009. doi: 10.1371/journal.pone.0071009

Li, Z., Kadivar, A., Pluta, J., Dunlop, J., and Wang, Z. (2012). Test–retest stability analysis of resting brain activity revealed by blood oxygen level-dependent functional MRI. *J. Magn. Reson. Imaging* 36, 344–354. doi: 10.1002/jmri.23670

Lieb, R., Becker, E., and Altamura, C. (2005). The epidemiology of generalized anxiety disorder in Europe. *Eur. Neuropsychopharmacol.* 15, 445–452. doi: 10.1016/j.euroneuro.2005.04.010

Linares, I. M., Trzesniak, C., Chagas, M. H., Hallak, J. E., Nardi, A. E., and Crippa, J. A. (2012). Neuroimaging in specific phobia disorder: a systematic review of the literature. *Rev. Bras. Psiquiatr.* 34, 101–111. doi: 10.1016/S1516-4446(12)70017-X

Lowe, M. J., Mock, B. J., and Sorenson, J. A. (1998). Functional connectivity in single and multislice echoplanar imaging using resting-state fluctuations. *Neuroimage* 7, 119–132. doi: 10.1006/nimg.1997.0315

MacDonald, A. W. III, Cohen, J. D., Stenger, V. A., and Carter, C. S. (2000). Dissociating the role of the dorsolateral prefrontal and anterior cingulate cortex in cognitive control. *Science* 288, 1835–1838. doi: 10.1126/science.288.5472.1835

Mathews, A., and MacLeod, C. (1985). Selective processing of threat cues in anxiety states. *Behav. Res. Ther.* 23, 563–569. doi: 10.1016/0005-7967(85)90104-4

Meyer, T., Qi, X. L., Stanford, T. R., and Constantinidis, C. (2011). Stimulus selectivity in dorsal and ventral prefrontal cortex after training in working memory tasks. *J. Neurosci.* 31, 6266–6276. doi: 10.1523/JNEUROSCI.6798-10.2011

Miller, E. K., and Cohen, J. D. (2001). An integrative theory of prefrontal cortex function. *Annu. Rev. Neurosci.* 24, 167–202. doi: 10.1146/annurev.neuro.24.1.167

Modi, S., Kumar, M., Kumar, P., and Khushu, S. (2015). Aberrant functional connectivity of resting state networks associated with trait anxiety. *Psychiatry Res.* 234, 25–34. doi: 10.1016/j.pscychresns.2015.07.006

Moon, C. M., Kang, H. K., and Jeong, G. W. (2015). Metabolic change in the right dorsolateral prefrontal cortex and its correlation with symptom severity in patients with generalized anxiety disorder: proton magnetic resonance spectroscopy at 3 Tesla. *Psychiatry Clin. Neurosci.* 69, 422–430. doi: 10.1111/pcn.12279

Nakamura, K., and Kubota, K. (1996). The primate temporal pole: its putative role in object recognition and memory. *Behav. Brain Res.* 77, 53–77. doi: 10.1016/0166-4328(95)00227-8

Ochsner, K. N., and Gross, J. J. (2005). The cognitive control of emotion. *Trends Cogn. Sci.* 9, 242–249. doi: 10.1016/j.tics.2005.03.010

Ohman, A. (2005). The role of the amygdala in human fear: automatic detection of threat. *Psychoneuroendocrinology* 30, 953–958. doi: 10.1016/j.psyneuen.2005.03.019

Oldfield, R. C. (1971). The assessment and analysis of handedness: the Edinburgh inventory. *Neuropsychologia* 9, 97–113. doi: 10.1016/0028-3932(71)90067-4

Olson, I. R., Plotzker, A., and Ezzyat, Y. (2007). The Enigmatic temporal pole: a review of findings on social and emotional processing. *Brain* 130(Pt 7), 1718–1731. doi: 10.1093/brain/awm052

O'Reilly, J. X., Beckmann, C. F., Tomassini, V., Ramnani, N., and Johansen-Berg, H. (2010). Distinct and overlapping functional zones in the cerebellum defined by resting state functional connectivity. *Cereb. Cortex* 20, 953–965. doi: 10.1093/cercor/bhp157

Pannekoek, J. N., Veer, I. M., van Tol, M.-J., van der Werff, S. J. A., Demenescu, L. R., Aleman, A., et al. (2013). Resting-state functional connectivity abnormalities in limbic and salience networks in social anxiety disorder without comorbidity. *Eur. Neuropsychopharmacol.* 23, 186–195. doi: 10.1016/j.euroneuro.2012.04.018

Patterson, K., Nestor, P. J., and Rogers, T. T. (2007). Where do you know what you know? The representation of semantic knowledge in the human brain. *Nat. Rev. Neurosci.* 8, 976–987. doi: 10.1038/nrn2277

Pehrs, C., Zaki, J., Schlochtermeier, L. H., Jacobs, A. M., Kuchinke, L., and Koelsch, S. (2015). The temporal pole top-down modulates the ventral visual stream during social cognition. *Cereb. Cortex*. doi: 10.1093/cercor/bhv226. [Epub ahead of print].

Phan, K. L., Fitzgerald, D. A., Nathan, P. J., Moore, G. J., Uhde, T. W., and Tancer, M. E. (2005). Neural substrates for voluntary suppression of negative affect: a functional magnetic resonance imaging study. *Biol. Psychiatry* 57, 210–219. doi: 10.1016/j.biopsych.2004.10.030

Phelps, E. A. (2006). Emotion and cognition: insights from studies of the human amygdala. *Annu. Rev. Psychol.* 57, 27–53. doi: 10.1146/annurev.psych.56.091103.070234

Phillips, M. L., Drevets, W. C., Rauch, S. L., and Lane, R. (2003). Neurobiology of emotion perception I: the neural basis of normal emotion perception. *Biol. Psychiatry* 54, 504–514. doi: 10.1016/S0006-3223(03)00168-9

Phillips, M. L., Ladouceur, C. D., and Drevets, W. C. (2008). A neural model of voluntary and automatic emotion regulation: implications for understanding the pathophysiology and neurodevelopment of bipolar disorder. *Mol. Psychiatry* 13, 833–857. doi: 10.1038/mp.2008.65

Power, J. D., Barnes, K. A., Snyder, A. Z., Schlaggar, B. L., and Petersen, S. E. (2012). Spurious but systematic correlations in functional connectivity MRI networks arise from subject motion. *Neuroimage* 59, 2142–2154. doi: 10.1016/j.neuroimage.2011.10.018

Roy-Byrne, P. P., and Wagner, A. (2004). Primary care perspectives on generalized anxiety disorder. *J. Clin. Psychiatry* 65(Suppl. 13), 20–26.

Sacchetti, B., Scelfo, B., and Strata, P. (2005). The cerebellum: synaptic changes and fear conditioning. *Neuroscientist* 11, 217–227. doi: 10.1177/1073858405276428

Shao, Y., Wang, L., Ye, E., Jin, X., Ni, W., Yang, Y., et al. (2013). Decreased thalamocortical functional connectivity after 36 hours of total sleep deprivation: evidence from resting state fMRI. *PLoS ONE* 8:e78830. doi: 10.1371/journal.pone.0078830

Shehzad, Z., Kelly, A. M. C., Reiss, P. T., Gee, D. G., Gotimer, K., Uddin, L. Q., et al. (2009). The resting brain: unconstrained yet reliable. *Cereb. Cortex* 19, 2209–2229. doi: 10.1093/cercor/bhn256

Shin, L. M., and Liberzon, I. (2010). The neurocircuitry of fear, stress, and anxiety disorders. *Neuropsychopharmacology* 35, 169–191. doi: 10.1038/npp.2009.83

Si, T.-M., Shu, L., Dang, W.-M., Su, Y.-A., Chen, J.-X., Dong, W.-T., et al. (2009). Evaluation of the reliability and validity of Chinese version of the Mini-International Neuropsychiatric Interview in patients with mental disorders. *Chin. Ment. Health J.* 23, 493–497. doi: 10.3969/j.issn.1000-6729.2009.07.011

Song, X.-W., Dong, Z.-Y., Long, X.-Y., Li, S.-F., Zuo, X.-N., Zhu, C.-Z., et al. (2011). REST: a toolkit for resting-state functional magnetic resonance imaging data processing. *PLoS ONE* 6:e25031. doi: 10.1371/journal.pone.0025031

Sridharan, D., Levitin, D. J., and Menon, V. (2008). A critical role for the right fronto-insular cortex in switching between central-executive and default-mode networks. *Proc. Natl. Acad. Sci. U.S.A.* 105, 12569–12574. doi: 10.1073/pnas.0800005105

Stefanacci, L., and Amaral, D. G. (2002). Some observations on cortical inputs to the macaque monkey amygdala: an anterograde tracing study. *J. Comp. Neurol.* 451, 301–323. doi: 10.1002/cne.10339

Stoodley, C. J. (2012). The cerebellum and cognition: evidence from functional imaging studies. *Cerebellum* 11, 352–365. doi: 10.1007/s12311-011-0260-7

Supple, W. F., Leaton, R. N., and Fanselow, M. S. (1987). Effects of cerebellar vermal lesions on species-specific fear responses, neophobia, and taste-aversion learning in rats. *Physiol. Behav.* 39, 579–586. doi: 10.1016/0031-9384(87)90156-9

Thomason, M. E., Dennis, E. L., Joshi, A. A., Joshi, S. H., Dinov, I. D., Chang, C., et al. (2011). Resting-state fMRI can reliably map neural networks in children. *Neuroimage* 55, 165–175. doi: 10.1016/j.neuroimage.2010.11.080

Wong, C., and Gallate, J. (2012). The function of the anterior temporal lobe: a review of the empirical evidence. *Brain Res.* 1449, 94–116. doi: 10.1016/j.brainres.2012.02.017

Yan, C.-G., Cheung, B., Kelly, C., Colcombe, S., Craddock, R. C., Di Martino, A., et al. (2013). A comprehensive assessment of regional variation in the impact of head micromovements on functional connectomics. *Neuroimage* 76, 183–201. doi: 10.1016/j.neuroimage.2013.03.004

Yeo, B. T. T., Krienen, F. M., Sepulcre, J., Sabuncu, M. R., Lashkari, D., Hollinshead, M., et al. (2011). The organization of the human cerebral cortex estimated by intrinsic functional connectivity. *J. Neurophysiol.* 106, 1125–1165. doi: 10.1152/jn.00338.2011

Conflict of Interest Statement: The authors declare that the research was conducted in the absence of any commercial or financial relationships that could be construed as a potential conflict of interest.

Advantages of publishing in Frontiers

OPEN ACCESS
Articles are free to read, for greatest visibility

COLLABORATIVE PEER-REVIEW
Designed to be rigorous – yet also collaborative, fair and constructive

FAST PUBLICATION
Average 85 days from submission to publication (across all journals)

COPYRIGHT TO AUTHORS
No limit to article distribution and re-use

TRANSPARENT
Editors and reviewers acknowledged by name on published articles

SUPPORT
By our Swiss-based editorial team

IMPACT METRICS
Advanced metrics track your article's impact

GLOBAL SPREAD
5'100'000+ monthly article views and downloads

LOOP RESEARCH NETWORK
Our network increases readership for your article

Frontiers
EPFL Innovation Park, Building I • 1015 Lausanne • Switzerland
Tel +41 21 510 17 00 • Fax +41 21 510 17 01 • info@frontiersin.org
www.frontiersin.org

Find us on